Thesis Title:

Development of a novel model to quantify nitrous oxide emissions in the biological nutrient removal process of wastewater treatment plants

---

A thesis submitted in fulfillment of the requirements for the degree

of

Doctor of Philosophy (PhD) in the Department of Life Sciences

at

Brunel University London

by

Theoni Maria Massara

September 2018

London

Abstract

This thesis aimed to develop a novel mathematical tool for the mitigation of nitrous oxide (N_2O) emissions in wastewater treatment plants (WWTPs). Considering that N_2O is a greenhouse gas with a grave global warming impact, tools for the prediction of N_2O production in WWTPs are essential to accurately estimate the emissions and effectively reduce them. The first chapter reviewed past studies focusing on the N_2O generation in WWTPs. The major findings underlined the need to optimise the applied WWTP processes and use models that consider multiple N_2O production pathways and changes of majorly influencing operational factors (e.g. dissolved oxygen, DO). The second chapter presented the development of an N_2O model following the widely accepted International Water Association (IWA) Activated Sludge Model (ASM) structure that described the operation of a full-scale anaerobic-anoxic-aerobic municipal WWTP. The simulation results showed that low-aeration strategies require optimisation to avoid unstable nitrification and increased N_2O production via the nitrification-related pathways. The third chapter introduced an ASM-type N_2O model for the operation of a real full-scale municipal WWTP that provided data for the model calibration. The simulation results indicated that lower DO setpoints than those documented during the monitoring campaign can be applied to decease energy requirements without observing higher N_2O emission. The fourth chapter explored the development of an N_2O model based on an alternative concept that describes the complex electron transfer processes of the bacterial populations involved in the N_2O production. The developed model was adapted to the operation of a real full-scale municipal WWTP that provided data for the model calibration and validation. The results showed how important the applied aeration regime is while considering mitigation strategies. This last chapter emphasised how errors/inconsistencies in the sampling campaigns can lead to the development of inaccurate models if these data are used for calibration/validation purposes.

List of Contents

List of Figures

List of Tables

List of Accompanying Material

Page

List of Definitions

Anammox	Anoxic ammonium oxidation
AND	Alternating Nitrification Denitrification
AO	Anoxic Oxic
AOB	Ammonia Oxidizing Bacteria
A^2/O	Anaerobic/Anoxic/Oxic treatment configuration
AOR	Ammonia Oxidation Rate
AS	Activated Sludge
ASM	Activated Sludge Model
ASMN	Activated Sludge Model for Nitrogen
BNR	Biological Nutrient Removal
C	Carbon
CF	Carbon Fibres
COD	Chemical Oxygen Demand
DFBBR	Denitrifying Fluidized Bed Bioreactor
DO	Dissolved Oxygen
EF	Emission Factor
FA	Free Ammonia
F/M	Food to Microorganisms ratio
FNA	Free Nitrous Acid
GHG	Greenhouse Gas
GWP	Global Warming Potential
GWRC	Global Water Research Coalition
HRT	Hydraulic Retention Time
IC	Inorganic Carbon
IPCC	Intergovernmental Panel on Climate Change
IWA	International Water Association
MLE	Modified Ludzack-Ettinger
MLSS	Mixed Liquor Suspended Solids
MLVSS	Mixed Liquor Volatile Suspended Solids
Mox	Oxidised mediator: electron carriers in oxidised form
Mred	Reduced mediator: electron carriers in reduced form
N	Nitrogen

NLR	Nitrogen Loading Rate
NOB	Nitrite Oxidizing Bacteria
OD	Oxidation Ditch
OHOs	Ordinary Heterotrophic Organisms
P	Phosphorus
PAOs	Phosphorus Accumulating Organisms
P.E.	Population Equivalent
PHAs	Polyhydroxyalkanoates
PNA	Partial Nitritation Anammox
PPs	Polyphosphates
SA	Sensitivity Analysis
SBR	Sequencing Batch Reactor
SE	Stripping Effectivity
SND	Simultaneous Nitrification Denitrification
SRT	Sludge Retention Time
SS	Suspended Solids
TN	Total Nitrogen
TKN	Total Kjeldahl Nitrogen
TP	Total Phosphorus
TSS	Total Suspended Solids
vNLR	volumetric Nitrogen Loading Rate
VSS	Volatile Suspended Solids
WWTP	Wastewater Treatment Plant

Preface

This PhD project aimed to develop, calibrate and validate a novel mathematical tool that can be used for the purposes of the online monitoring, control and mitigation of the carbon (C) footprint of wastewater treatment plants (WWTPs). Gaseous emissions are produced at various stages during the biological nutrient removal (BNR) in WWTPs. Strategies to decrease the required amount of energy for this operation may in fact cause greater harm due to the increase of greenhouse gas (GHG) emissions. Various GHG emissions are associated with the construction and operation of WWTPs; these include carbon dioxide (CO_2), methane (CH_4) and nitrous oxide (N_2O), with N_2O having a global warming potential (GWP) 265-298 times higher than the one of CO_2. The development of reliable and robust tools allowing the prediction of N_2O production and emission during the BNR in WWTPs is important for several reasons: (i) to accurately estimate the anticipated emissions, (ii) to immediately apply measures to reduce them, and (iii) to link them with a particular activity in the plant.

Thus, the key aims of the project can be summarised below:

- Develop a novel and flexible mathematical tool able to accurately predict the N_2O production and emission during the operation of a WWTP based on different approaches (i.e. International Water Association (IWA) Activated Sludge Model (ASM) structure; electron-carrier concept);
- Expand and adapt the developed versions of the model to describe the operation of different full-scale WWTPs;

- Calibrate/validate the proposed versions of the model by using real data from the operation of existing full-scale WWTPs to verify their reliability and accuracy;
- Suggest the most probable N_2O production pathway in each case along with the operational conditions that triggered the N_2O generation;
- Estimate the N_2O emission factor (EF) for each WWTP under investigation by using the developed model versions.

Hence, this research was conducted to answer to the following research questions:

- Which operational conditions majorly influence the N_2O production and emission during the BNR in WWTPs?
- Can previously developed and widely accepted modelling concepts (e.g. IWA ASM models, electron carrier models) be extended and adapted to describe the N_2O production and emission in different full-scale WWTPs?
- Which are the sources of uncertainty in this research?
- How can this research be improved and extended in the future?

To this end, this thesis was structured in the following way. First, a literature review that presented in detail all the pathways for N_2O production during the BNR in WWTPs, the most important parameters (e.g. dissolved oxygen (DO), temperature, pH, N_2O predecessors, etc.) influencing the N_2O production & emission in WWTPs, an assessment of the N_2O quantification techniques, a comparison of existing N_2O production/emission models, and suggestions for effective mitigation. Then, the IWA

ASM2d structure was expanded to develop an ASM-type N_2O model including all microbial N_2O production pathways, nitrogen (N), phosphorus (P) and chemical oxygen demand (COD) removal, N_2O stripping modelling, and prediction of the N_2O EF under changing DOs. Afterwards, this IWA ASM1 structure was adapted to describe the N_2O production and emission during the operation of the full-scale municipal SBR WWTP of La Roca del Valles (Barcelona, Spain). The developed model was calibrated with real data from the WWTP operation. The calibrated model version was then used to test if the reported emission trends can be successfully described under lower DOs. Next, the alternative approach to N_2O modelling (i.e. electron-carrier concept) was followed to create a multiple-pathway model describing the operation of a full-scale municipal SBR WWTP in Australia. This new version of the model was calibrated and validated using full-scale data from the intensive monitoring campaign of the plant under investigation. Furthermore, it was emphasised how potential errors in the sampling campaigns/methods/devices generate unreliable measurements. If these data are used for validation/calibration, they lead to inaccurate models. Finally, suggestions were made concerning the continuation and expansion of this research to new areas.

The results of each chapter are summarised below. Due to its high GWP, even a moderate N_2O quantity can importantly contribute to the final C-footprint of WWTPs. The biological pathways connected with the N_2O production during the BNR in WWTPs are nitrifier denitrification, hydroxylamine (NH_2OH) oxidation and heterotrophic denitrification; the first two occur through the activity of ammonia oxidizing bacteria (AOB). The major parameters influencing the N_2O emission during wastewater treatment are appraised in the first chapter. Indeed, different aspects that contribute either per se or combined to the

increase of N_2O emissions are listed: insufficient DO, nitrite (NO_2^-) accumulation, low COD:N, inhibited growth of the denitrifying bacterial population, absence of pH and/or temperature control. The accurate modelling of N_2O production and emission in WWTPs requires the inclusion of all biological production pathways as well as the possible abiotically driven N_2O generation under changing conditions (e.g. varying DOs and/or NO_2^- concentrations). Therefore, it can be concluded that the decrease of N_2O emission during the BNR in wastewater treatment relies upon the concurrence of different factors: application of the most appropriate N-removal process, optimum combination of operating conditions, and use of multiple-pathway models for the accurate prediction of N_2O emissions.

In the second chapter, a methodology to predict N_2O emissions during the BNR in WWTPs was presented. The developed N_2O estimation model considered the changing operational conditions (e.g. DO) within WWTPs. Based on the ASM structure, the proposed mathematical tool incorporated all biological N_2O production pathways for a municipal anaerobic/anoxic/oxic (A^2/O) WWTP with biological N, P and COD removal. A stripping effectivity (SE) coefficient was added to reflect the potential divergence of the stripping model from the actual stripping process. Partial nitrification resulting in high N_2O production via nitrifier denitrification was observed when the DO in the aerobic compartment ranged from 1.8 to 2.5 mg O_2 L^{-1}. The latter possibly suggests that decreased aeration strategies facilitate the attainment of a low overall C-footprint provided that complete nitrification is not compromised. The model predicted high N_2O emissions when low DO (~1.1 mg O_2 L^{-1}) and high influent ammonium (NH_4^+) concentration coincided. Further observation revealed that when the AOB population was higher than

the Nitrite Oxidizing Bacteria (NOB) respective one, NO_2^- accumulated. Hence, nitrifier denitrification was the preferred N_2O production pathway. Moreover, the effect of a sudden increase in the influent NH_4^+ load was investigated. It was noted that it resulted in the AOB growing at a faster rate compared to the NOB; thus, nitrifier denitrification pathway was considered once again as the N_2O hotspot. Finally, the developed model predicted that the highest N_2O EFs occurred under the following concurring conditions: enhancement of partial nitrification (i.e. low DO) along with increased importance of the stripping effect (i.e. high SEs).

In the third chapter, real N_2O emission data from the full-scale municipal SBR WWTP of La Roca del Valles (Barcelona, Spain) were used and the IWA ASM1 version was expanded and modified in the following way: adaptation to an SBR configuration performing COD and N removal, in addition to the inclusion of the biological and abiotic N_2O production. During the plant operation, two different cycle types were applied and monitored in terms of N_2O emissions; cycles of type B and C. Cycle B involved the alternation amongst two non-aerated (25-40 min) and two aerobic phases (15-40 min). The reaction phase for Cycle C included the sequence of two shorter non-aerated phases (25-29 min) with a longer aerobic one (66 min) between them. The representative DO profiles of cycles B and C as recorded by the La Roca del Valles WWTP operators were used to calibrate the developed model. The calibrated version agreed well with the provided N_2O emission data. It was then used for further simulations exploring if the monitored N_2O emission profiles can be satisfactorily described by simulating operation under different DOs. The optimal fit was attained under a DO setpoint of 1.6 mg O_2 L^{-1} for both aerobic phases of Cycle B and for a DO of 1.7 mg O_2 L^{-1} for the single aerobic phase

of Cycle C. The latter DO values were lower than the respective DO profiles reported by the plant operators during the monitoring campaign. Furthermore, the total N_2O EF predicted by the developed model differed between the two cycle types: 0.8% (Cycle B) and 1.5% (Cycle C). Although the total duration of aeration was approximately the same (Cycle B: 60 min; Cycle C: 66 min), the difference in the cycle configuration impacted on the final N_2O EF. The single longer aerobic phase of Cycle C enhanced the N_2O production via the nitrification-related routes and its subsequent emission through stripping for a slightly longer and non-interrupted period. Moreover, the N_2O production occurred only during the aerobic phases with the N_2O concentration peaks coinciding with the NO_2^- peaks for both cycles. Consequently, it can be concluded that nitrifier denitrification was the predominant AOB pathway for N_2O generation. Finally, no important NH_2OH consumption was noted, thus suggesting that the abiotic routes were poorly preferred under the conditions of the current study.

In the fourth chapter, a recent modelling approach based on the combination of the biological N_2O production pathways along with the complex electron transfer processes of the AOB and the denitrifiers was followed. The oxidation and reduction processes were dissociated, and electron carriers were inserted to describe the electron transfer from oxidation to reduction. The aim was to develop an electron carrier-type N_2O model integrating all the microbial production pathways and describing the operation of a full-scale municipal SBR WWTP in Australia. Data obtained during a two-day monitoring campaign were used to calibrate and validate the developed model. Key parameters relevant to the ammonium (NH_4^+) oxidation and the N_2O production dynamics required calibration. After calibration, the model was used for validation purposes. The model

predictions were compared against the profiles of the N-components, the DO and the N_2O as obtained on the second day of the intensive monitoring. The model was able to describe these trends. Under the intermittent aeration regime, nitrifier denitrification was the most contributing N_2O production pathway. The EF of the full-scale SBR WWTP was calculated as equal to 1% that was within the range of EFs reported for other full-scale municipal WWTPs in Australia.

Furthermore, the fact that potential failures in the sampling campaigns, methods and devices are likely to generate unreliable measurements was discussed in the final (fifth) chapter. If these data are used for the calibration and validation purposes of the developed mechanistic N_2O models, the robustness of this modelling cannot be guaranteed. The final section presents the possibility of extending this research to new areas in the future. The coupling of the developed mechanistic models with sophisticated statistical tools is suggested. The next goal is to perform multivariate statistical analysis of the datasets that were used for the calibration and validation of the mechanistic models analysed in the third and fourth chapter. The results concerning the most contributive N_2O generation pathways as well as the observations regarding the profiles of other parameters (e.g. DO, concentration of N-compounds, etc.) will be compared against the respective ones generated by the mechanistic modelling. In this way, the models proposed through this PhD project can be further improved. Finally, these actions will lead to an integrated tool combining both mechanistic and sophisticated statistical modelling that can be useful for mitigating the N_2O emissions during the BNR in WWTPs.

Acknowledgements

The candidate's full four-year PhD studentship was provided by the London Natural Environment Research Council Doctoral Training Partnership in which the nine following partners participated: University College London, Brunel University London, Birkbeck University of London, King's College London, Queen Mary University of London, Royal Holloway University of London, ZSL Institute of Zoology, Kew Royal Botanic Gardens and the Natural History Museum.

The PhD student was registered in Brunel University London and supervised by:

- Dr Evina Katsou, Senior Lecturer in Civil Engineering, Brunel University London,
- Dr Mark Scrimshaw, Reader in Environmental Chemistry, Brunel University London.

The project's title was: "Development of a novel model to quantify nitrous oxide emissions in the biological nutrient removal process of wastewater treatment plants". It was additionally supported and funded by the European Union research program C-FOOT-CTRL, which was under the auspices of the European Union Framework Program for Research and Innovation Horizon 2020. The partners were the following: Brunel University London (United Kingdom), National Technical University of Athens (Greece), Universitat Autònoma de Barcelona (Spain), the University of Queensland (Australia), Unisensor Sensorsysteme GmbH (Germany), Aeris Tecnologías Ambientales S.L. (Spain), Cobalt Water LLC (USA), DRH2O LLC (USA) and Green Tech Fund California I, PBC (USA).

I would like to thank the following people from the bottom of my heart:

- First, my wonderful supervisors, Dr Evina Katsou (Senior Lecturer in Civil Engineering at Brunel University London) and Dr Mark Scrimshaw (Reader in Environmental Chemistry at Brunel University London), for their collaboration, incessant support and guidance.
- Secondly, the amazing Prof. Simos Malamis (Assistant Professor at the Department of Water Resources and Environmental Engineering of the School of Civil Engineering at the National Technical University of Athens) for the superb collaboration and for kindly offering his 'to-the-point' consulting throughout my PhD.

At this point, I shall mention that my PhD 'journey' literally involved a lot of travelling and moving. I spent five months at Barcelona (Spain) and eight months at Brisbane (Australia) as a visiting PhD student at the Autonomous University of Barcelona (Department of Chemical, Biological and Environmental Engineering of the School of Engineering) and at the University of Queensland (Advanced Water Management Centre), respectively. I am deeply thankful towards Prof. Juan Antonio Baeza Labat (Autonomous University of Barcelona), Dr Albert Guisasola (Autonomous University of Barcelona), Prof. Zhiguo Yuan (University of Queensland), Dr Liu Ye (University of Queensland) and Dr Bing-Jie Ni (University of Queensland) who all honored me by working closely with me and supervising my progress.

Furthermore, I am grateful to NERC for the full four-year PhD studentship, as well to Prof. Mark Maslin (University College London) and Prof. Kevin Fowler (University College London) for coordinating the London NERC DTP. Moreover, I could never forget

my lovely colleagues at Brunel University London, Vasileia Vasilaki (PhD candidate) and Dr Peyo Stanchev (postdoctoral researcher) who offered precious help at various moments.

Apart from the practical and scientific help needed to complete my PhD, I asked for moral and emotional support many times. Therefore, I would like to thank my dear and absolutely lovely friends: Evina, Simos, Christina, Evi, Elena, Polly, Anda. This would not have been achieved without them in my life, without my knowing that they would always be there for me no matter what.

Moreover, I am thanking my loving and caring family for their sincere and unconditional love and support since the first day of my life. I cannot express how thankful I am to my mum Eleni, my brother Giorgos and my grandmother Poppy. Finally, I owe an awful lot to a marvellous dad, my dad, Giannis, to whom I am dedicating this work. Hoping that all this made me a better person and scientist, hoping that all this did happen for a reason and not in vain, I am finishing with some verses from ‘Helen’ by George Seferis translated in English by Edmund Keeley:

‘Tearful bird,
on sea-kissed Cyprus
consecrated to remind me of my country,
I moored alone with this fable,
if it’s true that it is a fable,
if it’s true that mortals will not again take up
the old deceit of the gods;
if it’s true
that in future years some other Teucer,
or some Ajax or Priam or Hecuba,

or someone unknown and nameless who nevertheless saw
a Scamander overflow with corpses,
isn't fated to hear
messengers coming to tell him
that so much suffering, so much life,
went into the abyss
all for an empty tunic, all for a Helen.'

Theoni-Maria Massara

Civil Engineer (MEng, MSc), PhD candidate

September 2018

London

Chapter I

Literature Review

Summary

N_2O production and emission occurs during the BNR in WWTPs. Due to having a GWP 265-298 times higher than CO_2, even a moderate N_2O quantity can importantly contribute to the final C-footprint of WWTPs. The conventional processes applied for the biological N-removal are nitrification and denitrification. Nevertheless, advanced methods such as nitritation/denitritation and completely autotrophic N-removal have also been implemented for the same purpose. The biological pathways connected with the N_2O production during the BNR in WWTPs are nitrifier denitrification, NH_2OH oxidation and heterotrophic denitrification; the first two occur through the activity of the AOB. The major parameters influencing the N_2O emission during wastewater treatment are appraised in this chapter. Indeed, different aspects that contribute either individually or combined to the increase of N_2O emissions are listed: insufficient DO, NO_2^- accumulation, low COD:N, inhibited growth of the denitrifying bacterial population, absence of pH and/or temperature control. An important observation is that the phenomenon of N_2O emission during the BNR is assessed using highly different methods amongst relevant past works. The accurate modelling of N_2O production and emission in WWTPs requires the inclusion of all biological production pathways as well as the possible abiotically driven N_2O generation under changing conditions (e.g. varying DOs and/or NO_2^- concentrations). Moreover, the establishment of quantification methods that precisely capture both the liquid and the gaseous N_2O trends will considerably enhance the calibration and validation of these models. Therefore, it can be concluded that the decrease of N_2O emission during the BNR in wastewater treatment relies upon the concurrence of different factors: application of the most appropriate N-removal process, optimum combination of

operating conditions, and use of multiple-pathway models for the accurate prediction of N_2O emissions.

Keywords

BNR, N_2O emission, nitritation/denitritation, Anammox, nitrifier denitrification, modelling.

1. Introduction

WWTPs operate for the pollutant removal and sanitation of wastewater. However, issues can arise with respect to the energy requirements and release of gaseous products during their operation (Hospido et al., 2004). Inside the European Union for example, the total treatment capacity of WWTPs exceeds 400 million population equivalents (P.E.). Hence, decreasing the energy needed to run the plants becomes increasingly important (Mamais et al., 2015). The long-established activated sludge (AS) process implemented during wastewater treatment is considered rather energy-consuming. Furthermore, production and emission of GHGs (i.e. N_2O, CO_2 and CH_4) is likely during the AS application (Hassani et al., 2011; Lijó et al., 2017). Therefore, it is essential to investigate the causes and hotspots of GHG production in WWTPs. The indirect CO_2 emission is calculated through the energy requirements of the plant, whereas direct CO_2 emissions can be reported in any of the treatment stages. CH_4 emission is noted in the sewerage and sludge treatment sections.

With a steady-state lifetime in the atmosphere of 116±9 years, N_2O is considered a highly important GHG (Prather et al., 2015). The larger the GWP of a gas (defined as the amount of energy the emissions of 1 ton of the gas will absorb over a given period, relative to the emissions of 1 ton of CO_2), the more it warms the Earth over this period. In a period of 100 years for example, the N_2O and CH_4 GWPs are estimated as 265-298 and 28-36 times higher, respectively, than the one of CO_2. Furthermore, the GWP values suggested by international organisations (e.g. Environmental Protection Agency) are updated occasionally; e.g. to reflect changes in the estimations of the GHGs lifetime in the atmosphere, and/or consider new estimates of the atmospheric GHG concentrations

that will affect the GWP calculation, etc. (IPCC, 2014). Moreover, the N_2O released in the stratosphere aggravates the stratospheric ozone depletion (Portmann et al., 2012). More importantly, the total GWP of the water cycle (i.e. considered as the sum of drinking water, wastewater treatment and effluent discharge, sludge processing and disposal) can be burdened by 26% because of the direct N_2O emissions happening during wastewater treatment (Frijns et al., 2008). The N_2O production in WWTPs can be largely variable because of several factors: initial N-load, influent composition and general operating/environmental conditions (Kampschreur et al., 2009; Yang et al. 2009; Ahn et al., 2010; Law et al., 2012a; Wang et al., 2014b; Li et al., 2015).

The conventional methods for N-removal from wastewater involve the biological processes of nitrification and denitrification. Nitrification includes a series of oxidations (i.e. ammonium (NH_4^+) → NO_2^- → nitrate (NO_3^-)), whereas denitrification a series of reductions (i.e. NO_3^- → NO_2^- → nitric oxide (NO) → N_2O → diatomic molecule N_2) (Kampschreur et al.,2009; Malamis et al., 2015). During nitritation/denitritation, NH_4^+ is oxidised to NO_2^- (nitritation) and, then, NO_2^- is reduced to N_2 (denitritation) (Turk and Mavinic, 1987; Frison et al., 2013). Compared to the conventional nitrification/denitrification, it can be less costly since it requires up to 25% and 40% less oxygen and external C, respectively. Moreover, it can decrease the sludge production by 25% (Malamis et al., 2015). In cases of nitrogenous effluents such as sludge reject water, the completely autotrophic N-removal over NO_2^- or deammonification as it is alternatively called, can also be applied (Malamis et al., 2015). Part of the entering NH_4^+ (around 60%) is oxidised to NO_2^- (Strous et al., 1998). The N-removal takes place via the anoxic ammonium oxidation (anammox) process; the remaining NH_4^+ is mainly oxidised to N_2

and minorly to NO_3^- (with the produced NO_2^- as electron acceptor) under anoxic conditions (Malamis et al., 2015). In all cases, N_2O can be accumulated and emitted. Therefore, the atmospheric N_2O and C-footprint of WWTPs are both likely to increase (Tallec et al., 2006; Zhu et al., 2008; Yang et al., 2009).

This chapter was written to serve the following purposes: a) to analyse the pathways for N_2O production during the biological N-removal in WWTPs, b) to summarise the major conclusions of previous works that examined the parameters (e.g. dissolved oxygen (DO), temperature, pH, N_2O predecessors, etc.) that majorly influence the N_2O production and emission during wastewater treatment, c) to assess the N_2O quantification techniques, d) to compare and contrast the mathematical models that have been presented to describe the N_2O generation during the biological nutrient removal BNR in WWTPs, and e) to use all this knowledge to suggest effective mitigation measures.

2. The pathways of N_2O production during the biological N-removal in WWTPs

N-removal during wastewater treatment can occur through various mechanisms, each of which requires the application of certain operating conditions along with the growth of the appropriate bacterial culture (Xavier et al., 2007; Ahn et al., 2008). During nitrification, NH_4^+ is firstly oxidised to NO_2^- by the AOB and, afterwards, the produced NO_2^- is oxidised to NO_3^- by the NOB. Denitrification involves a sequence of reductions performed by the heterotrophic denitrifying bacteria. Nitritation requires NO_2^- accumulation, whereas the NO_3^- formation must be hindered; hence, the AOB growth

must be promoted to the detriment of the NOB one. This can happen under conditions of high free ammonia (FA) (FA>1 mg NH_3 L^{-1}) or high free nitrous acid (FNA>0.02 mg HNO_2-N L^{-1}), low DO (0.4-1 mg O_2 L^{-1}) and elevated temperature (30-40 ^oC). During the completely autotrophic N-removal, the anammox bacteria use NO_2^- as electron acceptor to oxidise NH_4^+ to N_2 and NO_3^- (Kampschreur et al., 2009; Malamis et al., 2015).

The microbial pathways linked to the N_2O production during the BNR in WWTPs are basically three: NH_2OH oxidation, nitrifier denitrification and heterotrophic denitrification (Fig. 1) (Wunderlin et al., 2012, 2013; Ni and Yuan, 2015). The AOB-related N_2O generation is described as follows: first, the oxidation of ammonia (NH_3) to NH_2OH with the reduction of molecular oxygen catalysed by the ammonia monooxygenase (AMO). Then, NH_2OH is oxidised to NO_2^- catalysed by the hydroxylamine oxidoreductase (HAO) with oxygen as the electron acceptor. If the oxidation of NH_2OH to NO_2^- by the aid of the HAO enzyme is incomplete (e.g. under conditions of high ammonia oxidation rate (AOR) that lead to NH_2OH accumulation), N_2O can be generated as by-product (Fig. 1: NH_2OH oxidation pathway). Furthermore, the nitrite reductase (NirK) catalyses the NO_2^- reduction to NO, while the nitric oxide reductase (Nor) the NO conversion to N_2O (Fig. 1: nitrifier denitrification pathway). Although poorly successful in total N (TN) removal, nitrifier denitrification can be importantly contributive in the N_2O production; e.g. under oxygen-limiting conditions and high NO_2^- concentrations. (Hooper et al., 1997; Poughon et al., 2000; Chandran et al., 2011; Stein, 2011a, b; Law et al., 2012a; Ni and Yuan, 2015). In addition, N_2O can result as an intermediate of heterotrophic denitrification (Fig. 1) (von Schulthess and Gujer, 1996; Pan et al., 2012, 2013a; Ni and Yuan, 2015). Heterotrophic denitrification is a sequence of reductions with NO_2^-, NO and N_2O as intermediate

products. The following enzymes serve as catalysts for this series of reactions: the nitrate reductase (NaR), the nitrite reductase (NiR), the nitric oxide reductase (NOR) and the nitrous oxide reductase (N_2OR) (Ni and Yuan, 2015).

Chemical N_2O and NO production is also possible. However, the percentage of N_2O emitted due to chemical processes in biological systems is still under research and is considered to depend upon various factors (e.g. influent N-content, pH). In any case, the knowledge acquired through the current research suggests that most of the N_2O emitted in WWTPs is generated during biochemical processes. Therefore, this chapter does not focus on the purely chemical pathways as they are not regarded as significant N_2O and NO contributors in these scenarios (Schreiber et al., 2012).

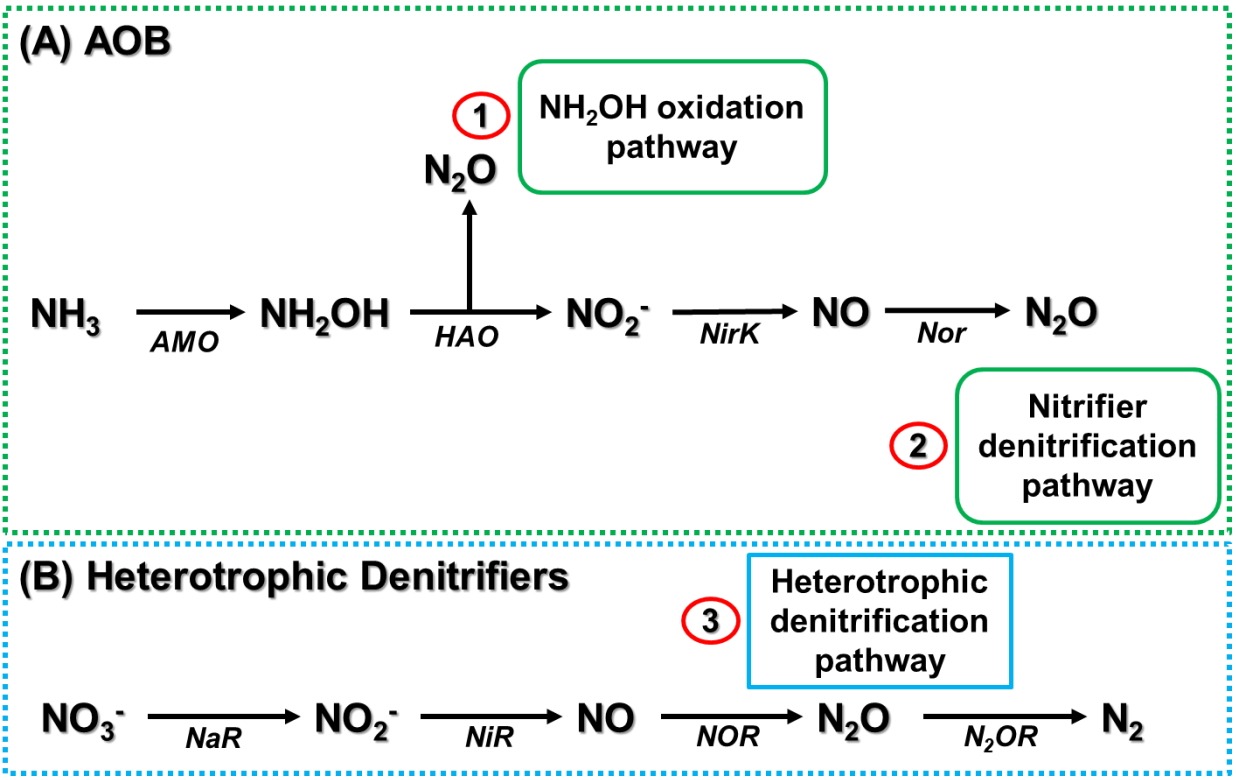

Figure 1: A simplified schematic representation of the biological pathways leading to N_2O production during the biological N-removal in WWTPs: (A) the two AOB pathways

(NH_2OH oxidation and nitrifier denitrification), and (B) the pathway activated by the heterotrophic denitrifiers (heterotrophic denitrification) (Ni and Yuan, 2015).

3. Parameters that influence the N_2O emissions during the biological N-removal in WWTPs

This section provides a critical overview of several lab-, pilot- and full-scale studies investigating the N_2O production and emission during the BNR in WWTPs. This overview aimed at unveiling the causes of N_2O production as well as at suggesting measures for the emission mitigation. The phenomenon of N_2O emission during wastewater treatment is highly variable because of numerous parameters including the nitrogen loading rate (NLR), the reactor configuration and operating conditions, the BNR process (conventional or advanced), the DO, the C-source, the pH, the temperature, etc., that will be examined in detail afterwards. The impact of each factor is investigated in the following subsections, while the major findings of all cited references are presented in Table 1.

Table 1: Overview of past lab-, pilot- and full-scale studies investigating the N_2O production and emission during the BNR in wastewater treatment (configuration, wastewater type and operating characteristics, HRT and NLR, main findings, N_2O production/EF and most contributive N_2O production pathway).

LAB-SCALE						
Reference	**Configuration**	**Wastewater type/Operating characteristics**	**HRT/NLR**	**Main findings**	**N_2O production/EF**	**Hotspot**
Ahn et al., 2011	1 bioreactor operated sequentially in nitrification & nitritation	• Synthetic • N-NH_4=500 mg L^{-1}	• HRT=1.1 d • NLR=455 mg N-NH_4 L^{-1} d^{-1}	Nitritation strategy: • reduced operating costs & energy requirements • optimisation needed against the C-footprint related to high N_2O emissions	N_2O emission: • 0.1±0.2% of influent N-NH_4 (nitrification) • 0.6±0.2% of influent N-NH_4 (nitritation)	Nitrifier denitrification
Law et al., 2011	SBR	• Synthetic with characteristics of anaerobic digester liquor • N-NH_4=1,000 mg L^{-1}	• HRT=1 d • NLR=1,000 mg N-NH_4 L^{-1} d^{-1}	• pH increase enhanced the AOR of the AOB culture • 6≤pH≤7: minimum N_2O production (0.2±0.01 mg N-N_2O h^{-1} g^{-1} VSS) • pH=8: maximum N_2O production (0.5±0.04 mg N-N_2O h^{-1} g^{-1} VSS)	Average N_2O emission: 0.6% of influent N-NH_4	AOB pathways at pH=8 (no clear predominance between the two pathways)
Zhu and Chen, 2011	1 SBR with acetic acid as C-source & 1 SBR with sludge fermentation liquid as C-source	• Municipal (real supplemented to attain desired NH_4-N, TN concentrations)	• HRT=0.7 d • NLR=51 mg N L^{-1} d^{-1}	• Sludge fermentation liquid as C-source increased the number of bacteria reducing N_2O to N_2	N_2O generation: • 0.5±0.03 mg N-N_2O mg^{-1} N-removed (acetic acid as C-source) • 0.1±0.02 mg N-N_2O mg^{-1} N-removed	Heterotrophic denitrification

		• Average initial N-NH_4=30 mg L^{-1} • Average initial TN=35.5 mg N L^{-1}			(sludge fermentation liquid as C-source)	
Quan et al., 2012	3 aerobic granular sludge SBRs	• Synthetic: mixture of municipal & pig manure digestate liquid • N_2O measurement in 3 10-day operational periods: influent N-NH_4=148, 106 & 74 mg L^{-1} (corresponding to COD:N ratios of 1:0.22, 1:0.15 & 1:0.11)	• HRT=0.3 d • NLR=493 mg N-NH_4 L^{-1} d^{-1} (influent N-NH_4=148 mg L^{-1}), 353 mg N-NH_4 L^{-1} d^{-1} (influent N-NH_4=106 mg L^{-1}), 247 mg N-NH_4 L^{-1} d^{-1} (influent N-NH_4=74 mg L^{-1})	• N_2O emissions decreased with the increase of aeration rate & COD:N ratio	N_2O emission (relative to influent N) at the aeration rates of 0.2, 0.6 & 1 L O_2 min^{-1}: • 8%, 6% & 4% (COD:N=1:0.22) • 7%, 5% & 4% (COD:N=1:0.15) • 4%, 3% & 2% (COD:N=1:0.11)	• Low DO (0.5-1.5 mg O_2 L^{-1}): heterotrophic denitrification • DO>1.5 mg O_2 L^{-1}: AOB pathways
Xie et al., 2012	AOB-enriched SBR system	• Synthetic • N-NH_4=1,000 mg L^{-1}	• HRT=0.5 d • NLR=2,000 mg N-NH_4 L^{-1} d^{-1}	• Low DO (e.g. DO<0.5 mg O_2 L^{-1}): AOB with NO_2^- as terminal electron acceptor responsible for N_2O emission	N_2O emission: 0.4% of total N-NH_4 oxidation	Nitrifier denitrification
Zhou et al., 2012	SBR	• Synthetic • N-NH_4=20 mg L^{-1}	• HRT=0.8 d • NLR=25 mg N-NH_4 L^{-1} d^{-1}	• Lowest COD:N(=0.6): very limited N_2O reduction with external C-source • COD:N=0.6-1.3: sharper increase in the N_2O	N_2O reduction rate (mg N-N_2O min^{-1} g $biomass^{-1}$) with COD:N ranging from 0.6 to 2.5:	Heterotrophic denitrification

				reduction rate with external C-source • COD:N=1.9-2.5: similar N_2O reduction rates regardless of C-source type	• 0.04-0.05 (internal C-source: PHA) • 0.003-0.05 (external C-source: sodium acetate)	
Hu et al., 2013	3 anoxic/oxic SBRs	• Synthetic mimicking urban • $N\text{-}NH_4$=55.4 mg L^{-1}	• HRT=0.6 d • NLR=92 mg $N\text{-}NH_4$ L^{-1} d^{-1}	• Sodium acetate (compared to glucose & soluble starch): optimal nutrient removal but highest N_2O emission (low denitrifiers diversity)	Percentage of TN-removed converted to N_2O: • 5% (C-source: glucose) • 9% (C-source: sodium acetate) • 3% (C-source: soluble starch)	Heterotrophic denitrification
Lochmatter et al., 2013	2 aerobic granular sludge SBRs	• Synthetic • $N\text{-}NH_4$=50 mg L^{-1}	• HRT=0.3 d • NLR=167 mg $N\text{-}NH_4$ L^{-1} d^{-1}	• N_2O emissions significantly decreased with higher COD loads & under AND conditions	Alternating high/low DO (AND)→ highest N_2O emission with the lowest COD loading rate (1.6 g COD $L^{-1}d^{-1}$) at the low-DO stage: 9% of influent N	• AND: heterotrophic denitrification • SND: all pathways possible

Shen et al., 2013	SBR	• Synthetic • N-NH_4=8, 18, 36, 52 mg L^{-1} (to examine different concentration effects on N_2O emissions)	• HRT=0.5 d • NLR=16 mg N-NH_4 L^{-1} d^{-1} (influent N-NH_4=8 mg L^{-1}), 36 mg N-NH_4 L^{-1} d^{-1} (influent N-NH_4=18 mg L^{-1}), 72 mg N-NH_4 L^{-1} d^{-1} (influent N-NH_4=36 mg L^{-1}), 104 mg N-NH_4 L^{-1} d^{-1} (influent N-NH_4=52 mg L^{-1})	• N_2O emissions mainly during nitrification • Nitrification: higher N_2O emissions with increased initial NH_4^+or NO_2^- concentrations	N_2O emissions: • 2.5% of the removed N-NH_4 (nitrification with high oxygen limitation) • 0.1-1.1% of the removed N-NH_4 (nitrification with low oxygen limitation)	Nitrifier denitrification
Chen et al., 2014	1 SBR with a sequence of anaerobic-oxic-anoxic phases & 1 anaerobic phase-cancelled SBR	• Synthetic • N-NH_4=31 mg L^{-1}	• HRT=0.5 d • NLR=62 mg N-NH_4 L^{-1} d^{-1}	• N_2O generation reduced by 42% in the anaerobic phase-cancelled SBR due to the enhanced heterotrophic denitrifiers' activity	N_2O generation: • 0.07±0.002 mg N-N_2O mg^{-1} TN-removed (anaerobic-anoxic-oxic SBR) • 0.04±0.003 mg N-N_2O mg^{-1} TN-removed (anaerobic phase-cancelled SBR)	Nitrifier denitrification
Eldyasti et al., 2014	DFBBR	• Municipal (synthetic)	• HRT=0.03 d • NLR=1,033 mg N L^{-1} d^{-1} (phases I &	• N_2O emissions decreased exponentially with biofilm thickness increase due to the slow-	N_2O emission: • 0.5% of influent TN (biofilm	Heterotrophic denitrification

		• TN=31±2 mg L^{-1} (phases I & III) • TN=51±3 mg L^{-1} (phase II)	III), 1,700 mg N L^{-1} d^{-1} (phase II)	growth denitrifiers retention & the limited N_2O diffusivity	thickness=680 μm) • 1.6% of influent TN (limited COD & biofilm thickness=230 μm)	
Wang et al., 2014a	2 SBRs: a control SBR & an experimental SBR achieving the NO_2^- pathway via an FNA treatment unit	• Synthetic: domestic wastewater & anaerobic digestion liquor • TKN=50 mg L^{-1} • Anaerobic digestion liquor addition: additional 20% N-load	• HRT=1 d • NLR=60 mg N L^{-1} d^{-1}	• FNA-based strategy for NO_2^- pathway: TN-removal substantially improved without negatively affecting N_2O emission	N_2O emission: • 1.5±0.4% of influent TN (control reactor) • 0.5±0.03% of influent TN (experimental reactor)	Nitrifier denitrification
Wang et al., 2014b	2 SBRs	• 1 SBR fed with real sludge reject water (N-NH_4=861±13 mg L^{-1}) & 1 SBR fed with synthetic reject water (N-NH_4=1,000 mg L^{-1})	• HRT=1 d • NLR=861 mg N-NH_4 L^{-1} d^{-1} (real sludge reject water), 1,000 mg N-NH_4 L^{-1} d^{-1} (synthetic sludge reject water)	• Nitritation systems with real anaerobic sludge digestion liquor: N_2O emissions via heterotrophic denitrification aided by the organic C in the liquor • FNA hindering effect: heterotrophic NO_2^- reduction possibly stopped at the N_2O formation stage	N_2O emission: • 3.1±0.2% of N-NH_4 oxidised (SBR with real digestion liquor) • 0.8±0.1% of N-NH_4 oxidised (SBR with synthetic digestion liquor)	Heterotrophic denitrification

Adouani et al., 2015	Batch reactor	• Synthetic • N-NH_4=6 mg L^{-1}	Batch experiments	• Low temperatures slowed down all denitrification enzyme activities (especially NO & N_2O reductase activities)	N_2O emission N-N_2O (N-denitrified)$^{-1}$: • 13% (20ºC) • 40% (10ºC) • 82% (5ºC)	Heterotrophic denitrification
Peng et al., 2015a	SBR	• Synthetic • N-NH_4=20 mg L^{-1}	• HRT=1 d • NLR=20 mg N-NH_4 L^{-1} d^{-1}	• N_2O EF increase with decreased DO & increased NO_2^- concentration • Nitrifier denitrification predominant in a wide range of DO & NO_2^- levels; NH_2OH oxidation dominant only at a high DO (e.g. 3.5 mg O_2 L^{-1}) with low NO_2^- (e.g.<10 mg N-NO_2^- L^{-1})	• Highest N_2O EFs at lowest DO (0.4 mg O_2 L^{-1}) & high NO_2^- (≥20 mg N-NO_2^- L^{-1}): 20-22% • Lowest N_2O EFs at highest DO (3.5 mg O_2 L^{-1}) & low NO_2^- (≤5 mg N-NO_2^- L^{-1}): 1.8-2%	Nitrifier denitrification
Peng et al., 2015b	SBR	• Synthetic • N-NH_4=20 mg L^{-1}	• HRT=1 d • NLR=20 mg N-NH_4 L^{-1} d^{-1}	• Linear relationship between N_2O production rate & IC concentration (IC range tested: 0-12 mmol C L^{-1}) • Alkalinity (mostly attributed to the IC) important for N_2O production in WWTPs	N_2O EF (specific N_2O production rate relative to specific AOR): increase from 2.5 to 5.5% with IC increase from 0 to 12 mmol C L^{-1}	AOB pathways
Poh et al., 2015	Gas tight, water-jacketed reactor	• Municipal (real) • N-NH_4=43 mg L^{-1}	Batch experiments	Temperature increase: • N_2O solubility decreased • more intensive stripping • N_2O (liquid) available for denitrification by	N_2O as primary electron acceptor: • 9.3 mg N-N_2O diffused to	Heterotrophic denitrification

				denitrifiers continuously decreasing	gas phase (25ºC) • 12.1 mg N-N_2O diffused to gas phase (35ºC)	
Song et al., 2015	Anoxic-Aerobic AS system	• Synthetic • Average N-NH_4=62 mg L^{-1}	• HRT=1 d • NLR=62 mg N-NH_4 L^{-1} d^{-1}	• Acetate-fed biomass: more abundant in bacteria capable of reducing N_2O	N_2O emission: • 2.3% of influent N (C-source: methanol) • 1.3% of influent N (C-source: acetate)	Heterotrophic denitrification
Zhang et al., 2016	SBR	• Synthetic (N-rich) • N-NH_4=200 mg L^{-1}	• HRT=0.7 d • NLR=286 mg N-NH_4 L^{-1} d^{-1}	Mannitol (instead of sodium acetate) as C-source: • N_2O emission reduced by 41% • NO_2^- accumulation ratio 20% lower	N_2O conversion rate (percentage of TN- removed converted to N_2O): • 21% (mannitol as C-source) • 41% (acetate as C-source)	Heterotrophic denitrification
Zhang et al., 2018	Expanded granular sludge bed anammox reactor	• Synthetic • N-NH_4=100 mg L^{-1}	• HRT=0.1 d • NLR=1,000 mg N-NH_4 L^{-1} d^{-1}	• High influent IC favoured the N_2O release from the anammox reactor • Essential to operate the reactor with an IC concentration enhancing the anammox process under an acceptable N_2O emission	Average N_2O emission: • 0.6% (IC=20 mg C L^{-1}) • 0.4% (IC=55 mg C L^{-1}) • 1% (IC=130 C mg L^{-1}) • 0.2% (IC=180 mg C L^{-1})	Denitrification inside the anammox granules

				• This study: optimal IC concentrations in the range of 55-130 mg C L^{-1}		
PILOT-SCALE						
Reference	**Configuration**	**Wastewater type/Operating characteristics**	**HRT/NLR**	**Main findings**	**N_2O production/EF**	**Hotspot**
Gabarro et al., 2014	Partial nitritation SBR	• Industrial (real: raw landfill leachate) • N-NH_4=2,000-2,300 mg L^{-1}	• HRT=0.5 d • NLR=4,000-4,600 mg N-NH_4 L^{-1} d^{-1}	• N_2O production: anoxic (60%) & aerobic (40%) • NO_2^- denitrification advancing faster than N_2O denitrification; high N_2O accumulation	N_2O production: 3.6% of influent TN	Heterotrophic denitrification
Pijuan et al., 2014	Continuous granular airlift nitritation reactor switched to SBR towards the end of study	• Sludge reject water produced in situ during the dewatering process of the anaerobic digester sludge from municipal WWTP • N-NH_4=726±50 mg L^{-1}	• HRT=0.5 d • NLR=1,452 mg N-NH_4 L^{-1} d^{-1}	• DO increase from 1 to 4.5 mg O_2 L^{-1}: N_2O emission decreased from 6% to 2.2% of N-oxidised • Higher DO: N_2O emission remained constant at 2.2% of N-oxidised • Two different mechanisms behind N_2O production; one DO-dependent & one not	N_2O emission: • 2.2% of oxidised N (airlift operation under DO>4.5 mg O_2 L^{-1}) • 19.3±7.5% of oxidised N (when shifting to SBR operation at DO>5 mg O_2 L^{-1})	• DO-dependent: nitrifier denitrification • non-DO-dependent: possibly chemical N_2O production
Frison et al., 2015	SBR	• Anaerobic supernatant produced from the co-digestion of the organic fraction of municipal	Acetic acid as C-source: • HRT=0.8 d • NLR=699 mg N-NH_4 L^{-1} d^{-1} Fermentation liquid as C-source: • HRT=0.5 d	N_2O emission decreased by: • maintaining the DO≥1.5 mg O_2 L^{-1} during the nitritation stage • applying an NLR respecting the system's N-removal capacity	N_2O emission: • 0.2% of influent N (SBR with DO=1.5 mg O_2 L^{-1}, vNLR=0.8 kg N m^{-3}, acetic	Nitrifier denitrification

		solid waste & waste AS • N-NH_4=559±75 mg L^{-1}	• NLR=1,118 mg N-NH_4 L^{-1} d^{-1}	• applying the aerobic/anoxic sequence	acid as C-source) • 1.5% of influent N (SBR with DO=1 mg O_2 L^{-1}, vNLR=1.1 kg N m^{-3}, fermentation liquid as C-source)	
Li et al., 2015	SBR	• Domestic (real) • Average N-NH_4=64 mg L^{-1}	• HRT=0.6 d • NLR=107 mg N-NH_4 L^{-1} d^{-1}	• AOR increase with pH & DO increase	N_2O accumulation ratio: • 29% (pH=6 & DO=1 mg O_2 L^{-1}) • 5% (pH=8.5 & DO=1 mg O_2 L^{-1}) • 12% (pH=6 & DO=3 mg O_2 L^{-1}) • 3% (pH=8.5 & DO=3 mg O_2 L^{-1})	Nitrifier denitrification
Zheng et al., 2015	OD	• Synthetic • N-NH_4=50 mg L^{-1}	• HRT=0.6 d • NLR=83 mg N-NH_4 L^{-1} d^{-1}	• High abundance of denitrifying bacteria & NOB inhibiting N_2O production • System shocks (e.g. N-overload, aeration failure) significantly increasing N_2O emission	N_2O emission: 0.03% of influent N	Nitrifier denitrification

Mannina et al., 2018	Integrated Fixed Film AS (IFAS) Membrane Bioreactor	• Municipal mixed with synthetic • N-NH_4=90 mg L^{-1} (phase I); 79 mg L^{-1} (phase II); 115 mg L^{-1} (phase III)	• HRT=21 d • NLR=4.3 mg N-NH_4 L^{-1} d^{-1} (phase I); 3.8 mg N-NH_4 L^{-1} d^{-1} (phase II); 5.5 mg N-NH_4 L^{-1} d^{-1} (phase III)	• Biofilms helpful in decreasing the N_2O emissions especially under stress conditions (e.g. low influent COD:N) • N_2O emissions mainly because of heterotrophic denitrification happening under low COD:N combined with a slightly increased DO	Total average N_2O emission: • 0.5% of influent N with biofilm (IFAS system) • 3.5% of influent N system operated without biofilm	Heterotrophic denitrification
FULL-SCALE						
Reference	**Configuration**	**Wastewater type/Operating characteristics**	**HRT/NLR**	**Main findings**	**N_2O production/EF**	**Hotspot**
Kampschreur et al., 2008	1 nitritation & 1 anammox reactor	• Sludge reject water (real: supernatant from centrifuged digested sludge from municipal WWTP) • TKN=1265±41 mg L^{-1}	• HRT=2.5 d • NLR=506 mg TKN L^{-1} d^{-1}	• Low DO or high NO_2^-: most likely causes of high N_2O emission by AOB • N_2O emission in the reject water treatment: same range as for the mainstream of AS processes	N_2O emission: • 1.7% of influent N (nitritation reactor) • 0.6% of influent N (anammox reactor)	• Nitritation reactor: nitrifier denitrification • Anammox reactor: both AOB pathways
De Mello et al., 2013	AS WWTP in Brazil	• Municipal (real) • N-NH_4=28±7 mg L^{-1}	• HRT=0.2 d • NLR=140 mg N-NH_4 L^{-1} d^{-1}	• N_2O production & emission during both aerated & non-aerated phases; emission higher during aeration (stripping)	N_2O emission from the aeration tank: 0.1% of influent TN	Nitrifier denitrification
Sun et al., 2014	AO process, an SBR & an OD	• Domestic (real) • TN=50-70 mg L^{-1}	• HRT=0.5 d • NLR=100-140 mg TN L^{-1} d^{-1}	• OD: optimal process for N_2O reduction • N_2O mitigation: DO control during nitrification	N_2O emission: • 1.4% of influent N (AO)	Heterotrophic denitrification after NO_2^- accumulation

		• N-NH_4=40-60 mg L^{-1}		& denitrification, high utilization rate of organic C during denitrification	• 2.7% of influent N (SBR) • 0.3% of influent N (OD)	during nitrification
Tumendelger et al., 2014	AS WWTP in Japan	• Municipal (real) • N-NH4=27, 29 & 35 mg L^{-1} at DO of 2.5, 2 & 1.5 mg O_2 L^{-1}, respectively	• HRT=0.5 d • NLR=54 mg N-NH_4 L^{-1} d^{-1} (N-NH_4=27 mg L^{-1}), 58 mg N-NH_4 L^{-1} d^{-1} (N-NH_4=29 mg L^{-1}), 70 mg N-NH_4 L^{-1} d^{-1} (N-NH_4=35 mg L^{-1})	• High aeration: NH_2OH oxidation pathway • Lower aeration: N_2O mainly produced through nitrifier denitrification; EF decreased	N_2O emission: • High aeration (DO=2.5-3 mg O_2 L^{-1}): 0.1% of influent N-NH_4 • Lower aeration (DO=1.5-2 mg O_2 L^{-1}): 0.03% of influent N-NH_4	• DO=2.5-3 mg O_2 L^{-1}: NH_2OH oxidation • DO=1.5-2 mg O_2 L^{-1}: Nitrifier denitrification
Castro-Barros et al., 2015	Partial nitritation-anammox granular sludge reactor	• Industrial (real: potato processing plant wastewater & sludge digestion reject water) • N-NH_4=340 mg L^{-1}	• HRT=0.2 d • NLR=1,700 mg N-NH_4 L^{-1} d^{-1}	• Intense aeration: higher N_2O emission rate due to larger N_2O formation rate & stripping • Transition from low to high aeration: N_2O emission rate negatively affected	Overall/average N_2O emission: 2% of influent N	NH_2OH oxidation pathway
Rodriguez-Caballero et al., 2015	SBR	• Municipal (real) • TN=69±5 mg L^{-1} • N-NH_4=39±2 mg L^{-1}	• HRT=1.5 d • NLR=46 mg TN L^{-1} d^{-1}	• N_2O emissions from the SBR accounted for the 60% of the WWTP C-footprint • Implementation of intermittent aeration with short oxic & anoxic phases: N_2O emissions	N_2O emission: 7% of influent N-NH_4	AOB pathways

				effectively minimized, desired effluent quality, electricity consumption unaffected		
Pan et al., 2016	Two-step plug-flow WWTP	• Municipal (real) • TKN=64±7 mg L^{-1} • N-NH_4=47±4 mg L^{-1}	• HRT=0.5 d • NLR=128 mg RKN L^{-1} d^{-1}	• Lower MLVSS in the 2nd step under the applied sludge return: higher biomass specific AOR leading to increased N_2O emissions	N_2O emission: • Overall plant: 1.9%±0.3% • 1st step: 0.7%±0.1% • 2nd step: 3.5%±0.5%	• 1st step: emissions mostly in aerobic zones (nitrification) • 2nd step: stripping (beginning of aerobic zones) of N_2O accumulated in anoxic zones (denitrification)

3.1 NLR

This section explores the effect that the NLR is likely to have on the N_2O production. For example, Quan et al. (2012) implemented three lab-scale aerobic granular SBRs to treat a mixture of municipal wastewater and liquid pig manure digestate. The N_2O emission was monitored in three ten-day operational periods. The applied NLRs were 448.5, 321.2 and 224.2 mg N L^{-1} d^{-1}, and the respective COD:N ratios were 1:0.22, 1:0.15 and 1:0.11 for each of the three operating modes. The corresponding maximum N_2O EFs were 8%, 7% and 4%. It was hypothesised that heterotrophic denitrification was aided by decreasing the NLR (or, equivalently, by increasing the COD:N). Hence, the facilitated heterotrophic denitrification process functioned as a mechanism of N_2O consumption. In the study by Xie et al. (2012), a lab-scale SBR was monitored in terms of N_2O emissions (0.4% of the total NH_4^+ oxidation). Nitrifier denitrification was considered as the responsible N_2O production pathway under the concurrence of the following conditions: high NLR (2,000 mg N L^{-1} d^{-1}), low DO (DO<0.5 mg O_2 L^{-1}) and a bacterial population enriched in AOB. This environment was regarded as favourable to nitritation and subsequent NO_2^- accumulation. Moreover, Frison et al. (2015) investigated the performance of a pilot-scale nitritation-denitritation SBR receiving as influent the reject water produced from the anaerobic co-digestion of sewage sludge and the organic fraction of municipal solid waste. Two different NLRs were applied; the first was 35% higher than the system's N-removal potential (2,077 mg N L^{-1} d^{-1}), whereas the second was respecting the system's treating capacity (1,080 mg N L^{-1} d^{-1}). The respective N_2O EFs were 1.5% and 0.2%. It was observed that operation under an NLR close to the system's N-removal capacity resulted in less NH_4^+ and NO_2^- accumulation. Thus, lower

N_2O production owing to nitrifier denitrification was expected. Furthermore, Zheng et al. (2015) explored the impact of enriching the influent NH_4^+ content (i.e. by applying a concentration five times higher) within a pilot-scale oxidation ditch (OD). During normal operation, the N_2O EF was estimated as low as 0.03%. The sudden change in the NH_4^+ load triggered a rapid emission increase by 39.3% (monitoring zone with DO stabilised at 0.8 mg O_2 L^{-1} after the shock) and by 113.1% (monitoring zone with DO stabilised at 0.2 mg O_2 L^{-1} after the shock). In both monitoring zones, DO decrease and NO_2^- accumulation were observed. Therefore, the responsible pathway for N_2O production was nitrifier denitrification, with its contribution depending on the DO of each zone.

All in all, the NLR can possibly influence the undisturbed completion of the nitrification and denitrification processes. The application of an NLR surpassing the system's N-removal capacity coinciding with conditions stimulating the N_2O generation pathways (e.g. low DO) is likely to increase the N_2O emission.

3.2 Reactor configuration and operating conditions

Here, the potential influence of the reactor configuration and the operating conditions was explored in terms of expected N_2O emissions.

3.2.1 Suspended-growth systems

First, Sun et al. (2014) compared three different full-scale wastewater treatment processes including an anoxic-oxic (AO) process, an SBR and an OD with respect to the N_2O generation. Generally, maintaining a proper DO during nitrification along with optimised utilization of the available C-source during denitrification were proposed to

ensure the completion of nitrification-denitrification and, thus, minimal NO_2^- and N_2O accumulation. More importantly, the OD presented a significantly lower EF (0.3% of influent N), compared to the SBR (2.7% of influent N) and the AO (1.4% of influent N). The analysis of the bacterial populations growing within the OD showed the richness of NOB and denitrifiers. The NOB enhanced the completion of nitrification and the avoidance of short-cut nitrification. The latter led to limited NO_2^- accumulation, hence decreasing the possibility of N_2O production through nitrifier denitrification. Moreover, the important denitrifying bacterial population fostered the N_2O consumption via heterotrophic denitrification. The pilot-scale experimental set-up implemented by Pijuan et al. (2014) was a continuous granular airlift nitritation reactor operated at high DO (>4.5 mg O_2 L^{-1}) treating reject water. It was shifted to an SBR mode towards the end of the study to reveal the potential impact on the N_2O emissions. Indeed, the EF varied significantly: only 2.2% of the oxidised N (airlift operation), in contrast to 19.3±7.5% of the oxidised N (SBR operation). This divergence was attributed to the SBR cycle configuration that included a short feeding phase (only 6 min). High N_2O emission occurred at the beginning of the cycle coinciding with phases with important NH_4^+ concentration. Therefore, NH_2OH oxidation was considered as the most likely N_2O production route.

In addition, the respective contribution of the AOB N_2O production pathways was found to depend upon the DO in the full-scale AS system monitored by Tumendelger et al. (2014). The NH_2OH oxidation pathway was predominant under high-DO conditions (2.5-3 mg O_2 L^{-1}) resulting in an N_2O EF equal to 0.1% of the influent NH_4^+. Lower DOs (1.5-2 mg O_2 L^{-1}) favoured the activation of the nitrifier denitrification pathway leading to a lower N_2O EF (0.03% of the influent NH_4^+). Furthermore, de Mello et al. (2013) noted

that N_2O production was possible during all phases (i.e. aerobic and anaerobic) in a full-scale AS WWTP. Nevertheless, the EF was higher during the aerated periods (0.1% of influent TN); the N_2O produced via nitrifier denitrification was stripped and emitted to the atmosphere. Lastly, Pan et al. (2016) focused on the N_2O emission patterns of a full-scale two-step plug-flow reactor treating municipal wastewater. A significant difference was noted in the EF between the first and the second step: 0.7%±0.1% (first step) and 3.5%±0.5% (second step). The second step was receiving as influent the wastewater that had already undergone the treatment of the first step; this caused dilution along with 40% lower mixed liquor volatile suspended solids (MLVSS) concentration. The higher specific AOR attained in this stage triggered the activation of both AOB pathways.

3.2.2 Attached-growth systems

Within a lab-scale fluidized bed bioreactor treating synthetic wastewater, Eldyasti et al. (2014) saw that increasing the biofilm thickness from 230 μm to 680 μm was accompanied by a decline in the N_2O EF from 1.6% of the influent TN to 0.5% of the influent TN. Similarly, the N_2O emission was found to differ as follows in the pilot-scale system operated by Mannina et al. (2018) for the treatment of municipal wastewater: 0.5% of the influent N with the system operated as an integrated fixed film AS membrane bioreactor, but 3.5% of the influent N with the system functioning without biofilm. The biofilm addition and expansion facilitated the retention of the denitrifying bacteria, thus enhancing the N_2O consumption through denitrification.

Inside the granular systems, both nitrifying and denitrifying bacteria can grow, hence rendering simultaneous nitrification-denitrification (SND) feasible (Quan et al., 2012). For example, in the lab-scale study by Quan et al. (2012) three aerobic granular

SBRs were set up for the co-treatment of municipal wastewater and liquid pig manure digestate at three aeration rates (0.2, 0.6 and 1 L air min^{-1}) and three COD:N ratios (1:0.22, 1:0.15 and 1:0.11). With NO_2^- as the only N-source, the specific N_2O generation rates via denitrification were 1.7, 1.6 and 1.3 mg N_2O g^{-1} SS min^{-1} at the aeration rates of 0.2, 0.6 and 1 L air min^{-1}, respectively, which were 41%, 45%, 40% higher than the respective ones with NO_3^- as the only N-source. The results indicated that: 1) the spatial structure of the granules created conditions favourable to incomplete denitrification which resulted in N_2O production, 2) the N_2O generation through the aerobic granules was mostly affected by NO_2^- accumulation, 3) the NO_3^- reduction rates were lower than those with NO_2^-, explaining the lower N_2O production with NO_3^- as the only N-source.

The anoxic or, even, micro-aerobic conditions needed for the denitrification process are never continually present within the aerobic granules. Certain configurations such as the OD or the biofilm bioreactors can possibly strengthen the denitrifying population activity and the resulting N_2O consumption through denitrification. Instead of paying attention to the bioreactor configuration though, optimizing the operating parameters (e.g. DO, aeration rate, phase duration, etc.) is more essential. For instance, the DO factor gravely influences nitrification and the related (AOB) pathways. As a further matter, the aeration strategy affects the N_2O stripping and the overall C-footprint of a WWTP. In this concept, the N_2O mitigation is mainly sought in the optimization of the operating parameters.

3.3 Biological N-removal processes

This section examines how the biological N-removal process applied each time along with certain operating conditions (e.g. DO levels, NO_2^- concentration, etc.) influences the N_2O production. The following N-removal alternatives are presented: nitrification-denitrification, SND, nitritation-denitritation and partial nitritation-anammox.

3.3.1 Nitrification-denitrification

Nitrification is a possible N_2O hotspot (e.g. works by Shen et al. (2013), Sun et al. (2014) and Li et al. (2015)). To run the nitrification undisturbedly and avoid the N_2O accumulation, operation under a proper DO is required. Moreover, conditions such as high DO, low temperatures, important NO_2^- concentrations, etc. hinder the completion of denitrification, thus raising the possibility of N_2O being produced via this pathway. On the contrary, prolonging an anoxic stage is likely to enhance the N_2O consumption via denitrification; in this case, the denitrifiers are offered more time to exhaust the available C-source and perform full denitrification. Completing both nitrification and denitrification is essential to avoid the intermediate N_2O production and emission (Gabarro et al., 2014; Sun et al., 2014; Adouani et al., 2015).

Between the two AOB pathways, nitrifier denitrification has a more important contribution in cases of low DOs, high NO_2^- concentrations, influent N-load above the system's treating capacity (Kampschreur et al., 2008; Wang et al., 2014a; Peng et al., 2015a, 2015b; Zheng et al., 2015). It shall be noted, though, that unveiling the relative contribution between the two AOB pathways (i.e. NH_2OH oxidation and nitrifier

denitrification) is not necessarily straightforward during an experiment (Law et al., 2011; Rodriguez-Caballero et al., 2015).

For example, Peng et al. (2015a) investigated the impact of changing DO and NO_2^- levels (with the DO and NO_2^- being changed independently) on an enriched nitrifying population in a lab-scale SBR treating synthetic wastewater. Nitrifier denitrification was the most contributive AOB pathway for a broad range of DO (e.g. 0.4-2.5 mg O_2 L^{-1}) and NO_2^- (e.g. 10-50 mg N-NO_2^- L^{-1}) values. NH_2OH oxidation was the N_2O hotspot for high DO (e.g. 3.5 mg O_2 L^{-1}) and low NO_2^- concentration (e.g.<10 mg N-NO_2^- L^{-1}). A lab-scale SBR treating municipal wastewater was operated under an anaerobic-aerobic-anoxic cycle configuration by Chen et al. (2014). N_2O generation was mainly noted during aeration due to nitrifier denitrification. After cancelling the anaerobic phase and extending the idle phase (i.e. the phase between the removal of the treated effluent and the beginning of the next cycle), N_2O emission dropped by 42%. N was removed mostly through the heterotrophic denitrification process that served as a mechanism of N_2O consumption. Rodriguez-Caballero et al. (2015) tested different aeration regimes in a full-scale SBR treating municipal wastewater. It was confirmed that a cycle configuration with a sequence of twenty/thirty-minute aerobic phases followed by short non-aerated periods was beneficial to the decrease of N_2O production. N_2O along with its precursors (i.e. NO and NO_2^-) were used up for the purposes of the full denitrification happening during the non-aerated stages.

Finally, it shall be mentioned that denitrification is also possible under micro-aerobic conditions. In environments such as the AS where aerobic and micro-aerobic conditions can concur, SND is likely (Krul and Veemingen, 1977; Ahn et al., 2010). Hence,

low DO along with a certain NH_4^+ and NO_2^- concentration are expected in this case. Especially in full-scale WWTPs though, N_2O production can follow any of the three microbial pathways (i.e. NH_2OH pathway, nitrifier denitrification and heterotrophic denitrification) during the BNR (Kim et al., 2010; Wunderlin et al., 2012; Lochmatter et al., 2013).

3.3.2 Nitritation-denitritation

Short-cut nitrification (nitritation) is an advanced N-removal process during which the AOB oxidise the NH_4^+ to NO_2^-. Afterwards, the produced NO_2^- undergoes denitritation, always by omitting the NO_3^- formation stage. When compared to conventional nitrification-denitrification, nitritation-denitritation is considered advantageous due to 25% lower oxygen demand in the aerobic stage, 40% lower COD demand in the anoxic phases, as well as limited sludge production along with a higher denitrification rate (1.5-2 times quicker) (Gustavsson, 2010). Therefore, short-cut nitrification can be ideal for wastewaters with low COD:N. Moreover, it can be performed with less energy and C-source requirements inside smaller anoxic tanks (Turk and Mavinic 1987). Hence, the low-DO conditions usually applied in such systems promote the AOB growth to the detriment of the NOB one. Besides, the short-cut nitrification schemes present high NO_2^- availability due to the NO_2^- generated during nitritation. Consequently, they are prone to high N_2O emissions, mainly through nitrifier denitrification.

A lab-scale bioreactor receiving an influent containing 500 mg N-NH_4^+ L^{-1} (i.e. high-strength wastewater) was operated in nitrification and nitritation modes by Ahn et al. (2011). The N_2O emission was more important during nitritation; the relatively low DO (1.1±0.4 mg O_2 L^{-1}) and affluent NO_2^- (91±6% NH_4^+ conversion to NO_2^-) facilitated the

enzymatic NirK and Nor activity, hence resulting in N_2O production through nitrifier denitrification. A lab-scale nitritation system treating anaerobic sludge digestion liquor was implemented by Wang et al. (2014b). It was observed that the NO_2^- produced during nitritation was later reduced to N_2O via heterotrophic denitrification. After regulating the DO around 1 mg O_2 L^{-1}, the NO_2^- reduction to N_2O was minimized. Pijuan et al. (2014) worked on a pilot-scale continuous granular airlift nitritation reactor treating reject water. The N_2O emission dropped from 6% to 2.2% of the oxidised N following the DO increase from 1 to 4.5 mg O_2 L^{-1}. With the further DO increase, the emissions remained stable at 2.2%, suggesting two different mechanisms contributing to the N_2O production: one influenced by the DO fluctuations (e.g. nitrifier denitrification) and one not (probably chemical). Desloover et al. (2012) have emphasized the importance of the NO_2^- accumulated after nitritation. It determines the activation of the nitrifier denitrification pathway under a low DO. Frison et al. (2015) tested the efficiency of nitritation-denitritation during the pilot-scale treatment of reject water produced from the anaerobic co-digestion of sewage sludge and the organic fraction of municipal solid waste. In line with Desloover et al. (2012), Frison et al. (2015) suggested that keeping the DO controlled at 1.5 mg O_2 L^{-1} or above during nitritation was effective in avoiding the NO_2^- accumulation and the related N_2O production.

3.3.3 Partial nitritation-anammox

The partial nitritation-anammox process begins with the AOB partially oxidizing NH_4^+ to NO_2^-. Afterwards, the anammox bacteria oxidise the remaining NH_4^+ using NO_2^- as electron acceptor. However, the growth of the annamox bacteria is highly unstable and dependent upon several parameters such as DO, temperature, free NH_3 and NO_3^-

concentration (Malamis et al., 2015; Ibrahim et al., 2015; Laureni et al., 2016). The first step of the process can constitute an N_2O hotspot since it involves the production of NO_2^- (usually under low DO). Even though it requires limited aeration to take place, the possibility of N_2O production (through nitrifier denitrification) can finally lead to a high overall C-footprint. On the other hand, the second (anammox) stage is not regarded as major N_2O hotspot. Generally, partial nitritation-anammox is destined to consume NO_2^-; a factor involved in the N_2O production pathways. Consequently, partial nitritation-anammox can play an active role in the N_2O mitigation strategies.

Kampschreur et al. (2008) noted a lower N_2O emission in the anammox compartment (0.6% of the influent N) of a full-scale two-stage partial nitritation-anammox system treating reject water. The EF in the nitritation reactor was 1.7% of the influent N. It was assumed that AOB from the nitritation section probably entered the anammox reactor. Under the NO_2^- presence and the low DO, the AOB probably activated the nitrifier denitrification N_2O production pathway. Castro-Barros et al. (2015) explored whether a partial nitritation-anammox full-scale plant can successfully treat sludge digestion reject water. NH_4^+ up to 0.1 kg N-NH_4^+ m^{-3} was accumulated during the non-aerated periods. In the subsequent aerated periods the accumulated NH_4^+ was subjected to oxidation. More importantly, the highest N_2O formation rate was achieved (0.06 kg N-N_2O m^{-3} d^{-1}). The aerobic conditions along with the NH_4^+ abundance stimulated the NH_2OH oxidation pathway. Furthermore, the anammox process was monitored in a lab-scale reactor treating synthetic wastewater by Zheng et al. (2018). The average N_2O emission decreased from 0.6% to 0.4% with the inorganic carbon (IC) provision increase from 20 to 55 mg C L^{-1}. The authors mentioned that a certain amount of denitrifiers was included

in the anammox population. It was suggested that the presence of these denitrifying bacteria enhanced the completion of heterotrophic denitrification and the subsequent consumption of N_2O as intermediate product of the process.

Although the advanced N-removal alternatives (e.g. nitritation-denitritation or partial nitritation-anammox) are applied to achieve operation under low energy requirements, N_2O production is always possible and often graver than in the cases of conventional N-removal. To avoid a final overall C-footprint higher than in the event of conventional treatment, the advanced N-removal schemes require process optimization.

3.4 C-source

During the biological N-removal in WWTPs, the C-source can differ in terms of composition and availability. Here, the influence of this factor on the N_2O generation is examined.

Zhu and Chen (2011) tested first sludge fermentation liquid and, secondly, acetic acid as C-sources for the operation of an anaerobic-aerobic lab-scale process for municipal wastewater treatment; the emissions dropped by 68.7% when sludge fermentation liquid was used. It was indicated that the existence of copper ions (Cu^{2+}) and propionic acid within the sludge fermentation liquid caused a decrease in the activity ratio of the following denitrifying enzymes: NOR:N_2OR (Fig. 1). Hence, the N_2O production via heterotrophic denitrification declined. In a similar study, Hu et al. (2013) tested three different C-sources (i.e. sodium acetate, glucose and soluble starch) to see how the N_2O production was affected in a lab-scale anoxic/oxic SBR fed with synthetic

wastewater. The N_2O conversion ratio (calculated as the percent of the TN-removed converted to N_2O) was 9% for sodium acetate, 5% for glucose and 3% for soluble starch. According to the microbial analysis, the denitrifying population diversity was poor in the case of sodium acetate. Therefore, the completion of heterotrophic denitrification was hindered, thus leading to N_2O production as an intermediate product. Furthermore, Song et al. (2015) compared methanol and acetate as C-sources for a lab-scale anoxic/aerobic AS system treating synthetic wastewater. The N_2O EF was 2.3% of the influent N for the methanol case, but significantly lower (1.3% of the influent N) with acetate as C-source. The microbial analysis revealed that acetate contained a higher population of denitrifiers reducing N_2O to N_2. Zhang et al. (2016) assessed mannitol and sodium acetate as potential C-sources for a lab-scale partial nitrification SBR implemented for the treatment of synthetic N-rich wastewater. The following N_2O conversion rates were reported: 21% for mannitol and 41% for sodium acetate. The bacterial analysis indicated that the N_2OR enzyme activity (Fig. 1) was less hindered by the NO_2^- presence in the partial nitrification system with mannitol used as C-source. Consequently, the completion of the heterotrophic denitrification process was facilitated in the mannitol case.

Peng et al. (2015b) underlined that the alkalinity (majorly related to the IC presence) is an important factor to consider while working on the mitigation of N_2O emissions in a lab-scale SBR system fed with synthetic wastewater. In cases of low IC availability, the *Nitrosomonas europaea* bacteria produce NO from NO_2^- with carbonic anhydrase (enzyme) as catalyst. Then, the reduction of NO to N_2O follows catalysed by NOR (Fig. 1) (Jahnke et al., 1984; Peng et al., 2015b). However, Peng et al. (2015b) reported a linear relationship between the IC concentration and the N_2O production in

their study; this was translated into decreased N_2O production under poor IC provision. The authors explained their results through the composition of the AOB population that was found poor in *Nitrosomonas europaea*.

Lastly, it shall be noted that in cases of low external C-source availability, internally stored compounds (e.g. polyhydroxyalkanoates (PHAs)) can be alternatively utilised. The latter is likely to increase the N_2O production during denitrification (Schalk-Otte et al., 2000). In this concept, Zhou et al. (2012) explored the influence of different COD:N ratios and C-sources (external: sodium acetate, internal: PHAs) on the N_2O consumption during denitrification in a lab-scale SBR operated to treat synthetic wastewater. With PHA as (internal) C-source, the COD:N increase from 0.6 to 1.3 improved the N_2O reduction rate from 0.04 to 0.05 mg N-N_2O min^{-1} g $biomass^{-1}$. While using sodium acetate as (external) C-source, N_2O was barely reduced (0.003 mg N-N_2O-N min^{-1} g $biomass^{-1}$) at the lowest COD:N (i.e. 0.6). The reduction rate was higher (0.02 mg N-N_2O min^{-1} g $biomass^{-1}$) for the higher COD:N (i.e. 1.3). At the highest COD:N applied (i.e. 1.9), similar N_2O reduction rates (0.05 mg N-N_2O min^{-1} g $biomass^{-1}$) were noted for both C-sources. According to the general observations of the study, the N_2O reduction during denitrification was enhanced at higher COD:N ratios; though this was slightly more noticeable under the use of external C-source.

All things considered, the C-source composition and availability is indeed an essential parameter to consider for the N_2O emission mitigation. For instance, there are certain C-source types that are more advantageous to the growth of denitrifiers. Moreover, it is important to ensure that the amount of the C-source is enough to consume

N_2O and run the heterotrophic denitrification process till the final step (N_2O reduction to N_2).

3.5 pH and temperature

The importance of pH and temperature on the N_2O production during the BNR in wastewater treatment is examined in this subsection. In a lab-scale partial nitritation SBR containing an enriched AOB population to treat sludge reject water under low-DO conditions (0.6±0.05 mg O_2 L^{-1}), Law et al. (2011) monitored the N_2O production with the pH ranging from 6 to 8.5. The minimum N_2O generation (0.2±0.01 mg N-N_2O h^{-1} g^{-1} VSS) was noted at 6<pH<7, and the maximum (0.5±0.04 mg N-N_2O h^{-1} g^{-1} VSS) at pH=8. Moreover, the AOR and the N_2O production rate were linearly correlated. The latter observation combined with the low DO of the study implied that the most possible N_2O production pathway was nitrifier denitrification. The pH effect was also studied by Li et al. (2015) for a pilot-scale municipal SBR performing nitrification. With the DO controlled at 3 mg O_2 L^{-1} and the pH increasing from 6 to 8.5, the maximum N_2O accumulation rate (0.3 mg N-N_2O g^{-1} MLSS L^{-1} h^{-1}) was reported for the lowest pH value (pH=6). On the other hand, the AOR increased with the pH increase; the maximum AOR (3.8 mg N-NH_4^+ g^{-1} MLSS L^{-1} h^{-1}) was observed at the maximum tested pH (pH=8.5). Differently from what was assumed by Law et al. (2011), Li et al. (2015) hypothesized that the electrons released with the AOR increase were principally used for the $O_2 \rightarrow H_2O$ reduction and secondarily for nitrifier denitrification. They underlined that it is probable to find no clear correlation between the AOR and the N_2O generation if the pH is majorly influential.

Adouani et al. (2015) studied the impact of temperature on the N_2O emissions during denitrification in a batch reactor fed with a synthetic solution containing acetate, NO_3^- and AS. Their results showed that the N_2O generation increased as the temperature decreased; the N_2O emissions rose from 13% to 40% and then to 82% of the total denitrified N at 20°C, 10°C and 5°C, respectively. The low temperatures decelerated all denitrification enzyme activities and, more importantly, the NO and N_2O reductase activities. Consequently, N_2O was produced through incomplete denitrification. Poh et al. (2015) conducted batch experiments on mixed liquor to see the effect of increasing temperature on the N_2O accumulation during denitrification. As soon as the temperature rose from 25°C to 35°C, the specific NO_3^-, NO_2^- and N_2O reduction rates showed an increase of 62% (5.8→9.4 mg N-NO_3^- g^{-1} VSS h^{-1}), 61% (4.9→7.9 mg N-NO_2^- g^{-1} VSS h^{-1}) and 41% (8→11.3 mg N-N_2O g^{-1} VSS h^{-1}), respectively. However, at 35°C, N_2O became less soluble in the mixed liquor, which meant that stripping was more intense. Considering that the N_2O gas is difficultly re-dissolved, the amount of dissolved N_2O available for the denitrification process was continuously decreasing as the experiment was proceeding. Thus, although higher temperatures are initially applied to enhance the denitrification kinetics, they are likely to generate more emissions.

With the view to mitigating the N_2O emissions, the pH can be maintained at ≥6 in order to enhance nitrification along with a high temperature (≥20°C) to boost the denitrifying enzymes' activity. However, an uncontrolled pH and temperature augmentation might produce an adverse result. For example, a pH increase above 7 can result in higher AOR and N_2O accumulation through the AOB pathways. Similarly, a

temperature increase over 25°C renders the N_2O produced during denitrification less soluble and facilitates its conversion to gas or, equivalently, its emission.

4. N_2O quantification and EF

As detailed in section 3, important N_2O emission can be noted during the N-removal processes in lab-, pilot- and full-scale WWTPs. However, the availability of standardized methods for the emission quantification is still limited. Hence, comparing the N_2O emissions amongst different WWTPs is a challenging process. It is essential to establish robust quantification methods and effective sampling strategies (Law et al., 2012a; Ye et al., 2014).

4.1 N_2O quantification

Here several N_2O quantification methods are described. In the case of fully-covered WWTPs, the N_2O emission can be calculated using the outflow gaseous N_2O concentration and the total gas flow rate. Nevertheless, most of the WWTPs are open schemes. In this case, the produced N_2O is measured by enclosing the emitted N_2O flux within a floating chamber (Law et al., 2012a; Marques et al., 2016). Afterwards, the grabbed N_2O samples are analysed either online (gas analysers) or offline (gas chromatography). Accurate measurements require humidity-free samples (Lim and Kim, 2014; Ye et al., 2014; Marques et al., 2014, 2016). The latter can be ensured by placing a filter at the inlet of the gas analysers as in the works by Law et al. (2011), Wang et al. (2014a) and Peng et al. (2015a, b).

Another quantification concept relies on the mass transfer from liquid to gas. Liquid N_2O can be produced during the biological N-removal in WWTPs and then turn into gas because of over-saturation or stripping (Marques et al., 2016). With Henry's coefficient for N_2O being equal to 0.024 M atm^{-1} (Kampschreur et al., 2009), N_2O is considered rather soluble in water and low in terms of stripping rate. The emission rate can be calculated by using the liquid N_2O concentration and the volumetric mass transfer coefficient (k_La). The latter combines the global transfer coefficient k_L and the interfacial area a (interphase transport between liquid and gas per unit of reactor volume). Considering that wastewater treatment occurs under conditions temporally and spatially variable, the k_La calculation is quite demanding. An additional issue is that the grab samples of liquid N_2O are taken with time intervals (Ye et al., 2014; Marques et al., 2016). For this reason, Mampaey et al. (2015) created a gas stripping tool measuring the liquid N_2O under aerated and non-aerated conditions on a minute time scale.

The importance of the sampling strategy was stressed by Daelman et al. (2013). They applied and compared different monitoring protocols on a 16-month N_2O emission dataset of a fully-covered full-scale municipal WWTP. The accurate estimation of the average annual N_2O emission demanded long-term, online/grab samples (including nightly and weekend sampling) to depict the seasonal trends. In addition, it was indicated that short-term high-frequency online sampling campaigns were required for the successful description of the diurnal dynamics.

Amongst the studies reviewed in Table 1, different quantification methods and sampling strategies were applied. De Mello et al. (2013) measured N_2O in a full-scale WWTP during all treatment phases (i.e. aerated and non-aerated) for 6 consecutive days.

During the aerated phases, air bubbles stripped from the liquid were captured using an upturned plastic funnel. Then, the bubbles (concentrated at the funnel headspace) were taken for further analysis. At the non-aerated stages, closed PVC chambers were used to measure the N_2O emission fluxes at the liquid-air interface. Samples were taken from the chambers using syringes. The authors continued measuring during the phase alternation throughout the whole campaign to cover possible temporal variations. Pijuan et al. (2014) and Rodriguez-Caballero et al. (2015) worked on a pilot- and full-scale SBR, respectively. Off-gas was continually collected from the reactor for 33 days corresponding to a total of 143 cycles. Especially for SBR set-ups, continuous N_2O sampling is needed to capture emission peaks and fluctuations. Furthermore, Tumendelger et al. (2014) took samples in 7 different locations along the whole length of the treatment line in full-scale WWTPs. Thus, the potential spatial variability was successfully portrayed. In this concept, Zheng et al. (2015) decided to sample in 14 different points belonging to 12 intensive sampling zones in a pilot-scale OD after ensuring steady-state operation. Finally, the importance of achieving steady state before staring the collection of N_2O measurements was also underlined in the lab-scale SBR study by Chen et al. (2014). All in all, the precise and successful description of N_2O dynamics requires continuous sampling covering multiple treatment locations during steady-state WWTP operation.

4.2 N_2O EF

During the biological N-removal in WWTPs, N_2O EFs are estimated as the amount of N_2O emitted relative to the influent N. According to the Intergovernmental Panel on Climate Change (IPCC) guideline of 2006, a single (standard) EF can be used in all cases

irrespective of the plant scale. Following this IPCC 2006 guideline, the older (standard) EF (i.e. 1% of the influent N-content) can now decrease and considered equal to 0.5% of the influent N-content. Although both factors are still used, it is debated whether they can accurately depict all cases of full-scale N_2O emission during wastewater treatment (Kampschreur et al., 2009; Law et al., 2012a).

Indeed, past works have shown that the N_2O emissions can importantly vary amongst different WWTPs. For example, Kampschreur et al. (2009) reported EFs (defined as the fraction of influent N emitted as N_2O) whose range varied upon the WWTP scale: 0-95% of the influent N for lab-scale schemes, 0-14.6% of the influent N for full-scale plants. The authors suggested that repeating the measurements in a more organized and carefully planned way was needed to produce more reliable and possibly less fluctuating results. Even among plants of the same scale, large differences can be noted. Law et al. (2012a) collected N_2O EF data within the range 0-25%; all information originated from full-scale WWTPs. This variability was attributed to the different operating conditions and configurations.

Moreover, the quantification method is another factor that can influence the final N_2O EF results (Law et al., 2012a; Lim and Kim, 2014). For example, Ahn et al. (2010) reported an average N_2O EF ranging daily from 0.01 to 1.8% (with respect to the influent Total Kjeldahl Nitrogen (TKN)) for twelve full-scale WWTPs in the U.S. applying different BNR and non-BNR processes (e.g. separate-stage BNR, step-feed non-BNR, OD, four-stage Bardenpho etc.); the observed difference in the EF was ascribed to the daily fluctuations of the influent N-load. For each process, online gas samples were taken both at the aerated and the non-aerated phases/compartments for a whole day. Rodriguez-

Caballero et al. (2014) also monitored the N_2O emission in a full-scale WWTP by taking online gaseous measurements during both the aerated and the non-aerated phases. The authors observed a diurnal decrease in the N_2O EF from 0.12 to 0.06% of the influent TKN because the nitrification process inside the bioreactor was instable. In both studies (i.e. Ahn et al., 2010; Rodriguez-Caballero et al., 2014), the successful description of the diurnal N_2O emission dynamics was achieved after executing continuous online sampling for a whole day.

Here it shall be underlined that there is no standardized way of calculating the N_2O production and emission amongst the studies reviewed in Table 1. The latter hinders the constructive comparison among these works. All things considered, the use of a single N_2O EF is potentially not representative of the N_2O emission for all WWTPs. As analysed in this section, the final EF results depend upon several factor such as the plant scale, the operating conditions and configurations, the possible temporal/spatial variations, the N_2O sampling protocol and quantification method. The precise calculation of the N_2O EF requires the development of tools able to continually and successfully capture both dissolved and gaseous N_2O dynamics at full scale.

5. Modelling the N_2O emissions during the BNR in WWTPs

The section is dedicated to the modelling of N_2O production and emission during the BNR in WWTPs. Several N_2O models have been suggested by extending the widely accepted activated sludge models (ASM), introduced by the International Water

Association (IWA) task group (Henze *et al.,* 1987, 2000). The IWA developed different ASM versions to describe different processes: organic matter oxidation and nitrification/denitrification (ASM1), biological phosphorus removal (ASM2 and ASM2d), internal storage and endogenous respiration (ASM3).

According to the initially proposed ASM versions, nitrification was modelled as one-step process without NO_2^- as an intermediate product. However, this fails to successfully describe events of system shocks and/or application of advanced BNR processes (e.g. nitritation/denitritation, completely autotrophic N-removal) (Gujer et al., 1999; Henze et al., 2000; Iacopozzi et al., 2007). Hence, ASM-type models have been developed with a two-step nitrification-denitrification structure (e.g. Iacopozzi et al., 2007; Guerrero et al., 2011; Ostace et al., 2011), thus allowing the estimation of the dissolved NO_2^- in the mixed liquor. As detailed in section 3.3, the NO_2^- dynamics is an essential factor to consider since NO_2^- is crucial for the N_2O production (e.g. via nitrifier denitrification). Nevertheless, these ASM extensions made no mention to the N_2O generation and emission.

It is essential to develop mathematical tools able to describe the N_2O production and emission with reference to every possible production pathway (e.g. AOB pathways, heterotrophic denitrification). The influence of the operational/process conditions is expected to be enlightened with the aid of such models, thus facilitating the design of effective mitigation strategies (Kampschreur et al., 2009; Law et al., 2012b; Ni and Yuan, 2015). A rough description of one-/multiple-pathway N_2O models is provided in the following sub-sections.

5.1 Nitrifier denitrification N_2O models

Nitrifier denitrification was the core of the model by Ni et al. (2011). They modelled nitrifier denitrification (with NO_2^- as the electron acceptor) occurring to produce NO and, finally, N_2O. According to their simulations, conditions of low DO (i.e. ≤1.5 mg O_2 L^{-1}) should be avoided since they were seen to inhibit nitrification and promote NO_2^- accumulation, subsequently leading to N_2O production through nitrifier denitrification pathway. Mampaey et al. (2013) chose to model nitrifier denitrification and NH_4^+ oxidation as concurring processes. The electrons released during the oxidation of NH_4^+ to NO_2^- were considered as being used for the AOB reduction of NO_2^- to NO and, finally, to N_2O. The application of the proposed model on a continuously aerated partial nitrification (SHARON) process indicated that the maximum N_2O emissions were noted for low DOs (i.e. DO≤1.5 mg O_2 L^{-1}). After running the process under intermittent aeration with aerobic and anoxic phases of equal duration, the same model was applied. Despite the varying DO profile this time, the maximum N_2O production was again noted during aeration and at low DO (i.e. DO≤1.5 mg O_2 L^{-1}). In both models, the DO factor was considered as having a pivotal role in N_2O generation through nitrifier denitrification. However, Ni et al. (2011) modelled NH_2OH as a model variable part of which was directly oxidised to N_2O, whereas Mampaey et al. (2013) described the NH_4^+ oxidation to NO_2^- as direct without the NH_2OH intermediate. Guo and Vanrolleghem (2014) developed a nitrifier denitrification model based on the assumptions by Mampaey et al. (2013) and Hiatt and Grady (2008a). A Haldane function was added to describe the DO influence on nitrifier denitrification and, thus, predict the NO_2^- accumulation at low DOs. Furthermore, different growth rates were assigned to each of the nitrifier denitrification steps (1st: $NO_2^- \rightarrow NO$; 2nd:

$NO \rightarrow N_2O$) to depict the varying AOB growth rate. They observed that the application of higher temperatures improved the nitrifier denitrification rates and, subsequently, the N_2O production though this pathway.

5.2 NH_2OH oxidation N_2O models

Law et al. (2012b) and Ni et al. (2013) focused on the other AOB pathway, the NH_2OH oxidation. First, Law et al. (2012b) investigated the correlation between the AOR and N_2O production rate for an enriched AOB culture performing NH_4^+ oxidation to NO_2^- in sludge reject water. The AOR increase was accompanied by an exponential increase to the N_2O production rate. The authors suggested that the predominant N_2O production pathway in this case was the NH_2OH/NOH; N_2O production is possible during the decomposition of the unstable nitrosyl radical (NOH) that is an intermediate of the NH_2OH oxidation. Nitrifier denitrification was possibly less contributive under the simulated experimental conditions: high NH_4^+ concentration (500 mg N-NH_4^+ L^{-1}) along with low DO levels (0.5-0.8 mg O_2 L^{-1}). Full-scale modelling was conducted by Ni et al. (2013) for an OD and an SBR plant based on the following series of oxidations: $NH_4^+ \rightarrow NH_2OH \rightarrow NO \rightarrow NO_2^-$. N_2O production was considered possible during the AOB reduction of NO with NH_2OH as the electron donor. The possibility for DO inhibition on the NO reduction was ignored. For both plant types, the maxima in the NH_4^+ concentrations coincided with those in the N_2O emissions. In the OD, the NH_4^+ concentration was seen to decrease without a simultaneous NO_2^- increase in the aerated zones. During the aerobic phases of the SBR operation, important amounts of NH_4^+ were accumulated leading to a high specific AOR and, finally, to an increased production of

intermediates such as NH_2OH. Therefore, NH_2OH oxidation was considered the responsible pathway for both simulated plant types.

5.3 Modelling both AOB N_2O production pathways

With a view to describing the electron transfer processes of the AOB metabolism, Ni et al. (2014) developed a model integrating the AOB oxidative ($NH_3 \rightarrow NH_2OH \rightarrow NO \rightarrow NO_2^-$) and reductive activity (including $NO_2^- \rightarrow N_2O$ and $NO \rightarrow N_2O$). The goal was to estimate the relative contribution of each AOB pathway to the N_2O generation under changing DOs and NO_2^- concentrations. The model was calibrated and validated using experimental data from two different bacterial cultures: the first was an enriched nitrifying culture from a lab-scale nitritation SBR treating synthetic anaerobic digester liquor (set-up studied by Law et al. (2013)), while the second was a nitrifying culture including both AOB and NOB to perform full nitrification. The NH_2OH oxidation pathway majorly contributed to the emissions under high DOs with extreme NO_2^- concentrations, whereas nitrifier denitrification was more influential under modest NO_2^- accumulation at low DO. Pocquet et al. (2016) created a two-pathway model including the following: (i) series of oxidations producing NO_2^- ($NH_3 \rightarrow NH_2OH \rightarrow NO \rightarrow NO_2^-$), (ii) NO reduction to N_2O combined with NH_2OH oxidation to NO_2^- (NH_2OH oxidation pathway), and (iii) nitrous acid (HNO_2) reduction to N_2O coupled with NH_2OH oxidation to NO_2^- (nitrifier denitrification pathway). In terms of inhibition factors, the AOB growth was considered non-inhibited (e.g. by NH_3 or HNO_2). On the contrary, a DO inhibition factor was imposed on the nitrifier denitrification process by limiting the N_2O production to a maximum with the DO decrease. During the simulations, the DO increase led to the

decrease of the N_2O EF. After the DO rise, the relative contribution of the nitrifier denitrification pathway started declining, in contrast to NH_2OH oxidation that began increasing its influence.

5.4 Heterotrophic denitrification N_2O models

In terms of heterotrophic denitrification modelling, the activated sludge model for nitrogen (ASMN) was proposed by Hiatt and Grady (2008a). Each of the (four) denitrification steps ($NO_3^- \rightarrow NO_2^- \rightarrow NO \rightarrow N_2O \rightarrow N_2$) was considered as a discrete reaction with its own specific growth rate. They mathematically validated their model by conducting simulations on a modified Ludzak-Ettinger (MLE) configuration: part of the NO_3^- produced in the aerobic reactor (nitrification) was entering the anoxic tank (denitrification) through internal recirculation (Hiatt and Grady, 2008b). According to their results, the mitigation of N_2O production required the provision of enough C-source to ensure the completion of denitrification in the anoxic reactor. An important observation, though, was that the ASMN did not acknowledge that the NO_x reduction and the C oxidation are processes with different kinetics catalysed by different enzymes. Hence, Pan et al. (2013a) developed their model by disconnecting the C-oxidation from the N-reduction. They assigned unique affinity constants to each denitrification step and introduced the ‘electron-carrier concept’: C-oxidation releasing electrons to carriers and NO_x reduction receiving them. The proposed model was calibrated and validated using experimental data from a lab-scale SBR containing a denitrifying culture fed with methanol (Pan et al., 2013b). As the provision of methanol shifted from continuous to pulse, increased electron competition

was noted. The N_2O reductase faced less electron availability under the decreased C-source supply. Thus, complete denitrification was hindered leading to N_2O accumulation.

5.5 Models integrating all biological N_2O production pathways

Ni et al. (2015) coupled the AOB modelling part suggested by Ni et al. (2014) and the heterotrophic denitrification mentions by Ni et al. (2013) in a single model. It was calibrated using data from a step-feed full-scale AS plant and, then, used to explain the important difference between the EFs of each step (first step: 0.7% of influent N, second step: 3.5% of influent N). A substantially higher specific N_2O production rate was observed in the second step along with considerable NO_3^- and NO_2^- levels in the anoxic zone, thus suggesting N_2O generation via heterotrophic denitrification. Under the applied sludge return ratio, the second step was receiving 70% less biomass than the first one. Returning around 30% of the total excess sludge to the second step was recommended as mitigation measure.

5.6 Modelling the combination of biological with biologically-driven N_2O production

Domingo-Felez and Smets (2016) combined the three biological N_2O production pathways with two biologically-driven abiotic N_2O production routes: (i) NH_2OH produced during nitrification can form nitroxyl (HNO) that dimerises (via hyponitrous acid ($H_2N_2O_2$)) to N_2O and H_2O at high pH, (ii) nitrosation of NH_2OH (with HNO_2 as nitrosating agent) can form N_2O inside nitritation reactors at low pH. Although the biological pathways are considered are as major N_2O production hotspots during the BNR in WWTPs, non-negligible abiotic N_2O generation can occur. For instance, Harper et al. (2015) examined

lab-scale batch data obtained during partial nitrification in synthetic wastewater. Under the approximately neutral pH of the study, the abiotic N_2O production was on average two orders of magnitude higher than the biological respective one. It was noted that the abiotic N_2O production was enhanced by the AS presence. Similarly, Soler-Jofra et al. (2016) saw that the NH_2OH concentration in a full-scale nitritation reactor treating reject water was ranging between 0.03 and 0.1 mg N-NH_2OH L^{-1}. Under this NH_2OH presence, almost one third of the total N_2O EF (calculated as the N_2O emitted with respect to the oxidised N during nitritation) resulted from the abiotic N_2O production.

Table 2: Review of the major findings of single- and multiple-pathway models estimating the N_2O dynamics during the BNR in WWTPs.

A. Single-pathway models	**B. Multiple-pathway models**
A1. Nitrifier denitrification	**B1. Both AOB pathways**
• Low DO (≤1.5 mg O_2 L^{-1}): nitrification inhibition, NO_2^- accumulation, higher N_2O emission (Ni et al., 2011; Mampaey et al., 2013) • Temperature increase: enhanced nitrifier denitrification rates causing higher N_2O emission (Guo and Vanrolleghem, 2014)	• NH_2OH oxidation pathway predominant at extremely low/high NO_2^- concentrations with high DO ≠ nitrifier denitrification dominant at low DO with moderate NO_2^- accumulation (Ni et al., 2014) • Maximum N_2O emission at high HNO_2 concentrations (0.6-1 µg N-NO_2 L^{-1}) with low DO (0.5-1 mg O_2 L^{-1}) (Pocquet et al., 2016)
A2. NH_2OH oxidation	**B2. All biological pathways**
• Pathway activated at high NH_4^+ levels (500 mg N-NH_4 L^{-1}) with low DO (0.5-0.8 mg O_2 L^{-1}) (Law et al., 2012b), or at high NH_4^+ concentrations without NO_2^- increase in aerated zones/phases (Ni et al., 2013)	• Anoxic conditions with low biomass content: NO_2^- accumulation & high NO_3^- levels enhancing heterotrophic denitrification pathway (Ni et al., 2015)
A3. Heterotrophic denitrification	**B3. Biological & biologically-driven pathways**
• Each denitrification step as a discrete reaction with a unique specific growth rate (Hiatt and Grady, 2008a) • Increased N_2O accumulation after decreasing the C-source loading rate (Pan et al., 2013a)	• Abiotic N_2O production possible in WWTPs & probably underestimated (Domingo-Felez and Smets, 2016)

5.7 Conclusions and directions for future modelling research

Table 2 presents the main point of each of the models analysed in subsections 5.1-5.6. As it was detailed in section 3, the AOB microbial production pathways are the major N_2O hotspots with their relative contribution depending on the DO and NO_2^- levels. In this regard, the two (AOB)-pathway models are more likely to successfully describe the N_2O emission in WWTPs, particularly if they take account of factors such as the DO and/or NO_2^- fluctuations (e.g. Ni et al., 2014), and/or the potential DO inhibitive effect on the maximum N_2O production (e.g. Pocquet et al., 2016). During the full-scale wastewater treatment though, all three biological N_2O production pathways are possible. Hence, they shall all be included for the purposes of successful full-scale modelling (Kampschreur et al., 2009; Law et al., 2012b; Ni and Yuan, 2015). In this concept, the inclusion of heterotrophic denitrification models including detailed kinetic description for each denitrification step under changing operating conditions (e.g. Pan et al., 2013a) is essential. Future full-scale modelling attempts shall focus on integrating all biological N_2O production pathways as potential emission contributors under varying operational conditions (e.g. DO, NO_2^- concentration, return sludge stream etc.); the latter without disregarding the possibility of abiotic N_2O production. However, it is noted that estimating the importance of abiotic (although biotically driven) N_2O generation in full-scale applications is still under research.

6. Actions to mitigate the N_2O emission in WWTPs

In this chapter, several past works dedicated to the phenomenon of N_2O production during the BNR in WWTPs were summarized. All these studies were analysed to unveil the factors majorly influencing the aspects of N_2O emission, quantification and modelling. The acquired knowledge served to suggest the following mitigation measures:

- Operate under optimum operating conditions. For example, DO is a crucial factor influencing the nitrification process, hence linked to the N_2O emission through the nitrification-related pathways (i.e. AOB production pathways). DO must be controlled at a level allowing the undisturbed completion of nitrification (e.g. at around 2 mg L^{-1}). The aeration rate is equally important. It shall be optimised to a level ensuring the occurrence of nitrification without raising the stripping intensity or the energy demands of the WWTP. Moreover, a WWTP should receive an influent N-load that does not surpass its treatment capacity to avoid NO_2^- accumulation. The same logic applies for the pH and temperature factors. For example, operating under pH≈7 and temperature around 20ºC aids the completion of nitrification-denitrification without excessive stripping or the accumulation of N_2O predecessors.
- Perform advanced N-removal (e.g. nitritation-denitritation or partial nitritation-anammox) only after optimising the process parameters. Even though these N-removal alternatives were suggested to decrease the energy requirements of WWTPs, they are likely to result in increased N_2O production. Therefore, running these processes after optimizating important parameters (e.g. DO) is critical to mitigate the emissions and achieve a moderate overall C-footprint.

- Provide enough C-source to increase the possibility of N_2O consumption through denitrification. The denitrifying bacteria require a sufficient C-source supply to perform denitrification till its final stage, thus consuming the intermediate N_2O product. In addition, the composition of the C-source can play an important role since several C-source types are more advantageous to the growth of the denitrifying bacteria.
- Estimate the EF by considering the plant scale as well as the special operating conditions of each WWTP. The estimated EF will help the operators realise if the plant emissions are beyond an accepted range and, hence, if mitigation strategies should be implemented.
- Apply a precise N_2O sampling and measurement protocol. Accurate sampling campaigns require sampling in various spots covering the whole treatment line for prolonged monitoring periods. Thus, potential spatial and/or temporal variabilities are more likely to be depicted. Continuous online measurements usually respond to this need. Future research should focus on the development of full-scale set-ups that simultaneously estimate both dissolved and gaseous N_2O dynamics.
- Utilise multiple-pathway N_2O models to predict the most contributive N_2O pathways and the most significant operating conditions in a WWTP under observation. Although the importance of abiotic N_2O production during the BNR in WWTPs is still under research, the successful full-scale N_2O modelling requires the integration of all production pathways (biological and abiotic) under varying conditions (e.g. different DO and/or NO_2^- levels).

All things considered, the N_2O production and emission during the BNR in WWTPs is a highly complex and dynamic issue influenced by multiple parameters. The development of novel and flexible multiple-pathway models validated upon real full-scale BNR data is crucial. Afterwards, operators will be able to accurately estimate the N_2O emission of existing plants or plants under construction and, finally, decide on the most appropriate mitigation plans.

References

Adouani, N., Limousy, L., Lendormi, T., Sire, O., 2015. N_2O and NO emissions during wastewater denitrification step: Influence of temperature on the biological process. Comptes Rendus Chim. 18: 15-22.

Ahn, J.H., Yu, R., Chandran, K., 2008. Distinctive microbial ecology and biokinetics of autotrophic ammonia and nitrite oxidation in a partial nitrification bioreactor. Biotechnol. Bioeng. 100: 1078-1087.

Ahn, J.H., Kim, S., Park, H., Rahm, B., Pagilla, K., Chandran, K., 2010. N_2O emissions from activated sludge processes, 2008-2009: results of a national monitoring survey in the United States. Environ. Sci. Technol. 44: 4505-4511.

Ahn, J.H., Kwan, T., Chandran, K., 2011. Comparison of partial and full nitrification processes applied for treating high-strength nitrogen wastewaters: Microbial ecology through nitrous oxide production. Environ. Sci. Technol. 45: 2734-2740.

Castro-Barros, C.M., Daelman, M.R.J., Mampaey, K.E., van Loosdrecht, M.C.M., Volcke, E.I.P., 2015. Effect of aeration regime on N_2O emission from partial nitritation-anammox in a full-scale granular sludge reactor. Water Res. 68: 793-803.

Chandran, K., Stein, L.Y., Klotz, M.G., van Loosdrecht, M.C.M., 2011. Nitrous oxide production by lithotrophic ammonia-oxidizing bacteria and implications for engineered nitrogen-removal systems. Biochem. Soc. Trans. 39: 1832-1837.

Chen, Y., Wang, D., Zheng, X., Li, X., Feng, L., Chen, H., 2014. Biological nutrient removal with low nitrous oxide generation by cancelling the anaerobic phase and extending the idle phase in a sequencing batch reactor. Chemosphere 109: 56-63.

Daelman, M.R.J., De Baets, B., van Loosdrecht, M.C.M., Volcke, E.I.P., 2013. Influence of sampling strategies on the estimated nitrous oxide emission from wastewater treatment plants. Water Res. 47: 3120-3130.

De Mello, W.Z. De, Ribeiro, R.P., 2013. Nitrous Oxide Emissions from an Intermittent Aeration Activated Sludge System of an Urban Wastewater Treatment Plant. Quim. Nova 36: 16-20.

Desloover, J., Vlaeminck, S.E., Clauwaert, P., Verstraete, W., Boon, N., 2012. Strategies to mitigate N_2O emissions from biological nitrogen removal systems. Curr. Opin. Biotechnol. 23: 474-482.

Domingo-Félez, C., Smets, B.F., 2016. A consilience model to describe N_2O production during biological N removal. Environ. Sci. Water Res. Technol. 2: 923-930.

Eldyasti, A., Nakhla, G., Zhu, J., 2014. Influence of biofilm thickness on nitrous oxide (N_2O) emissions from denitrifying fluidized bed bioreactors (DFBBRs). J. Biotechnol. 192: 281-290.

Frijns, J., Roorda, J., Mulder, M., 2008. Op weg naar een klimaatneutrale waterketen. H_2O. 41: 36-37.

Frison, N., Katsou, E., Malamis, S., Bolzonella, D., Fatone, F., 2013. Biological nutrients removal via nitrite from the supernatant of anaerobic co-digestion using a pilot-scale sequencing batch reactor operating under transient conditions. Chem. Eng. J. 230: 595-604.

Frison, N., Chiumenti, A., Katsou, E., Malamis, S., Bolzonella, D., Fatone, F., 2015. Mitigating off-gas emissions in the biological nitrogen removal via nitrite process treating anaerobic effluents. J. Clean. Prod. 93: 126-133.

Gabarro, J., González-Carcamo, P., Ruscalleda, M., Ganigue, R., Gich, F., Balaguer, M.D., Colprim, J., 2014. Anoxic phases are the main N_2O contributor in partial nitritation reactors treating high nitrogen loads with alternate aeration. Bioresour. Technol. 163: 92-99.

Guerrero, J., Guisasola, A., Baeza, J.A., 2011. The nature of the carbon source rules the competition between PAO and denitrifiers in systems for simultaneous biological nitrogen and phosphorus removal. Water Res. 45: 4793-4802.

Gujer, W., Henze, M., Mino, T., Van Loosdrecht, M., 1999. Activated Sludge Model No. 3. Water Sci. Technol. 39: 183-193.

Guo, L., and Vanrolleghem, P.A., 2014. Calibration and validation of an activated sludge model for greenhouse gases no. 1 (ASMG1): prediction of temperature-dependent N_2O emission dynamics. Bioprocess Biosyst. Eng. 37: 151-163.

Gustavsson D.J.I., 2010. Biological sludge liquor treatment at municipal wastewater treatment plants-a review. Vatten, 66: 179-192.

Harper, W.F., Takeuchi, Y., Riya, S., Hosomi, M., Terada, A., 2015. Novel abiotic reactions increase nitrous oxide production during partial nitrification: Modelling and experiments. Chem. Eng. J. 281: 1017-1023.

Hassani, A.H., Nejaei, A., Torabian, A., 2011. Excess sludge minimization in conventional activated sludge pilot plant by three chemical matters. Int. J. Environ. Res. 5: 981-988.

Henze, M., Grady Jr., C.P.L., Gujer, W., Marais, G.V.R., Matsuo, T., 1987. Activated Sludge Model No.1, IAWQ Scientific and Technical Report No.1. IWA Publishing, London, UK.

Henze, M., Gujer, W., Mino, T., van Loosdrecht, M.C.M., 2000. Activated Sludge Models ASM1, ASM2, ASM2d, and ASM3, IWA Scientific and Technical Report n.9. IWA Publishing, London, UK.

Hiatt, W.C., and Grady, C.P.L., 2008a. An updated process model for carbon oxidation, nitrification, and denitrification. Water Environ. Res. 80: 2145-2156.

Hiatt, W.C., Grady, C.P.L., 2008b. Application of the activated sludge model for nitrogen to elevated nitrogen conditions. Water Environ. Res. 80: 2134-2144.

Hooper, A.B., Vannelli, T., Bergmann, D.J., Arciero, D.M., 1997. Enzymology of the oxidation of ammonia to nitrite by bacteria. Antonie Van Leeuwenhoek. 71: 59-67.

Hospido, A., Moreira, M.T., Fernandez-Couto, M., Feijoo, G., 2004. LCA Case Studies: Environmental Performance of a Municipal Wastewater Treatment Plant. Munic. Wastewater Treat. Plant. 9: 261-271.

Hu, Z., Zhang, J., Li, S., Xie, H., 2013. Impact of carbon source on nitrous oxide emission from anoxic/oxic biological nitrogen removal process and identification of its emission sources. Environ. Sci. Pollut. Res. 20: 1059-1069.

Iacopozzi, I., Innocenti, V., Marsili-Libelli, S., Giusti, E., 2007. A modified Activated Sludge Model No. 3 (ASM3) with two-step nitrification-denitrification. Environ. Model. Softw. 22: 847-861.

Ibrahim, M., Yusof, N., Mohd Yusoff, M.Z., Hassan, M.A., 2015. Enrichment of anaerobic ammonium oxidation (anammox) bacteria for short start-up of the anammox process: a review. Desalin. Water Treat. 3994: 1-21.

IPCC, 2014. Climate Change 2014: Synthesis Report. Contribution of Working Groups I, II and III to the Fifth Assessment Report of the Intergovernmental Panel on Climate

Change. In: Core Writing Team, Pachauri R.K. and Meyer L.A. (Eds.), IPCC, Geneva, Switzerland.

Jahnke, L.S., Lyman, C., Hooper, A.B., 1984. Carbonic anhydrase, carbon dioxide levels and growth of Nitrosomonas. Arch. Microbiol. 140: 291-293.

Kampschreur, M.J., van der Star, W.R.L., Wielders, H.A., Mulder, J.W., Jetten, M.S.M., van Loosdrecht, M.C.M., 2008. Dynamics of nitric oxide and nitrous oxide emission during full-scale reject water treatment. Water Res. 42: 812-826.

Kampschreur, M.J., Temmink, H., Kleerebezem, R., Jetten, M.S.M., van Loosdrecht, M.C.M., 2009. Nitrous oxide emission during wastewater treatment. Water Res. 43: 4093-4103.

Kim, S.W., Miyahara, M., Fushinobu, S., Wakagi, T., Shoun, H., 2010. Nitrous oxide emission from nitrifying activated sludge dependent on denitrification by ammonia-oxidizing bacteria. Bioresour. Technol. 101: 3958-3963.

Krul, J.M., and Veeningen, R., 1977. The synthesis of the dissimilatory nitrate reductase under aerobic conditions in a number of denitrifying bacteria, isolated from activated sludge and drinking water. Water Res. 11: 39-43.

Laureni, M., Falås, P., Robin, O., Wick, A., Weissbrodt, D.G., Nielsen, J.L., Ternes, T.A., Morgenroth, E., Joss, A., 2016. Mainstream partial nitritation and anammox: Long-term process stability and effluent quality at low temperatures. Water Res. 101: 628-639.

Law, Y., Lant, P., Yuan, Z., 2011. The effect of pH on N_2O production under aerobic conditions in a partial nitritation system. Water Res. 45: 5934-5944.

Law, Y., Ye, L., Pan, Y., Yuan, Z., 2012a. Nitrous oxide emissions from wastewater treatment processes. Philos. Trans. R. Soc. Lond. B. Biol. Sci. 367: 1265-1277.

Law, Y., Ni, B.J., Lant, P., Yuan, Z., 2012b. N_2O production rate of an enriched ammonia-oxidizing bacteria culture exponentially correlates to its ammonia oxidation rate. Water Res. 46: 3409-3419.

Law, Y. Lant, P.A. Yuan, Z., 2013. The confounding effect of nitrite on N_2O production by an enriched ammonia-oxidizing culture. Environ. Sci. Technol. 47: 7186-7194.

Li, P., Wang, S., Peng, Y., Liu, Y., He, J., 2015. The synergistic effects of dissolved oxygen and pH on N_2O production in biological domestic wastewater treatment under nitrifying conditions. Environ. Technol. 36: 1623-1631.

Lijó, L., Malamis, S., González-García, S., Fatone, F., Moreira, M.T., Katsou, E., 2017. Technical and environmental evaluation of an integrated scheme for the co-treatment of wastewater and domestic organic waste in small communities. Water Res. 109: 173-185.

Lim, Y., and Kim, D.J., 2014. Quantification method of N_2O emission from full-scale biological nutrient removal wastewater treatment plant by laboratory batch reactor analysis. Bioresour. Technol. 165: 111-115.

Lochmatter, S., Gonzalez-Gil, G., Holliger, C., 2013. Optimised aeration strategies for nitrogen and phosphorus removal with aerobic granular sludge. Water Res. 47: 6187-6197.

Malamis, S., Katsou, E., Fatone, F., 2015. Integration of energy efficient processes in carbon and nutrient removal from sewage. In: Stamatelatou, K., Tsagarakis K.

(Eds.), Sewage Treatment Plants: Economic Evaluation of Innovative Technologies for Energy Efficiency. IWA Publishing, London, United Kingdom, pp.71-94.

Mamais, D., Noutsopoulos, C., Dimopoulou, A., Stasinakis, A., Lekkas, T.D., 2015. Wastewater treatment process impact on energy savings and greenhouse gas emissions. Water Sci. Technol. 71: 303-308.

Mampaey, K.E., Beuckels, B., Kampschreur, M.J., Kleerebezem, R., van Loosdrecht, M.C.M., Volcke, E.I.P., 2013. Modelling nitrous and nitric oxide emissions by autotrophic ammonia-oxidizing bacteria. Environ. Technol. 34: 1555-1566.

Mampaey, K.E., van Dongen, U.G.J.M., van Loosdrecht, M.C.M., Volcke, E.I.P., 2015. Novel method for online monitoring of dissolved N_2O concentrations through a gas stripping device. Environ. Technol. 36: 1680-1690.

Mannina, G., Ekama, G.A., Capodici, M., Cosenza, A., Di Trapani, D., Ødegaard, H., van Loosdrecht, M.M.C., 2018. Influence of carbon to nitrogen ratio on nitrous oxide emission in an Integrated Fixed Film Activated Sludge Membrane BioReactor plant. J. Clean. Prod. 176: 1078-1090.

Marques, R., Oehmen, A., Pijuan, M., 2014. Novel Microelectrode-Based Online System for Monitoring N_2O Gas Emissions during Wastewater Treatment. Environ. Sci. Technol. 48: 12816-12823.

Marques, R., Rodriguez-Caballero, A., Oehmen, A., Pijuan, M., 2016. Assessment of online monitoring strategies for measuring N_2O emissions from full-scale wastewater treatment systems. Water Res. 99: 171-179.

Ni, B.J., Ruscalleda, M., Pellicer-Nàcher, C., Smets, B.F., 2011. Modelling Nitrous Oxide Production during Biological Nitrogen Removal via Nitrification and Denitrification: Extensions to the General ASM Models. Environ. Sci. Technol. 45: 7768-7776.

Ni, B.J., Ye, L., Law, Y., Byers, C., Yuan, Z., 2013. Mathematical modelling of nitrous oxide (N_2O) emissions from full-scale wastewater treatment plants. Environ. Sci. Technol. 47: 7795-7803.

Ni, B.J., Peng, L., Law, Y., Guo, J., Yuan, Z., 2014. Modelling of Nitrous Oxide Production by Autotrophic Ammonia-Oxidizing Bacteria with Multiple Production Pathways. Environ. Sci. Technol. 48: 3916-3924.

Ni, B.J., and Yuan, Z., 2015. Recent advances in mathematical modelling of nitrous oxides emissions from wastewater treatment processes. Water Res. 87: 336-346.

Ni, B.J., Pan, Y., Van Den Akker, B., Ye, L., Yuan, Z., 2015. Full-Scale Modelling Explaining Large Spatial Variations of Nitrous Oxide Fluxes in a Step-Feed Plug-Flow Wastewater Treatment Reactor. Environ. Sci. Technol. 49: 9176-9184.

Ostace, G.S., Cristea, V.M., Agachi, P.Ş., 2011. Extension of Activated Sludge Model No. 1 with Two-step Nitrification and Denitrification Processes for Operation Improvement, Environ. Eng. Manag. J. 10: 1529-1544.

Pan, Y., Ni, B.J., Yuan, Z., 2013a. Modelling electron competition among nitrogen oxides reduction and N_2O accumulation in denitrification. Environ. Sci. Technol. 47: 11083-11091.

Pan, Y., Ni, B.J., Bond, P.L., Ye, L., Yuan, Z., 2013b. Electron competition among nitrogen oxides reduction during methanol-utilizing denitrification in wastewater treatment. Water Res. 47: 3273-3281.

Pan, Y., van den Akker, B., Ye, L., Ni, B.J., Watts, S., Reid, K., Yuan, Z., 2016. Unravelling the spatial variation of nitrous oxide emissions from a step-feed plug-flow full scale wastewater treatment plant. Sci. Rep. 6: 20792.

Peng, L., Ni, B.J., Ye, L., Yuan, Z., 2015a. The combined effect of dissolved oxygen and nitrite on N_2O production by ammonia oxidizing bacteria in an enriched nitrifying sludge. Water Res. 73: 29-36.

Peng, L., Ni, B.J., Ye, L., Yuan, Z., 2015b. N_2O production by ammonia oxidizing bacteria in an enriched nitrifying sludge linearly depends on inorganic carbon concentration. Water Res. 74: 58-66.

Pijuan, M., Torà, J., Rodríguez-Caballero, A., César, E., Carrera, J., Pérez, J., 2014. Effect of process parameters and operational mode on nitrous oxide emissions from a nitritation reactor treating reject wastewater. Water Res. 49: 23-33.

Pocquet, M., Wu, Z., Queinnec, I., Sperandio, M., 2016. A two-pathway model for N_2O emissions by ammonium oxidizing bacteria supported by the NO/N_2O variation. Water Res. 88: 948-959.

Poh, L.S., Jiang, X., Zhang, Z., Liu, Y., Ng, W.J., Zhou, Y., 2015. N_2O accumulation from denitrification under different temperatures. Appl. Microbiol. Biotechnol. 99: 9215-9226.

Portmann, R.W., Daniel, J.S., Ravishankara, A.R., 2012. Stratospheric ozone depletion due to nitrous oxide: influences of other gases. Philos. Trans. R. Soc. B Biol. Sci. 367: 1256-1264.

Poughon, L., Dussap, C.G., Gros, J.B., 2001. Energy model and metabolic flux analysis for autotrophic nitrifiers. Biotechnol. Bioeng. 72: 416-433.

Prather, M.J., Hsu, J., De Luca, N.M., Jackman, C.H., Oman, L.D., Douglass, A.R., Fleming, E.L., Strahan, S.E., Steenrod, S.D., Søvde, O.A., Isaksen, I.S. A., Froidevaux, L., and Funke, B., 2015. Measuring and modelling the lifetime of nitrous oxide including its variability. J. Geophys. Res. Atmos. 120: 5693-5705.

Quan, X., Zhang, M., Lawlor, P.G., Yang, Z., Zhan, X., 2012. Nitrous oxide emission and nutrient removal in aerobic granular sludge sequencing batch reactors. Water Res. 46: 4981-4990.

Rodriguez-Caballero, A., Aymerich, I., Poch, M., Pijuan, M., 2014. Evaluation of process conditions triggering emissions of green-house gases from a biological wastewater treatment system. Sci. Total Environ. 493: 384-391.

Rodriguez-Caballero, A., Aymerich, I., Marques, R., Poch, M., Pijuan, M., 2015. Minimizing N_2O emissions and carbon footprint on a full-scale activated sludge sequencing batch reactor. Water Res. 71: 1-10.

Schalk-Otte, S., Seviour, R.J, Kuenen, J.G., Jetten, M.S.M., 2000. Nitrous oxide (N_2O) production by Alcaligenes faecalis during feast and famine regimes. Water Res. 34: 2080-2088.

Schreiber, F., Wunderlin, P., Udert, K.M., Wells, G.F., 2012. Nitric oxide and nitrous oxide turnover in natural and engineered microbial communities: Biological pathways, chemical reactions, and novel technologies. Front. Microbiol. 3: 1-24.

Shen, L., Guan, Y., Wu, G., Zhan, X., 2013. N_2O emission from a sequencing batch reactor for biological N and P removal from wastewater. Front. Environ. Sci. Eng. 8: 776-783.

Soler-Jofra, A., Stevens, B., Hoekstra, M., Picioreanu, C., Sorokin, D., van Loosdrecht, M.C.M., Perez, J., 2016. Importance of abiotic hydroxylamine conversion on nitrous oxide emissions during nitritation of reject water. Chem. Eng. J. 287: 720-726.

Song, K., Harper, W.F., Hori, T., Riya, S., Hosomi, M., Terada, A., 2015. Impact of carbon sources on nitrous oxide emission and microbial community structure in an anoxic/oxic activated sludge system. Clean Technol. Environ. Policy. 17: 2375-2385.

Stein, L.Y., 2011a. Surveying N_2O-producing pathways in bacteria. Methods Enzymol. 486: 131-152.

Stein, L.Y., 2011b. Heterotrophic nitrification and nitrifier denitrification. In: Ward, B.B., Arp, D.J., Klotz M.G. (Eds.). Nitrification. American Society for Microbiology Press, Washington D.C., USA, pp. 95-114.

Strous, M., Heijnen, J.J., Kuenen, G.J., Jetten, M.M.S., 1998. The sequencing batch reactor as a powerful tool for the study of slowly growing anaerobic ammonium-oxidizing microorganisms. Appl. Microbiol. Biotechnol. 50: 589-596.

Sun, S., Bao, Z., Sun, D., 2014. Study on emission characteristics and reduction strategy of nitrous oxide during wastewater treatment by different processes. Environ. Sci. Pollut. Res. 22: 4222-4229.

Tallec, G., Garnier, J., Billen, G., Gousailles, M., 2006. Nitrous oxide emissions from secondary activated sludge in nitrifying conditions of urban wastewater treatment plants: Effect of oxygenation level. Water Res. 40: 2972-2980.

Tumendelger, A., Toyoda, S., Yoshida, N., 2014. Isotopic analysis of N_2O produced in a conventional wastewater treatment system operated under different aeration conditions. Rapid Commun. Mass Spectrom. 28: 1883-1892.

Turk, O., Mavinic, D.S., 1987. Benefits of using selective inhibition to remove nitrogen from highly nitrogenous wastes. Environ. Technol. Lett. 8: 419-426.

Von Schulthess, R., Gujer, W., 1996. Release of nitrous oxide (N_2O) from denitrifying activated sludge: Verification and application of a mathematical model. Water Res. 30: 521-530.

Wang, Q., Ye, L., Jiang, G., Hu, S., Yuan, Z., 2014a. Side-stream sludge treatment using free nitrous acid selectively eliminates nitrite oxidizing bacteria and achieves the nitrite pathway. Water Res. 55: 245-255.

Wang, Q., Jiang, G., Ye, L., Pijuan, M., Yuan, Z., 2014b. Heterotrophic denitrification plays an important role in N_2O production from nitritation reactors treating anaerobic sludge digestion liquor. Water Res. 62: 202-210.

Wunderlin, P., Mohn, J., Joss, A., Emmenegger, L., Siegrist, H., 2012. Mechanisms of N_2O production in biological wastewater treatment under nitrifying and denitrifying conditions. Water Res. 46: 1027-1037.

Wunderlin, P., Lehmann, M.F., Siegrist, H., Tuzson, B., Joss, A., Emmenegger, L., Mohn, J., 2013. Isotope Signatures of N_2O in a Mixed Microbial Population System: Constraints on N_2O Producing Pathways in Wastewater Treatment. Environ. Sci. Technol. 47: 1339-1348.

Xavier, J.B., De Kreuk, M.K., Picioreanu, C., Van Loosdrecht, M.C.M., 2007. Multi-scale individual-based model of microbial and bioconversion dynamics in aerobic granular sludge. Environ. Sci. Technol. 41: 6410-6417.

Xie, W.M., Ni, B.J., Li, W.W., Sheng, G.P., Yu, H.Q., Song, J., 2012. Formation and quantification of soluble microbial products and N_2O production by ammonia-oxidizing bacteria (AOB)-enriched activated sludge. Chem. Eng. Sci. 71: 67-74.

Yang, Q., Liu, X., Peng, C., Wang, S., Sun, H., Peng, Y., 2009. N_2O production during nitrogen removal via nitrite from domestic wastewater: Main sources and control method. Environ. Sci. Technol. 43: 9400-9406.

Ye, L., Ni, B.J., Law, Y., Byers, C., Yuan, Z., 2014. A novel methodology to quantify nitrous oxide emissions from full-scale wastewater treatment systems with surface aerators. Water Res. 48: 257-268.

Zhang, X., Wang, X., Zhang, J., Huang, X., Wei, D., Lan, W., Hu, Z., 2016. Reduction of nitrous oxide emissions from partial nitrification process by using innovative carbon source (mannitol). Bioresour. Technol. 218: 789-795.

Zhang, W., Wang, D., Jin, Y., 2018. Effects of inorganic carbon on the nitrous oxide emissions and microbial diversity of an anaerobic ammonia oxidation reactor. Bioresour. Technol. 250: 124-130.

Zheng, M., Tian, Y., Liu, T., Ma, T., Li, L., Li, C., Ahmad, M., Chen, Q., Ni, J., 2015. Minimization of nitrous oxide emission in a pilot-scale oxidation ditch: Generation, spatial variation and microbial interpretation. Bioresour. Technol. 179: 510-517.

Zhou, Y., Lim, M., Harjono, S., Ng, W.J., 2012. Nitrous oxide emission by denitrifying phosphorus removal culture using polyhydroxyalkanoates as carbon source. J. Environ. Sci. (China) 24: 1616-1623.

Zhu, X., and Chen, Y., 2011. Reduction of N_2O and NO Generation in Anaerobic-Aerobic (Low Dissolved Oxygen) Biological Wastewater Treatment Process by Using Sludge Alkaline Fermentation Liquid Environ. Sci. Technol. 45: 2137-2143.

Chapter II

Extend the activated sludge model to model nitrous oxide emissions in municipal anaerobic/anoxic/oxic wastewater treatment plants under changing operational conditions

Summary

A methodology to predict N_2O emissions during the BNR in WWTPs is presented. The developed N_2O estimation model considered the changing operational conditions (e.g. DO) within WWTPs. Based on the widely accepted and applied ASM models, the proposed mathematical tool incorporated the biological N_2O production pathways for a A^2/O WWTP with biological removal of organic matter, N and P. Precisely, three microbial N_2O production pathways were included: nitrifier denitrification, NH_2OH oxidation, and heterotrophic denitrification, with the first two being activated by the AOB. An SE coefficient was added to reflect the divergence of the stripping model from the actual stripping process. Partial nitrification resulting in high N_2O production via nitrifier denitrification was observed when the DO in the aerobic compartment ranged from 1.8 to 2.5 mg O_2 L^{-1}. The latter possibly suggests that decreased aeration strategies facilitate the attainment of a low overall carbon footprint provided that complete nitrification is not compromised. The model predicted high N_2O emissions when low DO (~1.1 mg O_2 L^{-1}) and high influent NH_4^+ concentration coincided. Further observation revealed that when the AOB population was higher than the NOB respective one, NO_2^- accumulated. Hence, nitrifier denitrification was the preferred N_2O production pathway. Moreover, the effect of a sudden increase in the influent NH_4^+ load was investigated. It was noted that it resulted in the AOB growing at a faster rate compared to the NOB; thus, nitrifier denitrification pathway was considered once again as the N_2O hotspot. Finally, the developed model predicted that the highest N_2O EFs occurred under the following concurring conditions: enhancement of partial nitrification (i.e. low DO) along with increased importance of the stripping effect (i.e. high SEs).

Keywords

N_2O, modelling, A^2/O, biological N_2O production pathways, N_2O stripping, changing operational conditions, N_2O EF

1. Introduction

N_2O is a GHG with a major GWP. Compared to other GHGs such as CH_4 and CO_2, N_2O's contribution to the phenomenon of global warming is importantly higher (IPCC, 2013). Moreover, the depletion of the ozone layer in the last century has been linked to the N_2O emission (Ravishankara et al., 2009). During the BNR in WWTPs, N_2O can be produced and emitted (Ahn et al., 2010; Foley et al., 2010). Besides, N_2O emissions can attribute to the C-footprint of WWTPs to the significant extent of 60 to 75% (Daelman et al., 2013; Rodríguez-Caballero et al., 2015).

The biological N_2O production pathways are associated with the biochemical processes of nitrification and denitrification that occur during the BNR. The nitrification-related pathways (i.e. nitrifier denitrification NH_2OH oxidation) are activated by the AOB. Furthermore, N_2O can be an intermediate product during heterotrophic denitrification; hence, the process is regarded as the third microbial N_2O production route (Wunderlin et al., 2012; Wunderlin et al., 2013; Ni and Yuan, 2015; Rodríguez-Caballero et al., 2015). The principal conditions under which the N_2O generation increases have been assessed and summarized as follows: inadequate DO at the nitrification stage, high NO_2^- levels throughout nitrification and denitrification and decreased COD:N during the denitrification process (Kampschreur et al., 2009; Desloover et al., 2012).

According to the findings of past studies, N_2O emissions have been reported as highly variable amongst different WWTPs. Therefore, the range of the resulting N_2O EFs can be considerable. For instance, the different configurations along with the dynamic operating conditions amongst the full-scale WWTPs examined by Law et al. (2012a) can explain why a wide EF range was recorded: 0-25% (Law et al., 2012a; Marques et al.,

2016). Similarly, the diurnal variability of the influent N-load was suggested as the condition justifying the difference in the EFs reported for twelve full-scale WWTPs in the United States (i.e. 0.01-1.8% when normalized to influent TKN) (Ahn et al., 2010). Moreover, Rodriguez-Caballero et al. (2014) observed the N_2O production in a full-scale municipal WWTP. Nitrification within the bioreactor was non-stable. Hence, the N_2O EF was reported to decrease from 0.12 to 0.06% of the influent TKN throughout the day. Another important factor influencing the EF calculation is the N_2O quantification method and frequency (Law et al., 2012a; Lim and Kim, 2014). In both works by Ahn et al. (2010) and Rodriguez-Caballero et al. (2014), the temporal emission trends were successfully depicted because of the continuous online recording of the N_2O emissions. In quest of an accurate monitoring protocol, Daelman et al. (2013) compared different monitoring scenarios using the N_2O emission data collected after the 16-month operation of a fully covered municipal WWTP in the Netherlands. The authors suggested that the average annual emission in addition to the seasonal trends can be precisely captured via continuous online and intermittent (nightly and weekend) sampling. The accurate recording of the emissions' diurnal variation demanded short-term high-frequency sampling campaigns (Daelman et al., 2013). Therefore, it can be deduced that the N_2O EF calculation of a WWTP can be highly demanding due to numerous reasons: configuration type, N_2O sampling strategy and quantification method.

In this concept, the development of mathematical models estimating the N_2O emission during the BNR in WWTPs is crucial to achieve optimal plant operation and mitigation of the emissions. The advances in the domain of N_2O modelling are continuous. Different models including different production pathways and based on various

assumptions are constantly emerging (Ni and Yuan, 2015; Pocquet et al., 2016). For example, nitrifier denitrification was the core of the models by Ni et al. (2011) and Mampaey et al. (2013). According to the model developed by Ni et al. (2011), low DO (i.e. ≤1.5 mg O_2 L^{-1}) enhanced partial nitrification that resulted in NO_2^- accumulation and, therefore, in activating the nitrifier dentification pathway. Likewise, Mampaey et al. (2013) noted increased N_2O production and emission during the aerobic phases with the DO controlled at relatively low levels (i.e. ≤1.5 mg O_2 L^{-1}). Law et al. (2012b) and Ni et al. (2013) described the second AOB production pathway (i.e. NH_2OH oxidation) in their models. While working on an enriched AOB culture, Law et al. (2012b) observed that the increase in AOR was correlated with the increase in the N_2O production rate. Similarly, Ni et al. (2013) saw that NH_4^+ was likely to accumulate during the aerated phases, thus raising the AOR and NH_2OH production; NH_2OH was generated as by-product of the NH_4^+ oxidation.

However, it has been noted that the two AOB production pathways are likely to simultaneously contribute to the N_2O production during the BNR in WWTPs. Consequently, two-(AOB) pathway models have been suggested (Chandran et al., 2011; Wunderlin et al., 2012; Pocquet et al., 2016). Ni et al. (2014) developed such a model and investigated the conditions that influence the relative contribution of each AOB pathway. The NH_2OH oxidation pathway was preferred for extremely low/high NO_2^- concentrations coinciding with high DO, whereas nitrifier denitrification under moderate NO_2^- concentration combined with low DO. Moreover, the NH_2OH oxidation pathway contribution was slightly higher under conditions of moderate NO_2^- concentration and high DO. Similarly, the relative contribution of the NH_2OH oxidation pathway was gradually

elevated with the DO increase according to the two-(AOB) pathway model by Pocquet et al. (2016).

The heterotrophic denitrification pathway was described in the ASMN by Hiatt and Grady (2008). The ASMN regarded each denitrification step as a distinct reaction with its own specific rate. Pan et al. (2013) distinguished C-oxidation from N-reduction in their denitrification model and considered the electron competition amongst the different denitrification phases.

Notwithstanding, N_2O production can follow any of the three microbial production pathways during the BNR in WWTPs. For that reason, models integrating all pathways are essential to elucidate the trends of N_2O production/consumption and suggest effective mitigation strategies, particularly for the needs of full-scale N_2O modelling (Kampschreur et al., 2009; Ni and Yuan, 2015). For example, the spatial variations in the N_2O flux of a step-feed two-pass full-scale activated sludge plant were successfully explained through the development of a three-pathway model by Ni et al. (2015). In the latter, the authors merged the two-(AOB) pathway modelling with the description of heterotrophic denitrification suggested by Ni et al. (2014) and Ni et al. (2013), respectively.

Models integrating all the biological N_2O production pathways are considered as the most fit for illuminating the impact of changing operating conditions (e.g. DO, NO_2^- concentration, etc.) and clarifying any time/space-related variability in the emissions. Hence, they can serve as a tool helping WWTP operators decide on the most suitable mitigation plan.

The successful full-scale modelling of N_2O emissions requires the development of tools considering all production routes in addition to the importance of parameters such as the aeration patterns, the DO profiles and the N_2O transfer from liquid to gas. The ASM proposed by the IWA task group are a widely popular tool for the BNR description during wastewater treatment. The ASM structure has been expanded to include one or more of the N_2O production pathways and, then, used to investigate the effect of changing conditions (e.g. influent N-load or COD:N, DO, etc.) (Ni et al., 2011; Ni et al., 2013). However, these ASM extensions disregarded the removal of other nutrients (e.g. P) as well as the modelling of the N_2O stripping process. Besides, they focused on either one or two of the biological N_2O production pathways; not on all three of them.

Thus, the aim of this chapter was the development of an ASM-type N_2O model that: (i) included all microbial N_2O production pathways, (ii) considered N, P and COD removal, (iii) proposed an approach to N_2O stripping modelling, and (iv) predicted the N_2O EF under changing DOs. To achieve this goal, the IWA ASM2d structure was enriched with all biological N_2O production routes and a calculation of the N_2O EF. The developed model's continuity was also checked to discover potential typos, conceptual errors and inconsistencies. Lastly, a sensitivity analysis (SA) was conducted to detect the model parameters that were significantly sensitive to the N_2O EF.

2. Materials and Methods

2.1 Basic description of the simulated WWTP and influent composition

The proposed model described the N, P and COD removal within a WWTP with three continuous stirred tank reactors and one settler that operated under an A^2/O configuration (Fig. 2).

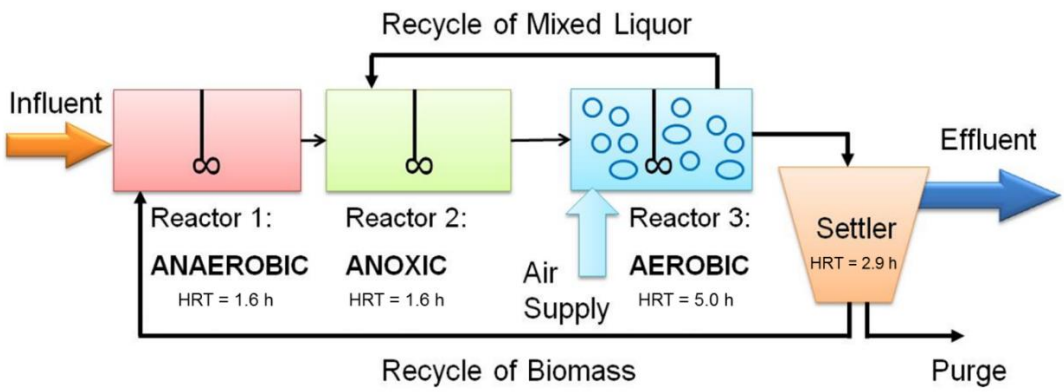

Figure 2: The A^2/O WWTP configuration simulated in the developed model.

The first reactor (HRT=1.6 h) in the simulated A^2/O configuration was anaerobic. This anaerobic environment was advantageous to the growth and prevalence of the phosphorus accumulating organisms (PAOs) over the ordinary heterotrophic organisms (OHOs), thus favouring P-removal. The second (anoxic) reactor (HRT=1.6 h) was receiving NO_3^- via the internal recycle of the mixed liquor that was then subjected to denitrification by the OHOs or the denitrifying PAOs. Nitrification, P and COD removal were occurring in the third (aerobic) reactor (HRT=5 h) of the A^2/O configuration. Afterwards, the treated effluent was entering the settler. Two streams were coming out: the final effluent and an external recycle of biomass that was going back to the first (anaerobic) reactor. The WWTP operated under a total HRT of 11 h. The ratios of the

purge, internal and external recirculation streams were 0.007, 2 and 1/3, respectively, with reference to the influent flowrate. The three reactors in the A^2/O WWTP were simulated under the following typical DO setpoints: 0 mg O_2 L^{-1} (anaerobic and anoxic) and 3 mg O_2 L^{-1} (aerobic).

The influent composition was simulated as representative of the influent treated at the municipal full-scale A^2/O WWTP of Manresa (Spain). The influent components included inert soluble material (S_I), inert particulate organic material (X_I), slowly biodegradable substrates (X_S), and fermentable, readily biodegradable organic substrates (S_F) fractions as follows: S_I=0.07*COD, X_I=0.11*COD, X_S=0.6*COD, and S_F=0.4*COD. The rest of the COD state variables were fixed at zero. The influent composition and properties are presented in Table 3 (Machado et al., 2014).

Table 3: Influent composition (pH=7 and T=20 ºC)

Composition	**mg L^{-1}**
$N\text{-}NH_4^+$	20
BOD_5	170
COD	420
Total N	35
$N\text{-}NO_3^-$	2.6
$P\text{-}PO_4^{3-}$	9
TKN (Kjeldahl N)	33
TSS	189

2.2 Model description

The basic structure of the proposed model followed the principles of the IWA ASM2d. The latter is an ASM version that describes the activity of the heterotrophs, the nitrifiers and the PAOs during the BNR in WWTPs (Henze et al., 2000). Nevertheless, the

main purpose of this work was to create a model that can successfully depict the N_2O production/consumption/emission trends for a full-scale municipal WWTP performing N, P and COD removal. Hence, parameters and process rates concerning the stoichiometry and kinetics of the three biological N_2O production pathways were inserted. The AOB pathways' description was based on the hypotheses formulated by Pocquet et al. (2016), whereas heterotrophic denitrification on the assumptions of the Hiatt and Grady (2008) model. All the included processes were modified accordingly to represent the activity of the AOB, heterotrophic biomass and PAOs. Consequently, the final model structure was regarded as able to describe all the biological pathways for the N_2O production and consumption during the BNR in WWTPs in the most holistic way (Fig. 3).

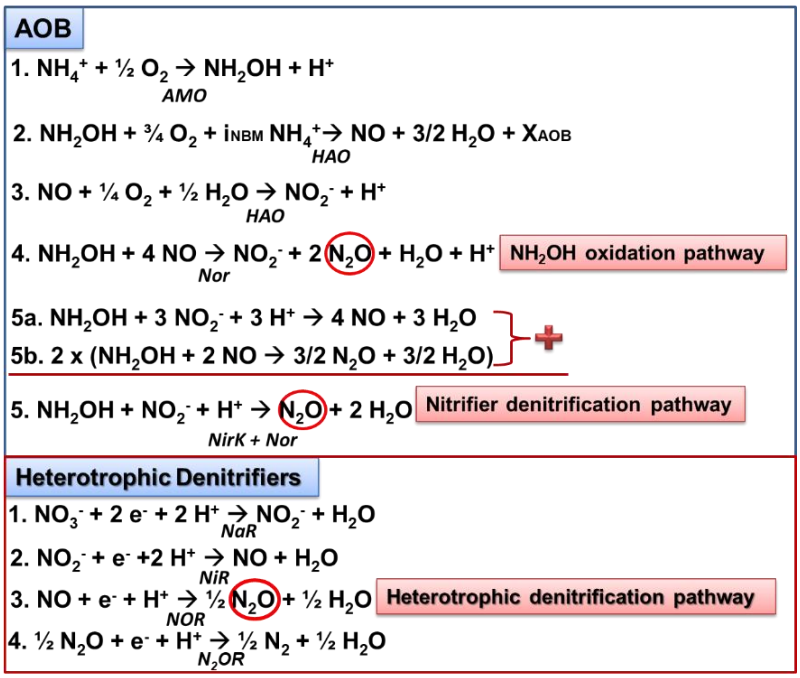

Figure 3: The three biological pathways of N_2O production included in the proposed model: (i) NH_2OH oxidation (AOB pathway), (ii) nitrifier denitrification (AOB pathway), and (iii) heterotrophic denitrification (Ni and Yuan, 2015; Pocquet et al., 2016).

As shown in Fig. 3, five reactions were included to describe the two AOB pathways following the assumptions made by Pocquet et al. (2016): (1) NH_4^+ oxidation to NH_2OH, (2) NH_2OH oxidation to NO, (3) NO oxidation to NO_2^-, (4) NO reduction to N_2O combined with NH_2OH oxidation to NO_2^- (N_2O production via the NH_2OH oxidation pathway), (5) NO_2^- reduction combined with NH_2OH oxidation to produce N_2O (N_2O production via nitrifier denitrification). Reaction (5) coupled two 'sub-reactions' with NO as an intermediate product (Fig. 3: reactions 5a and 5b). Moreover, Fig. 3 presents the four steps of the heterotrophic denitrification pathway. The enzymes that catalyse each step of the three pathways are: AMO (NH_4^+ monooxygenase), HAO (NH_2OH oxidoreductase), Nor (NO reductase), NirK (NO_2^- reductase) for the AOB, and NaR (NO_3^- reductase), NiR (NO_2^- reductase), NOR (NO reductase), and N_2OR (N_2O reductase) for the heterotrophs (Fig. 3) (Ni and Yuan, 2015; Pocquet et al., 2016). Pocquet et al. (2016) suggested grouping together the NO_2^- reduction to NO (NirK enzyme) and the reduction of NO to N_2O (Nor enzyme) in a single 'hyper-reaction' (Fig. 3: nitrifier denitrification pathway; reaction 5). They formulated the hypothesis that the Nor enzyme (Fig. 3: nitrifier denitrification pathway; reaction 5b) was instantly consuming the NO generated with NirK as catalyst (Fig. 3: nitrifier denitrification pathway; reaction 5a). Reaction 5a (Fig. 3: nitrifier denitrification pathway) was considered as happening at a high rate to ensure that NO loops were avoided in the simulations.

P-removal also constituted part of the developed model. Following the respective IWA ASM2d structure proposed by Henze et al. (2000), the following processes were inserted to depict the PAO activity during the BNR in WWTPs: storage of PHAs, aerobic storage of polyphosphates (PPs), aerobic growth of PAOs and lysis of PHAs, PPs and

PAOs. More importantly, the processes of anoxic PP storage and anoxic PAO growth were extended to all four potential electron acceptors existing in the model: i.e. NO_3^-, NO_2^-, NO and N_2O.

The dynamic model was developed in Matlab® and solved using the *ode15s* function. The settling process was modelled as in the study by Takács et al. (1991). Finally, the attainment of steady state for the model components was ensured by simulating WWTP operation under a stable influent composition for a long period of time (i.e. 200 d).

All kinetic parameters were normalized for 20 ºC as suggested in the ASM2d version presented by Henze et al. (2000). The AOB decay and growth rates followed the Hiatt and Grady (2008) proposed values; i.e. μ_{AOB}=0.8 d^{-1}, b_{AOB}=0.1 d^{-1}, respectively. Especially for the NOB population, two different combinations of decay and growth rate values were tested to examine the respective effect on the nitrification process; the first from Hiatt and Grady (2008) (i.e. μ_{NOB}=0.8 d^{-1}, b_{NOB}=0.1 d^{-1}), and the second from Jubany et al. (2008) (i.e. μ_{NOB}=1 d^{-1}, b_{NOB}=0.2 d^{-1}).

2.3 Modelling approach to the N_2O EF

The N_2O EF was calculated in three different ways. The first set of calculations followed the most conservative approach according to which both the stripped N_2O and the N_2O in the effluent (N_2O-EF_{TOTAL}, Eq. 1.1) were considered. Secondly, only the stripping contribution (N_2O-EF_{GAS}, Eq. 1.2) was included in the N_2O EF. Thirdly, the N_2O

EF was estimated by involving exclusively the N_2O contained in the effluent ($N_2O\text{-}EF_{EFF}$, Eq. 1.3).

$$\mathbf{N_2O\text{-}EF_{TOTAL}}(\%) = \mathbf{100} \cdot \frac{\mathbf{N_2O_{ST}+N_2O_{EFF}}}{\mathbf{N_{IN}}} \quad \textbf{(Equation 1.1)}$$

$$\mathbf{N_2O\text{-}EF_{GAS}}\ (\%) = \mathbf{100} \cdot \frac{\mathbf{N_2O_{ST}}}{\mathbf{N_{IN}}} \quad \textbf{(Equation 1.2)}$$

$$\mathbf{N_2O\text{-}EF_{EFF}}\ (\%) = \mathbf{100} \cdot \frac{\mathbf{N_2O_{EFF}}}{\mathbf{N_{IN}}} \quad \textbf{(Equation 1.3)}$$

The N_2O_{ST} stands for the N_2O stripped from the aerobic reactor, N_2O_{EFF} for the N_2O in the effluent, and N_{IN} for the total influent N-content. Eq. 2 explains how N_{IN} was calculated.

$$\mathbf{N_{IN}}\ (\mathbf{g\ N} \cdot \mathbf{d^{-1}}) = \mathbf{Q_{EFF}} \cdot (\mathbf{S_{NH4}} + \mathbf{S_{NO3}} + \mathbf{S_F} \cdot \mathbf{i_{NS_F}} + \mathbf{X_S} \cdot \mathbf{i_{NX_S}} + \mathbf{S_I} \cdot \mathbf{i_{NS_I}} + \mathbf{X_I} \cdot \mathbf{i_{NX_I}})$$

(Equation 2)

With the flowrate denoted by Q_{EFF} ($m^3\ d^{-1}$), the remaining terms appear as in the initial ASM2d version proposed by Henze et al. (2000); S_{NH4}, S_{NO3}, S_F, X_S, S_I and X_I represent the influent concentrations for NH_4^+ (g NH_4^+-N m^{-3}), NO_3^- (g NO_3^--N m^{-3}), fermentable substrate (g COD m^{-3}), slowly biodegradable substrate (g COD m^{-3}), inert soluble substrate (g COD m^{-3}) and inert particulate substrate (g COD m^{-3}), respectively. i_{NS_F}, i_{NX_S}, i_{NS_I} and i_{NX_I} symbolize the N-content (g N g^{-1}COD) of S_F, X_S, S_I and X_I, respectively.

The effluent N_2O (N_2O_{EFF}) calculation was conducted using the N_2O concentration (g N m^{-3}) in the aerobic reactor (N_2O_{AE}) as in Eq. 3:

$$\mathbf{N_2O_{EFF}\ (g\,N \cdot d^{-1}) = Q_{EFF} \cdot N_2O_{AE}} \qquad \textbf{(Equation 3)}$$

Eq. 4 details how the amount of stripped N_2O (N_2O_{ST}) was estimated; with k_La_{N2O} as the volumetric mass transfer coefficient for N_2O, V_{AE} as the volume of the aerobic reactor and 'SE' as the 'stripping effectivity' factor. Different SE values from 0 to 1 were tested to explore the impact of the proposed stripping modelling approach on the N_2O EF.

$$\mathbf{N_2O_{ST}\ (g\,N \cdot d^{-1}) = k_La_{N_2O} \cdot V_{AE} \cdot N_2O_{AE} \cdot SE} \qquad \textbf{(Equation 4)}$$

The volumetric mass transfer coefficient (k_La) combines the global transfer coefficient k_L with the interfacial area a (i.e. the interphase transport surface between liquid and gas per unit of reactor volume). Precisely, the k_La_{N2O} was calculated using Higbie's penetration model as shown in Eq. 5 (Capela et al., 2001):

$$\mathbf{k_La_{N_2O}(d^{-1}) = k_La_{O_2} \cdot \sqrt{\frac{Dif_{N2O}}{Dif_{O2}}}} \qquad \textbf{(Equation 5)}$$

$\mathbf{k_La_{O_2}}$ stands for the volumetric mass transfer of oxygen in the aerobic reactor. It was automatically calculated by use of the DO control system integrated in the proposed model. Dif_{N2O} is the molecular diffusivity of N_2O in water ($2.11*10^{-9}$ m^2 s^{-1} at 20 ºC) and Dif_{O2} the molecular diffusivity of oxygen in water ($2.01*10^{-9}$ m^2 s^{-1} at 20 ºC) (Lide, 2007).

2.4 Continuity check

Following the method suggested by Hauduc et al. (2010) who checked and corrected seven published ASM-type models, the proposed model was tested in terms of potential typos, inconsistencies, gaps and/or conceptual errors. According to this methodology, the multiplication of the stoichiometric matrix (available in the Accompanying Material section) by the composition matrix (i.e. conversion factors of each state variable to COD, N, P, charge and total suspended solids (TSS)) produces the continuity matrix. The latter matrix was produced and analysed. The tolerance permitting its acceptance was fixed at 10^{-15} as indicated by Hauduc et al. (2010). The stoichiometric and composition matrix, as well as the continuity check are provided in detail in the Accompanying Material section.

2.5 SA

Part of the simulations was dedicated to a SA to discover the model parameters that were most sensitive to changes in the $N_2O\text{-}EF_{TOTAL}$ (Eq. 1.1). Reichert and Vanrolleghem (2001) linked the relative sensitivity ($S_{i,j}$) of an output (y_i) with reference to an input parameter (θ_j) as presented in Eq. 6:

$$\mathbf{S_{i,j} = \frac{\theta_j}{y_i} \cdot \frac{\partial y_i}{\partial \theta_j}} \qquad \textbf{(Equation 6)}$$

With the $N_2O\text{-}EF_{TOTAL}$ at steady state as the model output, the SA was conducted for all kinetic/stoichiometric parameters and conversion factors that are detailed in the

Accompanying Material section. The only exceptions made were the factors concerning the S_I production during hydrolysis (f_{SI}) and the S_I P-content (i_{PSI}); they were assumed as null. Moreover, the anoxic growth factor (n_G) was set at 0.9 (instead of 1) to calculate the forward difference. Furthermore, the parameters concerning the NOB growth and decay were considered equal to the Hiatt and Grady (2008) proposed values. Hence, the SA was carried out for a whole of 104 parameters.

The sensitivity of each parameter was estimated using the central difference method. To eliminate the influence of the perturbation factor on the final parameter ranking, a range of different perturbation factors (i.e. 0.01-10%) was tested. More importantly, two different steady-state scenarios (i.e. high (3 mg O_2 L^{-1}) and low (1 mg O_2 L^{-1}) DO in the aerobic reactor) were deployed to elucidate the causes of increased N_2O emissions with the influent NH_4^+ set at 30 mg NH_4^+-N L^{-1} and the SE at 0.5. Section 3 details and discusses all simulation results.

3. Results and Discussion

3.1 The effect of DO on the nitrification process and the generation of N_2O emissions

The proposed model was used to explore the impact of a changing DO (from 0 to 4 mg O_2 L^{-1}) in the aerobic reactor on the process of nitrification and the generation of N_2O emissions. The changes in the N_2O-EF_{TOTAL}, AOB and NOB populations and NH_4^+, NO_2^- and NO_3^- concentrations in relation to the varying DO are presented in Fig. 4.

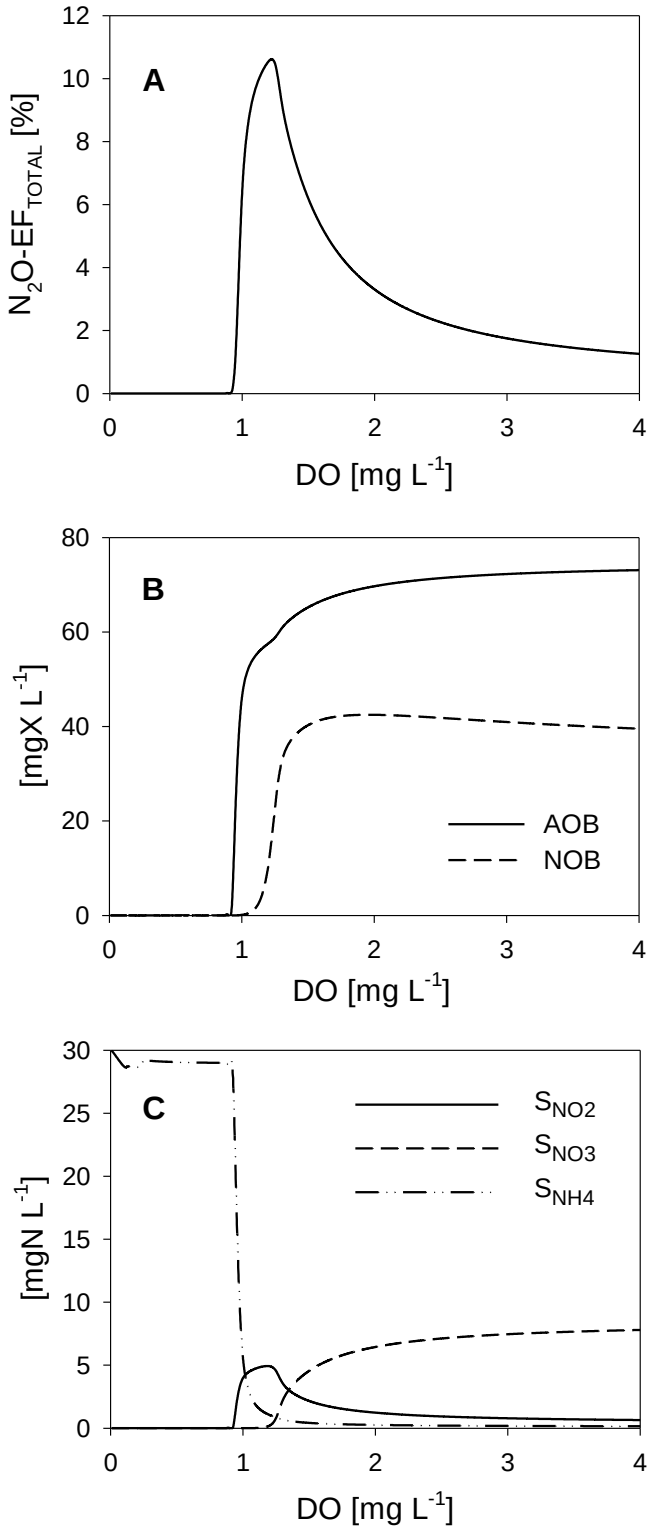

Figure 4: The impact of the changing DO within the aerobic reactor on the steady-state values of the: (A) N_2O EF, (B) AOB and NOB populations, and (C) NO_2^-, NO_3^- and NH_4^+,

concentrations. The SE was 1, while the NOB growth and decay parameters were considered as equal to the Hiatt and Grady (2008) proposed values.

According to the trends observed in Fig. 4B and 4C, there was no growth of the AOB/NOB populations under low DOs (i.e. for DO<0.8 mg O_2 L^{-1}). Similarly, no NO_2^-/NO_3^- was generated under these low-DO conditions. On the contrary, the NH_4^+ concentration was seen to increase from its initial influent value (i.e. 20 mg NH_4^+-N L^{-1}). The latter can be attributed to the NH_4^+ released during hydrolysis. Moreover, there was no NH_4^+ consumption since the low DO inhibited nitrification. The gradual DO increase from 0.8 mg O_2 L^{-1} stimulated the growth of the AOB population. Nevertheless, the NOB growth was observed when the DO concentration reached the value of approximately 1.1 mg O_2 L^{-1} (Fig. 4B). The reported DO values (i.e. 0.8 and 1.1 mg L^{-1}) regarding the commencement of the AOB and NOB growth can be justified via their different affinity constants. The NOB affinity constant for oxygen is lower than the AOB respective one (Wiesmann, 1994). In this concept, the success of strategies promoting partial nitrification (i.e. NH_4^+ oxidation to NO_2^-) relies on maintaining the DO at proper levels (Guisasola et al., 2010).

Accordingly, the AOB population was richer than the NOB respective one for a DO range from 0.8 to 1.1 mg O_2 L^{-1} (Fig. 4B). Furthermore, NH_4^+ was consumed to produce NO_2^- through partial nitrification (Fig. 4C). With the DO ranging from 0.8 to 1.1 mg O_2 L^{-1}, an importantly high N_2O EF was noted (≈10.5%) (Fig. 4A). NO_2^- was accumulated via partial nitrification and, subsequently, N_2O was produced through nitrifier denitrification. At such low-DO environments, oxygen is replaced by the accumulated NO_2^- in its function as final electron acceptor. Therefore, the AOB are most likely to activate the nitrifier

denitrification N_2O production pathway (Tallec et al., 2006; Kampschreur et al., 2008; Desloover et al., 2012).

Similar trends have been observed in past works that examined the favoured N_2O production route under different DOs. For instance, the preferred N_2O production pathway was explored within an enriched AOB culture contained in a lab-scale partial nitrification reactor that was implemented to treat anaerobic digester liquor. Three different DO values were applied: 0.6, 1.3 and 2.3 mg O_2 L^{-1}. Nitrifier denitrification was found to be the major emission contributor at the lowest DO levels (Law et al., 2013). Moreover, a lab-scale SBR fed with synthetic wastewater and provided with an enriched nitrifying sludge was examined in terms of the DO impact on the N_2O emissions. Increasing the DO from 0.2 to 3 mg O_2 L^{-1} was accompanied by a decreasing contribution of the nitrifier denitrification pathway (Peng et al., 2014).

As soon as the DO reached 1.5 mg O_2 L^{-1} and onwards, the AOB and NOB populations became almost stable around 70 and 40 mg biomass L^{-1}, respectively (Fig. 4B). The DO increase favoured complete nitrification, thus promoting the NO_2^- consumption and NO_3^- production as indicated in Fig. 4C. The nitrifier denitrification pathway was slowly abandoned as proven by the continuous N_2O-EF_{TOTAL} decline that started at a DO≈1.5 mg O_2 L^{-1} and continued as the applied DO was increasing. Especially at high DOs (i.e. >3 mg O_2 L^{-1}), the observed N_2O-EF_{TOTAL} was below 2%, hence importantly decreased (Fig. 4A).

The results produced by the proposed model suggest that increasing the DO can foster the mitigation of N_2O emission. Nevertheless, such high-DO strategies can be disadvantageous in terms of energy requirements. The energy needed to perform

nitrification is likely to negatively contribute to the C-footprint of WWTPs. For example, the electricity required for the nitrifying process corresponded to 13% of the C-footprint of a plug-flow (three-pass) full-scale municipal WWTP in the UK (Aboobakar et al., 2013). The intermittent aeration strategies have been suggested as an alternative to lower the cost of aeration by 33-45%. Nonetheless, they cannot guarantee the undisturbed activity of the nitrifiers, thus potentially interrupting the nitrification process. Therefore, additional N_2O emission can occur and increase the C-footprint of the plant (Dotro et al., 2011). Before applying low-aeration regimes, the possibility of N_2O process emissions shall be weighed (Aboobakar et al., 2013). Low DOs raise the likelihood of N_2O production and emissions that can add to a WWTP's C-footprint. In this concept, different DOs shall be tested to conclude to a DO range that ensures normal plant operation and undisturbed nitrification without excessive energy consumption. According to the proposed model, this DO interval can be 1.8-2.5 mg O_2 L^{-1}.

3.2 The impact of different NOB growth and decay parameter values on the N_2O EF

Two different sets of values for the NOB growth and decay rate were included in the simulations to investigate their respective effect on the N_2O EF. The first set followed the Hiatt and Grady (2008) proposed values (μ_{NOB}=0.8 d^{-1}, b_{NOB}=0.1 d^{-1}), while the second set was suggested by Jubany et al. (2008) (μ_{NOB}=1 d^{-1}, b_{NOB}=0.2 d^{-1}).

Especially for the treatment of wastewaters with high NH_4^+ concentration, the process of short-cut biological N-removal has been proposed. It occurs in two stages: first, partial nitrification/nitritation (NH_4^+ oxidation to NO_2^-) and, then, denitritation (NO_2^-

reduction to N_2) (Jubany et al., 2009). In contrast to the conventional nitrification-denitrification schemes, this novel process is beneficial with respect to COD requirements (40% lower during denitrification) and denitrification rate (63% higher) (Turk and Mavinic, 1987). Moreover, 25% less oxygen is needed for nitrification since the 'nitratation' stage (i.e. NO_2^- oxidation to NO_3^-) is omitted (Peng and Zhu, 2006). To achieve partial nitrification/nitritation, certain temperature, pH and DO conditions are needed to enhance the AOB growth to the detriment of the NOB one (Jubany et al., 2009). By keeping the pH and temperature unchanged during all simulations (T=20 ºC and pH=7), this work gave emphasis to the DO impact on the nitrification stages. Low DO is generally regarded as advantageous to partial nitrification and NO_2^- accumulation (Ruiz et al., 2003; Guisasola et al., 2005; Soliman and Eldyasti, 2016).

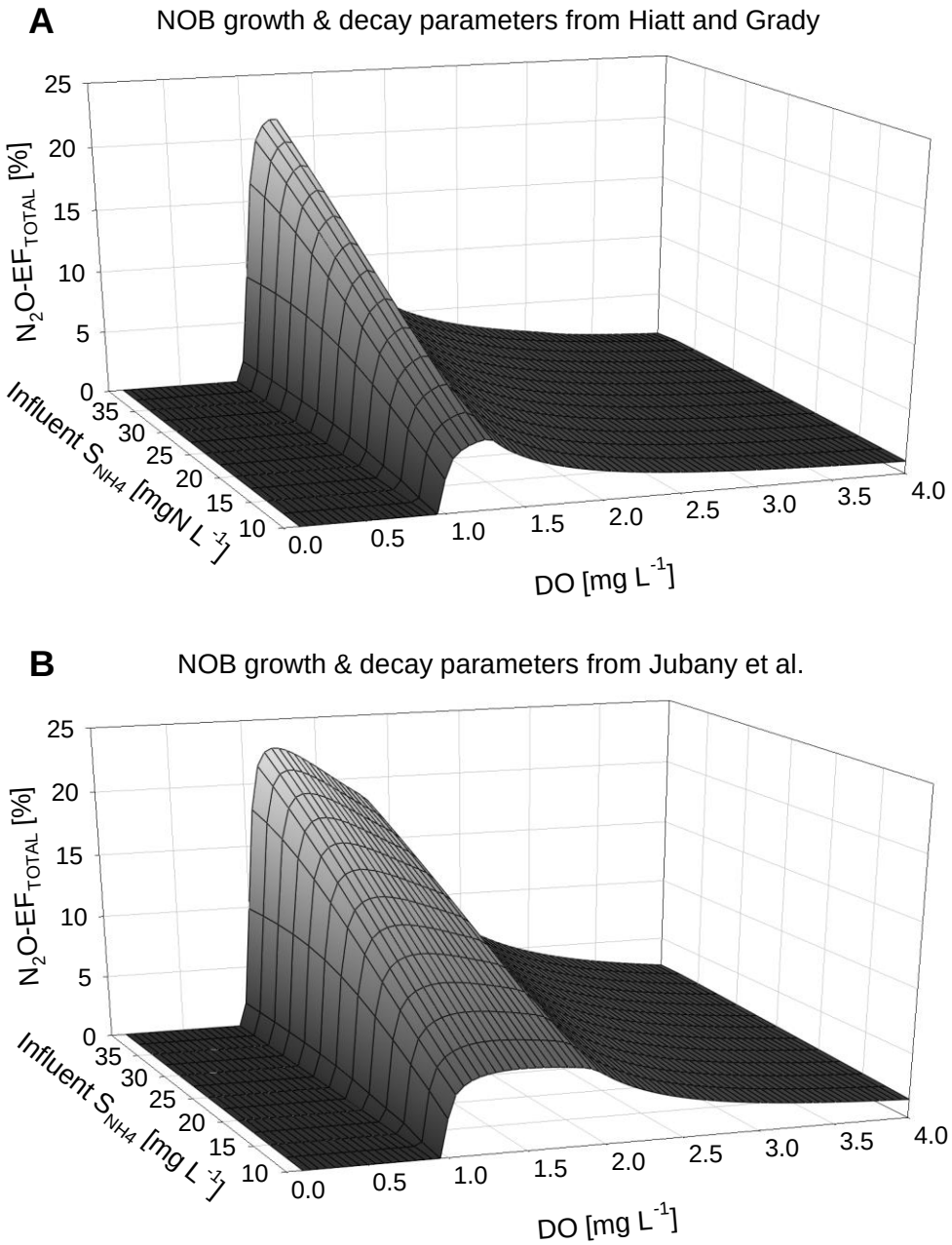

Figure 5: The steady-state N_2O EF with respect to different DO setpoints in the aerobic reactor (0 to 4 mg O_2 L^{-1}) and influent S_{NH4} concentrations (10 to 40 mg NH_4^+-N L^{-1}). The applied SE was 1. A) NOB growth and decay rates as in Hiatt and Grady (2008). B) NOB growth and decay rates as in Jubany et al. (2008).

The evolution of the N_2O-EF_{TOTAL} was observed while the DO setpoint in the aerobic reactor was changing from 0 to 4 mg O_2 L^{-1} and the influent NH_4^+ from 10 to 40 mg NH_4^+-N L^{-1} (Fig. 5). During this set of simulations, the maximum SE (i.e. SE=1) was applied. Hence, it became possible to estimate the N_2O-EF_{TOTAL} for increasing DO and influent NH_4^+ values under full striping contribution to the EF (i.e. worst-case scenario in terms of expected emissions). After testing each of the proposed combinations for the NOB growth/decay rates (the first from Hiatt and Grady (2008) and the second from Jubany et al. (2008)), the N_2O-EF_{TOTAL} was seen to fluctuate in a comparable way. No N_2O emissions were noted within the 0-0.8 mg O_2 L^{-1} range since no nitrification was happening. With the DO increasing beyond 0.8 mg O_2 L^{-1}, partial nitrification started. With the DO ranging from 0.8 to 1.8 mg O_2 L^{-1}, the highest EFs were noted. The occurring partial nitrification resulted in NO_2^- accumulation and, thus, activation of the nitrifier denitrification pathway. The highest N_2O-EF_{TOTAL} (≈22%) was noticed under the following concurring conditions: DO≈1.1 mg L^{-1}, influent N-NH_4^+=40 mg L^{-1} (i.e. the highest tested) and SE=1. With the DO surpassing 1.8 mg O_2 L^{-1}, the NO_2^- started being consumed via full nitrification, hence allowing the N_2O-EF_{TOTAL} to attain an importantly lower value (≈2% for DO>2.5 mg O_2 L^{-1}). Analogously, Pijuan et al. (2014) investigated the DO impact in a pilot-scale airlift system with granular biomass performing nitritation to treat reject wastewater. The DO increase from 1 to 4.5 mg O_2 L^{-1} provoked an N_2O EF reduction from 6% to 2.2% of N-oxidized. In a lab-scale nitritation reactor receiving synthetic wastewater, Rathnayake et al. (2015) saw that the DO rise from 0.6 to 2.3 mg O_2 L^{-1} stimulated a decrease in the N_2O EF from 2.9 to 1.4%.

Furthermore, the evolution of the N_2O-EF_{TOTAL} with respect to the influent NH_4^+ concentration showed that the emissions increased as the influent NH_4^+ load became higher (Fig. 5). Therefore, streams with lower initial NH_4^+ content are likely to result in lower EFs. Similarly, Frison et al. (2015) implemented a pilot-scale SBR for the treatment of reject water to explore the influence of two different combinations between the N-loading rate and the DO (first combination: volumetric N-loading rate=1.1 kg N m^{-3} d^{-1} & DO=1 mg O_2 L^{-1}; second combination: volumetric N-loading rate=0.8 kg N m^{-3} d^{-1} & DO=1.5 mg O_2 L^{-1}). Shifting from the first to the second combination resulted in an N_2O EF decrease from 1.5 to 0.2% of the influent N-load. Applying a higher DO along with an influent N-load that respected the system's treatment capacity inhibited the NO_2^- accumulation and, hence, the increase of the N_2O emissions. Likewise, the developed model estimated an increase in the N_2O-EF_{TOTAL} if higher NH_4^+ in the influent coincided with lower DOs.

Nevertheless, the N-removal via NO_2^- was extended with the NOB growth and decay parameters proposed by Jubany et al. (2008). The DO intervals inside which nitritation was observed were ≈0.8<DO<1.8 mg O_2 L^{-1} with the parameters suggested by Hiatt and Grady (2008), in contrast to ≈0.8<DO<2.2 mg O_2 L^{-1} with the ones recommended by Jubany et al. (2008) (Fig. 5). It shall be noted, though, that the model parameter majorly affecting the process is the NOB half-saturation coefficient for oxygen. It was 1.2 mg O_2 L^{-1} according to the study by Hiatt and Grady (2008) but considered as equal to 1.8 mg O_2 L^{-1} (Guisasola et al., 2005; Jubany et al., 2009) for the purposes of the work by Jubany et al. (2008). The latter (higher) value broadens the DO range inside

which the NOB activity is suppressed, thus prolonging nitritation and raising the likelihood of increased N_2O emissions.

3.3 The stripping modelling influence on the N_2O EF

The aerobic sections where nitrification occurs are regarded as the principal N_2O generation sites in WWTPs. The produced N_2O will be stripped during aeration and released to the atmosphere (Law et al., 2012a; Mannina et al., 2016).

As detailed in section 2.3, the modelling approach to the N_2O stripping incorporated the k_La. Moreover, it included the SE as a coefficient depicting the deviation of the model estimation (Eq. 4) from an ideal representation of how stripping happens in reality (SE=1). Eq. 4 was formulated based on the following assumptions: i) the air bubbles do not contain N_2O even when they ascend the reactor, ii) liquid-phase N_2O and DO are homogeneous, and iii) the k_La remains unchanged along the whole liquid depth. The impact of an increasing DO (from 0 to 4 mg O_2 L^{-1}) under the highest initial influent NH_4^+ content (i.e. 40 mg NH_4^+-N L^{-1}) was explored for varying SEs (i.e. 0, 0.1, 0.25, 0.5, 0.75, 1) using the NOB growth/decay parameters by Hiatt and Grady (2008). The maximum N_2O EFs were noted for a DO around 1.2 mg O_2 L^{-1} for all the applied SEs. The simulation results regarding the maximum N_2O-EF_{TOTAL} (i.e. including both the stripped N_2O and the N_2O released in the effluent) and the maximum N_2O-EF_{GAS} (describing only the stripped N_2O contribution) with respect to different SEs are shown in Fig. 6. Fig. 6 was produced after applying the following conditions: DO≈1.2 mg O_2 L^{-1} (as the worst-

case scenario that provides the maximum EFs), initial influent NH_4^+ content=40 mg NH_4^+-N L^{-1}, and NOB growth/decay parameters by Hiatt and Grady (2008).

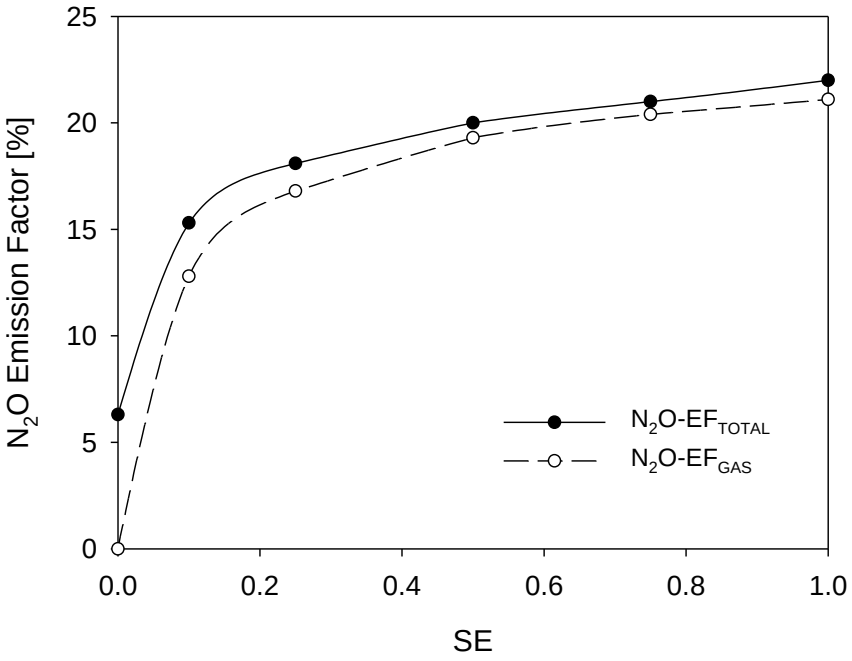

Figure 6: The maximum N_2O EF (N_2O-EF_{TOTAL} including both the stripped N_2O and the N_2O released in the effluent; N_2O-EF_{GAS} describing only the stripped N_2O contribution) reported for different SE values (0, 0.1, 0.25, 0.5, 0.75, 1). The DO was considered equal to 1.2 mg O_2 L^{-1} (the maximum EFs occurred for this DO value), the influent NH_4^+ was 40 mg NH_4^+-N L^{-1}, and the NOB growth/decay parameters followed the Hiatt and Grady (2008) proposed values.

As indicated in Fig. 6, both the N_2O-EF_{TOTAL} and the N_2O-EF_{GAS} evolved in a comparable way for all the SE values tested. Their absolute values were slightly different, though. Precisely, the maximum N_2O-EF_{GAS} rose from 0% (SE=0) to ~21.1% (SE=1), whereas the maximum N_2O-EF_{TOTAL} from 6.3% (SE=0) and ~22% (SE=1). Hence, the EFs generally increased with the SE increase. This trend was more abrupt initially (SE:

0→0.1) and smoother onwards (SE: 0.25→1) (Fig. 6). Under a lower SE value, the N_2O is more likely to follow the heterotrophic denitrification pathway (reaction 4 of denitrification in Fig. 3). Thus, there is higher likelihood of its consumption through denitrification. Finally, it was noticed that the N_2O-EF_{TOTAL} was consistently higher than the N_2O-EF_{GAS}, although not to an important extent (Fig. 6). Therefore, it can be deduced that the stripped N_2O and, subsequently, the SE value were key factors that majorly affected the final EF results.

3.4 Modelling the N_2O emissions while disturbing the normal WWTP operation

Another target was to investigate the results produced by the proposed model while simulating perturbations of the influent concentration under varying combinations of DOs and SEs. The latter was considered useful since the transition period after a system shock facilitates the accumulation of intermediates that are likely to generate N_2O. As an indicative example, the abrupt increase in the influent NH_4^+ content (as a step increase from 20 to 30 mg NH_4^+-N L^{-1} on the 10th day of the plant operation) was analysed for different applied DOs and SEs in the aerobic reactor.

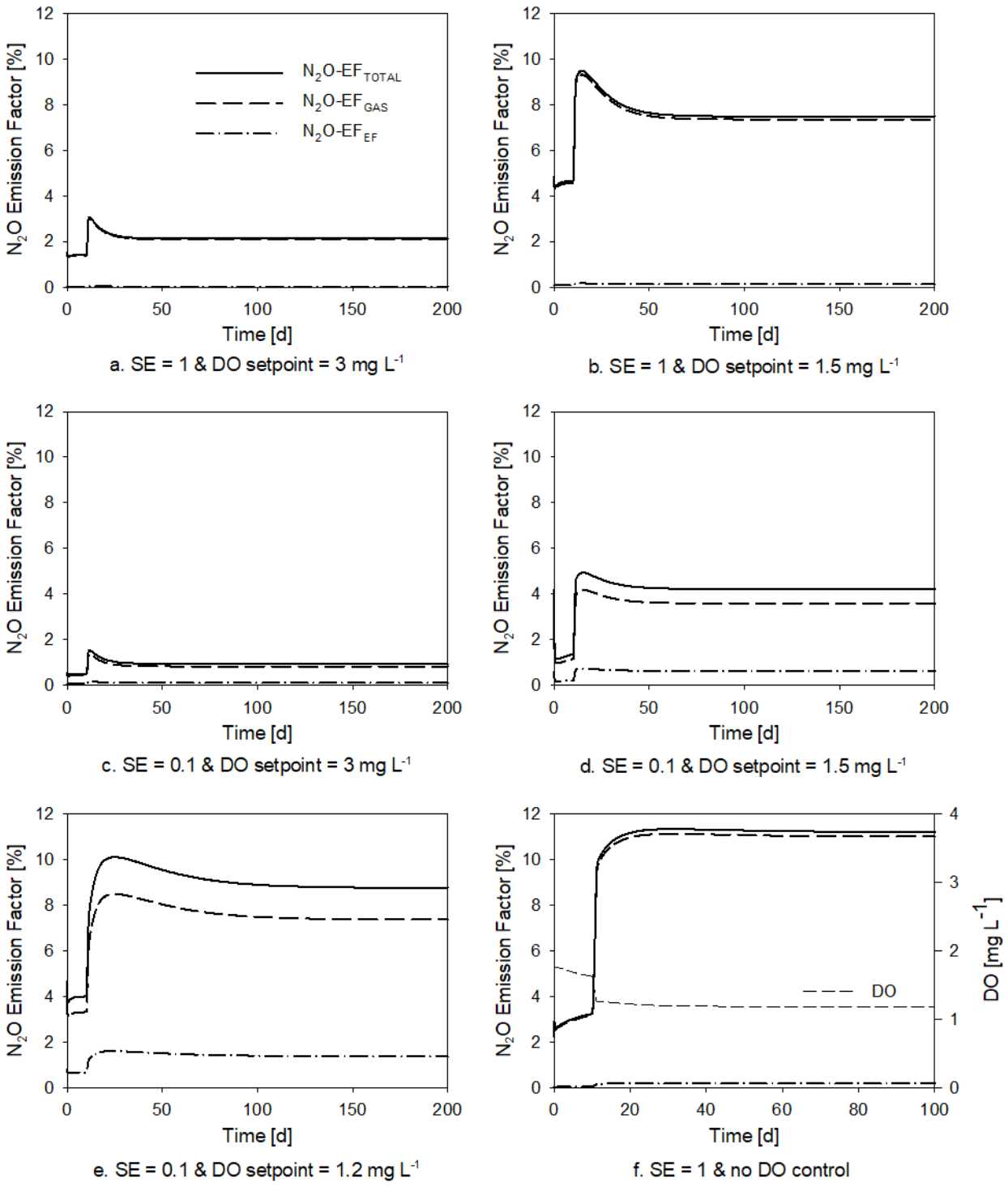

Figure 7: The impact of increasing the influent NH_4^+ concentration (from 20 to 30 mg NH_4^+-N L^{-1}) on the N_2O EF at the 10th day of the plant operation. Different SE values (1

and 0.1) and DO setpoints (3 mg O_2 L^{-1}, 1.5 mg O_2 L^{-1}, 1.2 mg O_2 L^{-1} and no DO control) were tested.

SE equal to 1 was applied for scenarios a and b to see how the simulated system reacts to the sudden influent NH_4^+ increase under full stripping conditions. The abrupt rise in the influent NH_4^+ concentration immediately triggered an escalation in the N_2O emission. The N_2O-EF_{TOTAL} evolved as detailed hereafter: 1.4→3.1% until the 12th day of operation (scenario a) and 4.5→9.6% until the 17th day (scenario b). Afterwards, it presented a smooth downward trend till its stabilisation at ~2.1% after the 30th day (scenario a), and at ~7.5% after the 40th day (scenario b) (Fig. 7). The major difference between scenarios a and b was the applied DO; it was importantly lower in case b. As already analysed in Fig. 5A, higher EFs are likely in this event. Under this (low) DO, the AOB perform nitritation. Hence, NO_2^- accumulation and N_2O production through nitrifier denitrification are anticipated (Kuenen et al., 2008; Peng et al., 2015; Jin et al., 2016). As a matter of fact, experimental studies have featured low DO (i.e. <1.5 mg O_2 L^{-1}) as highly helpful to the nitritation process and the resulting NO_2^- accumulation but detrimental to the NOB growth (Garrido et al., 1997; Bae et al., 2001; Ciudad et al., 2005; Blackburne et al., 2008).

For both scenarios a and b, the decreasing trend of the EF can be translated into a gradual NOB growth that initiated the oxidation of the accumulated NO_2^-. It was observed, though, that the EF failed to return to its initial value, meaning that the developed NOB population was inadequate to oxidize all the accumulated NO_2^- amount (Fig. 7). Fig. 8 presents the AOB and NOB evolution under the application of scenarios a and b. After the system shock on the 10th day of operation, the AOB growth was steadily

higher than the NOB respective one. Indeed, past findings support the fact that an increased NH_4^+ loading under a controlled DO setpoint promotes the AOB activity over the NOB one (Peng et al., 2015).

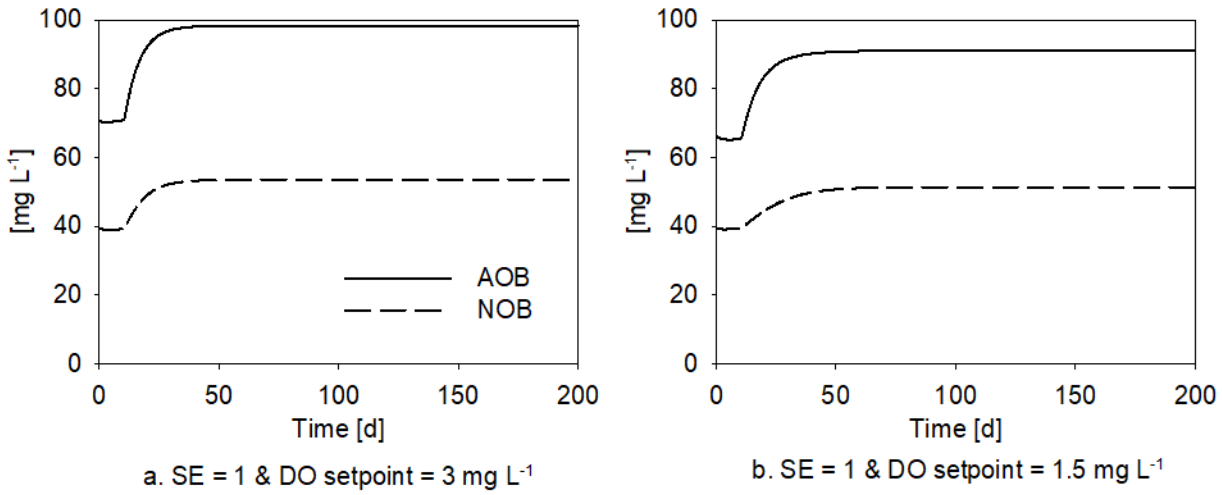

Figure 8: The AOB and NOB evolution after increasing the influent NH_4^+ concentration (from 20 to 30 mg NH_4^+-N L^{-1}) on the 10th day of the WWTP operation. Different DO control setpoints (3 and 1.5 mg O_2 L^{-1}) were tested with the SE equal to 1.

While operating under the same DO control setpoint, different SEs were applied to observe the full (SE=1) versus the limited (SE=0.1) stripping effect (comparison between scenarios a and c, and comparison between scenarios b and d in Fig. 7). The general trends were always similar: the N_2O-EF_{TOTAL} quickly increasing after the system shock, then slightly decreasing to get finally stabilized around a value always higher than the one held before the influent NH_4^+ enrichment. The lower SE value (i.e. 0.1) can justify the obvious distance between the N_2O-EF_{TOTAL} and N_2O-EF_{GAS} lines. The emission was lesser for scenarios c and d (i.e. SE=0.1 cases) with more N_2O simulated as dissolved and released in the effluent (Fig. 7). By lowering the SE to 0.1, the WWTP is considered

as operating under less powerful stripping. The latter allows more N_2O to stay within the aerobic reactor. Hence, a higher amount of N_2O is expected to return to the anoxic reactor via the recycling stream and end up being consumed during denitrification. Furthermore, scenario e described operation under conditions manifestly inhibiting the NOB activity and promoting nitritation (DO=1.2 mg O_2 L^{-1} & SE=0.1); emissions above 9% were noted.

Nevertheless, all scenarios from a to e included DO control. The latter was added to simulate how the system can continually operate under the desired DO setpoint despite potential fluctuations in the aeration. On the other hand, scenario f described operation under no DO control. In this case, the increase of the influent NH_4^+ loading was found to have a more evident effect since it lowered the DO concentration. Hence, the system shifted from full to partial nitrification which can justify the higher EF.

A general increase in the N_2O emissions was the simulated system's response to the disturbance of its normal operation (i.e. increase of the influent NH_4^+ concentration from 20 to 30 mg NH_4^+-N L^{-1} on the 10th day of the WWTP operation) under all the applied SEs and DOs. The system shock impacted on both the AOB and the NOB. However, the AOB restored their growth faster and more effectively than the NOB. Therefore, partial nitrification and N_2O production via nitrifier denitrification were observed. The extent of the emissions varied according to the applied SE and DO. Higher emissions occurred under the combination of high SEs and low DOs. This can be explained through the following: increased SE values raised the stripping importance while lower DOs created conditions favourable to partial nitrification. Especially in the case of no DO control, the EF significantly increased because the operating condition was intensely advantageous to partial nitrification.

3.5 SA

Under an influent NH_4^+ of 30 mg NH_4^+-N L^{-1} and an SE equal to 0.5, two different scenarios were implemented for the SA: the first was a 'high-DO' scenario (DO in the aerobic reactor=3 mg O_2 L^{-1}) to simulate conditions that favour the completion of the nitrification process, while the second was a 'low-DO' one (DO in the aerobic reactor=1 mg O_2 L^{-1}) to simulate an environment favourable to partial nitrification. Table 2 presents the results of the SA (i.e. the 40 most sensitive parameters to the N_2O-EF_{TOTAL}) in descending order according to their $S_{i,j}$ absolute value that was calculated using Eq. 6. The signs of the Sij are also provided: a positive sensitivity index suggests that the parameter increase is accompanied by an increase in the N_2O-EF_{TOTAL}, while the opposite happens in the case of negative sensitivity. Moreover, the results were produced upon a perturbation factor of 0.01% as the value proposed by De Pauw (2005) who recommended the use of a factor with equal derivative values for forward and backward differences. In any case, the choice of the perturbation factor had no important influence on the parameter ranking (data not shown).

Table 4: The results of the SA for the two different scenarios tested (first: DO_{AE} =3 mg O_2 L^{-1}; second: DO_{AE} =1 mg O_2 L^{-1}). In both cases the influent NH_4^+ was considered equal to 30 mg NH_4^+-N L^{-1} and the SE equal to 0.5. The DO control setpoint in the aerobic reactor is denoted by DO_{AE}.

Order	DO_{AE}=3 mg O_2 L^{-1}		DO_{AE}=1 mg O_2 L^{-1}	
	Parameter	Si,j	Parameter	Si,j
1	μ_{NOB}	-2.138	Y_{AOB}	2.233
2	η_G	1.489	η_G	1.978
3	b_{NOB}	1.059	q_{AOB_AMO}	1.407
4	$q_{AOB\_N2O\_ND}$	0.997	Y_{PAO}	1.108

Order	DO_{AE}=3 mg O_2 L^{-1}		DO_{AE}=1 mg O_2 L^{-1}	
	Parameter	Si,j	Parameter	Si,j
5	μ_{AOB_HAO}	-0.926	b_{AOB}	-1.024
6	$K_{I\_O2\_AOB}$	0.878	η_{G5}	-0.947
7	Y_{AOB}	0.863	K_{OH5}	-0.853
8	K_{HNO2_AOB}	-0.857	$q_{AOB\_N2O\_ND}$	0.841
9	K_{NO2_NOB}	0.851	K_{O2_AOB1}	-0.738
10	Y_{PAO}	0.739	i_{NXS}	0.674
11	K_{O2_NOB}	0.629	Y_H	-0.470
12	η_{G5}	-0.620	Y_{PO4}	-0.435
13	K_{OH5}	-0.470	q_{PP}	0.400
14	K_{N2O_Den}	0.435	μ_{PAO}	-0.386
15	i_{NXS}	0.428	i_{NBM}	-0.375
16	b_{PAO}	-0.408	K_{HNO2_AOB}	-0.360
17	SE	0.375	i_{NSF}	0.338
18	Y_H	-0.364	$K_{I\_O2\_AOB}$	0.299
19	K_{MAX_P}	0.259	K_{MAX_P}	0.292
20	i_{NBM}	-0.247	SE	0.223
21	μ_{PAO}	0.246	K_{NH2OH_AOB}	-0.209
22	i_{NSF}	0.207	$K_{O2\_AOB\_ND}$	0.198
23	$K_{O2\_AOB\_ND}$	0.192	μ_{AOB_HAO}	-0.175
24	D_{O2}	-0.187	K_{N2O_Den}	0.170
25	D_{N2O}	-0.187	K_{S5}	0.166
26	K_{P_P}	-0.169	K_F	-0.157
27	K_{O2_AOB2}	0.167	Y_{PHA}	-0.149
28	K_{S5}	0.151	K_{NH4_AOB}	-0.137
29	b_H	0.149	n_{fe_H}	-0.134
30	Y_{PO4}	-0.135	K_{O2_P}	-0.132
31	K_{P_NOB}	0.122	b_H	0.121
32	q_{AOB_AMO}	-0.120	D_{O2}	-0.111
33	q_{PHA}	0.118	D_{N2O}	-0.111
34	K_H	-0.101	b_{PAO}	-0.101
35	K_F	-0.099	K_H	-0.098
36	n_{fe_H}	-0.094	k_La	0.089
37	Y_{PHA}	-0.094	K_{O2_AOB2}	0.082
38	q_{PP}	0.085	K_{IPP_P}	-0.074
39	η_{G3}	0.077	i_{PXS}	-0.073
40	i_{PXS}	-0.064	b_{PP}	-0.071

The parameter ranking was different between the two tested scenarios. For the first ‘high-DO’ scenario (DO in the aerobic reactor=3 mg O_2 L^{-1}), first the NOB-, then the

AOB- and finally the PAO-related parameters emerged as the most sensitive to the N_2O-EF_{TOTAL}. The sensitivity of the parameters linked to the NOB activity is essential to unveil the mechanisms of NO_2^- accumulation. As detailed in section 3.1, the NO_2^- dynamics will determine partial nitrification, nitrifier denitrification and the resulting N_2O emission. For the second 'low-DO' scenario (DO in the aerobic reactor=1 mg O_2 L^{-1}), the parameters describing the AOB activity were the most sensitive. Under these low-DO conditions, the NOB growth is inhibited (Fig. 4B). The plant performs partial nitrification (section 3.1) and, subsequently, the NOB parameters lose their sensitivity.

For both simulated operational modes, the sensitivity of the anoxic growth factor (η_G) (i.e. the stoichiometric factor involved in the anoxic growth of heterotrophs and PAOs) presented an important sensitivity. It is indeed a parameter whose change will considerably affect the model stoichiometry because it participates in all the anoxic processes. Furthermore, it can be linked to the N_2O-EF_{TOTAL} since the anoxic conditions are those that potentially lead to N_2O consumption through denitrification. Another interesting observation is that the SE was only in the 17th and 20th place in the parameter ranking of the high- and low-DO scenario, respectively. As shown in Fig. 6, the SE increase substantially affected the N_2O-EF_{TOTAL} while rising from 0 to 0.2. Its additional increase from 0.2 up to 1 had a minor effect on the EF. During the SA simulations, the SE was within the 0.2-1 range. Its relative sensitivity would have been higher if its reference value had been below 0.2. In addition, the conversion factors referring to the N-content (i_{NXS}, i_{NSF}) of state variables X_S and S_F were found closely linked to the N_2O-EF_{TOTAL}. Given that they are implicated in the N_{IN} calculation (Eq. 2), they do influence the estimation of the N_2O-EF_{TOTAL} (Eq. 1.1).

Next, Table 4 was re-observed from another perspective: to find if any of the model parameters appear with an important sensitivity (i.e. within the first ten places of the parameter ranking) for both scenarios. The η_G, the $q_{AOB\_N2O\_ND}$ (maximum N_2O production rate for the nitrifier denitrification pathway), the Y_{PAO} (PAOs yield coefficient) and the Y_H (yield coefficient for the heterotrophs) appeared in the first ten places for both simulated operational modes; all with a positive sensitivity index. Hence, decreasing their values coincides with a decrease of the N_2O-EF_{TOTAL}. The η_G, Y_{PAO} and Y_H, precisely, are included in the stoichiometry of processes happening under anoxic conditions. In this anoxic environment, N_2O can be consumed via heterotrophic denitrification, thus leading to a lower final EF. Finally, the $q_{AOB\_N2O\_ND}$ kinetic parameter emerged as highly sensitive for both scenarios. It describes the N_2O production rate for the nitrifier denitrification pathway. With its sensitivity being high for both the high- and the low-DO scenario, nitrifier denitrification is probably the most important N_2O hotspot while designing N_2O mitigation strategies.

4. Conclusions

This chapter was dedicated to the development of an ASM-type model describing the COD, N and P removal for a municipal full-scale A^2/O WWTP. More importantly, the model incorporated all the biological pathways for N_2O production to analyse the N_2O dynamics and estimate the resulting EF of the plant. The most substantial conclusions are provided below:

- Low or intermittent aeration strategies are frequently adopted with a view to reducing the energy requirements of WWTPs. According to the developed model, the application of an aerobic DO from 0.8 to 1.8 mg O_2 L^{-1} will promote the AOB activity over the NOB one. Hence, the system will move from full to partial nitrification. Subsequently, NO_2^- accumulation will be noted resulting in N_2O production via nitrifier denitrification. The latter can lead to a high overall C-footprint for the WWTP considering the significant N_2O GWP. Therefore, operation under decreased aeration is desired only to the extent that it does not hinder the completion of the nitrification process.
- An SE factor (ranging from 0 to 1) was used to depict the divergence of the stripping modelling from the actual striping process. Lower SE values allowed the maintenance of higher N_2O concentrations in the mixed liquor. The latter enhanced N_2O consumption through denitrification.
- An increase of the influent NH_4^+ concentration from 20 to 30 mg NH_4^+-N L^{-1} on the 10th day of the WWTP operation was simulated under various SE and DO values to see the effect on the N_2O emissions. Higher EFs were noted in the low-DO cases that were favourable to nitrifier denitrification. Moreover, this concurred with the application of high SEs that reflected a more intense stripping.
- The SA revealed that the NOB-related parameters had no significant effect over the N_2O-EF while examining a low-DO scenario due to absence of NOB growth. On the contrary, they emerged as highly important under the high-DO condition since they influence the NO_2^- oxidation. n_G, $q_{AOB\_N2O\_ND}$, Y_{PAO} and Y_H were in the top ten places of the parameter ranking for both the high- and the low-DO scenario.

n_G, Y_{PAO} and Y_H affect the N_2O-EF since they relate to N_2O consumption through denitrification. Finally, the high sensitivity of the $q_{AOB\_N2O\_ND}$ parameter points out to the fact that nitrifier denitrification is likely to be the most contributive N_2O production pathway.

References

Aboobakar, A., Cartmell, E., Stephenson, T., Jones, M., Vale, P., Dotro, G., 2013. Nitrous oxide emissions and dissolved oxygen profiling in a full-scale nitrifying activated sludge treatment plant. Water Res. 47: 524-534.

Ahn, J.H., Kim, S., Park, H., Rahm, B., Pagilla, K., Chandran, K., 2010. N_2O emissions from activated sludge processes, 2008-2009: results of a national monitoring survey in the United States. Environ. Sci. Technol. 44: 4505-4511.

Bae, W., Baek, S., Chung, J., Lee, Y., 2001. Optimal operational factors for nitrite accumulation in batch reactors, Biodegradation. 12: 359-366.

Blackburne, R., Yuan, Z., Keller, J., 2008. Partial nitrification to nitrite using low dissolved oxygen concentration as the main selection factor. Biodegradation. 19: 303-312.

Capela, S., Roustan, M., Heduit, A., 2001. Transfer number in fine bubble diffused aeration systems. Water Sci. Technol. 43: 145-152.

Chandran, K.; Stein, L.Y.; Klotz, M.G.; van Loosdrecht, M.C.M., 2011. Nitrous oxide production by lithotrophic ammonia-oxidizing bacteria and implications for engineered nitrogen-removal systems. Biochem. Soc. Trans. 39: 1832-1837.

Ciudad, G., Rubilar, O., Muñoz, P., Ruiz, G., Chamy, R., Vergara, C., Jeison, D., 2005. Partial nitrification of high ammonia concentration wastewater as a part of a shortcut biological nitrogen removal process. Process Biochem. 40: 1715-1719.

Daelman, M.R.J., De Baets, B., van Loosdrecht, M.C.M., Volcke, E.I.P., 2013. Influence of sampling strategies on the estimated nitrous oxide emission from wastewater treatment plants. Water Res. 47: 3120-3130.

Desloover, J., Vlaeminck, S.E., Clauwaert, P., Verstraete, W., Boon, N., 2012. Strategies to mitigate N_2O emissions from biological nitrogen removal systems. Curr. Opin. Biotechnol. 23: 474-482.

Dotro, G., Jefferson, B., Jones, M., Vale, P., Cartmell, E., Stephenson, T., 2011. A review of the impact and potential of intermittent aeration on continuous flow nitrifying activated sludge. Environ. Technol. 32: 1685-1697.

Foley, J., de Haas, D., Yuan, Z., Lant, P., 2010. Nitrous oxide generation in full-scale biological nutrient removal wastewater treatment plants. Water Res. 44: 831-844.

Frison, N., Chiumenti, A., Katsou, E., Malamis, S., Bolzonella, D., Fatone, F., 2015. Mitigating off-gas emissions in the biological nitrogen removal via nitrite process treating anaerobic effluents. J. Clean. Prod. 93: 126-133.

Garrido, J.M., Van Benthum, W.A.J., Van Loosdrecht, M.C.M., Heijnen, J.J., 1997. Influence of dissolved oxygen concentration on nitrite accumulation in a biofilm airlift suspension reactor. Biotechnol. Bioeng. 53: 168-178.

Guisasola, A., Jubany, I., Baeza, J.A., Carrera, J., Lafuente, J., 2005. Respirometric estimation of the oxygen affinity constants for biological ammonium and nitrite oxidation. J. Chem. Technol. Biotechnol. 80: 388-396.

Guisasola, A., Marcelino, M., Lemaire, R., Baeza, J.A., Yuan, Z., 2010. Modelling and simulation revealing mechanisms likely responsible for achieving the nitrite pathway through aeration control. Water Sci. Technol. 61: 1459-1465.

Hauduc, H., Rieger, L., Takács, I., Héduit, A., Vanrolleghem, P.A., Gillot, S., 2010. A systematic approach for model verification: application on seven published activated sludge models. Water Sci. Technol. 61: 825-839.

Henze, M., Gujer, W., Mino, T., van Loosdrecht, M.C.M., 2000. Activated Sludge Models ASM1, ASM2, ASM2d, and ASM3. IWA Scientific and Technical Report n.9., IWA Publishing, London.

Hiatt, W.C., and Grady, C.P.L., 2008. An updated process model for carbon oxidation, nitrification, and denitrification. Water Environ. Res. 80: 2145-2156.

IPCC, 2013. In: Stocker, T.F., Qin, D., Plattner, G.-K., Tignor, M., Allen, S.K., Boschung, J., Nauels, A., Xia, Y., Bex, V., Midgley, P.M. (Eds.), Climate Change 2013: The Physical Science Basis. Contribution of Working Group I to the Fifth Assessment Report of the Intergovernmental Panel on Climate Change. Cambridge University Press, Cam-bridge, United Kingdom and New York, NY, USA (1535 pp.).

Jin, Y., Wang, D., Zhang, W., 2016. Effects of substrates on N_2O emissions in an anaerobic ammonium oxidation (anammox) reactor. Springerplus. 1-12.

Jubany, I., Carrera, J., Lafuente, J., Baeza, J.A., 2008. Start-up of a nitrification system with automatic control to treat highly concentrated ammonium wastewater: Experimental results and modelling. Chem. Eng. J. 144: 407-419.

Jubany, I., Lafuente, J., Baeza, J.A., Carrera, J., 2009. Total and stable washout of nitrite oxidizing bacteria from a nitrifying continuous activated sludge system using automatic control based on Oxygen Uptake Rate measurements. Water Res. 43: 2761-2772.

Kampschreur, M.J., van der Star, W.R.L., Wielders, H.A., Mulder, J.W., Jetten, M.S.M., van Loosdrecht, M.C.M., 2008. Dynamics of nitric oxide and nitrous oxide emission during full-scale reject water treatment. Water Res. 42: 812-826.

Kampschreur, M.J., Temmink, H., Kleerebezem, R., Jetten, M.S.M., van Loosdrecht, M.C.M., 2009. Nitrous oxide emission during wastewater treatment. Water Res. 43: 4093-4103.

Kuenen, J.G., 2008. Anammox bacteria: from discovery to application. Nat. Rev. Microbiol. 6: 320-326.

Law, Y., Ye, L., Pan, Y., Yuan, Z., 2012a. Nitrous oxide emissions from wastewater treatment processes. Philos. Trans. R. Soc. Lond. B. Biol. Sci. 367: 1265-1277.

Law, Y., Ni, B.J., Lant, P., Yuan, Z., 2012b. N_2O production rate of an enriched ammonia-oxidising bacteria culture exponentially correlates to its ammonia oxidation rate. Water Res. 46: 3409-3419.

Law, Y., Lant, P., Yuan, Z., 2013. The confounding effect of nitrite on N_2O production by an enriched ammonia-oxidizing culture. Environ. Sci. Technol. 47: 7186-7194.

Lide, D.R., 2007. CRC Handbook of Chemistry and Physics. 87th ed., CRC Press/Taylor and Francis Group, Boca Raton.

Lim, Y., and Kim, D.J., 2014. Quantification method of N_2O emission from full-scale biological nutrient removal wastewater treatment plant by laboratory batch reactor analysis. Bioresour. Technol. 165: 111-115.

Machado, V.C., Lafuente, J.J., Baeza, J.A., 2014. Activated sludge model 2d calibration with full-scale WWTP data: Comparing model parameter identifiability with influent and operational uncertainty. Bioprocess Biosyst. Eng. 37: 1271-1287.

Mampaey, K.E., Beuckels, B., Kampschreur, M.J., Kleerebezem, R., van Loosdrecht, M.C.M., Volcke, E.I.P., 2013. Modelling nitrous and nitric oxide emissions by autotrophic ammonia-oxidizing bacteria. Environ. Technol. 34: 1555-1566.

Mannina, G., Cosenza, A., Di Trapani, D., Laudicina, V.A., Morici, C., Ødegaard, H., 2016. Nitrous oxide emissions in a membrane bioreactor treating saline wastewater contaminated by hydrocarbons. Bioresour. Technol. 219: 289-297.

Marques, R., Rodríguez-Caballero, A., Oehmen, A., Pijuan, M., 2016. Assessment of online monitoring strategies for measuring N_2O emissions from full-scale wastewater treatment systems. Water Res. 99: 171-179.

Ni, B.J., Ruscalleda, M., Pellicer-Nàcher, C., Smets, B.F., 2011. Modelling Nitrous Oxide Production during Biological Nitrogen Removal via Nitrification and Denitrification: Extensions to the General ASM Models. Environ. Sci. Technol. 45: 7768-7776.

Ni, B.J., Ye, L., Law, Y., Byers, C., Yuan, Z., 2013. Mathematical modelling of nitrous oxide (N_2O) emissions from full-scale wastewater treatment plants. Environ. Sci. Technol. 47: 7795-7803.

Ni, B.J., Peng, L., Law, Y., Guo, J., Yuan, Z., 2014. Modelling of Nitrous Oxide Production by Autotrophic Ammonia-Oxidizing Bacteria with Multiple Production Pathways. Environ. Sci. Technol. 48: 3916-3924.

Ni, B.J. and Yuan, Z., 2015. Recent advances in mathematical modelling of nitrous oxides emissions from wastewater treatment processes. Water Res. 87: 336-346.

Ni, B.J., Pan, Y., Van Den Akker, B., Ye, L., Yuan, Z., 2015. Full-Scale Modelling Explaining Large Spatial Variations of Nitrous Oxide Fluxes in a Step-Feed Plug-Flow Wastewater Treatment Reactor. Environ. Sci. Technol. 49: 9176-9184.

Pan, Y., Ni, B.J., Yuan, Z., 2013. Modelling electron competition among nitrogen oxides reduction and N_2O accumulation in denitrification. Environ. Sci. Technol. 47: 11083-11091.

Pan, M., Hu, Z., Liu, R., Zhan, X., 2015. Effects of loading rate and aeration on nitrogen removal and N_2O emissions in intermittently aerated sequencing batch reactors treating slaughterhouse wastewater at 11 ºC. Bioprocess Biosyst. Eng. 38: 681-689.

Peng, Y., and Zhu, G., 2006. Biological nitrogen removal with nitrification and denitrification via nitrite pathway. Appl. Microbiol. Biotechnol. 73: 15-26.

Peng, L., Ni, B.J., Erler, D., Ye, L., Yuan, Z., 2014. The effect of dissolved oxygen on N_2O production by ammonia-oxidizing bacteria in an enriched nitrifying sludge. Water Res. 66: 12-21.

Peng, L., Ni, B.J., Ye, L., Yuan, Z., 2015. The combined effect of dissolved oxygen and nitrite on N_2O production by ammonia oxidizing bacteria in an enriched nitrifying sludge. Water Res. 73: 29-36.

Pijuan, M., Torà, J., Rodríguez-Caballero, A., César, E., Carrera, J., Pérez, J., 2014. Effect of process parameters and operational mode on nitrous oxide emissions from a nitritation reactor treating reject wastewater. Water Res. 49: 23-33.

Pocquet, M., Wu, Z., Queinnec, I., Spérandio, M., 2016. A two-pathway model for N_2O emissions by ammonium oxidizing bacteria supported by the NO/N_2O variation. Water Res. 88: 948-959.

Rathnayake, R.M.L.D., Oshiki, M., Ishii, S., Segawa, T., Satoh, H., Okabe, S., 2015. Effects of dissolved oxygen and pH on nitrous oxide production rates in autotrophic partial nitrification granules. Bioresour. Technol. 197: 15-22.

Ravishankara, A.R., Daniel, J.S., Portmann, R.W., 2009. Nitrous Oxide (N_2O): The dominant ozone-depleting substance emitted in the 21st century. Science. 326: 123 LP-125.

Reichert, P., Vanrolleghem, P.A., 2001. Identifiability and uncertainty analysis of the river water quality model no. 1 (RWQM1). Water Sci. Technol. 43: 329-338.

Rodríguez-Caballero, A., Aymerich, I., Poch, M., Pijuan, M., 2014. Evaluation of process conditions triggering emissions of green-house gases from a biological wastewater treatment system. Sci. Total Environ. 493: 384-391.

Rodríguez-Caballero, A., Aymerich, I., Marques, R., Poch, M., Pijuan, M., 2015. Minimizing N_2O emissions and carbon footprint on a full-scale activated sludge sequencing batch reactor. Water Res. 71: 1-10.

Ruiz, G., Jeison, D., Chamy, R., 2003. Nitrification with high nitrite accumulation for the treatment of wastewater with high ammonia concentration. Water Res. 37: 1371-1377.

Soliman, M., and Eldyasti, A., 2016. Development of partial nitrification as a first step of nitrite shunt process in a Sequential Batch Reactor (SBR) using Ammonium Oxidizing Bacteria (AOB) controlled by mixing regime. Bioresour. Technol. 221: 85-95.

Tallec, G., Garnier, J., Billen, G., Gousailles, M., 2006. Nitrous oxide emissions from secondary activated sludge in nitrifying conditions of urban wastewater treatment plants: Effect of oxygenation level. Water Res. 40: 2972-2980.

Takács, I., Patry, G.G., Nolasco, D., 1991. A dynamic model of the clarification-thickening process. Water Res. 25: 1263-1271.

Turk, O., and Mavinic, D.S., 1987. Benefits of using selective inhibition to remove nitrogen from highly nitrogenous wastes. Environ. Technol. Lett. 8: 419-426.

Wiesmann, U., 1994. Biological nitrogen removal from wastewater. In: A. Fiechter (Eds.), Advances in Biochemical Engineering Bio- technology. Springer-Verlag, Berlin, pp. 113-154.

Wunderlin, P., Mohn, J., Joss, A., Emmenegger, L., Siegrist, H., 2012. Mechanisms of N_2O production in biological wastewater treatment under nitrifying and denitrifying conditions. Water Res. 46: 1027-1037.

Wunderlin, P., Lehmann, M.F., Siegrist, H., Tuzson, B., Joss, A., Emmenegger, L., Mohn, J., 2013. Isotope Signatures of N_2O in a Mixed Microbial Population System: Constraints on N_2O Producing Pathways in Wastewater Treatment. Environ. Sci. Technol. 47: 1339-1348.

Chapter III

Modelling the nitrous oxide emission in a full-scale activated sludge sequencing batch reactor

Summary

The development of mathematical tools describing the N_2O dynamics in WWTPs under changing operating conditions will enhance the emission mitigation as well as the optimised plant design and operation. Real N_2O emission data from the full-scale municipal SBR plant of La Roca del Valles (Barcelona, Spain) were used in order to: (i) develop and calibrate an ASM-type model describing the N_2O dynamics of full-scale municipal SBRs, (ii) investigate if the trends of the real N_2O emission data can be successfully described by simulating the plant operation under DO setpoints lower than those reported during the monitoring campaign. The widely accepted ASM1 structure was now expanded and modified in the following way: adaptation to an SBR configuration performing COD and N removal, in addition to the inclusion of the biological and abiotic N_2O production. During the plant operation, two different cycle types were applied and monitored in terms of N_2O emissions; cycles of type B and C. Cycle B involved the alternation amongst two non-aerated (25-40 min) and two aerobic phases (15-40 min). The reaction phase for Cycle C included the sequence of two shorter non-aerated phases (25-29 min) with a longer aerobic one (66 min) between them. Both the experimental data and the developed model linked the emissions with air flow or, equivalently, with the aerobic phases. The representative DO profiles of cycles B and C as recorded by the La Roca del Valles WWTP operators [i.e. Cycle type B: DO=2.3 mg O_2 L^{-1} (1st aerobic phase)/1.9 mg O_2 L^{-1} (2nd aerobic phase), Cycle type C: DO=2.3 mg O_2 L^{-1} (single aerobic phase)] were used to calibrate the developed model while simulating cycles B and C. The calibrated model agreed well with the provided N_2O emission monitoring data. Hence, it was considered representative enough of the La Roca WWTP operation, thus allowing

its use for further simulations to explore if the monitored emission profiles can be satisfactorily described while simulating operation under different DOs. The optimal fit was attained under a DO setpoint of 1.6 mg O_2 L^{-1} for both aerobic phases of Cycle B and for a DO of 1.7 mg O_2 L^{-1} for the single aerobic phase of Cycle C. The latter DO values were lower than the respective DO profiles reported by the plant operators during the monitoring campaign. However, slight divergences in the 2nd emission peak of Cycle B were observed. The latter can be attributed to an actual N_2O denitrification rate lower than the value predicted by the model. Therefore, a higher final N_2O concentration was observed at the end of the non-aerated phase during the monitoring campaign with this N_2O amount being stripped at the beginning of the consequent (2nd) aerobic phase of Cycle B. Furthermore, the total N_2O EF predicted by the developed model differed between the two cycle types: 0.8% (Cycle B) and 1.5% (Cycle C). Although the total duration of aeration was approximately the same (Cycle B: 60 min; Cycle C: 66 min), the difference in the cycle configuration impacted on the final N_2O EF. The single longer aerobic phase of Cycle C enhanced the N_2O production via the nitrification-related routes and its subsequent emission through stripping for a slightly longer and non-interrupted period. Moreover, the N_2O production occurred only during the aerobic phases with the N_2O concentration peaks coinciding with the NO_2^- peaks for both cycles. Consequently, it can be concluded that nitrifier denitrification was the predominant AOB pathway for N_2O generation. The optimal fit was obtained for a rather low DO setpoint (1.6 mg O_2 L^{-1} for cycle B and 1.7 mg O_2 L^{-1} for cycle C). This observation agrees with past findings regarding the AOB pathways' relative contribution; compared to incomplete NH_2OH oxidation, nitrifier denitrification has been suggested as increasingly contributing with the

DO decrease. Finally, no important NH_2OH consumption was noted, thus suggesting that the abiotic routes were poorly preferred under the conditions of the current study.

Keywords

N_2O emissions, SBR, full-scale modelling, real full-scale N_2O emission data, cycle configuration

1. Introduction

During wastewater treatment, GHGs, including CO_2, N_2O and CH_4, can be produced and emitted (Lijó et al., 2017). The calculation of indirect CO_2 emission relates to the energy consumption of a WWTP, whereas direct CO_2 emission occurs during all the treatment stages. CH_4 emission is mainly noted in the sewerage and sludge treatment compartments (IPCC, 2007). N_2O production and emission is mostly observed during the BNR (Pan et al., 2016). In a period of 100 years, N_2O presents the highest GWP among the GHGs. Compared to the GWP of CO_2, N_2O's GWP is 265-298 times higher, whereas CH_4 has a GWP only 28-36 times higher (IPCC, 2014). Moreover, it is estimated that direct N_2O emissions in WWTPs influence the total GWP of the water cycle (considered as the sum of drinking water production, wastewater treatment and effluent discharge, sludge processing and disposal) by 26% (Frijns et al., 2008). Furthermore, the wide variation in N-loads, influent characteristics and operational/environmental conditions amongst WWTPs justify the variability of N_2O production and emission (Kampschreur et al., 2009; Yang et al., 2009; Ahn et al., 2010; Law et al., 2012; Wang et al., 2014; Li et al., 2015).

Within this context, the online monitoring of N_2O emissions in full-scale WWTPs with different configurations has gained importance in recent years (Rodriguez-Caballero et al., 2015). For instance, Daelman et al. (2013) examined 416-day emission data from a full-scale fully covered municipal WWTP in the Netherlands. They stressed the significance of long-term sampling to successfully describe the average N_2O dynamics, along with the necessity for online monitoring to capture the diurnal trends. Aboobakar et al. (2013) studied 8-week, continuous, online monitoring data of dissolved and gaseous

N_2O, DO and NH_4^+ loading in a full-scale nitrifying AS plant in the UK. The results showed that the diurnal and spatial variability of the N_2O emissions had a direct correlation with the DO levels. The reported N_2O emissions were translated into over 34,000 CO_2 equivalents year^{-1}, thus adding 13% to the C-footprint resulting from the energy requirements of the monitored plant. Hence, the authors emphasized the need to further investigate and understand the emission patterns by applying real-time control with a view to achieving efficient, low-energy operation and N_2O emission mitigation. Moreover, N_2O emission was monitored for ten weeks in a municipal plug-flow full-scale WWTP in Spain (Rodriguez-Caballero et al., 2014). The dynamics of the N_2O emission were found to be highly variable due to the instability of the nitrification process within the bioreactor. Abrupt aeration stops in the nitrifying zones caused emission peaks that increased the overall plant EF. Furthermore, the analysis of the 12-month online emission data from a full-scale municipal WWTP in Finland revealed strong correlation of the diurnal N_2O emission with the changes in the influent biological oxygen demand and the NH_4^+ load in the aerobic zones (Kosonen et al., 2016). Finally, Spinelli et al. (2018) presented a critical analysis of the online monitored N_2O emissions in a full-scale MLE municipal WWTP in Italy. According to their observations, the emission hotspots occurred under conditions of low COD:N and increased stripping.

In this regard, the development of mathematical tools describing the N_2O dynamics in WWTPs under changing operating conditions will enhance the emission mitigation as well as the optimised WWTP design and operation. The use of full-scale emission data to calibrate and validate such dynamic models is essential to predict the extent of the emissions as well as the operating conditions that shall be applied to ensure the emission

mitigation (Mannina et al., 2016; Pocquet et al., 2016). The IWA ASM models (Henze et al., 2000) are commonly accepted for the description of COD and nutrient removal in WWTPs. However, they disregard N_2O production and quantification. In terms of biological N_2O production during the BNR in WWTPs, the major pathways are three and related to the biochemical processes of nitrification-denitrification: nitrifier denitrification, incomplete NH_2OH oxidation and heterotrophic denitrification; the first two routes are activated by the AOB (Wunderlin et al., 2012; Rodriguez-Caballero et al., 2015). Considering that biological N_2O production is generally regarded as the main hotspot in WWTPs, N_2O emission linked to abiotic N_2O production is often underestimated although it can occur to a non-negligible extent. The following pathways have been suggested, especially under conditions of acidic pH (e.g. pH≤5): (i) the NH_2OH produced during nitrification can form nitroxyl (HNO) which reacts with hyponitrous acid ($H_2N_2O_2$) to generate N_2O and H_2O, and (ii) the nitrosation of NH_2OH (with HNO_2 as nitrosation agent) that can form N_2O inside nitritation reactors. Apart from the importance of the pH parameter however, recent studies have concluded that further research is needed to discover other potentially significant factors. Moreover, the research on the determination of the process rates, kinetic parameter values, potential participating enzymes/catalysts, as well as of the N_2O amount produced through the abiotic pathways in biological systems is still ongoing (Schreiber et al., 2012; Harper et al., 2015; Domingo-Félez and Smets, 2016, 2019; Soler-Jofra et al., 2016; Su et al., 2019).

Real N_2O emission data from the full-scale municipal SBR plant of La Roca del Valles (Barcelona, Spain) used in a previous study by Rodriguez-Caballero et al. (2015) were provided. The aims of this chapter were: (i) to create an ASM-type model describing

the N_2O dynamics of full-scale municipal SBR plants, (ii) calibrate the developed model with the provided data, and (iii) use the calibrated model version to test if the emission data trends can be successfully described under lower DOs than those reported during the monitoring campaign. To attain these objectives, the widely accepted ASM1 structure that has been suggested by the IWA to describe organic matter oxidation and the processes of nitrification and denitrification was used but expanded and modified in the following way: adaptation to an SBR configuration performing COD and N removal, in addition to the inclusion of the biological and abiotic N_2O production.

2. Materials and Methods

2.1. Brief description of the WWTP

The real N_2O emission data used in the current study were obtained during the online monitoring of the full-scale municipal WWTP of La Roca del Valles (Barcelona, Spain). The plant has a capacity of 48,000 P.E. (Rodriguez-Caballero et al., 2015). A schematic representation of the La Roca del Valles WWTP is provided in Fig. 9.

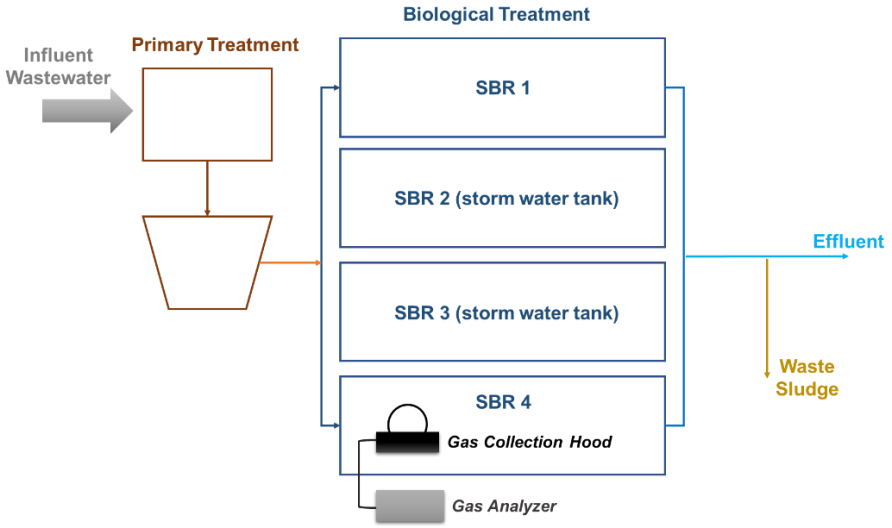

Figure 9: Schematic representation of the full-scale municipal WWTP of La Roca del Valles (Barcelona, Spain; 48,000 P.E.) (adapted by Rodriguez-Caballero et al., 2015).

The La Roca WWTP includes a primary treatment unit followed by a biological treatment section (with four identical SBRs) where COD and N removal is performed. The working volume of each SBR is 4,684 m^3. After decantation, the effluent is discharged to the receiving river. Furthermore, there is a line of waste sludge that is withdrawn to undergo external treatment (Rodriguez-Caballero et al., 2015).

2.2 Different cycle configurations and SBR operation

As seen in Fig. 9, only two of the SBRs (i.e. SBR 1 and SBR 4) were operating during the monitoring period, while the other two (i.e. SBR 2 and SBR 3) were used as storm water storage tanks. The SBRs functioned under different cycle configurations with a total duration of 260-265 min including a reaction phase of 120-125 min, continuing with settling and decanting of 65 min each. When the SBR 1 was in the reaction phase, the

SBR 4 was in the decanting stage and vice versa. Hence, the operators were able to perform continuous wastewater treatment. The wastewater was treated in an alternation of aerobic and non-aerated phases whose number, length and sequence depended upon the cycle configuration applied each time (see Fig. 10) (Rodriguez-Caballero et al., 2015).

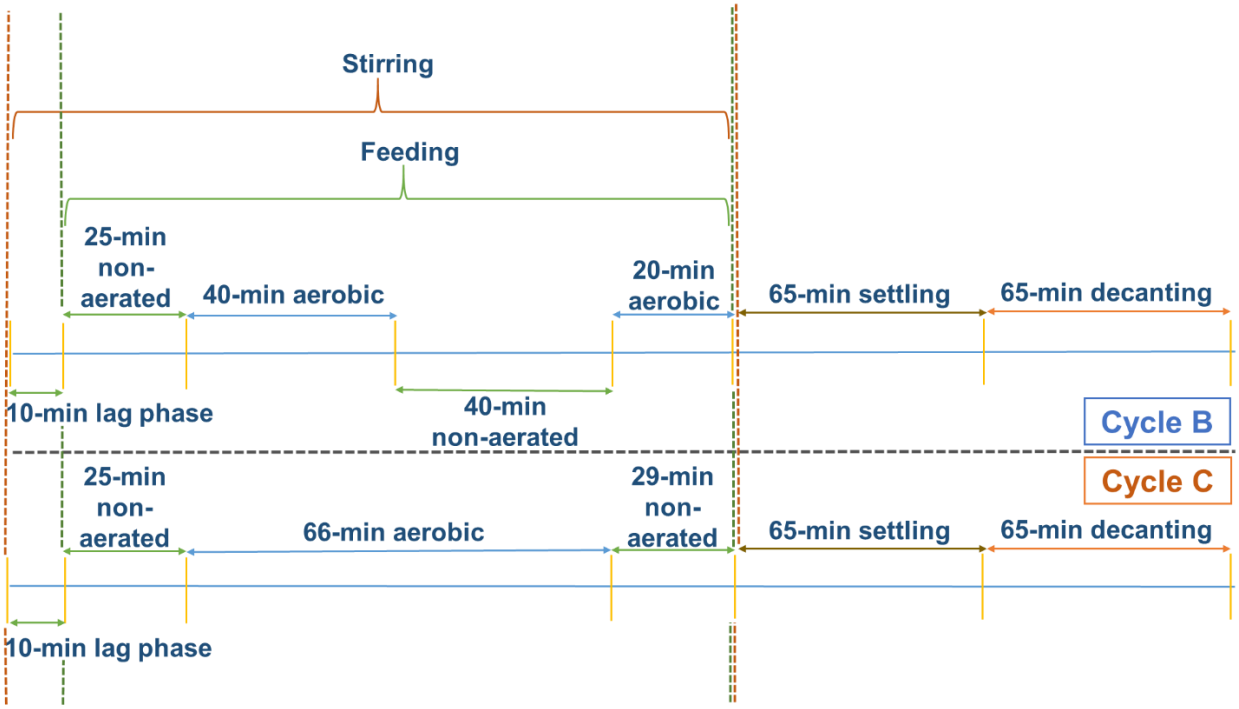

Figure 10: The different cycle configurations (i.e. Cycle B and Cycle C) that were applied in the full-scale municipal WWTP of La Roca del Valles (Barcelona, Spain) and simulated in the developed model (adapted by Rodriguez-Caballero et al., 2015).

During the plant operation, two different cycle types were applied and monitored in terms of N_2O emissions; cycles of type B and cycles of type C. They both began with a 10-min lag phase during which the mixed liquor was stirred before the feeding started. Cycle B involved the alternation amongst two non-aerated (25-40 min) and two aerobic phases (15-40 min). The reaction phase for Cycle C included the sequence of two shorter

non-aerated phases (25-29 min) with a long aerobic one (66 min) between them (see Fig. 10) (Rodriguez-Caballero et al., 2015).

2.3 Online monitoring of N_2O emissions

Continuous online monitoring of the N_2O emissions was conducted for 33 days from February to March 2014 for the SBR 4 (Fig. 9). During this period, a total of 143 cycles was recorded. Gas from the SBR was collected using a commercial gas collection hood (AC'SCENT® Flux Hood) that was connected to a commercial gas analyzer (VA-3000, Horiba, Japan). Moreover, the gas analyzer included a sample conditioning system (series CSS, M&C Tech group). The off gas was continually captured from the bioreactor headspace (at 0.5 L air min^{-1}, precisely), with the obtained data being recorded every 15 s. Furthermore, data revealing the dissolved N_2O trends were logged via a microsensor (In Situ Amplifier System, Unisense A/S, Aarhus, Denmark) (Rodriguez-Caballero et al., 2015).

2.4. Analyses of the wastewater samples

Details on the operational parameters and wastewater characteristics in the influent, bioreactor and effluent are provided in Table 5.

Table 5: Operating parameters and influent, AS and effluent characteristics (adapted by Rodriguez-Caballero et al., 2015).

Parameter	Average value ± standard deviation
Influent	
Flow ($m^3 d^{-1}$) *	6553 ± 228
COD (mg L^{-1}) *	604 ± 37
TKN (mg N L^{-1}) *	69 ± 5
NH_4^+ (mg N-NH_4^+ L^{-1}) *	39 ± 2
TP (mg P L^{-1}) *	7.5 ± 0.5
pH	7.7 ± 0.04
Bioreactor	
NH_4^+ (mg N-NH_4^+ L^{-1}) *	8 ± 5
NO_2^- (mg N-NO_2^- L^{-1}) **	0.5 ± 0.03
NO_3^- (mg N-NO_3^-- L^{-1}) **	<0.06
MLSS (mg L^{-1}) *	3100 ± 58
MLVSS/MLSS (%)	81 ± 0.5
HRT (d)	1.5 ± 0.02
SRT (d)	26 ± 2
Temperature (^oC) *	20 ± 0.5
Effluent	
COD (mg L^{-1}) *	66 ± 8
TKN (mg N L^{-1}) *	7.5 ± 0.8
NH_4^+ (mg N-NH_4^+ L^{-1}) *	3.3 ± 0.6
TP (mg P L^{-1}) *	1.4 ± 0.1
* Provided either by the operators (2-3 samples per week), or by the automatic control system/online sensors installed in the plant.	
** Average values resulting from the chemical analyses. Samples were grabbed in 20 different SBR cycles (sampling frequency: 20-120 min).	

Samples taken from the influent wastewater as well as from the treated effluent were analyzed in terms of their COD, TKN and NH_4^+ content. Moreover, the MLSS, MLVSS, NH_4^+, NO_2^- and NO_3^- were monitored in the bioreactor. Automatic refrigerated samplers were used to take grab samples from the mixed liquor with a frequency varying between 20 and 120 min (depending on the cycle) to measure the concentrations of the

N-compounds (i.e. NH_4^+, NO_2^- and NO_3^-). First, the samples were filtered though Millipore filter units (0.22 mm pore size). Then, they were characterized according to the standard methods (APHA, 1998), or the method of ion chromatography for the NO_2^- and NO_3^- ions. Moreover, the NH_4^+ concentration was monitored throughout the plant operation both at the influent entry point and within the SBR using two online ion-selective electrodes (ammo::lyser™) linked to a monitoring station (S::CAN Messtechnik GmbH, Austria). While the monitoring campaign was taking place at the SBR 4, a portable DO sensor equipped with a thermometer (YSI Inc. USA) was utilized to record DO and temperature (Rodriguez-Caballero et al., 2015).

2.5 Model description

The kinetic model was developed to describe the simultaneous N and COD removal for the full-scale municipal SBR WWTP of La Roca del Valles (Barcelona, Spain; 48,000 P.E.) by adapting and extending the IWA ASM1 structure to describe the La Roca SBR operation and the cycle configurations (see Fig. 10) with a view to estimating the N_2O dynamics in a holistic way. The latter was achieved by including not only the biological N_2O pathways (i.e. nitrifier denitrification, incomplete NH_2OH hydroxylamine oxidation and heterotrophic denitrification), but also the proposed abiotic production routes (i.e. NH_2OH decomposition to N_2O, and N-nitrosation of NH_2OH with HNO_2 as nitrosating agent) (Harper et al., 2015; Soler-Jofra et al., 2016; Domingo-Félez and Smets, 2016).

AOB

1. $NH_4^+ + ½\ O_2 \rightarrow NH_2OH + H^+$
2. $NH_2OH + ¾\ O_2 + i_{NBM}\ NH_4^+ \rightarrow NO + 3/2\ H_2O + X_{AOB}$
3. $NO + ¼\ O_2 + ½\ H_2O \rightarrow NO_2^- + H^+$
4. $NH_2OH + 4\ NO \rightarrow NO_2^- + 2\ N_2O + H_2O + H^+$ — NH_2OH oxidation

5a. $NH_2OH + 3\ NO_2^- + 3\ H^+ \rightarrow 4\ NO + 3\ H_2O$
5b. $NH_2OH + 2\ NO \rightarrow 3/2\ N_2O + 3/2\ H_2O$
[(5a) + 2 * (5b)]/3 = (5)

5. $NH_2OH + NO_2^- + H^+ \rightarrow N_2O + 2\ H_2O$ — Nitrifier denitrification

Heterotrophic Denitrifiers

1. $NO_3^- + 2\ e^- + 2\ H^+ \rightarrow NO_2^- + H_2O$
2. $NO_2^- + e^- + 2\ H^+ \rightarrow NO + H_2O$
3. $NO + e^- + H^+ \rightarrow ½\ N_2O + ½\ H_2O$ — Heterotrophic denitrification pathway
4. $½\ N_2O + e^- + H^+ \rightarrow ½\ N_2 + ½\ H_2O$

Abiotic N_2O production

1. $4NH_2OH \rightarrow N_2O + 2NH_3 + 3H_2O$ — NH_2OH decomposition to N_2O
2. $NH_2OH + HNO_2 \rightarrow N_2O + 2H_2O$ — N-nitrosation of NH_2OH (HNO_2 as nitrosating agent)

Figure 11: The five pathways for the N_2O production considered in the model: NH_2OH oxidation pathway (AOB-biological), nitrifier denitrification (AOB-biological), heterotrophic denitrification (biological), NH_2OH decomposition to N_2O (abiotic), and N-nitrosation of NH_2OH with HNO_2 as nitrosating agent (abiotic) (adapted by Domingo-Félez and Smets, 2016).

The final model was developed in Matlab® and solved using the *ode15s* function that is a variable order method recommended for stiff systems. Steady-state, especially for the particulate components, was achieved by running the model for a high number of cycles (i.e. >200). Tables presenting the stoichiometric and kinetic parameters, the model

stoichiometry, and the process rates of the integrated processes are given in detail in the Accompanying Material section.

2.6 N_2O EF modelling

After running the model for a high number of cycles (i.e. >200) to ensure that the simulated system had reached steady state conditions (especially for the particulate components of the model), the N_2O EF resulting from the last cycle was calculated in the following way: considering both the stripped N_2O and the N_2O in the effluent. This approach was regarded the most conservative possible estimation ($N_2O\text{-}EF_{TOTAL}$, Eq. 1), as first suggested and analysed in the previous chapter:

$$\mathbf{N_2O\text{-}EF_{TOTAL}}(\%) = \mathbf{100} \cdot \frac{\mathbf{N_2O_{ST}+N_2O_{EFF}}}{\mathbf{N_{IN}}}$$

(Equation 1)

Where N_2O_{ST} is the amount of N_2O stripped from the reactor, N_2O_{EFF} the N_2O in the effluent of the SBR and N_{IN} the total N-content of the influent that was calculated according to Eq. 2:

$$\mathbf{N_{IN}\ (g\ N) = V_{FEED} \cdot (S_{NH4} + S_S \cdot i_{NS_S} + X_S \cdot i_{NX_S})}$$

(Equation 2)

Where V_{FEED} is the volume of wastewater that is fed into the reactor (m^3), and with rest of the terms following the ASM1 nomenclature as proposed in the study of Henze et al. (2000): S_{NH4}, S_S and X_S the influent concentrations for NH_4^+ (g N-NH_4^+ m^{-3}), readily

soluble substrate S_S (g COD m^{-3}) and slowly biodegradable substrate X_S (g COD m^{-3}), respectively. i_{NS_S} and i_{NX_S} are defined as the N-content (g N g^{-1} COD) of S_S and X_S, respectively.

The N_2O in the effluent (N_2O_{EFF}) was calculated using the volume of the water extracted from the SBR $V_{EXTRACT}$ (m^3) and the N_2O concentration (g N-N_2O m^{-3}) in the last cycle ($N_2O_{LAST\ CYCLE}$) as in Eq. 3:

$$\mathbf{N_2O_{EFF}\ (g\ N - N_2O) = V_{EXTRACT} \cdot N_2O_{LAST\ CYCLE}}$$

(Equation 3)

A separate section in the Matlab code was dedicated to the SBR function inside which the changing SBR volume during its operation (i.e. V in m^3) and the accumulation of the N_2O stripped in each cycle (i.e. N_2O_{ST} in g N-N_2O) were simulated as extra variables. For the purposes of the stripping modelling, the volumetric mass transfer coefficient for N_2O (i.e. k_La_{N2O} in d^{-1}) along with the SE factor were implemented. SE values in the range 0-1 were applied to investigate the impact of this typical modelling approach on the N_2O EF. The volumetric mass transfer coefficient (k_La) combines the global transfer coefficient k_L along with the interfacial area a (interphase transport surface between liquid and gas per unit of reactor volume). The k_La_{N2O} resulted from Eq. 4 following Higbie's penetration model (Capela et al., 2001):

$$\mathbf{k_La_{N_2O}(d^{-1}) = k_La_{O_2} \cdot \sqrt{\frac{Dif_{N2O}}{Dif_{O2}}}}$$

(Equation 4)

As seen in Eq. 4, the kLa_{N2O} is correlated with the volumetric mass transfer coefficient of oxygen (i.e. kLa_{O2} in d^{-1}). The latter was automatically calculated by including the DO control system in the model. Dif_{N2O} is the molecular diffusivity of N_2O in water ($2.11 \cdot 10^{-9}$ m^2 s^{-1} at 20 ºC) and Dif_{O2} the molecular diffusivity of oxygen in water ($2.01 \cdot 10^{-9}$ m^2 s^{-1} at 20 ºC) (Lide, 2007).

3. Results and Discussion

3.1 Model calibration

DO plays an important role during the nitrification/denitrification stages. Insufficient DO provision during nitrification, or high DO levels during denitrification have been identified as conditions likely to result in high N_2O emission (Kampschreur et al., 2009; Desloover et al., 2012). Moreover, minor N_2O emissions usually occur during the non-aerated phases of the BNR because of the negligible stripping (Ahn et al., 2010). In accordance with the above, both the experimental data and the developed model linked the emissions with air flow or, equivalently, with the aerobic phases.

Rodriguez-Caballero et al. (2015) provided the representative DO profiles of cycles B and C as recorded by the La Roca del Valles WWTP operators. Precisely, the DO was reported to be around 2.3 mg O_2 L^{-1} during the 1st aerobic phase and approximately equal to 1.9 mg O_2 L^{-1} during the 2nd aerobic phase of cycle B. Furthermore, the long aerobic phase of cycle C was operated under a DO of around 2.3 mg O_2 L^{-1}. These DO data were used to calibrate the developed model while simulating cycles B and C. Within the calibration attempt, the SE parameter was also evaluated.

Finally, all other operating, design, stoichiometric and kinetic parameters of the model were based either upon the detailed plant description by the study of Rodriguez-Caballero et al. (2015), or on relevant past studies (e.g. Henze et al., 2000; Jubany, 2007; Hiatt and Grady, 2008; Jubany et al., 2008; Harper et al., 2015; Pocquet et al., 2016). The only kinetic parameter that was calibrated due to the absence of reliable information on a range of appropriate values was the rate constant $k_{abiotic\_1}$ (in L mg N^{-1} d^{-1}) for the 1st abiotic N_2O production route integrated in the model (i.e. NH_2OH decomposition to N_2O).

The total N_2O emission (in g N-N_2O d^{-1}) for a cycle was an additional simulated variable. The evolution of this variable in time was used for calculating the instantaneous N_2O emission. As seen in Fig. 12, a good fitting to the recorded N_2O emission data occurred under the following coinciding conditions: i) by following the DO profiles of cycles B and C as recorded by the plant operators [i.e. Cycle type B: DO=2.3 mg O_2 L^{-1} (1st aerobic phase)/1.9 mg O_2 L^{-1} (2nd aerobic phase), Cycle type C: DO=2.3 mg O_2 L^{-1} (single aerobic phase)], ii) by testing different SE values in the range 0-1 (an SE=0.11 contributed to a quite successful description of the N_2O emission monitoring data in both cases), and iii) by calibrating the $k_{abiotic\_1}$ at 0.17 L mg N^{-1} d^{-1} for both cycles B and C.

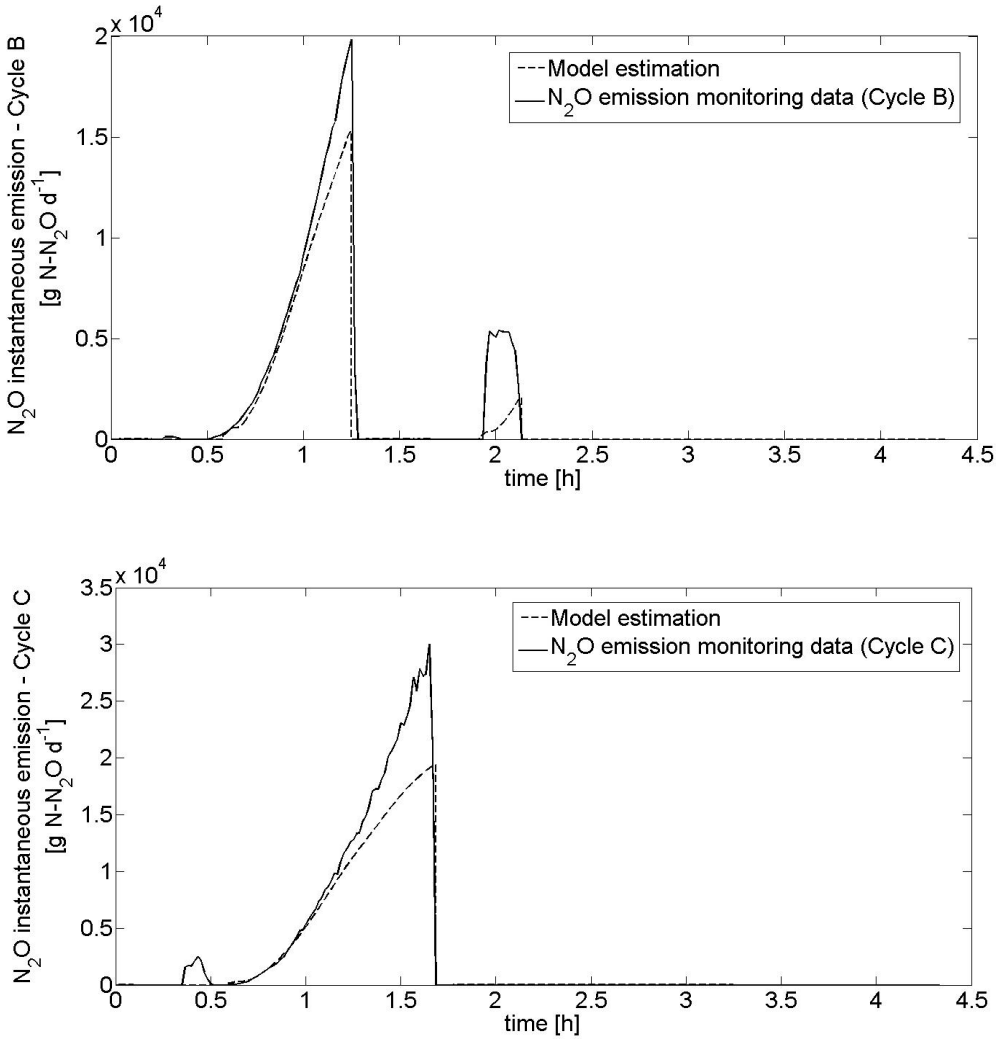

Figure 12: The model estimation concerning the N_2O emission (in g N-N_2O d^{-1}) during cycles B and C compared to the respective N_2O emission monitoring data after calibration.

The calibration was successful as shown in Fig. 12. Precisely, the application of the DO profiles provided by the plant operators, in addition to the calibration of the SE and $k_{abiotic\_1}$ values at 0.11 and 0.17 L mg N^{-1} d^{-1}, respectively, for both cycles were found to give a good description of the N_2O emission monitoring data. Hence, it was assumed that this (calibrated) version of the model was representative enough of the La Roca

WWTP operation, thus allowing its use for further simulations concerning the plant performance.

3.2 Operation of the La Roca WWTP under different DO setpoints

3.2.1 Operation under an optimal DO setpoint during the aerobic phases

According to the Global Water Research Coalition (GWRC), the nitrification-related microbial routes (i.e. the two AOB pathways) are considered as major hotspots for N_2O emissions in full-scale domestic WWTPs (Foley et al., 2011). During nitrification, insufficient aeration has an inhibitory effect (Kampschreur et al., 2009; Desloover et al., 2012), and can therefore lead to increased emissions through the AOB pathways. In this regard, the calibrated version of the developed model that was discussed in section 3.1 was used to re-run the model. This time the simulations were conducted in quest of a different DO setpoint during the aerobic phase(s) of each cycle potentially lower than the DO applied during the plant operation yet ensuring an acceptable description of the N_2O emission monitoring data.

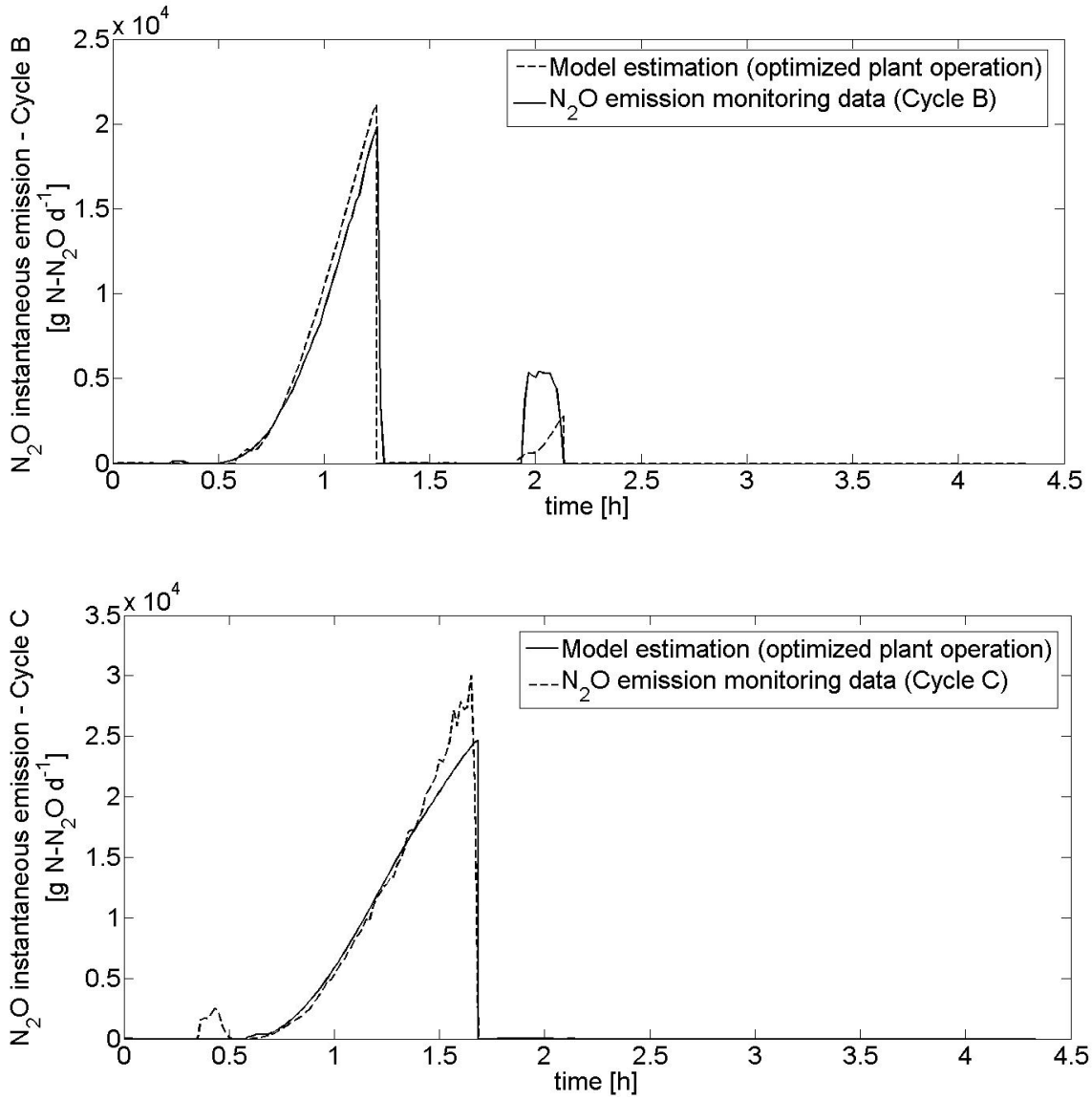

Figure 13: The model estimation concerning the N_2O emission (in g N-N_2O d^{-1}) during cycles B and C compared to the respective N_2O emission monitoring data. The model provided this fit by applying a DO setpoint of 1.6 mg O_2 L^{-1} for both aerobic phases of Cycle B, as well as a DO of 1.7 mg O_2 L^{-1} for the single aerobic phase of Cycle C.

The results after the DO setpoint optimization are shown in Fig. 13 for both cycles B and C. A first observation is that the optimization process generated simulation results that were agreed well with the provided N_2O emission data. This optimal fit was attained

under a DO setpoint of 1.6 mg O_2 L^{-1} during both aerobic phases of Cycle B, as well as a DO of 1.7 mg O_2 L^{-1} for the single aerobic phase of Cycle C. The latter DO values were indeed lower than the respective DO profiles reported by the plant operators during the monitoring campaign; i.e. Cycle type B: DO=2.3 mg O_2 L^{-1} (1st aerobic phase) and 1.9 mg O_2 L^{-1} (2nd aerobic phase), Cycle type C: DO=2.3 mg O_2 L^{-1} (single aerobic phase). To decrease the energy requirements of a plant, operators often test lower DO setpoints and perform advanced N-removal processes (e.g. short-cut nitrification). However, these processes are likely to constitute N_2O hotspots. Hence, it is important to find the minimal DO below which excessive N_2O emission is expected. In this concept, the DO setpoints resulting from these simulations (i.e. 1.6 mg O_2 L^{-1} for both aerobic phases of Cycle B, and 1.7 mg O_2 L^{-1} for the aerobic phase of Cycle C) can be suggested to the La Roca WWTP operators as suitable to achieve operation under lower DOs without risking to observe higher N_2O emissions. Nevertheless, it is noted that this version of the model was unable to precisely capture the emission peak at the beginning of the 2nd aerobic phase of Cycle B (Fig. 13); especially the part of the emissions recorded at the very beginning of the peak. As seen in Fig. 14, the developed model predicts total N_2O consumption via the denitrification happening during the non-aerated phase before the 2nd aerobic phase of Cycle B. However, the respective N_2O emission monitoring data presented a non-negligible N_2O concentration very early in the beginning of the 2nd aerobic phase of Cycle B (Fig. 13). It can be hypothesized that these emissions were recorded because of the stripping of the N_2O not consumed during the previous non-aerated phase. This effect can be related to an actual N_2O denitrification rate during the non-aerated phase lower than the value predicted by the model. Hence, a higher final

N_2O concentration was noted at the end of the non-aerated phase during the monitoring campaign with this N_2O amount being stripped at the beginning of the consequent aerobic phase. This divergence was not observed in cycle C since only one (long) aerobic phase existed in this case (Fig. 14).

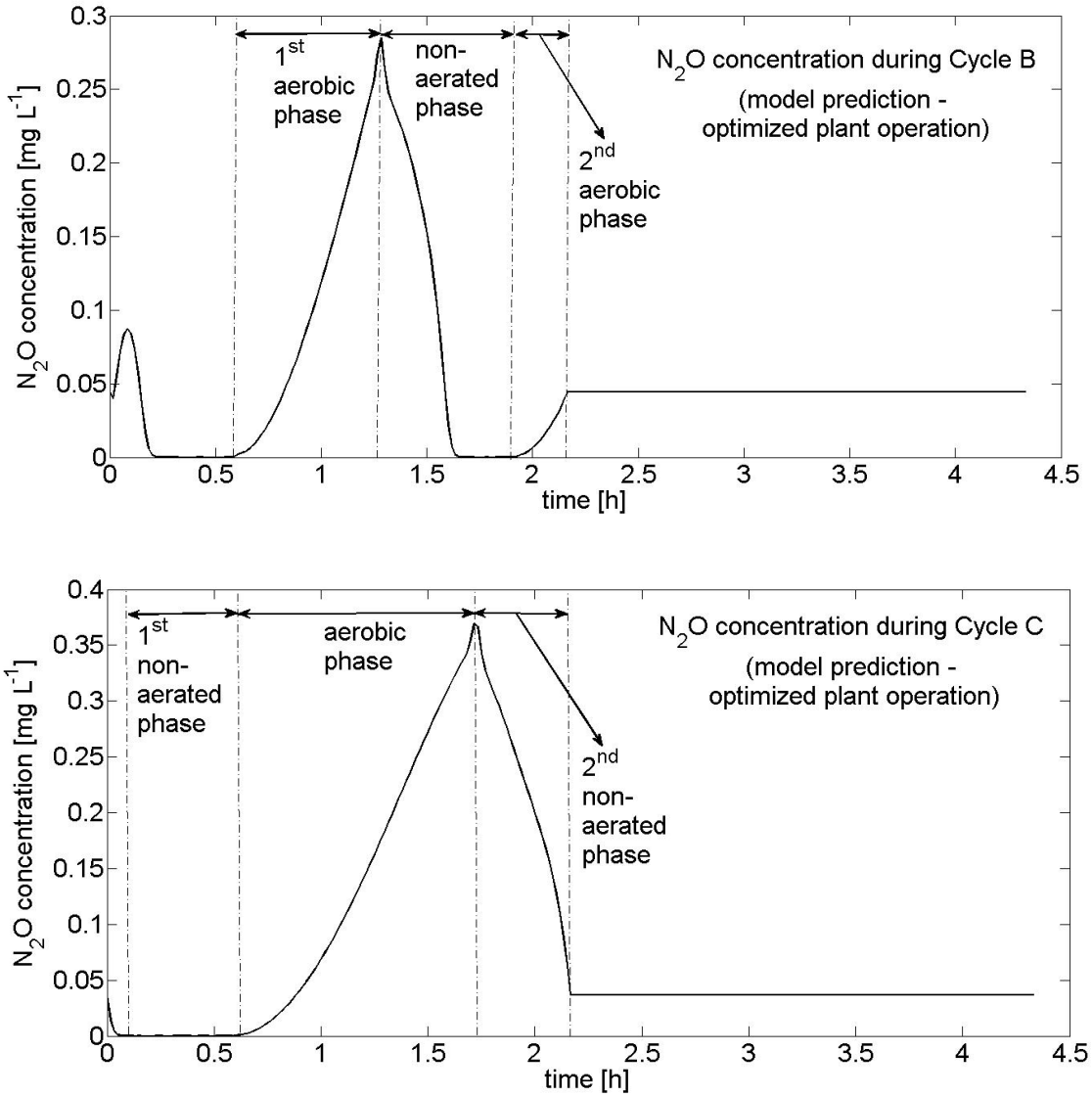

Figure 14: The evolution of the N_2O concentration during Cycles B and C after the DO setpoint optimization according to the developed model.

3.2.2 Plant operation under an optimal DO setpoint: impact of the cycle configuration on the N_2O EF

The total N_2O EF predicted by this last version of the developed model differed between the two cycle types: 0.8% (Cycle B) and 1.5% (Cycle C). Although the total aerobic phase duration is approximately the same for both cycles (Cycle B: 60 min; Cycle C: 66 min), the difference in the cycle configuration possibly impacted on the final N_2O EF. Cycle B included the following sequence of phases: non-aerated (25 min), aerobic (40 min), non-aerated (40 min) and aerobic (20 min). On the contrary, Cycle C had a different cycle configuration: non-aerated (25 min), aerobic (66 min) and non-aerated (20 min). It can be deduced that the single longer aerobic phase of Cycle C promoted the N_2O production via the nitrification-related routes and its subsequent emission through stripping for a longer, non-interrupted period (Rodriquez-Caballero et al., 2015). Moreover, the evolution of the N components in Fig. 15 provides some additional explanation. For both cycles, the N_2O produced during the aerobic phase(s) was partly consumed in the following non-aerated phase. The rest of this N_2O amount was probably stripped, hence explaining the resulting N_2O EF. The N_2O produced during the single longer aerobic phase of Cycle C was higher than the N_2O generated during the 1st aerobic phase of Cycle B. Although Cycle B also involved a 2nd aerobic phase, the associated N_2O production was very small. Moreover, the total N_2O production of Cycle B was lower than the respective one of Cycle C, thus justifying the difference between the EFs. The configuration of Cycle C provided the most favorable conditions for the highest N_2O production predicted by the developed model due to the following: i) longer, non-interrupted N_2O production during the unique longer aerobic phase (66 min), ii) enhanced

stripping during this single and slightly extended aeration period, and iii) low consumption of the N_2O produced in the subsequent non-aerated phase.

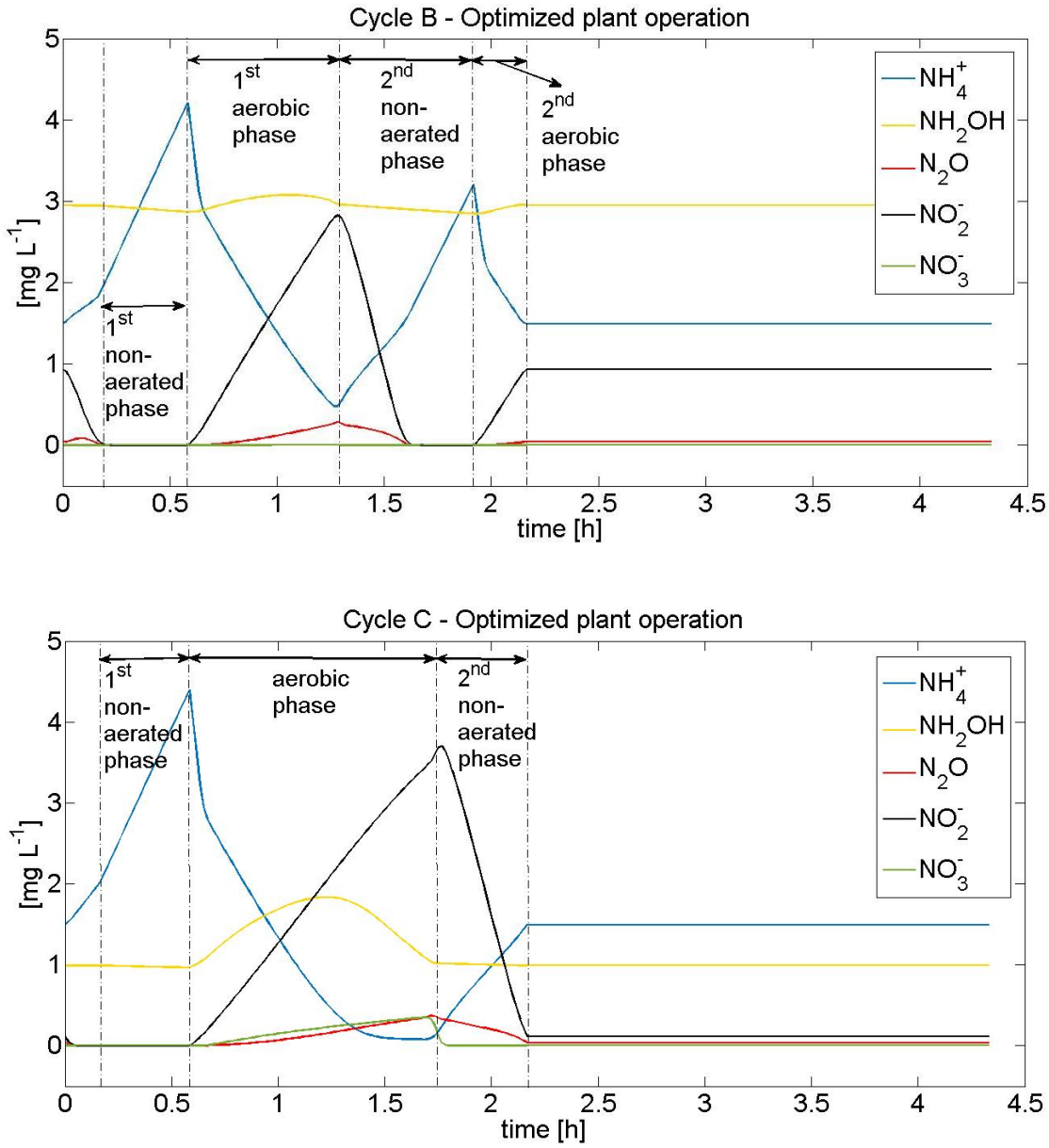

Figure 15: The evolution of the NH_4^+, NH_2OH, N_2O, NO_2^- and NO_3^- concentrations during Cycles B and C.

3.2.3 Predominant N_2O production pathway

As shown in Fig. 14, N_2O production occurred only during the aerated phases. Moreover, the N_2O concentration peaks coincided with the NO_2^- peaks for both cycles. This was observed for both the single aerobic phase of cycle C as well as for the 1st aerobic phase of cycle B. The 2nd aerobic phase of Cycle B was accompanied by small N_2O production. Consequently, nitrifier denitrification was the predominant AOB pathway for N_2O generation. The optimal fit was obtained for a rather low DO setpoint (1.6 mg O_2 L^{-1} for cycle B and 1.7 mg O_2 L^{-1} for cycle C). This observation agrees with past studies regarding the AOB pathways relative contribution; compared to incomplete NH_2OH oxidation, nitrifier denitrification has been suggested as increasingly contributing with the DO decrease (Anderson et al., 1993; Sutka et al., 2006; Kampschreur et al., 2008).

Comparable results have been reported in similar experimental studies. For instance, Rassamee et al. (2011) operated a lab-scale SBR fed with real municipal wastewater under an anoxic phase followed by a longer aerobic one (113 min and 480 min, respectively) with the DO ranging from 1 to 3 mg O_2 L^{-1} during aeration. They observed that nitrifier denitrification was the N_2O hotspot under low DO (i.e. 2 mg O_2 L^{-1}) and moderate NO_2^- accumulation (i.e. <5 mg NO_2^--N L^{-1}). In the lab-scale study performed by Peng et al. (2014), the performance of a lab-scale SBR treating domestic wastewater was observed under NO_2^- accumulation of <1.5 mg NO_2^--N L^{-1}. The applied cycle configuration included 260 min of aerobic feeding followed by 20 min of aeration. With the DO gradually increasing from 0.2 to 3 mg O_2 L^{-1}, the contribution of the nitrifier dentification and NH_2OH oxidation pathways changed from 95 to 66% and from 5 to 34%, respectively; nitrifier dentification was the main contributor pathway. In another study,

Peng et al. (2015) applied an SBR fed with domestic wastewater under a cycle configuration comprising 260 min of aerobic feeding and 20 min of further aeration. With the DO ranging from 0.4 to 3.5 mg O_2 L^{-1} and the average NO_2^- concentration from 5 to 50 mg NO_2^--N L^{-1}, nitrifier dentification emerged as the most preferred N_2O production pathway; NH_2OH oxidation was the principal N_2O production route only under the combination of high DO (i.e. 3.5 mg O_2 L^{-1}) with low average NO_2^- concentration (i.e. <10 mg NO_2^--N L^{-1}).

As mentioned in section 2.5, the developed model also incorporated 2 abiotic pathways for N_2O production: i.e. NH_2OH decomposition to N_2O, and N-nitrosation of NH_2OH with HNO_2 as nitrosating agent. However, as seen in Fig. 15 there was no important NH_2OH consumption (or, equivalently, decrease in the NH_2OH concentration), thus suggesting that the abiotic routes were poorly preferred. All the simulations were repeated by de-activating the processes rates related to the abiotic pathways. No significant difference in the final results was detected (data not shown). The abiotic contribution to N_2O emissions has been generally considered minor in wastewater treatment although significant in soils and atmospheric chemistry (Schreiber et al., 2012; Liu et al., 2017). For example, Heil et al. (2014) executed lab-scale experiments on an aqueous solution containing NH_2OH, NO_2^-, iron (Fe^{3+}) and copper (Cu^{2+}), all of which are commonly found in soils. Abiotic N_2O production was noted with a specific site preference of 34-35‰. As far as wastewater treatment is concerned, Terada et al. (2017) confirmed the possibility of abiotic N_2O production in the absence of AOB-enriched biomass in a lab-scale nitritation SBR treating synthetic inorganic wastewater. Although these findings indicate the likelihood of abiotic N_2O production, they also suggest certain conditions that

are likely to enhance this; e.g. pH≤5 (Domingo-Félez and Smets, 2019; Su et al., 2019). However, the La Roca WWTP that provided the full-scale N_2O emission data and operational/influent characteristics for the development and calibration of the model operated under no such conditions. Therefore, no important contribution of the abiotic N_2O production pathways was anticipated; fact that was additionally supported by the simulation results.

4. Conclusions

In this chapter, the IWA ASM1 model was expanded and modified to describe the N_2O dynamics for the full-scale SBR WWTP of La Roca del Valles (Barcelona, Spain). The developed model included all known pathways for N_2O production: biological (i.e. nitrifier denitrification, NH_2OH oxidation, and heterotrophic denitrification) and abiotic (NH_2OH decomposition to N_2O, and N-nitrosation of NH_2OH with HNO_2 as nitrosating agent). Real N_2O emission data from the WWTP operation were used to calibrate the mathematical model and explore the possibility of plant operation under DO setpoints lower than the ones applied during the monitoring campaign. Two different cycle configurations were applied and monitored in terms of N_2O emissions; cycles of type B and cycles of type C. Cycle B involved the alternation amongst two non-aerated (25-40 min) and two aerated phases (15-40 min). Cycle C included two shorter non-aerated phases (25-29 min) with a long aerated one (66 min) between them. These two cycle configurations were integrated into the model. The following conclusions were reached:

- Considering the significance of the DO parameter during the nitrification/denitrification stages, both the experimental data and the developed model linked the emissions with air flow or, equivalently, with the aerated phases. With a view to calibrating the developed model, the representative DO profiles of cycles B and C as recorded by the La Roca del Valles WWTP operators were used [i.e. Cycle type B: DO=2.3 mg O_2 L^{-1} (1st aerobic phase)/1.9 mg O_2 L^{-1} (2nd aerobic phase), Cycle type C: DO=2.3 mg O_2 L^{-1} (single aerobic phase)]. The calibrated version of the model provided a rather good description of the N_2O monitoring data for both cycle types. Therefore, the calibrated model was regarded as representative enough of the La Roca WWTP operation.
- The calibrated model was used to explore whether a potentially lower DO setpoint than the one applied during the plant operation can ensure an acceptable description of the N_2O emission monitoring data. The optimal fit was achieved for a DO setpoint of 1.6 mg O_2 L^{-1} during both aerobic phases of Cycle B, as well as a DO of 1.7 mg O_2 L^{-1} for the single aerobic phase of Cycle C. The latter DO values were indeed lower than the respective DO profiles reported by the plant operators during the monitoring campaign. However, slight divergences in the 2nd emission peak of Cycle B were observed. The latter can be attributed to an actual N_2O denitrification rate lower than the value predicted by the model. Hence, a higher final N_2O concentration was noted at the end of the non-aerated phase during the monitoring campaign with this N_2O amount being stripped at the beginning of the consequent (2nd) aerobic phase of Cycle B.

- The total N_2O EF predicted by the optimised version of the model differed between the two cycle types: 0.8% (Cycle B) and 1.5% (Cycle C). Although the total aerobic phase duration was approximately the same for both cycles (Cycle B: 60 min; Cycle C: 66 min), the difference in the cycle configuration impacted on the final N_2O EF. The single longer aerobic phase of Cycle C enhanced the N_2O production via the nitrification-related routes and its subsequent emission through stripping for a longer, non-interrupted period. Hence, it can be deduced that applying cycle configurations with an alternation amongst multiple aerobic and non-aerated phases of moderate length (e.g. like Cycle B) can possibly reinforce the N_2O emission mitigation.
- For both cycle types, N_2O production was noted only during the aerated phases coinciding with the NO_2^- peaks. Consequently, nitrifier denitrification was considered the predominant pathway for N_2O generation. The optimal fit was obtained for a rather low DO setpoint (1.6 mg O_2 L^{-1} for cycle B and 1.7 mg O_2 L^{-1} for cycle C). This observation agrees with past studies regarding the AOB pathways relative contribution; compared to incomplete NH_2OH oxidation, nitrifier denitrification has been suggested as increasingly contributing with the DO decrease. Finally, no important NH_2OH consumption was observed, thus suggesting that the abiotic routes were poorly preferred under the conditions of the current study.

References

Aboobakar, A., Cartmell, E., Stephenson, T., Jones, M., Vale, P., Dotro, G., 2013. Nitrous oxide emissions and dissolved oxygen profiling in a full-scale nitrifying activated sludge treatment plant, Water Res. 47: 524-534.

Ahn, J.H., Kim, S., Park, H., Rahm, B., Pagilla, K., Chandran, K., 2010. N_2O emissions from activated sludge processes, 2008-2009: results of a national monitoring survey in the United States. Environ. Sci. Technol. 44:4505-4511.

Anderson, I., Poth, M., Homstead, J., Burdige, D., 1993. A comparison of NO and N_2O nitrifier Alcaligenes faecalis. Appl. Environ. Microbiol. 59: 3525-3533.

APHA, 1998. Standard Methods for Examination of Water and Wastewater, 20th ed. American Public Health Association, Washington, DC.

Capela, S., Roustan, M., Heduit, A., 2001. Transfer number in fine bubble diffused aeration systems. Water Sci. Technol. 43: 145-152.

Daelman, M.R.J., De Baets, B., van Loosdrecht, M.C.M., Volcke, E.I.P., 2013. Influence of sampling strategies on the estimated nitrous oxide emission from wastewater treatment plants. Water Res. 47: 3120-3130.

Desloover, J., Vlaeminck, S.E., Clauwaert, P., Verstraete, W., Boon, N., 2012. Strategies to mitigate N_2O emissions from biological nitrogen removal systems. Curr. Opin. Biotechnol. 23: 474-482.

Domingo-Félez, C., Smets, B.F., 2016. A consilience model to describe N_2O production during biological N removal. Environ. Sci. Water Res. Technol. 2: 923-930.

Domingo-Félez, C., Smets, B.F., 2019. Regulation of key N_2O production mechanisms during biological water treatment. Curr. Opin. Biotechnol. 57: 119-126.

Foley, J., Yuan, Z., Keller, J., Senante, E., Chandran, K., Willis, J., Shah, A., van Loosdrecht, M.C.M., van Voorthuizen, E., 2011. N_2O and CH_4 Emission from Wastewater Collection and Treatment Systems: State of the Science Report and Technical Report. IWA Publishing, London, United Kingdom.

Frijns, J., Roorda, J., Mulder, M., 2008. Op weg naar een klimaatneutrale waterketen. H_2O. 41: 36-37.

Harper, W.F., Takeuchi, Y., Riya, S., Hosomi, M., Terada, A., 2015. Novel abiotic reactions increase nitrous oxide production during partial nitrification: Modeling and experiments. Chem. Eng. J. 281: 1017-1023.

Heil, J., Wolf, B., Brüggemann, N., Emmenegger, L., Tuzson, B., Vereecken, H., Mohn, J., 2014. Site-specific 15N isotopic signatures of abiotically produced N_2O. Geochim. Cosmochim. Acta. 139: 72-82.

Henze, M., Gujer, W., Mino, T., van Loosdrecht, M., 2000. Activated Sludge Models ASM1, ASM2, ASM2d and ASM3. IWA Publishing, London, United Kingdom.

Hiatt, W.C., Grady, C.P.L., 2008. An updated process model for carbon oxidation, nitrification, and denitrification. Water Environ. Res. 80: 2145-2156.

Jubany, I., 2007. Operation, modeling and automatic control of complete and partial nitrification of highly concentrated ammonium wastewater. PhD thesis in Chemical Engineering, Universitat Autònoma de Barcelona, Spain. http://tdx.cat/handle/10803/5310; accessed 15.03.2016.

Jubany, I., Carrera, J., Lafuente, J., Baeza, J.A., 2008. Start-up of a nitrification system with automatic control to treat highly concentrated ammonium wastewater: Experimental results and modelling. Chem. Eng. J. 144: 407-419.

IPCC, 2007. Climate Change 2007: The Physical Science Basis. Cambridge University Press, Cambridge, United Kingdom.

IPCC, 2014. Climate Change 2014: Synthesis Report. Contribution of Working Groups I, II and III to the Fifth Assessment Report of the Intergovernmental Panel on Climate Change. In: Core Writing Team, Pachauri R.K. and Meyer L.A. (Eds.), IPCC, Geneva, Switzerland.

Kampschreur, M. J., Tan, N. C. G., Kleerebezem, R., Picioreanu, C., Jetten, M.S.M., van Loosdrecht, M.C.M., 2008. Effect of dynamic process conditions on nitrogen oxide emission from a nitrifying culture. Environ. Sci. Technol. 42: 429-435.

Kampschreur, M.J., Temmink, H., Kleerebezem, R., Jetten, M.S.M., van Loosdrecht, M.C.M., 2009. Nitrous oxide emission during wastewater treatment. Water Res. 43: 4093-4103.

Kosonen, H., Heinonen, M., Mikola, A., Haimi, H., Mulas, M., Corona, F., Vahala, R., 2016. Nitrous Oxide Production at a Fully Covered Wastewater Treatment Plant: Results of a Long-Term Online Monitoring Campaign, Environ. Sci. Technol. 50: 5547-5554.

Law, Y., Ye, L., Pan, Y., Yuan, Z., 2012. Nitrous oxide emissions from wastewater treatment processes. Philos. Trans. R. Soc. Lond. Ser. B Biol. Sci. 367:1265-1277.

Li, P., Wang, S., Peng, Y., Liu, Y., He, J., 2015. The synergistic effects of dissolved oxygen and pH on N_2O production in biological domestic wastewater treatment under nitrifying conditions. Environ. Technol. 36:1623-1631.

Lide, D.R., 2007. CRC Handbook of Chemistry and Physics. 87th ed., CRC Press/Taylor and Francis Group, Boca Raton.

Lijó, L., Malamis, S., González-García, S., Fatone, F., Moreira, M.T., Katsou, E., 2017. Technical and environmental evaluation of an integrated scheme for the co-treatment of wastewater and domestic organic waste in small communities. Water Res. 109: 173-185.

Liu, S., Han, P., Hink, L., Prosser, J.I., Wagner, M., Brüggemann, N., 2017. Abiotic Conversion of Extracellular NH_2OH Contributes to N_2O Emission during Ammonia Oxidation, Environ. Sci. Technol. 51: 13122-13132.

Mannina, G., Ekama, G., Caniani, D., Cosenza, A., Esposito, G., Gori, R., Garrido-baserba, M., Rosso, D., Olsson, G., 2016. Greenhouse gases from wastewater treatment-A review of modelling tools. Sci. Total Environ. 551-552: 254-270.

Pan, Y., van den Akker, B., Ye, L., Ni, B.-J., Watts, S., Reid, K., Yuan, Z., 2016. Unravelling the spatial variation of nitrous oxide emissions from a step-feed plug-flow full scale wastewater treatment plant. Sci. Rep. 6: 20792.

Peng, L., Ni, B.J., Erler, D., Ye, L., Yuan, Z., 2014. The effect of dissolved oxygen on N_2O production by ammonia-oxidizing bacteria in an enriched nitrifying sludge. Water Res. 66: 12-21.

Peng, L., Ni, B., Ye, L., Yuan, Z., 2015. The combined effect of dissolved oxygen and nitrite on N 2 O production by ammonia oxidizing bacteria in an enriched nitrifying sludge. Water Res. 73: 29-36.

Pocquet, M., Wu, Z., Queinnec, I., Sperandio, M., 2016. A two-pathway model for N_2O emissions by ammonium oxidizing bacteria supported by the NO/N_2O variation. Water Res. 88: 948-959.

Rassamee, V., Sattayatewa, C., Pagilla, K., Chandran, K., 2011. Effect of oxic and anoxic conditions on nitrous oxide emissions from nitrification and denitrification processes, Biotechnol. Bioeng. 108: 2036-2045.

Rodriguez-Caballero, A., Aymerich, I., Poch, M., Pijuan, M., 2014. Evaluation of process conditions triggering emissions of green-house gases from a biological wastewater treatment system, Sci. Total Environ. 493: 384-391.

Rodriguez-Caballero, A., Aymerich, I., Marques, R., Poch, M., Pijuan, M., 2015. Minimizing N_2O emissions and carbon footprint on a full-scale activated sludge sequencing batch reactor. Water Res. 71: 1-10.

Schreiber, F., Wunderlin, P., Udert, K.M., Wells, G.F., 2012. Nitric oxide and nitrous oxide turnover in natural and engineered microbial communities: Biological pathways, chemical reactions, and novel technologies. Front. Microbiol. 3: 1-24.

Soler-Jofra, A., Stevens, B., Hoekstra, M., Picioreanu, C., Sorokin, D., van Loosdrecht, M.C.M., Perez, J., 2016. Importance of abiotic hydroxylamine conversion on nitrous oxide emissions during nitritation of reject water. Chem. Eng. J. 287: 720-726.

Spinelli, M., Eusebi, A.L., Vasilaki, V., Katsou, E., Frison, N., Cingolani, D., Fatone, F., 2018. Critical analyses of nitrous oxide emissions in a full scale activated sludge system treating low carbon-to-nitrogen ratio wastewater, J. Clean. Prod. 190: 517-524.

Su, Q., Domingo-Félez, C., Mark Jensen, M., Smets, B.F., 2019. Abiotic Nitrous Oxide (N_2O) Production Is Strongly pH Dependent but Contributes Little to Overall N_2O Emissions in Biological Nitrogen Removal Systems. Environ. Sci. Technol. 53: 3508-3516.

Terada, A., Sugawara, S., Hojo, K., Takeuchi, Y., Riya, S., Harper, W.F., Yamamoto, T., Kuroiwa, M., Isobe, K., Katsuyama, C., Suwa, Y., Koba, K., Hosomi, M., 2017. Hybrid Nitrous Oxide Production from a Partial Nitrifying Bioreactor: Hydroxylamine Interactions with Nitrite. Environ. Sci. Technol. 51: 2748-2756.

Wang, Q., Jiang, G., Ye, L., Pijuan, M., Yuan, Z., 2014. Heterotrophic denitrification plays an important role in N2O production from nitritation reactors treating anaerobic sludge digestion liquor. Water Res. 62:202-210.

Wunderlin, P., Mohn, J., Joss, A., Emmenegger, L., Siegrist, H., 2012. Mechanisms of N_2O production in biological wastewater treatment under nitrifying and denitrifying conditions. Water Res. 46: 1027-1037.

Chapter IV

Modelling the nitrous oxide emission in a full-scale municipal sequencing batch reactor wastewater treatment plant using the concept of electron carriers

Summary

N_2O can be produced and emitted during the BNR in WWTPs. Having an important GWP, the water utilities consider the N_2O emissions as significantly contributing to the C-footprint of WWTPs. The N_2O production during the BNR is linked to the activity of the AOB and the heterotrophic denitrifiers. Nitrifier denitrification, incomplete NH_2OH oxidation and heterotrophic denitrification are the biological pathways activated by the AOB and the heterotrophic denitrifiers. Hence, the mathematical modelling of the N_2O production and emission in WWTPs is expected to facilitate the design of effective mitigation strategies, improve the WWTP operation and enable the precise estimation of the anticipated onsite N_2O emission. Several single/multiple-pathway N_2O models have been proposed as extensions to the widely accepted IWA ASM structure. However, different more recent modelling approaches were based on the combination of the description of the biological N_2O production pathways along with the complex electron transfer processes of the AOB and the denitrifiers. The oxidation and reduction processes were dissociated, and electron carriers were inserted to describe the electron transfer from oxidation to reduction. The aim of this work was to develop an electron carrier-type N_2O model integrating all the microbial production pathways and describing the operation of a full-scale municipal SBR WWTP in Australia. Data obtained during a two-day intensive monitoring campaign were used to calibrate and validate the developed model. Key parameters relevant to the NH_4^+ oxidation and the N_2O production dynamics required calibration. After calibration, the model was able to depict the experimental trends obtained with data of the first day of the intensive monitoring. The calibrated version of the model was then used for validation purposes. The model predictions were compared

against the profiles of the N components, the DO and the N_2O as obtained on the second day of the intensive monitoring. The model was able to describe these trends. Under the intermittent aeration regime, nitrifier denitrification was the most contributing N_2O production pathway. The EF of the full-scale municipal SBR WWTP was calculated as equal to 1% that was within the range of EFs reported for other full-scale municipal WWTPs in Australia.

Keywords

N_2O emissions, SBR, full-scale modelling, electron carrier concept, intensive monitoring data

1. Introduction

N_2O can be produced during the BNR in WWTPs and, afterwards, be emitted to the atmosphere (Kampschreur et al., 2009; Foley et al., 2010; Ahn et al., 2011; Ye et al., 2014). Moreover, it reacts with the stratospheric ozone, thus contributing to the ozone layer depletion (Portmann et al., 2012; Ye et al., 2014). Having a GWP 265-298 times higher than CO_2 (IPCC, 2014), the water utilities consider the N_2O emissions as likely to importantly aggravate the C-footprint of WWTPs (Kampschreur et al., 2009; Ahn et al., 2011; Ni et al., 2013, 2015).

The N_2O production during the BNR is linked to the AOB and the heterotrophic denitrifiers (Kampschreur et al., 2009; Lu and Chandran, 2010; Ni et al., 2013). The AOB can contribute to the N_2O generation via two pathways. First, N_2O can result as the final product of nitrifier denitrification with NO_2^- as the terminal electron acceptor. Secondly, N_2O can be generated as an intermediate product of the incomplete NH_2OH oxidation to NO_2^-. Moreover, N_2O is an intermediate product of the heterotrophic denitrification process. The latter is a sequence of reductions: NO_3^- to NO_2^-, NO_2^- to NO, NO to N_2O and, finally, N_2O to N_2. Therefore, N_2O emission can be noted if denitrification is disturbed and remains incomplete (Kim et al., 2010; Chandran et al., 2011; Stein, 2011; Ni et al., 2013). The major factors affecting these bioprocesses have been reviewed and include DO levels, COD:N, C-source composition, pH, temperature, etc. (Kampschreur et al., 2009; Lu and Chandran, 2010; Pan et al., 2012; Ni et al., 2013).

In this concept, the mathematical modelling of the N_2O production and emission in WWTPs has gained importance and the results can be used to facilitate the design of effective mitigation strategies (Ni et al., 2013, 2015; Pocquet et al., 2016). Furthermore,

the development of accurate N_2O models will enhance the BNR operation and optimization and enable the precise estimation of the anticipated onsite N_2O emission (Ni et al., 2013; 2014). Several single/multiple-pathway N_2O models have been proposed as extensions to the ASM structure introduced by the IWA task group (Henze et al., 1987, 2000). For example, multiple-pathway ASM-type models have emerged exploring how the relative contribution of each pathway changes depending on the DO level (Pocquet et al., 2016. Pocquet et al. (2016) found that nitrifier denitrification was the N_2O hotspot under low-DO conditions. On the contrary, the NH_2OH oxidation contribution increased with the DO increase. Furthermore, Hiatt and Grady (2008) focused on the heterotrophic denitrification pathway. They introduced the ASMN that described each denitrification step as a discrete reaction with a unique specific rate.

Although widely accepted in the scientific world, the original IWA ASM versions were developed with a view to describing the following processes: organic matter oxidation and nitrification/denitrification (ASM1), biological phosphorus removal (ASM2 and ASM2d), internal storage and endogenous respiration (ASM3). According to these initial versions though, nitrification was modelled as one-step process (i.e. oxidation of NH_4^+ to NO_3^-) and denitrification as a one-step reduction of NO_3^- to N_2. However, this does not represent how the BNR occurs in WWTPs (Gujer et al., 1999; Henze et al., 2000; Iacopozzi et al., 2007; Pan et al., 2013). To accurately describe the BNR as well as the N_2O production during the BNR, modifications were made; all nitrification/denitrification steps and biological N_2O production pathways were added. Hence, the ASM-type N_2O models were developed.

Alternative N_2O modelling approaches that are not based on the IWA ASM structure were also suggested. They described the biological N_2O production during the BNR in WWTPs through the electron transfer processes related to the metabolism of the AOB and denitrifying bacterial populations (e.g. Pan et al., 2013; Ni et al., 2014). The oxidation and reduction processes were dissociated. Electron carriers were inserted as a component describing the electron transfer from oxidation to reduction. The Mred (reduced mediator) and Mox (oxidised mediator) were introduced as model components representing the electron carriers in reduced and oxidised form, respectively. Although the electron carrier pool is rather small, the Mox and Mred availability was assumed as continuous. Moreover, this modelling approach regarded the recirculation between the Mox and Mred as follows: an Mox increase making up for an Mred decrease and vice versa ($Mred \rightleftharpoons Mox + 2e^- + 2H^+$), with the total concentration of the electron carriers (Ctot) kept stable (SMred + SMox = Ctot) (Sipkema et al., 2000; Gyan et al., 2006; Pan et al., 2013; Ni et al., 2014).

Hence, the aim of this work was to develop an electron carrier-type N_2O model integrating all the microbial production pathways describing the operation of a full-scale municipal SBR in Australia. To this end, full-scale data from a two-day intensive monitoring campaign of the plant were used for the model calibration and validation.

2. Materials and Methods

2.1 Brief description of the WWTP

The full-scale SBR WWTP receives an average daily flow of 23.9 ML d^{-1}. The wastewater treated in the plant is mainly municipal with sporadic minor contributions of industrial wastewater, surface water run-off and infiltrated groundwater. The scheme consists of six (identical) tanks; five tanks were online and one offline for routine maintaining at the time of the study. Each SBR tank (working volume=6,000 m^3) was operated independently of the others and received around 20% of the total wastewater flow. One of the online tanks, namely SBR 1, was monitored and analysed in this chapter. First, the influent was passing through an anoxic selector and, then, through SBR 1 (AWMC, 2014). A schematic representation of SBR 1 is provided in Fig. 16.

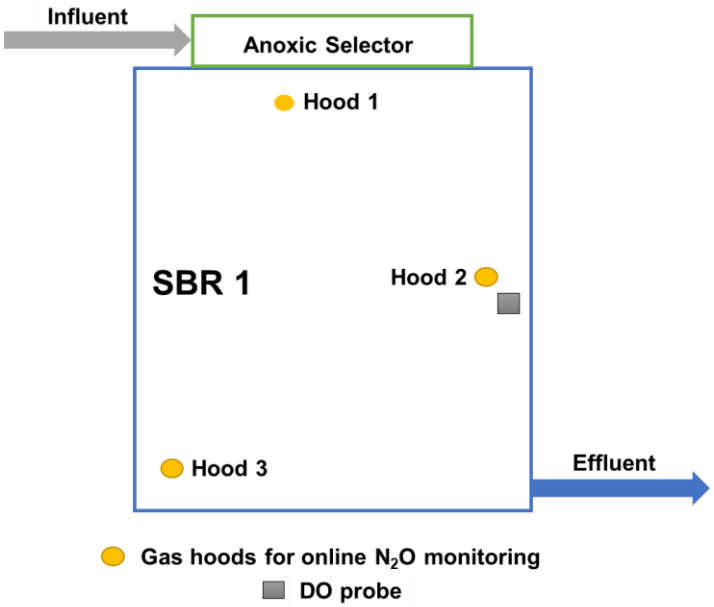

Figure 16: Schematic representation of the SBR 1 operating in the full-scale municipal SBR WWTP under investigation.

2.2 SBR cycle configuration

The SBR cycle configuration involved the following sequence of phases: 108 min of continuous feeding (intermittent aeration), 54 min for the reaction (intermittent aeration), 54 min of settling and 54 min of decanting. The intermittent aeration regime during the feeding and reaction phases included the recurrence of aeration (30-45 min) and non-aeration (15-60 min). A DO probe was placed at the SBR to provide online DO measurements (Fig. 16). This data was used by the plant operators to control the air flow and achieve intermittent aeration (AWMC, 2014).

2.3 Online N_2O measurements

SBRs are supposed to be completely mixed. Therefore, the GHG emission is expected to be homogeneous along the whole tank. For the purposes of this study though, online N_2O gas hoods were placed in three different locations to cover the possibility of non-maintaining the desired mixing/aeration conditions. As indicated in Fig. 16, the first hood was placed next to the influent inlet to capture the emissions of this zone. Similarly, the second and third hood were situated in the middle of the SBR tanks and at the effluent outlet, respectively (Fig. 16). The online data from all three hoods were included in the calculation of the overall N_2O emission; each hood was considered as representing 1/3 of the SBR tank surface. The data provided for the calibration/validation of the proposed model were obtained through an intensive two-day monitoring campaign. The N_2O emissions at the three chosen sampling locations (Fig. 16) were captured using gas hoods floating over the mixed liquor and connected to a continuous online analyser

(Horiba). The Horiba analyser was simultaneously recording N_2O and DO (DO from the middle of the SBR tank) on a minute time scale (AWMC, 2014).

2.4 Analyses of the wastewater samples

Details on the influent and effluent characteristics are provided in Table 6. During the intensive monitoring campaign, samples were taken within the SBR (i.e. from hood 2, Fig. 16) and analysed for their NH_4^+, NO_3^- and NO_2^- content at the beginning of the SBR cycle and at the end of each phase (AWMC, 2014).

Table 6: Influent and effluent characteristics of the SBR plant (adapted by AWMC, 2014).

Parameter	Average value ± standard deviation
Influent	
COD (mg L^{-1})	494 ± 78
NH_4^+ (mg N-NH_4^+ L^{-1})	35 ± 3
NO_3^- (mg N-NO_3^- L^{-1})	4.7 ± 1.3
NO_2^- (mg N-NO_2^-- L^{-1})	Not detectable
Effluent	
COD (mg L^{-1})	173 ± 36
NH_4^+ (mg N-NH_4^+ L^{-1})	NA
NO_3^- (mg N-NO_3^- L^{-1})	8.1 ± 0.9
NO_2^- (mg N-NO_2^-- L^{-1})	0.4 ± 0.2

The collected samples were filtered using 0.45 mm disposable sterile filters (Millipore, Millex GP). The NH_4^+, NO_3^- and NO_2^- content of the filtered samples was measured using the Lachat QuickChem8000 Flow Injection Analyser (Lachat Instrument, Milwaukee, USA). The COD was analysed according to Standard Methods (APHA, 1995).

2.5 Model description

The kinetic model was developed to describe the N_2O dynamics for the SBR 1 of the full-scale municipal SBR WWTP under investigation by adapting and extending relevant past models proposed by Ni et al. (2014) and Pan et al. (2013). The new version of the model was now modified to describe the SBR 1 operation and cycle configuration (section 2.2) with a view to estimating the N_2O dynamics in a holistic way. The latter was achieved by including all biological N_2O production pathways (i.e. nitrifier denitrification, NH_2OH oxidation and heterotrophic denitrification) as indicated in Fig. 17:

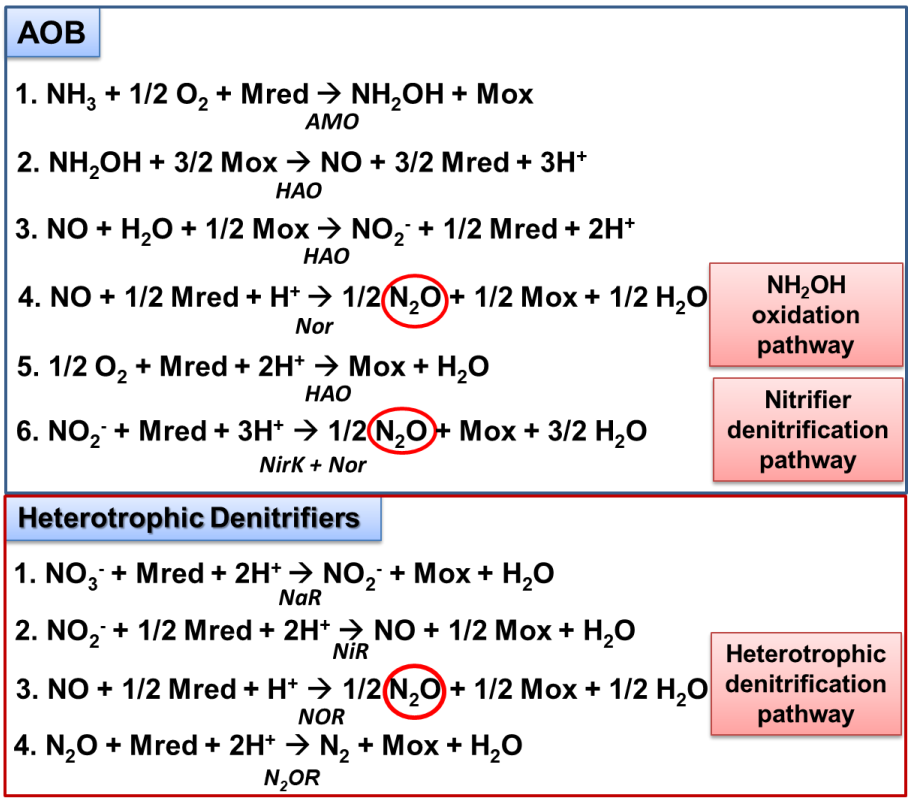

Figure 17: The three biological pathways for N_2O production considered in the model: NH_2OH oxidation pathway (AOB pathway), nitrifier denitrification (AOB pathway), and the heterotrophic denitrification pathway (adapted by Pan et al., 2013; Ni et al., 2014).

Mred and Mox stand for the electron carriers in the reduced and oxidised form, respectively. As presented in Fig. 17, NH_3 is first oxidised to NH_2OH (reaction 1 in the AOB section) catalysed by the AMO enzyme. Here, Mred offers two electrons to the oxygen atom and gets oxidised to Mox. Afterwards, the AOB oxidise the produced NH_2OH to NO_2^- with NO as intermediate product and HAO as a catalyst (Fig. 17: reaction 1 in the AOB section). Mox receives four electrons after the NH_2OH oxidation and is reduced to Mred. The NO that was generated will then produce N_2O (Fig. 17: reaction 4 in the AOB section; NH_2OH oxidation pathway) helped by the Nor enzyme; Mred offers one electron to NO and is re-oxidised to Mox. The AOB produce energy through the electron transfer. According to reaction 5 (Fig. 17: AOB section), Mred gives electrons to reduce O_2 and is re-oxidized to Mox aided through the HAO enzymatic activity. NO_2^- can replace O_2 as electron acceptor and finally produce N_2O (Fig. 17: reaction 6 in the AOB section; nitrifier denitrification pathway); Mred offers electrons to reduce NO_2^- and is re-oxidised to Mox. The NO_2^- reduction was simulated as one-step. The latter was assumed so as not to associate the two AOB pathways through NO. If NO was considered an intermediate of the NO_2^- reduction, it would then be available for oxidation to NO_2^-. Hence, NO and NO_2^- loops would be noted (Ni et al., 2014). Furthermore, the heterotrophic denitrification was modelled as a sequence of four reductions (Fig. 17: heterotrophic denitrification section). Each time Mred gives two electrons to the respective N-oxide (i.e. NO_3^-, NO_2^-, NO and N_2O) and is re-oxidised to Mox. The enzymes catalysing reactions 1-4 in the heterotrophic denitrification sequence (Fig. 17: heterotrophic denitrification section) are the NO_3^-, NO_2^-, NO and N_2O reductases (i.e. NaR, NiR, NOR and N_2OR, respectively) (Pan et al., 2013).

The final model was developed in Aquasim (Reichert, 1998) that has been used for the modelling purposes of similar past studies (e.g. Pan et al., 2013, 2016; Ni et al., 2014, 2015). Steady-state operation was simulated by running the model for a high number of days (i.e. >80 d) and a sludge retention time (SRT) of 15 d. Tables presenting the stoichiometric and kinetic parameters, the model stoichiometry, and the process rates of the integrated processes are given in detail in the Accompanying Material section.

2.6 N_2O EF modelling

The N_2O EF resulting from the last cycle was determined in the following way: equal to the percentage of the influent N-load emitted as N_2O (N_2O-EF, Eq. 1):

$$\mathbf{N_2O - EF}(\%) = \mathbf{100} \cdot \frac{\mathbf{N_2O_{emission}}}{\mathbf{N_{IN}}}$$

(Equation 1)

N_{IN} was considered as equal to the sum of NH_4^+, NO_2^- and NO_3^- contained in the influent. It was calculated as indicated in Eq. 2:

$$\mathbf{N_{IN}\ (mmol\ N) = V_{FEED} \cdot (S_{NH4} + S_{NO3} + S_{NO2})}$$

(Equation 2)

Where V_{FEED} is the volume of wastewater that is fed into the reactor (L), and with rest of the terms following the nomenclature as proposed in the studies by Ni et al. (2014) and Pan et al (2013): S_{NH4}, S_{NO3} and S_{NO2} the influent concentrations for NH_4^+ (mmol N-NH_4^+ L^{-1}), NO_3^- (mmol N-NO_3^- L^{-1}) and NO_2^- (mmol N-NO_2^- L^{-1}), respectively.

A separate section in the Aquasim code was dedicated to the SBR function inside which the changing SBR volume during its operation (i.e. V in L) and the accumulation of the N_2O emitted in each cycle (i.e. $N_2O_{emission}$ in mmol N-N_2O) were simulated. For the purposes of the N_2O emission modelling, the volumetric mass transfer coefficient for N_2O (i.e. k_La_{N2O} in h^{-1}) was used. The volumetric mass transfer coefficient (k_La) combines the global transfer coefficient k_L along with the interfacial area a (interphase transport surface between liquid and gas per unit of reactor volume) (Ye et al., 2014). The k_La_{N2O} resulted from Eq. 3 following Higbie's penetration model (Capela et al., 2001):

$$\mathbf{k_L a_{N_2O}(h^{-1}) = k_L a_{O_2} \cdot \sqrt{\frac{Dif_{N2O}}{Dif_{O2}}}}$$

(Equation 3)

As seen in Eq. 3, the k_La_{N2O} is correlated with the volumetric mass transfer coefficient of O_2 (i.e. kLa_{O2} in h^{-1}). Dif_{N2O} is the molecular diffusivity of N_2O in water ($2.11 \cdot 10^{-9}$ m^2 s^{-1} at 20 ºC) and Dif_{O2} the molecular diffusivity of O_2 in water ($2.01 \cdot 10^{-9}$ m^2 s^{-1} at 20 ºC) (Lide, 2007). The kLa_{O2} at time t_1 was calculated using Eq. 4 (adapted by Ye et al. (2014)):

$$\mathbf{kLa_{O2_{t_1}}(h^{-1}) = \left(\frac{MO_2}{V_{working}}\right) * \left(\frac{t_1 - t_0}{DO_{sat} - DO(t_1)}\right)}$$

(Equation 4)

Where MO_2 is the total oxygen demand during a cycle (mmol O_2 h^{-1}), $V_{working}$ the working SBR volume (L), DO_{sat} is the O_2 saturation concentration in water under atmospheric conditions (≈8.5 g O_2 m^{-3} at 22 ºC according to Tchobanoglous et al. (2003)),

t_1 the time (in h) at which the DO(t_1) measurement (mmol O_2 L^{-1}) was taken, and t_0 (in h) the previous measurement time. DO measurements were taken every minute. The MO_2 and DO(t) data were provided by the plant operators.

3. Results and Discussion

3.1 Model calibration

The model calibration was done using the NH_4^+, NO_2^- and NO_3^-, DO and gaseous N_2O data obtained by the plant operators on the first day of the intensive monitoring campaign. The calibration process followed the method proposed by similar past studies on the development of models following the electron-carrier concept (i.e. Pan et al., 2013; Ni et al., 2014, 2015). Certain model parameters were indicated as 'key parameters' with reference to the available measured data by the sensitivity analysis tool incorporated in the Aquasim program (as suggested by Ni et al. (2015)): the specific maximum NH_3 oxidation rate (r_{NH3_Ox}), the O_2 affinity constant for NH_3 oxidation (K_{O2_NH3}), the specific maximum NO_2^- reduction rate (r_{NO2_red}), the specific maximum NO reduction rate (r_{NO_red}), and the specific maximum O_2 reduction rate (r_{O2_red}). They were then calibrated using the secant method integrated in Aquasim (Reichert, 1998; Ni et al., 2015). First, parameters relevant to the NH_3 oxidation (i.e. r_{NH3_Ox} and K_{O2_NH3}) were calibrated using the NH_4^+, NO_2^- and NO_3^-, and DO calibration data. Secondly, the parameters related to the N_2O production (i.e. r_{NO2_red}, r_{NO_red} and r_{O2_red}) were calibrated using the provided gaseous N_2O data.

All other stoichiometric and kinetic parameters followed values proposed in literature. Both the calibrated parameters as well as those adapted from literature are presented in detail in the Accompanying Material section. Furthermore, it must be noted that the values of the calibrated parameters resulted as comparable to the respective ones suggested by similar past modelling studies (e.g. Ni et al., 2014, 2015). The results produced by the developed model after calibration along with the respective experimental data are presented in Fig. 18 and 19. As it can be seen, the calibrated version of the proposed model agreed well with the provided (real) data used for calibration purposes.

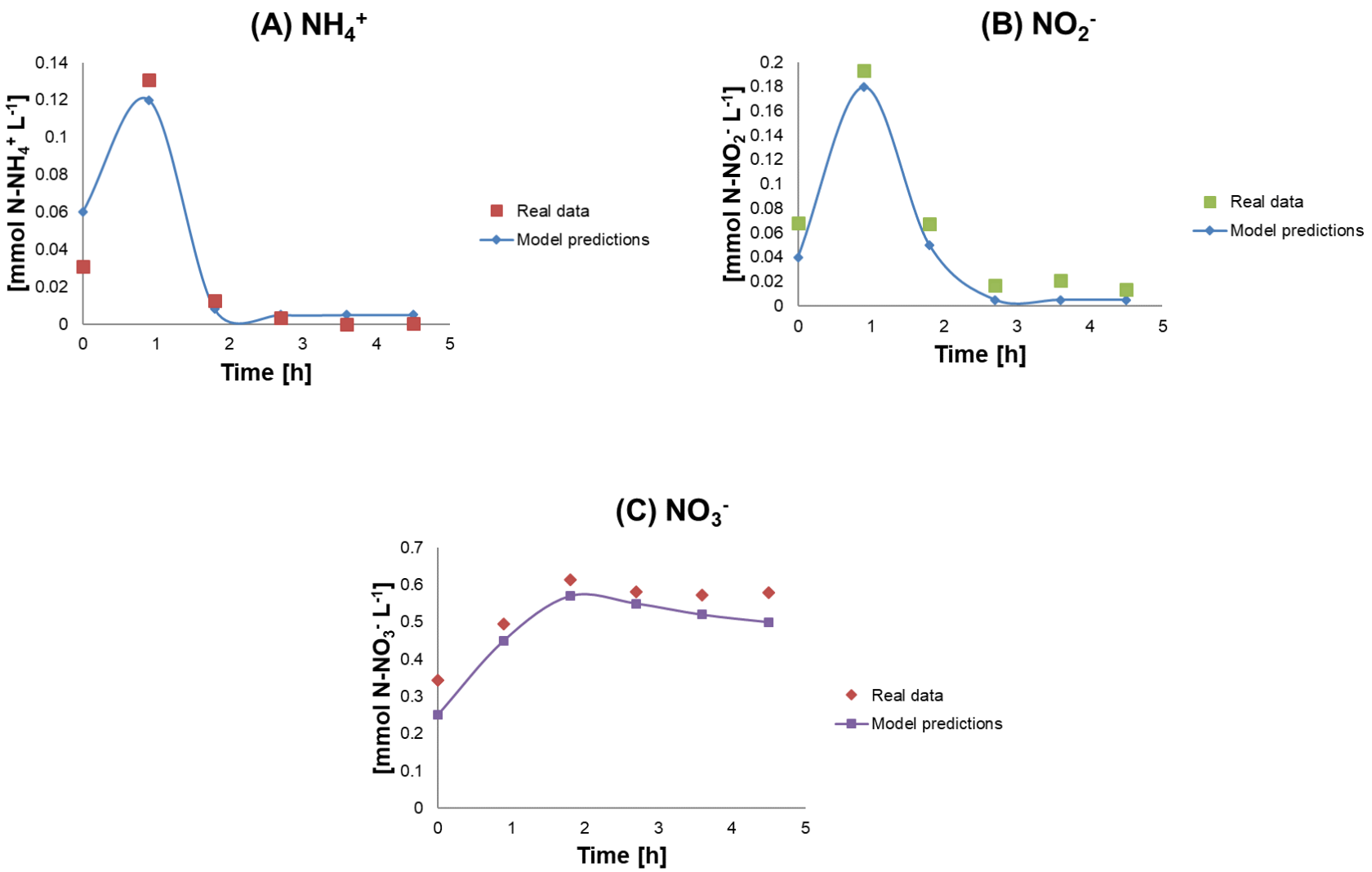

Figure 18: Model calibration results using the data of the first day of the intensive monitoring campaign concerning the NH_4^+, NO_2^- and NO_3^- profiles. The markers indicate the real data, and the lines the model prediction.

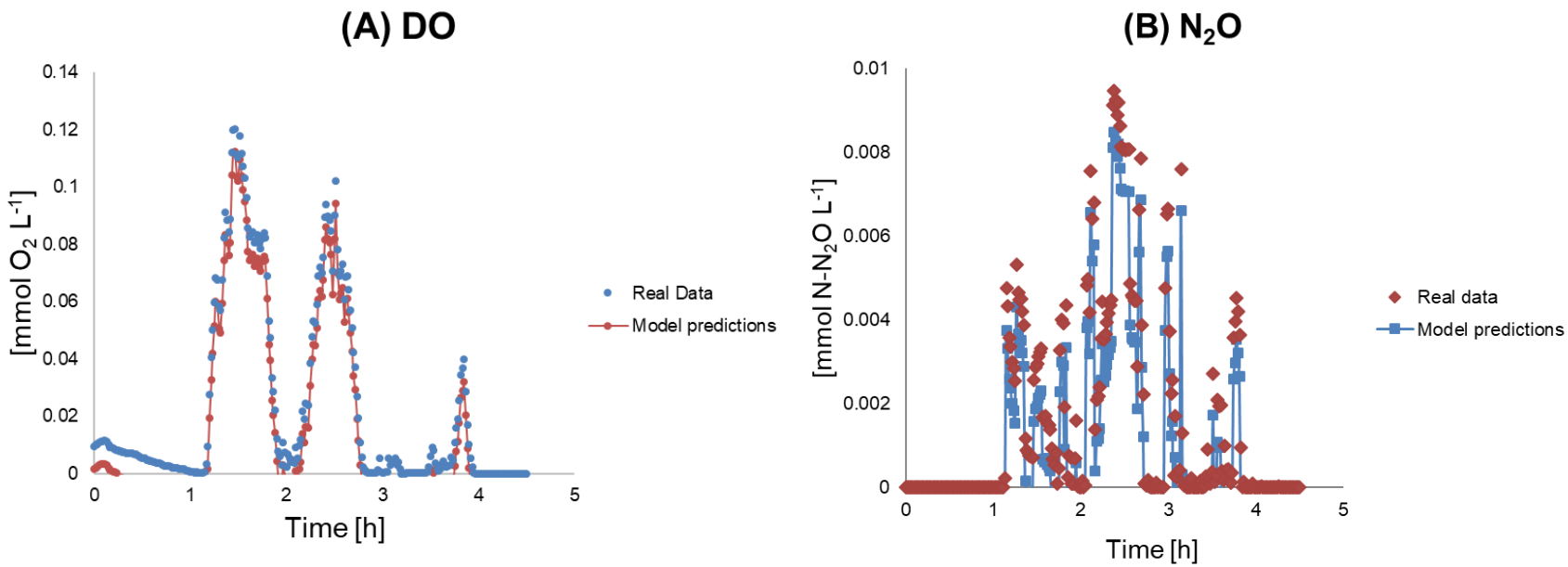

Figure 19: Model calibration results using the data of the first day of the intensive monitoring campaign concerning the N_2O and DO profiles. The markers indicate the real data, and the lines the model prediction.

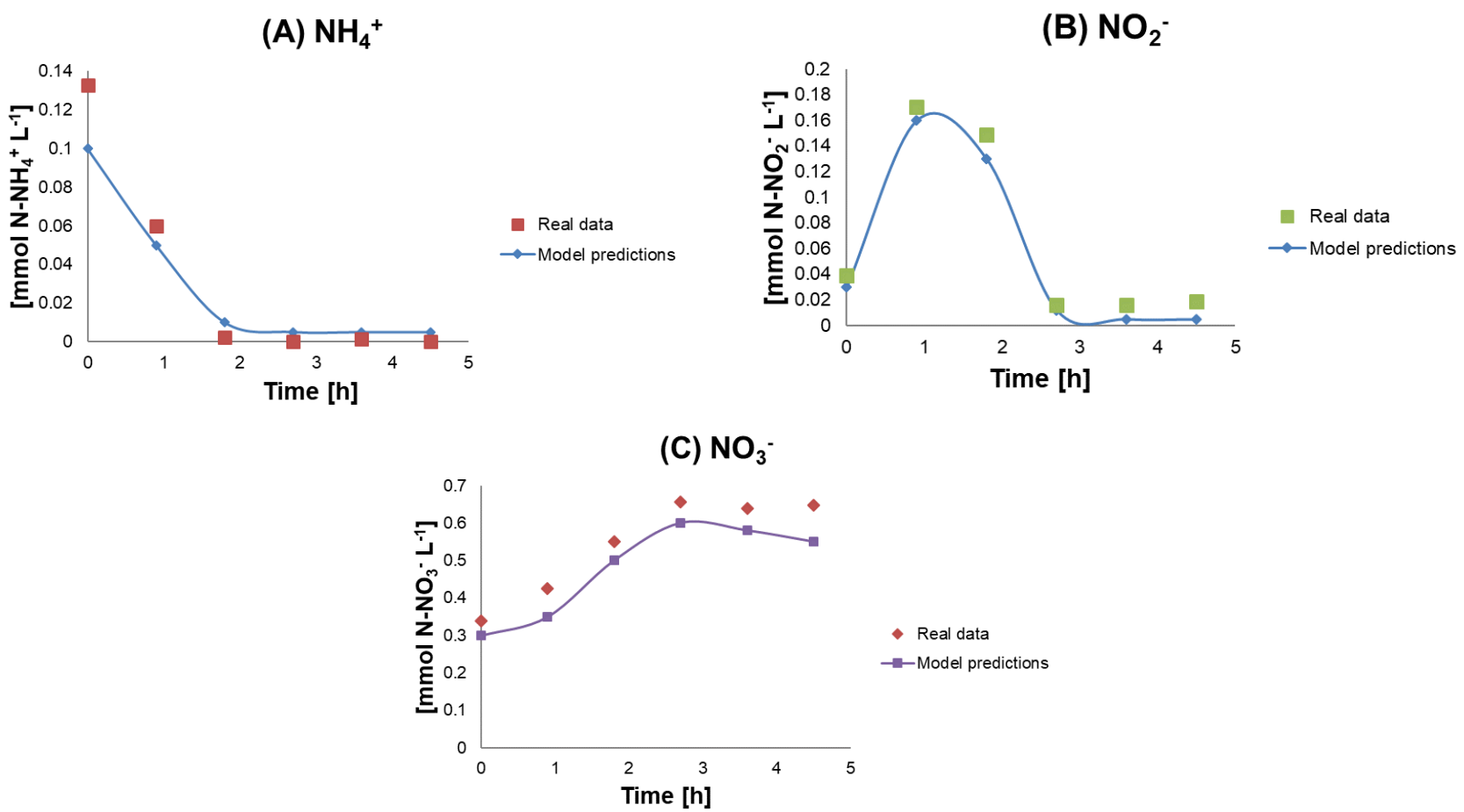

Figure 20: Model validation results using the data of the second day of the intensive monitoring campaign concerning the NH_4^+, NO_2^- and NO_3^- profiles. The markers indicate the real data, and the lines the model prediction.

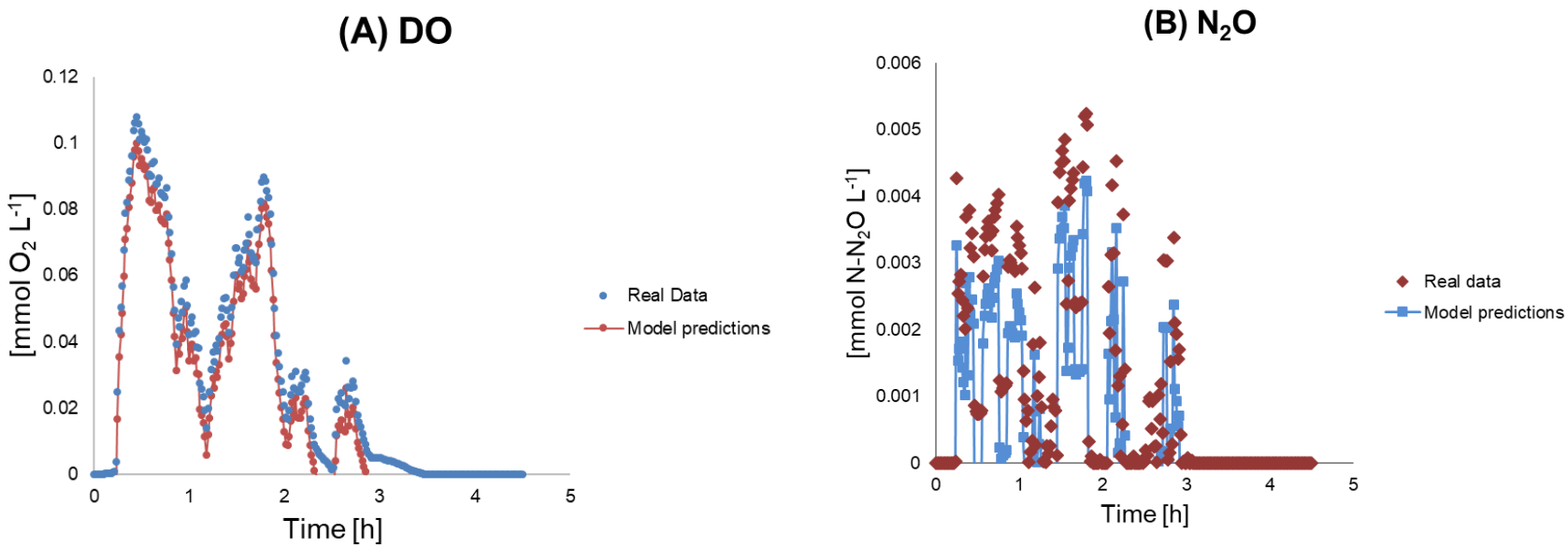

Figure 21: Model validation results using the data of the second day of the intensive monitoring campaign concerning the N_2O and DO profiles. The markers indicate the real data, and the lines the model prediction.

3.2 Model validation

The calibrated version of the developed model was used for validation purposes. The model predictions were compared against the NH_4^+, NO_2^-, NO_3^-, DO and N_2O data obtained on the second day of the intensive monitoring campaign (Fig. 20 and 21).

The calibrated version of the developed model can provide an accurate prediction of the NH_4^+, NO_2^-, NO_3^-, DO and N_2O profiles as measured on the second day of the intensive sampling campaign. In terms of the most contributive N_2O production pathway, the following possible explanations were given. The NO_3^- slightly increased (Fig. 20C) from its initial value suggesting that some of the produced NH_4^+ was oxidised to NO_3^- (complete nitrification). Considering that no significant NO_3^- decrease was observed, it was assumed that no important heterotrophic denitrification was happening. Moreover, the initial NO_3^- value (Fig. 20C) was higher than the NH_4^+ and NO_2^- ones (Fig. 20A and 20B, respectively). Before entering the SBR tank, the influent had passed through an anoxic selector. Hence, the initial NO_3^- value observed at the beginning of the SBR cycle (Fig. 20C) can be probably considered as remaining NO_3^- from some minor (incomplete) heterotrophic denitrification activity in this anoxic compartment. Under the intermittent aeration regime (Fig. 21A), the increase in the DO provided the conditions for the initiation of the nitrification process. The NO_2^- concentration began increasing levels (Fig. 20B) and the first N_2O emissions appeared (Fig. 21B). After approximately 1 h of operation, the DO was at lower levels than before (Fig. 21A). The NH_4^+ and NO_2^- concentrations presented a deceasing trend (Fig. 20A and 20B). N_2O emission was observed approximately till the 3rd hour of operation (Fig. 21B) when the NH_4^+ and NO_2^- concentrations reached very low levels (Fig. 20A and 20B). Therefore, nitrifier denitrification was proposed as the most

possible N_2O production pathway. Similarly, past studies exploring the relative contribution of the AOB pathways under fluctuating DO revealed that nitrifier denitrification was majorly contributive under a wide range of DOs, whereas NH_2OH oxidation was more likely while operating consistently under a relatively high DO (i.e. >0.11 mmol O_2 L^{-1}) (Peng et al., 2015; Pocquet et al., 2016). Furthermore, past works investigating the operation of full-scale SBR plants treating municipal wastewater under intermittent aeration suggested that nitrifier denitrification was the principal N_2O production hotspot (Rodriquez-Caballero et al., 2015).

Finally, the N_2O EF of the full-scale SBR WWTP modelled within this study was found equal to 1%. The latter result is within the 0.2-1.9% range of EFs reported for other full-scale municipal WWTPs in Australia (AWMC, 2014).

4. Conclusions

A kinetic model integrating all the biological N_2O production pathways was developed in this study based on the electron carrier concept. The model described the operation of a full-scale municipal SBR in Australia. Data obtained during a two-day intensive monitoring campaign were used to calibrate and validate the developed model. The results of this work can be summarised in the following points:

- Key parameters relevant to the NH_4^+ oxidation and N_2O production dynamics required calibration. After calibration, the model satisfactorily depicted the NH_4^+, NO_2^-, NO_3^-, DO and N_2O profiles as they were provided though the data of the first day of intensive monitoring.

- The calibrated version of the model was used for validation purposes. The model predictions were compared against the NH_4^+, NO_2^-, NO_3^-, DO and N_2O profiles as they were provided though the data of the second day of the intensive monitoring. The model was able to describe these trends.
- Under the intermittent aeration regime, nitrifier denitrification was suggested as the most possible N_2O production pathway. The EF of the full-scale municipal SBR WWTP was calculated as equal to 1% that is within the range of EFs reported for other full-scale municipal WWTPs in Australia.

Finally, the present version of the developed model can be easily adapted to describe the operational characteristics of other SBR plants, or even other configurations as well after further modifications. Thus, it can serve as a flexible electron carrier-type N_2O prediction tool.

References

Advanced Water Management Centre (AWMC), 2014. Final Project Report for Quantifying Fugitive Greenhouse Gas Emissions from Bolivar WWTP. South Australia Water Corporation & The University of Queensland, Brisbane, Australia.

Ahn, J.H., Kwan, T., Chandran, K., 2011. Comparison of partial and full nitrification processes applied for treating high-strength nitrogen wastewaters: microbial ecology through nitrous oxide production. Environ. Sci. Technol. 45: 2734-2740.

APHA, 1995. Standard methods for the examination of water and wastewater. American Public Health Association, Washington DC, USA.

Capela, S., Roustan, M., Heduit, A., 2001. Transfer number in fine bubble diffused aeration systems. Water Sci. Technol. 43: 145-152.

Chandran, K., Stein, L.Y., Klotz, M.G., van Loosdrecht, M.C.M., 2011. Nitrous oxide production by lithotrophic ammonia-oxidizing bacteria and implications for engineered nitrogen-removal systems. Biochem. Soc. Trans. 39: 1832-1837.

Foley, J., de Haas, D., Yuan, Z., Lant., P., 2010. Nitrous oxide generation in full-scale biological nutrient removal wastewater treatment plants. Water Res. 44: 831-844.

Gujer, W., Henze, M., Mino, T., Van Loosdrecht, M., 1999. Activated Sludge Model No. 3. Water Sci. Technol. 39: 183-193.

Gyan, S., Shiohira, Y., Sato, I., Takeuchi, M., Sato, T., 2006. Regulatory loop between redox sensing of the NADH/NAD^+ ratio by Rex (YdiH) and oxidation of NADH by NADH dehydrogenase Ndh in Bacillus subtilis. J. Bacteriol. 188: 7062-7071.

Henze, M., Grady Jr., C.P.L., Gujer, W., Marais, G.V.R., Matsuo, T., 1987. Activated Sludge Model No.1, IAWQ Scientific and Technical Report No.1. IWA Publishing, London, UK.

Henze, M., Gujer, W., Mino, T., van Loosdrecht, M.C.M., 2000. Activated Sludge Models ASM1, ASM2, ASM2d, and ASM3, IWA Scientific and Technical Report n.9. IWA Publishing, London, UK.

Hiatt, W.C., and Grady, C.P.L., 2008. An updated process model for carbon oxidation, nitrification, and denitrification. Water Environ. Res. 80: 2145-2156.

Iacopozzi, I., Innocenti, V., Marsili-Libelli, S., Giusti, E., 2007. A modified Activated Sludge Model No. 3 (ASM3) with two-step nitrification-denitrification. Environ. Model. Softw. 22: 847-861.

IPCC, 2014. Climate Change 2014: Synthesis Report. Contribution of Working Groups I, II and III to the Fifth Assessment Report of the Intergovernmental Panel on Climate Change. In: Core Writing Team, Pachauri R.K. and Meyer L.A. (Eds.), IPCC, Geneva, Switzerland.

Kampschreur, M.J., Temmink, H., Kleerebezem, R., Jetten, M.S.M., van Loosdrecht, M.C.M., 2009. Nitrous oxide emission during wastewater treatment. Water Res. 43: 4093-4103.

Kim, S.W., Miyahara, M., Fushinobu, S., Wakagi, T., Shoun, H., 2010. Nitrous oxide emission from nitrifying activated sludge dependent on denitrification by ammonia-oxidizing bacteria. Bioresour. Technol. 101: 3958-3963.

Lide, D.R., 2007. CRC Handbook of Chemistry and Physics. 87th ed., CRC Press/Taylor and Francis Group, Boca Raton.

Lu, H., and Chandran, K., 2010. Factors promoting emissions of nitrous oxide and nitric oxide from denitrifying sequencing batch reactors operated with methanol and ethanol as electron donors. Biotechnol. Bioeng. 106: 390-398.

Ni, B.J., Ye, L., Law, Y., Byers, C., Yuan, Z., 2013. Mathematical modelling of nitrous oxide (N_2O) emissions from full-scale wastewater treatment plants. Environ. Sci. Technol. 47: 7795-7803.

Ni, B.J., Peng, L., Law, Y., Guo, J., Yuan, Z., 2014. Modelling of nitrous oxide production by autotrophic ammonia-oxidizing bacteria with multiple production pathways Environ. Sci. Technol. 48: 3916-3924.

Ni, B.J., Pan, Y., Van Den Akker, B., Ye, L., Yuan, Z., 2015. Full-Scale Modelling Explaining Large Spatial Variations of Nitrous Oxide Fluxes in a Step-Feed Plug-Flow Wastewater Treatment Reactor. Environ. Sci. Technol. 49: 9176-9184.

Pan, Y., Ye, L., Ni, B.J., Yuan, Z., 2012. Effect of pH on N_2O reduction and accumulation during denitrification by methanol utilizing denitrifiers. Water Res. 46: 4832-4840.

Pan, Y., Ye, L., Yuan, Z., 2013. Modelling Electron Competition among Nitrogen Oxides Reduction and N_2O Accumulation in Denitrification. Environ. Sci. Technol. 47: 11083-11091.

Pan, Y., van den Akker, B., Ye, L., Ni, B.-J., Watts, S., Reid, K., Yuan, Z., 2016. Unravelling the spatial variation of nitrous oxide emissions from a step-feed plug-flow full scale wastewater treatment plant. Sci. Rep. 6: 20792.

Peng, L., Ni, B.J., Ye, L., Yuan, Z., 2015. The combined effect of dissolved oxygen and nitrite on N_2O production by ammonia oxidizing bacteria in an enriched nitrifying sludge. Water Res. 73: 29-36.

Pocquet, M., Wu, Z., Queinnec, I., Sperandio, M., 2016. A two-pathway model for N_2O emissions by ammonium oxidizing bacteria supported by the NO/N_2O variation. Water Res. 88: 948-959.

Portmann, R.W., Daniel, J.S., Ravishankara, A.R., 2012. Stratospheric ozone depletion due to nitrous oxide: influences of other gases. Philos. Trans. R. Soc. B Biol. Sci. 367: 1256-1264.

Reichert, P., 1998. AQUASIM 2.0-Computer Program for the Identification and Simulation of Aquatic Systems; EAWAG: Dübendorf, Switzerland.

Rodriguez-Caballero, A., Aymerich, I., Marques, R., Poch, M., Pijuan, M., 2015. Minimizing N_2O emissions and carbon footprint on a full-scale activated sludge sequencing batch reactor. Water Res. 71: 1-10.

Sipkema, E.M., de Koning, W., Ganzeveld, K.J., Janssen, D.B., Beenackers, A.A.C.M., 2000. NADH-regulated metabolic model for growth of methylosinus trichosporium OB3b. Model presentation, parameter estimation, and model validation. Biotechnol. Prog. 16: 176-188.

Stein, L.Y., 2011. Surveying N_2O-producing pathways in bacteria. Methods Enzymol. 486: 131-152.

Tchobanoglous, G., Burton, F.L., Stensel, H.D., 2003. Wastewater Engineering, Treatment and Reuse. 4th ed. McGraw Hill Boston, USA.

Ye, L., Ni, B.J., Law, Y., Byers, C., Yuan, Z., 2014. A novel methodology to quantify nitrous oxide emissions from full-scale wastewater treatment systems with surface aerators. Water Res. 48: 257-268.

Chapter V

Conclusions and Further Work

1. Introduction

This PhD project aimed to develop, calibrate and validate a novel mathematical tool that can be used for the purposes of the online monitoring, control and mitigation of the C-footprint of WWTPs. Gaseous emissions are produced at various stages during the BNR in WWTPs. Strategies to decrease the required amount of energy for this operation may in fact cause greater harm due to the increase of GHG (e.g. N_2O) emissions. Thus, the development of a reliable and robust tool allowing the prediction of N_2O production and emission during the BNR in WWTPs is important to accurately estimate the anticipated emissions and apply measures to reduce them.

To deliver this PhD project, the following steps were taken. First, a review of relevant past studies was conducted to provide a holistic and comprehensive perspective on the real on-field N_2O emissions during the BNR in WWTPs by covering several important aspects of N_2O production/emission during the BNR processes. The principal aims of this first chapter were: i) to introduce the mechanisms involved in the N_2O production during the BNR in WWTPs, ii) to review past studies that revealed the operational parameters with the greatest impact on the N_2O emissions during the BNR in municipal wastewater and sludge reject water treatment, iii) to report the relevant mathematical modelling that has been developed for the simulation of N_2O production/emission during the BNR processes, and iv) to propose potential mitigation strategies. The major findings suggested that it is important for the plant operators to optimise the treatment process (especially in terms of significant operating parameters such as DO, temperature, pH, etc.), and perform long-term measurement campaigns covering the whole length of the treatment line to capture spatial and/or temporal

variations. Moreover, the need to consider multiple N_2O production pathways as well as the changes of majorly influencing operational factors (e.g. DO) to create accurate N_2O was highlighted and taken into consideration for the development of the models presented in the second, third and fourth chapter.

In the second chapter, the goal was to extend the widely applied IWA ASM2d structure to develop an N_2O model describing the operation of a full-scale A^2/O municipal WWTP by: (i) considering N, P and organic matter removal, (ii) integrating all the microbial pathways for N_2O production/consumption during the BNR in WWTPs, (iii) estimating the N_2O EF under different DO levels. According to the major conclusions reached after the simulations, the application of low-aeration strategies by plant operators is recommended only to the extent that it does not disturb the nitrification process. The attempt to improve the C-footprint of a WWTP under a lower aeration regime requires optimisation. If not, nitrification can be unstable, and a higher overall footprint is likely to be noted due to the N_2O produced through the AOB pathways.

In the third chapter, the IWA ASM1 version was now used but expanded and modified in the following way: adaptation to a full-scale municipal SBR WWTP performing organic matter and N-removal, in addition to the inclusion of the biological and abiotic N_2O production. Real N_2O emission data from the full-scale municipal SBR plant of La Roca del Valles in Spain were provided to calibrate the developed model. The calibrated model was used to investigate if lower DOs than the ones applied during the plant operation could satisfactorily represent the monitored plant performance. Indeed, the simulation results indicated that lower DO setpoints than those documented during the monitoring campaign can lead to similar emission trends. Hence, the operation under

these lower DO setpoints can be suggested to the plant operators as a strategy to decrease the plant's C-footprint.

Furthermore, it was considered useful to also explore an alternative concept in terms of full-scale N_2O modelling (i.e. electron carrier concept). Hence, the fourth chapter focused on the development of an N_2O production model that simultaneously described the biological N_2O production pathways and the complex electron transfer processes of the involved bacterial populations. The objectives were to: (i) to adapt the developed model to the characteristics of a full-scale municipal SBR WWTP in Australia, and (ii) calibrate/validate the model using real data from a two-day intensive monitoring campaign of the WWTP. Under the intermittent aeration applied in the plant, nitrifier denitrification was the major N_2O hotspot, suggesting that the operators should pay attention to the applied aeration regime while considering mitigation strategies.

This last chapter considers how potential errors/inconsistencies in the sampling campaigns, methods and devices will generate unreliable measurements. The latter is likely to lead to the development of inaccurate models if these data are used for validation/calibration purposes. The chapter ends with suggestions for extending this research to new areas in the future.

2. Sources of uncertainty

The various sampling, monitoring and calculation methods can importantly affect the N_2O measurements, thus adding to the uncertainties of full-scale N_2O quantification. Although there is a gradual movement towards process- and operation-based quantification, there is currently no common quantifying protocol.

For instance, the floating chamber method that is widely applied in WWTPs for gaseous N_2O sampling was initially introduced for soil monitoring purposes. Hence, its ability to accurately represent the N_2O emissions occurring during the BNR in wastewater treatment can be questioned. Significant variability can be noted in terms of the chamber configuration, the chamber area and material, the choice of the monitored parameters, and the methodology followed to calculate the N_2O flux. Furthermore, the calculation of the N_2O flux depends on several factors including the sampling campaign, the bioreactor configuration, and the operational conditions (e.g. periods/compartments of aeration or non-aeration). Although the EF can be importantly influenced by the N_2O flux calculation, the uncertainty related to the flux measurements in full-scale WWTPs has been scarcely reported.

Moreover, the continuous monitoring of dissolved N_2O is important to elucidate the pathways of N_2O production at full-scale. It shall be noted that short-term measurement campaigns are likely to miss seasonal/annual peaks and fluctuations, thus leading to an inaccurate estimation of the N_2O EF. Commercial gas analysers are increasingly being used and considered a reliable tool. Nevertheless, there are still limited mentions with respect to their accuracy, detection limits and calibration requirements.

Consequently, it can be deduced that there are multiple sources of uncertainty and error regarding the monitoring campaigns and equipment. All in all, future research should focus on the successful full-scale application of online standardized set-ups that continually estimate both dissolved and gaseous N_2O dynamics. The reliable measurements obtained through such devices will facilitate the development of robust N_2O production models.

3. Extending this research to new areas

As it was demonstrated throughout this this thesis, the N_2O emission occurring during the BNR in WWTPs involves many influential parameters. The development of dynamic models which consider all pathways of N_2O production and have been calibrated and validated upon data originating from real full-scale BNR schemes is essential. Then, operators will be able to predict the potential N_2O emissions of a scheme under construction or directly interfere in the operation of an existing one to achieve the desired mitigation.

The models developed through this PhD research can serve as prediction tools for the estimation of N_2O production and emission in WWTPs. Especially the ASM-type models presented in Chapters II and III are based on the widely accepted IWA ASM structure and can be easily adapted to different plant configurations. Nevertheless, they lack validation upon real full-scale emission data. Hence, their application on different full-scale WWTPs that can provide calibration/validation data could be the object of future research. The model presented in Chapter IV is based on the concept of electron carriers. However, this concept is relatively new. Few similar full-scale studies are available for comparative purposes. Moreover, the developed model was calibrated and validated upon real full-scale WWTP data resulting from a short monitoring campaign (i.e. 2 days). It would be interesting to investigate its application in different full-scale schemes that can provide calibration/validation data resulting from longer monitoring campaigns.

As previously underlined, real data are needed for the calibration and validation of the developed N_2O models. However, this extends the discussion to the following aspect: the robustness of the models depends on the quality of the provided measurements for

the calibration/validation process. The uncertainties related to various factors such as the quantification methods and devices and the often poorly designed monitoring campaigns that fail to capture temporal and/or spatial emission variations, etc. generate unreliable data. If used for calibration and validation, these inaccurate measurements will subsequently lead to the development of incorrect models.

Apart from the mechanistic N_2O modelling that has been the focus of this PhD project though, multivariate statistics are another mathematical tool that can spot the relationships between the N_2O emissions and influential parameters (e.g. DO, NO_2^- levels, etc.) for the whole monitoring period or for selected operating subperiods. Such statistical analyses are expected to deepen the understanding of the data acquired during the N_2O monitoring campaigns, hence enhancing the calibration and validation of the mechanistic N_2O production models. The results of such analyses can be used by plant operators to improve a WWTP's performance in the following ways: (i) predict the most influential operational parameters, and (ii) design more efficient monitoring campaigns.

Another goal is to perform multivariate analysis of the WWTP datasets that were used for the calibration and validation of the mechanistic models presented in the third and fourth chapter. The results concerning the most contributive N_2O generation pathways as well as the observations regarding the profiles of other parameters (e.g. DO, concentration of N-compounds, etc.) will be compared against the respective ones generated by the mechanistic modelling. In this way, the models proposed through this PhD project can be further improved. Finally, these actions will lead to an integrated tool combining both mechanistic and sophisticated statistical tools that can be useful for mitigating the N_2O emissions during the BNR in WWTPs.

Accompanying Material

Accompanying Material of Chapter II

i. Model Components

Component	Denotation	Units
S_{O2}	Dissolved Oxygen	g O_2 m^{-3}
S_F	Fermentable, readily biodegradable, organic substrate	g COD m^{-3}
S_A	Fermentation products (acetate)	g COD m^{-3}
S_{NH4}	Ammonium	g N-NH_4^+ m^{-3}
S_{NH2OH}	Hydroxylamine	g N-NH_2OH m^{-3}
S_{N2O}	Nitrous oxide	g N-N_2O m^{-3}
S_{NO}	Nitric oxide	g N-NO m^{-3}
S_{NO2}	Nitrite	g N-NO_2^- m^{-3}
S_{NO3}	Nitrate	g N-NO_3^- m^{-3}
S_{PO4}	Phosphate	g P-PO_4^{3-} m^{-3}
S_I	Soluble, inert, bon-biodegradable organics	g COD m^{-3}
S_{ALK}	Bicarbonate alkalinity	mole HCO_3^- m^{-3}
S_{N2}	Nitrogen	g N m^{-3}
X_I	Particulate, inert, non-biodegradable organics	g COD m^{-3}
X_S	Slowly biodegradable substrate	g COD m^{-3}
X_H	Heterotrophic biomass	g COD m^{-3}
X_{PAO}	Phosphorus Accumulating Organisms	g COD m^{-3}
X_{PP}	Polyhydroxyalkanoates	g COD m^{-3}
X_{PHA}	Polyphosphates	g COD m^{-3}
X_{AOB}	Ammonium oxidizing bacteria	g COD m^{-3}
X_{NOB}	Nitrite oxidizing bacteria	g COD m^{-3}
X_{TSS}	Total suspended solids	g TSS m^{-3}
X_{MeOH}	Metal hydroxides	g TSS m^{-3}
X_{MeP}	Metal phosphate ($MePO_4$)	g TSS m^{-3}

ii. Conversion Factors

Typical Conversion Factors				
Symbol	**Denotation**	**Value**	**Units**	**Reference**
i_{NSF}	N-content of fermentable substrates S_F	0.03	g N (g COD)$^{-1}$	Henze et al., 2000
i_{PSF}	P-content of S_F	0.01	g P (g COD)$^{-1}$	Henze et al., 2000
i_{NSI}	N-content of inert soluble COD S_I	0.01	g N (g COD)$^{-1}$	Henze et al., 2000
i_{PSI}	P-content of S_I	0	g P (g COD)$^{-1}$	Henze et al., 2000
i_{NXI}	N-content of inert particulate COD X_I	0.02	g N (g COD)$^{-1}$	Henze et al., 2000
i_{PXI}	P-content of X_I	0.01	g P (g COD)$^{-1}$	Henze et al., 2000
i_{TSSXI}	Total Suspended Solids (TSS) to COD ratio for X_I	0.75	g TSS (g COD)$^{-1}$	Henze et al., 2000
i_{NXS}	N-content of slowly biodegradable substrate X_S	0.04	g N (g COD)$^{-1}$	Henze et al., 2000
i_{PXS}	P-content of X_S	0.01	g P (g COD)$^{-1}$	Henze et al., 2000
i_{TSSXS}	TSS to COD ratio for X_S	0.75	g TSS (g COD)$^{-1}$	Henze et al., 2000
i_{NBM}	N-content of heterotrophic biomass (X_H), P-accumulating organisms (X_{PAO}) and autotrophic nitrifiers (X_{AOB} and X_{NOB})	0.07	g N (g COD)$^{-1}$	Henze et al., 2000
i_{PBM}	P-content of X_H, X_{PAO}, X_{AOB} and X_{NOB}	0.02	g P (g COD)$^{-1}$	Henze et al., 2000
i_{TSSBM}	TSS to COD ratio for X_H, X_{PAO}, X_{AOB} and X_{NOB}	0.9	g TSS (g COD)$^{-1}$	Henze et al., 2000

iii. Stoichiometric Parameters

Typical Stoichiometric Parameters				
Symbol	**Denotation**	**Value**	**Units**	**Reference**
Y_H	Yield coefficient of X_H	0.625	g COD (g COD)$^{-1}$	Henze et al., 2000
Y_{PHA}	Polyhydroxyalkanoate (PHA) requirement for Polyphosphate (PP) storage	0.2	g COD (g P)$^{-1}$	Henze et al., 2000
Y_{PAO}	Yield coefficient for PAO	0.625	g COD (g COD)$^{-1}$	Henze et al., 2000
Y_{PO4}	PP requirement (PO_4 release) per PHA stored	0.4	g P (g COD)$^{-1}$	Henze et al., 2000
Y_{AOB}	Yield coefficient for the Ammonia Oxidizing Bacteria (AOB)	0.18	g COD (g COD)$^{-1}$	Jubany et al., 2008
Y_{NOB}	Yield coefficient for the Nitrite Oxidizing Bacteria (NOB)	0.08	g COD (g COD)$^{-1}$	Jubany et al., 2008
f_{SI}	Production of S_I in hydrolysis	0	g COD (g COD)$^{-1}$	Henze et al., 2000
f_{XI}	Fraction of X_I generated in biomass lysis	0.1	g COD (g COD)$^{-1}$	Henze et al., 2000
n_G	Anoxic growth factor	1	dimensionless	Hiatt and Grady, 2008

iv. Kinetic Parameters (wherever temperature-dependent the value was taken for 20 ºC)

Part A: Hydrolysis Processes				
Symbol	**Denotation**	**Value**	**Units**	**Reference**
K_H	Hydrolysis rate constant	3	d^{-1}	Henze et al., 2000
K_{O2_H}	Saturation/inhibition coefficient for O_2	0.2	g O_2 m^{-3}	Henze et al., 2000
K_{x_H}	Saturation coefficient for particulate COD	0.1	g X_S (g X_H) $^{-1}$	Henze et al., 2000
n_{NO3_H}	Anoxic hydrolysis reduction factor	0.6	Dimensionless	Henze et al., 2000
n_{NO2_H}	Anoxic hydrolysis reduction factor	0.6	Dimensionless	Massara et al., 2018
K_{NO3_H}	Saturation/inhibition coefficient for NO_3^-	0.5	g N m^{-3}	Henze et al., 2000
K_{NO2_H}	Saturation/inhibition coefficient for NO_2^-	0.5	g N m^{-3}	Massara et al., 2018
n_{fe_H}	Anaerobic hydrolysis reduction factor	0.4	Dimensionless	Henze et al., 2000

Part B: Heterotrophic Biomass X_H				
Symbol	**Denotation**	**Value**	**Units**	**Reference**
μ_H	Maximum growth rate on substrate	6	g X_S (g X_H) $^{-1}d^{-1}$	Henze et al., 2000
KO_2	Saturation/inhibition coefficient for O_2	0.2	g O_2 m^{-3}	Henze et al., 2000
K_F	Saturation coefficient for growth on S_F	4	g COD m^{-3}	Henze et al., 2000
K_{NH4}	Saturation coefficient for NH_4^+ (nutrient)	0.05	g N m^{-3}	Henze et al., 2000
K_P	Saturation coefficient for PO_4^{3-} (nutrient)	0.01	g P m^{-3}	Henze et al., 2000
K_{ALK}	Saturation coefficient for alkalinity (HCO_3^-)	0.1	mole HCO_3^- m^{-3}	Henze et al., 2000
K_A	Saturation coefficient for growth on acetate S_A	4	g COD m^{-3}	Henze et al., 2000
K_{NO3}	Saturation/inhibition coefficient for NO_3^-	0.5	g N m^{-3}	Henze et al., 2000
K_{NO2}	Saturation/inhibition coefficient for NO_2^-	0.5	g N m^{-3}	Massara et al., 2018
n_{NO3_D}	Reduction factor for denitrification	0.8	Dimensionless	Henze et al., 2000
q_{fe}	Maximum rate for fermentation	3	g S_F (g X_H) $^{-1}d^{-1}$	Henze et al., 2000
K_{fe_H}	Saturation coefficient for fermentation of S_F	4	g COD m^{-3}	Henze et al., 2000
b_H	Rate constant for lysis and decay	0.4	d^{-1}	Henze et al., 2000
μ_{H_Den}	Maximum specific growth rate of heterotrophs	6.25	d^{-1}	Hiatt and Grady, 2008
n_{G3}	Anoxic growth factor ($NO_2^- \rightarrow NO$)	0.16	Dimensionless	Hiatt and Grady, 2008
n_{G4}	Anoxic growth factor ($NO \rightarrow N_2O$)	0.35	Dimensionless	Hiatt and Grady, 2008
n_{G5}	Anoxic growth factor ($N_2O \rightarrow N_2$)	0.35	Dimensionless	Hiatt and Grady, 2008
K_{S3}	Half-saturation coefficient for substrate	20	mg COD L^{-1}	Hiatt and Grady, 2008
K_{S4}	Half-saturation coefficient for substrate	20	mg COD L^{-1}	Hiatt and Grady, 2008
K_{S5}	Half-saturation coefficient for substrate	40	mg COD L^{-1}	Hiatt and Grady, 2008
K_{NO2_Den}	Half-saturation coefficient for NO_2-N	0.2	mg N L^{-1}	Hiatt and Grady, 2008
K_{OH4}	Half-saturation coefficient for O_2	0.1	mg O_2 L^{-1}	Hiatt and Grady, 2008
K_{N2O_Den}	Half-saturation coefficient for N_2O-N	0.05	mg N L^{-1}	Hiatt and Grady, 2008
K_{OH3}	Half-saturation coefficient for O_2	0.1	mg O_2 L^{-1}	Hiatt and Grady, 2008
K_{NO_Den}	Half-saturation coefficient for NO-N	0.05	mg N L^{-1}	Hiatt and Grady, 2008
K_{OH5}	Half-saturation coefficient for O_2	0.1	mg O_2 L^{-1}	Hiatt and Grady, 2008
K_{I3NO}	NO inhibition coefficient ($NO_2^- \rightarrow NO$)	0.5	mg N L^{-1}	Hiatt and Grady, 2008
K_{I4NO}	NO inhibition coefficient ($NO \rightarrow N_2O$)	0.3	mg N L^{-1}	Hiatt and Grady, 2008
K_{I5NO}	NO inhibition coefficient ($N_2O \rightarrow N_2$)	0.075	mg N L^{-1}	Hiatt and Grady, 2008

Part C: PAOs				
Symbol	**Denotation**	**Value**	**Units**	**Reference**
q_{PHA}	Rate constant for storage of X_{PHA}	3	g X_{PHA} (g X_{PAO})$^{-1}$ d^{-1}	Henze et al., 2000
K_{A_P}	Saturation coefficient for growth on acetate S_A	4	g COD m^{-3}	Henze et al., 2000
K_{ALK_P}	Saturation coefficient for alkalinity (HCO_3^-)	0.1	mole HCO_3^- m^{-3}	Henze et al., 2000
q_{PP}	Rate constant for storage of X_{PP}	1.5	g X_{PP} (g X_{PAO})$^{-1}$ d^{-1}	Henze et al., 2000
K_{O2_P}	Saturation/inhibition coefficient for O_2	0.2	g O_2 m^{-3}	Henze et al., 2000
K_{P_P}	Saturation coefficient for P in storage of PP	0.2	g P m^{-3}	Henze et al., 2000
K_{PHA_P}	Saturation coefficient for PHA	0.01	g X_{PHA} (g X_{PAO})$^{-1}$	Henze et al., 2000
K_{MAX_P}	Maximum ratio of X_{PP}/X_{PAO}	0.34	g X_{PP} (g X_{PAO})$^{-1}$	Henze et al., 2000
K_{PP_P}	Saturation coefficient for PP	0.01	g X_{PP} (g X_{PAO})$^{-1}$	Henze et al., 2000
K_{IPP_P}	Inhibition coefficient for PP storage	0.02	g X_{PP} (g X_{PAO})$^{-1}$	Henze et al., 2000
K_{PO4_P}	Saturation coefficient for PO_4^{3-}	0.01	g P m^{-3}	Henze et al., 2000
n_{NO3_P}	Anoxic hydrolysis reduction factor	0.6	Dimensionless	Henze et al., 2000
n_{NO2_P}	Anoxic hydrolysis reduction factor	0.6	Dimensionless	Massara et al., 2018
K_{NO3_P}	Saturation/inhibition coefficient for NO_3^-	0.5	g N m^{-3}	Henze et al., 2000
K_{NO2_P}	Saturation/inhibition coefficient for NO_2^-	0.5	g N m^{-3}	Massara et al., 2018
μ_{PAO}	Maximum growth rate of PAO	1	d^{-1}	Henze et al., 2000
b_{PAO}	Rate for lysis of X_{PAO}	0.2	d^{-1}	Henze et al., 2000
b_{PP}	Rate for lysis of X_{PP}	0.2	d^{-1}	Henze et al., 2000
b_{PHA}	Rate for lysis of X_{PHA}	0.2	d^{-1}	Henze et al., 2000

Part D: Nitrifying Organisms				
Symbol	**Denotation**	**Value**	**Units**	**Reference**
μ_{AOB_HAO}	Maximum AOB growth rate	0.78	d^{-1}	Hiatt and Grady, 2008
q_{AOB_AMO}	Maximum rate for the AMO reaction	5.2008	mg N (mg COD)$^{-1}$ d^{-1}	Pocquet et al., 2016
K_{O2_AOB1}	AOB affinity constant for O_2 (AMO reaction)	1	mg O_2 L^{-1}	Pocquet et al., 2016
K_{NH4_AOB}	AOB affinity constant for NH_4^+	0.2	mg N L^{-1}	Pocquet et al., 2016
K_{O2_AOB2}	AOB affinity constant for O_2 (HAO reaction)	0.6	mg O_2 L^{-1}	Pocquet et al., 2016
K_{NH2OH_AOB}	AOB affinity constant for NH_2OH	0.9	mg N L^{-1}	Pocquet et al., 2016
q_{AOB_HAO}	Maximum rate for HAO reaction	5.2008	mg N (mg COD)$^{-1}$ d^{-1}	Pocquet et al., 2016
$K_{NO\_AOB\_HAO}$	AOB affinity constant for NO (from HAO)	0.0003	mg N L^{-1}	Pocquet et al., 2016
$q_{AOB\_N2O\_NN}$	Maximum N_2O production rate by NH_2OH oxidation pathway	0.0078	mg N (mg COD)$^{-1}$ d^{-1}	Pocquet et al., 2016
$K_{NO\_AOB\_NN}$	AOB affinity constant for NO (from NirK)	0.008	mg N L^{-1}	Pocquet et al., 2016
$K_{O2\_AOB\_ND}$	AOB constant for O_2 effect on the nitrifier denitrification pathway	0.5	mg O_2 L^{-1}	Pocquet et al., 2016
$K_{I\_O2\_AOB}$	N_2O constant for production inhibition by O_2	0.8	mg O_2 L^{-1}	Pocquet et al., 2016
K_{HNO2_AOB}	AOB affinity constant for HNO_2	0.004	mg N L^{-1}	Pocquet et al., 2016
$q_{AOB\_N2O\_ND}$	Maximum N_2O production rate by the nitrifier denitrification pathway	1.3008	mg N (mg COD)$^{-1}$ d^{-1}	Pocquet et al., 2016
K_{ALK_AOB}	Saturation coefficient for alkalinity (HCO_3^-)	0.1	mole HCO_3^- m^{-3}	Massara et al., 2018
K_{P_AOB}	Saturation coefficient for PO_4^{3-} (nutrient)	0.01	g P m^{-3}	Massara et al., 2018
μ_{NOB} (1st tested)	Maximum NOB growth rate	0.78	d^{-1}	Hiatt and Grady, 2008
μ_{NOB} (2nd tested)	Maximum NOB growth rate	1.02	d^{-1}	Jubany et al., 2008
K_{O2_NOB} (1st tested)	Half-saturation coefficient for O_2	1.2	mg O_2 L^{-1}	Hiatt and Grady, 2008
K_{O2_NOB} (2nd tested)	Half-saturation coefficient for O_2	1.75	mg O_2 L^{-1}	Jubany et al., 2008
K_{ALK_NOB}	Saturation coefficient for alkalinity (HCO_3^-)	0.1	mole HCO_3^- m^{-3}	Massara et al., 2018
K_{NO2_NOB}	Saturation coefficient for NO_2^-	0.5	mg N L^{-1}	Massara et al., 2018
K_{P_NOB}	Saturation coefficient for PO_4^{3-} (nutrient)	0.01	g P m^{-3}	Massara et al., 2018
b_{AOB}	Decay rate of AOB	0.096	d^{-1}	Hiatt and Grady, 2008
b_{NOB} (1st tested)	Decay rate of NOB	0.096	d^{-1}	Hiatt and Grady, 2008
b_{NOB} (2nd tested)	Decay rate of NOB	0.17	d^{-1}	Jubany et al., 2008

Part E: Precipitation of P with $Fe(OH)_3$				
Symbol	**Denotation**	**Value**	**Units**	**Reference**
k_{PRE}	Rate constant for P precipitation	1	m^3 (g $Fe(OH)_3)^{-1}$ d^{-1}	Henze et al., 2000
k_{RED}	Rate constant for redissolution	0.6	d^{-1}	Henze et al., 2000
$K_{ALK\ PR}$	Saturation coefficient for alkalinity (HCO_3^-)	0.5	mole HCO_3^- m^{-3}	Henze et al., 2000

v. Conversion Factors Matrix (ici)

Component	COD	N	P	Charge	TSS
S_{O2}	-1				
S_F	1	i_{NSF}	i_{PSF}		
S_A	1			-1/64	
S_{NH4}		1		1/14	
S_{NH2OH}	-8/7	1			
S_{N2O}	-16/7	1			
S_{NO}	-20/7	1			
S_{NO2}	-24/7	1		-1/14	
S_{NO3}	-32/7	1		-1/14	
S_{PO4}			1	-1.5/31	
S_I	1	i_{NSI}	i_{PSI}		
S_{ALK}				-1	
S_{N2}	-24/14	1			
X_I	1	i_{NXI}	i_{PXI}		i_{TSSXI}
X_S	1	i_{NXS}	i_{PXS}		i_{TSSXS}
X_H	1	i_{NBM}	i_{PBM}		i_{TSSBM}
X_{PAO}	1	i_{NBM}	i_{PBM}		i_{TSSBM}
X_{PP}			1	-1/31	3.23
X_{PHA}	1				0.6
X_{AOB}	1	i_{NBM}	i_{PBM}		i_{TSSBM}
X_{NOB}	1	i_{NBM}	i_{PBM}		i_{TSSBM}
X_{TSS}					-1
X_{MeOH}					1
X_{MeP}			31.0/150.8		1

vi. Stoichiometric Matrix

Part A: Hydrolysis Processes				
Process	**1**	**2**	**3**	**4**
Component	**Aerobic Hydrolysis**	**Anoxic Hydrolysis (1st step: $NO_3^- \rightarrow NO_2^-$)**	**Anoxic Hydrolysis (2nd step: $NO_2^- \rightarrow N_2$)**	**Anaerobic Hydrolysis**
S_{O2}				
S_F	$1-f_{SI}$	$1-f_{SI}$	$1-f_{SI}$	$1-f_{SI}$
S_A				
S_{NH4}	$i_{NXS}-(1-f_{SI})\cdot i_{NSF}$	$i_{NXS}-(1-f_{SI})\cdot i_{NSF}$	$i_{NXS}-(1-f_{SI})\cdot i_{NSF}$	$i_{NXS}-(1-f_{SI})\cdot i_{NSF}$
S_{NH2OH}				
S_{N2O}				
S_{NO}				
S_{NO2}				
S_{NO3}				
S_{PO4}	$i_{PXS}-(1-f_{SI})\cdot i_{PSF}$	$i_{PXS}-(1-f_{SI})\cdot i_{PSF}$	$i_{PXS}-(1-f_{SI})\cdot i_{PSF}$	$i_{PXS}-(1-f_{SI})\cdot i_{PSF}$
S_I	f_{SI}	f_{SI}	f_{SI}	f_{SI}
S_{ALK}[1]				
S_{N2}				
X_I				
X_S	-1	-1	-1	-1
X_H				
X_{PAO}				
X_{PP}				
X_{PHA}				
X_{AOB}				
X_{NOB}				
X_{TSS}[2]				
X_{MeOH}				
X_{MeP}				

[1] The alkalinity stoichiometric coefficient for each one of the processes was calculated by multiplying its column of process coefficients by the fourth column of the Conversion Factors Matrix.

[2] The TSS stoichiometric coefficient for each one of the processes was calculated by multiplying its column of process coefficients by the fifth column of the Conversion Factors Matrix.

Part B: Heterotrophic Biomass X_H

Process	5	6	7	8	9	10	11	12	13	14	15	16
			S_F: Anoxic growth of X_H				S_A: Anoxic growth of X_H					
Component	**Aerobic growth on S_F**	**Aerobic growth on S_A**	**1st step: $NO_3^- \rightarrow NO_2^-$**	**2nd step: $NO_2^- \rightarrow NO$**	**3rd step: $NO \rightarrow N_2O$**	**4th step: $N_2O \rightarrow N_2$**	**1st step: $NO_3^- \rightarrow NO_2^-$**	**2nd step: $NO_2^- \rightarrow NO$**	**3rd step: $NO \rightarrow N_2O$**	**4th step: $N_2O \rightarrow N_2$**	**Fermentation**	**Lysis**
S_{O2}	$1-(1/Y_H)$	$1-(1/Y_H)$										
S_F	$-1/Y_H$		$-1/(Y_H \cdot n_G)$	$-1/(Y_H \cdot n_G)$	$-1/(Y_H \cdot n_G)$	$-1/(Y_H \cdot n_G)$					-1	
S_A		$-1/Y_H$					$-1/(Y_H \cdot n_G)$	$-1/(Y_H \cdot n_G)$	$-1/(Y_H \cdot n_G)$	$-1/(Y_H \cdot n_G)$	1	
S_{NH4}	$-i_{NBM} +1/Y_H \cdot i_{NSF}$	$-i_{NBM}$	$-i_{NBM}+1/Y_H \cdot i_{NSF}$	$-i_{NBM} +1/Y_H \cdot i_{NSF}$	$-i_{NBM} +1/Y_H \cdot i_{NSF}$	$-i_{NBM} +1/Y_H \cdot i_{NSF}$	$-i_{NBM}$	$-i_{NBM}$	$-i_{NBM}$	$-i_{NBM}$	i_{NSF}	$i_{NBM}-i_{NXI} \cdot f_{XI} -(1-f_{XI}) \cdot i_{NXS}$
S_{NH2OH}												
S_{N2O}					$(1-Y_H \cdot n_G) /((4/7) \cdot Y_H \cdot n_G)$	$-(1-Y_H \cdot n_G) /((4/7) \cdot Y_H \cdot n_G)$			$(1-Y_H \cdot n_G) /((4/7) \cdot Y_H \cdot n_G)$	$-(1-Y_H \cdot n_G) /((4/7) \cdot Y_H \cdot n_G)$		
S_{NO}				$(1-Y_H \cdot n_G) /((4/7) \cdot Y_H \cdot n_G)$	$-(1-Y_H \cdot n_G) /((4/7) \cdot Y_H \cdot n_G)$			$(1-Y_H \cdot n_G) /((4/7) \cdot Y_H \cdot n_G)$	$-(1-Y_H \cdot n_G) /((4/7) \cdot Y_H \cdot n_G)$			
S_{NO2}			$(1-Y_H \cdot n_G) /((8/7) \cdot Y_H \cdot n_G)$	$-(1-Y_H \cdot n_G) /((4/7) \cdot Y_H \cdot n_G)$			$(1-Y_H \cdot n_G) /((8/7) \cdot Y_H \cdot n_G)$	$-(1-Y_H \cdot n_G) /((4/7) \cdot Y_H \cdot n_G)$				
S_{NO3}			$-(1-Y_H \cdot n_G) /((8/7) \cdot Y_H \cdot n_G)$				$-(1-Y_H \cdot n_G) /((8/7) \cdot Y_H \cdot n_G)$					
S_{PO4}	$-i_{PBM} +1/Y_H \cdot i_{PSF}$	$-i_{PBM}$	$-i_{PBM}+1/Y_H \cdot i_{PSF}$	$-i_{PBM}+1/Y_H \cdot i_{PSF}$	$-i_{PBM}+1/Y_H \cdot i_{PSF}$	$-i_{PBM}+1/Y_H \cdot i_{PSF}$	$-i_{PBM}$	$-i_{PBM}$	$-i_{PBM}$	$-i_{PBM}$	i_{PSF}	$i_{PBM}-i_{PXI} \cdot f_{XI} -(1-f_{XI}) \cdot i_{PXS}$
S_I												
S_{ALK}												
S_{N2}						$(1-Y_H \cdot n_G)$				$(1-Y_H \cdot n_G)$		

						$/((4/7)\cdot Y_H\cdot n_G)$				$/((4/7)\cdot Y_H\cdot n_G)$	
X_I											f_{XI}
X_S											$1-f_{XI}$
X_H	1	1	1	1	1	1	1	1	1	1	-1
X_{PAO}											
X_{PP}											
X_{PHA}											
X_{AOB}											
X_{NOB}											
X_{TSS}											
X_{MeOH}											
X_{MeP}											

Part C: PAOs

Process	17	18	19	20	21	22	23	24	25	26	27	28	29	30
			Anoxic storage of X_{PP}					Anoxic growth of X_{PAO}						
Component	**Storage of X_{PHA}**	**Aerobic storage of X_{PP}**	**1st step: $NO_3^- \rightarrow NO_2^-$**	**2nd step: $NO_2^- \rightarrow NO$**	**3rd step: $NO \rightarrow N_2O$**	**4th step: $N_2O \rightarrow N_2$**	**Aerobic growth of X_{PAO}**	**1st step: $NO_3^- \rightarrow NO_2^-$**	**2nd step: $NO_2^- \rightarrow NO$**	**3rd step: $NO \rightarrow N_2O$**	**4th step: $N_2O \rightarrow N_2$**	**Lysis of X_{PAO}**	**Lysis of X_{PP}**	**Lysis of X_{PHA}**
S_{O2}		$-Y_{PHA}$					$1-1/Y_{PAO}$							
S_F														
S_A	-1													1
S_{NH4}							$-i_{NBM}$	$-i_{NBM}$	$-i_{NBM}$	$-i_{NBM}$	$-i_{NBM}$	$i_{NBM}-i_{NXI}\cdot f_{XI}-(1-f_{XI})\cdot i_{NXS}$		
S_{NH2OH}														
S_{N2O}					$Y_{PHA}/(4/7)$	$-Y_{PHA}/(4/7)$				$(1-Y_{PAO}\cdot n_G)/((4/7)\cdot Y_{PAO}\cdot n_G)$	$-(1-Y_{PAO}\cdot n_G)/((4/7)\cdot Y_{PAO}\cdot n_G)$			
S_{NO}				$Y_{PHA}/(4/7)$	$-Y_{PHA}/(4/7)$				$(1-Y_{PAO}\cdot n_G)/((4/7)\cdot Y_{PAO}\cdot n_G)$	$-(1-Y_{PAO}\cdot n_G)/((4/7)\cdot Y_{PAO}\cdot n_G)$				
S_{NO2}			$Y_{PHA}/(8/7)$	$-Y_{PHA}/(4/7)$				$(1-Y_{PAO}\cdot n_G)/((8/7)\cdot Y_{PAO}\cdot n_G)$	$-(1-Y_{PAO}\cdot n_G)/((4/7)\cdot Y_{PAO}\cdot n_G)$					
S_{NO3}			$-Y_{PHA}/(8/7)$					$-(1-Y_{PAO}\cdot n_G)/((8/7)\cdot Y_{PAO}\cdot n_G)$						
S_{PO4}	Y_{PO4}	-1	-1	-1	-1	-1	$-i_{PBM}$	$-i_{PBM}$	$-i_{PBM}$	$-i_{PBM}$	$-i_{PBM}$	$i_{PBM}-i_{PXI}\cdot f_{XI}-(1-f_{XI})\cdot i_{PXS}$	1	
S_I														
S_{ALK}														
S_{N2}						$Y_{PHA}/(4/7)$					$(1-Y_{PAO}\cdot n_G)/((4/7)\cdot Y_{PAO}\cdot n_G)$			
X_I												f_{XI}		
X_S												$1-f_{XI}$		
X_H														
X_{PAO}							1	1	1	1	1	-1		

X_{PP}	$-Y_{PO4}$	1	1	1	1	1							-1	
X_{PHA}	1	$-Y_{PHA}$	$-Y_{PHA}$	$-Y_{PHA}$	$-Y_{PHA}$	$-Y_{PHA}$	$-1/Y_{PAO}$	$-1/Y_{PAO}$	$-1/Y_{PAO}$	$-1/Y_{PAO}$	$-1/Y_{PAO}$			-1
X_{AOB}														
X_{NOB}														
X_{TSS}														
X_{MeOH}														
X_{MeP}														

Part D: Nitrifying Organisms								
Process	**31**	**32**	**33**	**34**	**35**	**36**	**37**	**38**
Component	**NH_3 oxidation to NH_2OH coupled with O_2 consumption**	**NH_2OH oxidation to NO coupled with O_2 reduction (*AOB growth here)**	**NO oxidation to NO_2^- coupled with O_2 reduction**	**NO reduction to N_2O coupled with the NH_2OH oxidation to NO_2^- (N_2O from the NH_2OH oxidation pathway)**	**HNO_2 reduction to N_2O coupled with NH_2OH oxidation to NO_2^- (N_2O from the nitrifier denitrification pathway)**	**Aerobic growth of NOB**	**Lysis of AOB**	**Lysis of NOB**
S_{O2}	-8/7	$-(12/7-Y_{AOB})/Y_{AOB}$	-4/7			$-((8/7)-Y_{NOB})/Y_{NOB}$		
S_F								
S_A								
S_{NH4}	-1	$-i_{NBM}$				$-i_{NBM}$	$i_{NBM}-i_{NXI}\cdot f_{XI}-(1-f_{XI})\cdot i_{NXS}$	$i_{NBM}-i_{NXI}\cdot f_{XI}-(1-f_{XI})\cdot i_{NXS}$
S_{NH2OH}	1	$-1/Y_{AOB}$		-1	-1			
S_{N2O}				4	2			
S_{NO}		$1/Y_{AOB}$	-1	-4				
S_{NO2}			1	1	-1	$-1/Y_{NOB}$		
S_{NO3}						$1/Y_{NOB}$		
S_{PO4}		$-i_{PBM}$				$-i_{PBM}$	$i_{PBM}-i_{PXI}\cdot f_{XI}-(1-f_{XI})\cdot i_{PXS}$	$i_{PBM}-i_{PXI}\cdot f_{XI}-(1-f_{XI})\cdot i_{PXS}$
S_I								
S_{ALK}								
S_{N2}								
X_I							f_{XI}	f_{XI}
X_S							$1-f_{XI}$	$1-f_{XI}$
X_H								
X_{PAO}								
X_{PP}								
X_{PHA}								
X_{AOB}		1					-1	
X_{NOB}						1		-1
X_{TSS}								
X_{MeOH}								
X_{MeP}								

Part E: Precipitation of P with $Fe(OH)_3$		
Process	**39**	**40**
Component	**Precipitation**	**Redissolution**
S_{O2}		
S_F		
S_A		
S_{NH4}		
S_{NH2OH}		
S_{N2O}		
S_{NO}		
S_{NO2}		
S_{NO3}		
S_{PO4}	-1	1
S_I		
S_{ALK}		
S_{N2}		
X_I		
X_S		
X_H		
X_{PAO}		
X_{PP}		
X_{PHA}		
X_{AOB}		
X_{NOB}		
X_{TSS}		
X_{MeOH}	-3.45	3.45
X_{MeP}	4.87	-4.87

vii. Process Rates

Part A: Hydrolysis Processes		
Process	**Description**	**Process rate**
1	Aerobic hydrolysis	$K_H \cdot S_{O2}/(K_{O2\_H}+S_{O2}) \cdot (X_S/X_H)/(K_{x\_H}+(X_S/X_H)) \cdot X_H$
2	Anoxic hydrolysis (NO_3^-)	$K_H \cdot n_{NO3\_H} \cdot K_{O2\_H}/(K_{O2\_H}+S_{O2}) \cdot S_{NO3}/(K_{NO3\_H}+S_{NO3}) \cdot (X_S/X_H)/(K_{x\_H}+(X_S/X_H)) \cdot X_H$
3	Anoxic hydrolysis (NO_2^-)	$K_H \cdot n_{NO2\_H} \cdot K_{O2\_H}/(K_{O2\_H}+S_{O2}) \cdot S_{NO2}/(K_{NO2\_H}+S_{NO2}) \cdot (X_S/X_H)/(K_{x\_H}+(X_S/X_H)) \cdot X_H$
4	Anaerobic hydrolysis	$K_H \cdot n_{fe\_H} \cdot K_{O2\_H}/(K_{O2\_H}+S_{O2}) \cdot (K_{NO2\_H}/(K_{NO2\_H}+(S_{NO3}+S_{NO2})) \cdot (X_S/X_H)/(K_{x\_H}+(X_S/X_H)) \cdot X_H$
Part B: Heterotrophic Biomass X_H		
Process	**Description**	**Process rate**
5	Aerobic growth on S_F	$\mu_H \cdot S_F/(K_F+S_F) \cdot S_F/(S_F+S_A) \cdot S_{O2}/(K_{O2}+S_{O2}) \cdot S_{NH4}/(K_{NH4}+S_{NH4}) \cdot S_{PO4}/(K_P+S_{PO4}) \cdot S_{ALK}/(K_{ALK}+S_{ALK}) \cdot X_H$
6	Aerobic growth on S_A	$\mu_H \cdot S_A/(K_A+S_A) \cdot S_A/(S_F+S_A) \cdot S_{O2}/(K_{O2}+S_{O2}) \cdot S_{NH4}/(K_{NH4}+S_{NH4}) \cdot S_{PO4}/(K_P+S_{PO4}) \cdot S_{ALK}/(K_{ALK}+S_{ALK}) \cdot X_H$
7	S_F: Anoxic growth of heterotrophs ($NO_3^- \rightarrow NO_2^-$)	$\mu_H \cdot n_{NO3\_D} \cdot S_F/(K_F+S_F) \cdot S_F/(S_F+S_A) \cdot K_{O2}/(K_{O2}+S_{O2}) \cdot S_{NO3}/(K_{NO3}+S_{NO3}) \cdot S_{NH4}/(K_{NH4}+S_{NH4}) \cdot S_{PO4}/(K_P+S_{PO4}) \cdot S_{ALK}/(K_{ALK}+S_{ALK}) \cdot X_H$
8	S_F: Anoxic growth of heterotrophs ($NO_2^- \rightarrow NO$)	$\mu_H \cdot n_{G3} \cdot S_F/(K_{S3}+S_F) \cdot S_F/(S_F+S_A) \cdot S_{NO2}/(K_{NO2\_Den}+S_{NO2}) \cdot K_{OH3}/(K_{OH3}+S_{O2}) \cdot S_{NH4}/(K_{NH4}+S_{NH4}) \cdot S_{PO4}/(K_P+S_{PO4}) \cdot S_{ALK}/(K_{ALK}+S_{ALK}) \cdot X_H$
9	S_F: Anoxic growth of heterotrophs ($NO \rightarrow N_2O$)	$\mu_H \cdot n_{G4} \cdot S_F/(K_{S4}+S_F) \cdot S_F/(S_F+S_A) \cdot S_{NO}/(K_{NO\_Den} + S_{NO} + S_{NO}^2/K_{I4NO}) \cdot K_{OH4}/(K_{OH4}+S_{O2}) \cdot S_{NH4}/(K_{NH4}+S_{NH4}) \cdot S_{PO4}/(K_P+S_{PO4}) \cdot S_{ALK}/(K_{ALK}+S_{ALK}) \cdot X_H$
10	S_F: Anoxic growth of heterotrophs ($N_2O \rightarrow N_2$)	$\mu_H \cdot n_{G5} \cdot S_F/(K_{S5}+S_F) \cdot S_F/(S_F+S_A) \cdot S_{N2O}/(K_{N2O\_Den}+S_{N2O}) \cdot K_{OH5}/(K_{OH5}+S_{O2}) \cdot S_{NH4}/(K_{NH4}+S_{NH4}) \cdot S_{PO4}/(K_P+S_{PO4}) \cdot S_{ALK}/(K_{ALK}+S_{ALK}) \cdot X_H$
11	S_A: Anoxic growth of heterotrophs ($NO_3^- \rightarrow NO_2^-$)	$\mu_H \cdot n_{NO3\_D} \cdot S_A/(K_A+S_A) \cdot S_A/(S_F+S_A) \cdot K_{O2}/(K_{O2}+S_{O2}) \cdot S_{NO3}/(K_{NO3}+S_{NO3}) \cdot S_{NH4}/(K_{NH4}+S_{NH4}) \cdot S_{PO4}/(K_P+S_{PO4}) \cdot S_{ALK}/(K_{ALK}+S_{ALK}) \cdot X_H$
12	S_A: Anoxic growth of heterotrophs ($NO_2^- \rightarrow NO$)	$\mu_H \cdot n_{G3} \cdot S_A/(K_{S3}+S_A) \cdot S_A/(S_F+S_A) \cdot S_{NO2}/(K_{NO2\_Den}+S_{NO2}) \cdot K_{OH3}/(K_{OH3}+S_{O2}) \cdot S_{NH4}/(K_{NH4}+S_{NH4}) \cdot S_{PO4}/(K_P+S_{PO4}) \cdot S_{ALK}/(K_{ALK}+S_{ALK}) \cdot X_H$
13	S_A: Anoxic growth of heterotrophs ($NO \rightarrow N_2O$)	$\mu_H \cdot n_{G4} \cdot S_A/(K_{S4}+S_A) \cdot S_A/(S_F+S_A) \cdot S_{NO}/(K_{NO\_Den} + S_{NO} + S_{NO}^2/K_{I4NO}) \cdot K_{OH4}/(K_{OH4}+S_{O2}) \cdot S_{NH4}/(K_{NH4}+S_{NH4}) \cdot S_{PO4}/(K_P+S_{PO4}) \cdot S_{ALK}/(K_{ALK}+S_{ALK}) \cdot X_H$
14	S_A: Anoxic growth of heterotrophs ($N_2O \rightarrow N_2$)	$\mu_H \cdot n_{G5} \cdot S_A/(K_{S5}+S_A) \cdot S_A/(S_F+S_A) \cdot S_{N2O}/(K_{N2O\_Den}+S_{N2O}) \cdot K_{OH5}/(K_{OH5}+S_{O2}) \cdot S_{NH4}/(K_{NH4}+S_{NH4}) \cdot S_{PO4}/(K_P+S_{PO4}) \cdot S_{ALK}/(K_{ALK}+S_{ALK}) \cdot X_H$
15	Fermentation	$q_{fe} \cdot K_{O2}/(K_{O2}+S_{O2}) \cdot K_{NO2}/(K_{NO2}+(S_{NO3}+S_{NO2})) \cdot S_F/(K_{fe\_H}+S_F) \cdot S_{ALK}/(K_{ALK}+S_{ALK}) \cdot X_H$
16	Lysis	$b_H \cdot X_H$

Part C: PAOs		
Process	**Description**	**Process rate**
17	Storage of X_{PHA}	$q_{PHA} \cdot S_A/(K_{A\_P}+S_A) \cdot S_{ALK}/(K_{ALK\_P}+S_{ALK}) \cdot (X_{PP}/X_{PAO})/(K_{PP\_P}+(X_{PP}/X_{PAO})) \cdot X_{PAO}$
18	Aerobic storage of X_{PP}	$q_{PP} \cdot S_{O2}/(K_{O2\_P}+S_{O2}) \cdot S_{PO4}/(K_{P\_P}+S_{PO4}) \cdot S_{ALK}/(K_{ALK\_P}+S_{ALK}) \cdot (X_{PHA}/X_{PAO})/(K_{PHA\_P}+(X_{PHA}/X_{PAO})) \cdot (K_{MAX\_P}-(X_{PP}/X_{PAO}))/(K_{IPP\_P}+K_{MAX\_P}-(X_{PP}/X_{PAO})) \cdot X_{PAO}$
19	Anoxic storage of X_{PP} ($NO_3^- \rightarrow NO_2^-$)	$q_{PP} \cdot n_{NO3\_P} \cdot S_{NO3}/(K_{NO3\_P}+S_{NO3}) \cdot K_{O2\_P}/(K_{O2\_P}+S_{O2}) \cdot S_{PO4}/(K_{P\_P}+S_{PO4}) \cdot S_{ALK}/(K_{ALK\_P}+S_{ALK}) \cdot (X_{PHA}/X_{PAO})/(K_{PHA\_P}+(X_{PHA}/X_{PAO})) \cdot (K_{MAX\_P}-(X_{PP}/X_{PAO}))/(K_{IPP\_P}+K_{MAX\_P}-(X_{PP}/X_{PAO})) \cdot X_{PAO}$
20	Anoxic storage of X_{PP} ($NO_2^- \rightarrow NO$)	$q_{PP} \cdot n_{G3} \cdot S_{NO2}/(K_{NO2\_Den}+S_{NO2}) \cdot K_{OH3}/(K_{OH3}+S_{O2}) \cdot S_{PO4}/(K_{P\_P}+S_{PO4}) \cdot S_{ALK}/(K_{ALK\_P}+S_{ALK}) \cdot (X_{PHA}/X_{PAO})/(K_{PHA\_P}+(X_{PHA}/X_{PAO})) \cdot (K_{MAX\_P}-(X_{PP}/X_{PAO}))/(K_{IPP\_P}+K_{MAX\_P}-(X_{PP}/X_{PAO})) \cdot X_{PAO}$
21	Anoxic storage of X_{PP} ($NO \rightarrow N_2O$)	$q_{PP} \cdot n_{G4} \cdot S_{NO}/(K_{NO\_Den} + S_{NO}+S_{NO}^2/K_{I4NO}) \cdot K_{OH4}/(K_{OH4}+S_{O2}) \cdot S_{PO4}/(K_{P\_P}+S_{PO4}) \cdot S_{ALK}/(K_{ALK\_P}+S_{ALK}) \cdot (X_{PHA}/X_{PAO})/(K_{PHA\_P}+(X_{PHA}/X_{PAO})) \cdot (K_{MAX\_P}-(X_{PP}/X_{PAO}))/(K_{IPP\_P}+K_{MAX\_P}-(X_{PP}/X_{PAO})) \cdot X_{PAO}$
22	Anoxic storage of X_{PP} ($N_2O \rightarrow N_2$)	$q_{PP} \cdot n_{G5} \cdot S_{N2O}/(K_{N2O\_Den}+S_{N2O}) \cdot K_{OH5}/(K_{OH5}+S_{O2}) \cdot S_{PO4}/(K_{P\_P}+S_{PO4}) \cdot S_{ALK}/(K_{ALK\_P}+S_{ALK}) \cdot (X_{PHA}/X_{PAO})/(K_{PHA\_P}+(X_{PHA}/X_{PAO})) \cdot (K_{MAX\_P}-(X_{PP}/X_{PAO}))/(K_{IPP\_P}+K_{MAX\_P}-(X_{PP}/X_{PAO})) \cdot X_{PAO}$
23	Aerobic growth of X_{PAO}	$\mu_{PAO} \cdot S_{O2}/(K_{O2\_P}+S_{O2}) \cdot S_{PO4}/(K_{P\_P}+S_{PO4}) \cdot S_{NH4}/(K_{NH4}+S_{NH4}) \cdot S_{ALK}/(K_{ALK\_P}+S_{ALK}) \cdot (X_{PHA}/X_{PAO})/(K_{PHA\_P}+(X_{PHA}/X_{PAO})) \cdot X_{PAO}$
24	Anoxic growth of X_{PAO} ($NO_3^- \rightarrow NO_2^-$)	$\mu_{PAO} \cdot n_{NO3\_P} \cdot S_{NO3}/(K_{NO3\_P}+S_{NO3}) \cdot K_{O2\_P}/(K_{O2\_P}+S_{O2}) \cdot S_{PO4}/(K_{P\_P}+S_{PO4}) \cdot S_{NH4}/(K_{NH4}+S_{NH4}) \cdot S_{ALK}/(K_{ALK\_P}+S_{ALK}) \cdot (X_{PHA}/X_{PAO})/(K_{PHA\_P}+(X_{PHA}/X_{PAO})) \cdot X_{PAO}$
25	Anoxic growth of X_{PAO} ($NO_2^- \rightarrow NO$)	$\mu_{PAO} \cdot n_{G3} \cdot S_{NO2}/(K_{NO2\_Den}+S_{NO2}) \cdot K_{OH3}/(K_{OH3}+S_{O2}) \cdot S_{PO4}/(K_{P\_P}+S_{PO4}) \cdot S_{NH4}/(K_{NH4}+S_{NH4}) \cdot S_{ALK}/(K_{ALK\_P}+S_{ALK}) \cdot (X_{PHA}/X_{PAO})/(K_{PHA\_P}+(X_{PHA}/X_{PAO})) \cdot X_{PAO}$
26	Anoxic growth of X_{PAO}: ($NO \rightarrow N_2O$)	$\mu_{PAO} \cdot n_{G4} \cdot S_{NO}/(K_{NO\_Den} + S_{NO}+S_{NO}^2/K_{I4NO}) \cdot K_{OH4}/(K_{OH4}+S_{O2}) \cdot S_{PO4}/(K_{P\_P}+S_{PO4}) \cdot S_{NH4}/(K_{NH4}+S_{NH4}) \cdot S_{ALK}/(K_{ALK\_P}+S_{ALK}) \cdot (X_{PHA}/X_{PAO})/(K_{PHA\_P}+(X_{PHA}/X_{PAO})) \cdot X_{PAO}$
27	Anoxic growth of X_{PAO}: ($N_2O \rightarrow N_2$)	$\mu_{PAO} \cdot n_{G5} \cdot S_{N2O}/(K_{N2O\_Den}+S_{N2O}) \cdot K_{OH5}/(K_{OH5}+S_{O2}) \cdot S_{PO4}/(K_{P\_P}+S_{PO4}) \cdot S_{NH4}/(K_{NH4}+S_{NH4}) \cdot S_{ALK}/(K_{ALK\_P}+S_{ALK}) \cdot (X_{PHA}/X_{PAO})/(K_{PHA\_P}+(X_{PHA}/X_{PAO})) \cdot X_{PAO}$
28	Lysis of X_{PAO}	$b_{PAO} \cdot S_{ALK}/(K_{ALK\_P}+S_{ALK}) \cdot X_{PAO}$
29	Lysis of X_{PP}	$b_{PP} \cdot S_{ALK}/(K_{ALK\_P}+S_{ALK}) \cdot X_{PP}$
30	Lysis of X_{PHA}	$b_{PHA} \cdot S_{ALK}/(K_{ALK\_P}+S_{ALK}) \cdot X_{PHA}$
Part D: Nitrifying Organisms		
Process	**Description**	**Process rate**
31	NH_3 oxidation to NH_2OH with oxygen consumption	$q_{AOB\_AMO} \cdot S_{O2}/(K_{O2\_AOB1}+S_{O2}) \cdot S_{NH4}/(K_{NH4\_AOB}+S_{NH4}) \cdot X_{AOB}$
32	NH_2OH oxidation to NO with oxygen reduction	$\mu_{AOB\_HAO} \cdot S_{O2}/(K_{O2\_AOB2}+S_{O2}) \cdot S_{NH2OH}/(K_{NH2OH\_AOB}+S_{NH2OH}) \cdot S_{NH4}/(S_{NH4}+10^{-12}) \cdot S_{PO4}/(K_{P\_AOB}+S_{PO4}) \cdot S_{ALK}/(K_{ALK\_AOB}+S_{ALK}) \cdot X_{AOB}$

	(X_{AOB} growth)	
33	NO oxidation to NO_2^- with oxygen reduction	$q_{AOB\_HAO} \cdot S_{O2}/(K_{O2\_AOB2}+S_{O2}) \cdot S_{NO}/(K_{NO\_AOB\_HAO}+S_{NO}) \cdot X_{AOB}$
34	NO reduction to N_2O with the NH_2OH oxidation to NO_2^- (N_2O from NH_2OH oxidation)	$q_{AOB\_N2O\_NN} \cdot S_{NH2OH}/(K_{NH2OH\_AOB}+S_{NH2OH}) \cdot S_{NO}/(K_{NO\_AOB\_NN}+S_{NO}) \cdot X_{AOB}$
35	HNO_2 reduction to N_2O with NH_2OH oxidation to NO_2^- (N_2O from nitrifier denitrification)	$q_{AOB\_N2O\_ND} \cdot S_{NH2OH}/(K_{NH2OH\_AOB}+S_{NH2OH}) \cdot S_{HNO2}/(K_{HNO2\_AOB}+S_{HNO2}) \cdot fS_{O2} \cdot X_{AOB}$ $fS_{O2}= S_{O2}/(K_{O2\_AOB\_ND} + (1-2\cdot(K_{O2\_AOB\_ND}/K_{I\_O2\_AOB})^{1/2})\cdot S_{O2} + ((S_{O2}^2)/K_{I\_O2\_AOB}))$ • $S_{HNO2}=(S_{NO2}/(Ka\cdot 10^{pH} + 1)\cdot(47/14))$ (Jubany, 2007) • $Ka=\exp(-2300/(273+T))$ (Jubany, 2007) • T=20ºC & pH=7 (Massara et al., 2018)
36	Aerobic growth of X_{NOB}	$\mu_{NOB} \cdot S_{O2}/(K_{O2\_NOB}+S_{O2}) \cdot S_{NO2}/(K_{NO2\_NOB}+S_{NO2}) \cdot S_{PO4}/(K_{P\_NOB}+S_{PO4}) \cdot S_{ALK}/(K_{ALK\_NOB}+S_{ALK}) \cdot X_{NOB}$
37	Lysis of AOB	$b_{AOB} \cdot X_{AOB}$
38	Lysis of NOB	$b_{NOB} \cdot X_{NOB}$
Part E: Precipitation of P with $Fe(OH)_3$		
Process	**Description**	**Process rate**
39	Precipitation	$k_{PRE} \cdot S_{PO4} \cdot X_{MeOH}$
40	Redissolution	$k_{RED} \cdot S_{ALK}/(K_{ALK\_PR}+S_{ALK}) \cdot X_{MeP}$

viii. Link to the Continuity Check Matrix File

The continuity matrix (in the form of Excel file) can be accessed through the link provided below:

http://dx.doi.org/10.1016/j.cej.2017.10.119

References (Accompanying Material of Chapter II)

Henze, M., Gujer, W., Mino, T., van Loosdrecht, M.C.M., 2000. Activated Sludge Models ASM1, ASM2, ASM2d, and ASM3. IWA Scientific and Technical Report n.9., IWA Publishing, London.

Hiatt, W.C., and Grady, C.P.L., 2008. An updated process model for carbon oxidation, nitrification, and denitrification. Water Environ. Res. 80: 2145-2156.

Jubany, I., 2007. Operation, modelling and automatic control of complete and partial nitrification of highly concentrated ammonium wastewater. PhD thesis in Chemical Engineering, Universitat Autònoma de Barcelona, Spain. http://tdx.cat/handle/10803/5310, (accessed 15.03.2016).

Jubany, I., Carrera, J., Lafuente, J., Baeza, J.A., 2008. Start-up of a nitrification system with automatic control to treat highly concentrated ammonium wastewater: Experimental results and modelling. Chem. Eng. J. 144: 407-419.

Massara, T.M., Solís, B., Guisasola, A., Katsou, E., Baeza, J.A., 2018. Development of an ASM2d-N_2O model to describe nitrous oxide emissions in municipal WWTPs under dynamic conditions. Chem. Eng. J. 335: 185-196.

Pocquet, M., Wu, Z., Queinnec, I., Spérandio, M., 2016. A two-pathway model for N_2O emissions by ammonium oxidizing bacteria supported by the NO/N_2O variation. Water Res. 88: 948-959.

Accompanying Material of Chapter III

i. Model Components

Component	Denotation	Units
S_{O2}	Dissolved Oxygen	g O_2 m^{-3}
S_S	Readily biodegradable substrate	g COD m^{-3}
S_{NH4}	Ammonium	g N-NH_4^+ m^{-3}
S_{NH2OH}	Hydroxylamine	g N-NH_2OH m^{-3}
S_{N2O}	Nitrous oxide	g N-N_2O m^{-3}
S_{NO}	Nitric oxide	g N-NO m^{-3}
S_{NO2}	Nitrite	g N-NO_2^- m^{-3}
S_{NO3}	Nitrate	g N-NO_3^- m^{-3}
S_{PO4}	Phosphate	g P-PO_4^{3-} m^{-3}
S_I	Soluble, inert, bon-biodegradable organics	g COD m^{-3}
S_{ALK}	Bicarbonate alkalinity	mole HCO_3^- m^{-3}
S_{N2}	Nitrogen	g N m^{-3}
X_I	Particulate, inert, non-biodegradable organics	g COD m^{-3}
X_S	Slowly biodegradable substrate	g COD m^{-3}
X_H	Heterotrophic biomass	g COD m^{-3}
X_{AOB}	Ammonium oxidizing bacteria	g COD m^{-3}
X_{NOB}	Nitrite oxidizing bacteria	g COD m^{-3}
X_{TSS}	Total suspended solids	g TSS m^{-3}

ii. Conversion Factors

Typical Conversion Factors				
Symbol	**Denotation**	**Value**	**Units**	**Reference**
i_{NSF}	N-content of fermentable substrates S_F	0.03	g N (g COD)$^{-1}$	Henze et al., 2000
i_{PSF}	P-content of S_F	0.01	g P (g COD)$^{-1}$	Henze et al., 2000
i_{NSI}	N-content of inert soluble COD S_I	0.01	g N (g COD)$^{-1}$	Henze et al., 2000
i_{PSI}	P-content of S_I	0	g P (g COD)$^{-1}$	Henze et al., 2000
i_{NXI}	N-content of inert particulate COD X_I	0.02	g N (g COD)$^{-1}$	Henze et al., 2000
i_{PXI}	P-content of X_I	0.01	g P (g COD)$^{-1}$	Henze et al., 2000
i_{TSSXI}	Total Suspended Solids (TSS) to COD ratio for X_I	0.75	g TSS (g COD)$^{-1}$	Henze et al., 2000
i_{NXS}	N-content of slowly biodegradable substrate X_S	0.04	g N (g COD)$^{-1}$	Henze et al., 2000
i_{PXS}	P-content of X_S	0.01	g P (g COD)$^{-1}$	Henze et al., 2000
i_{TSSXS}	TSS to COD ratio for X_S	0.75	g TSS (g COD)$^{-1}$	Henze et al., 2000
i_{NBM}	N-content of heterotrophic biomass ($X_H$and autotrophic nitrifiers (X_{AOB} and X_{NOB})	0.07	g N (g COD)$^{-1}$	Henze et al., 2000
i_{PBM}	P-content of X_H, X_{AOB} and X_{NOB}	0.02	g P (g COD)$^{-1}$	Henze et al., 2000
i_{TSSBM}	TSS to COD ratio for X_H, X_{AOB} and X_{NOB}	0.9	g TSS (g COD)$^{-1}$	Henze et al., 2000

iii. Stoichiometric Parameters

Typical Stoichiometric Parameters				
Symbol	**Denotation**	**Value**	**Units**	**Reference**
Y_H	Yield coefficient of X_H	0.625	g COD (g COD)$^{-1}$	Henze et al., 2000
Y_{AOB}	Yield coefficient for the Ammonia Oxidizing Bacteria (AOB)	0.18	g COD (g COD)$^{-1}$	Jubany et al., 2008
Y_{NOB}	Yield coefficient for the Nitrite Oxidizing Bacteria (NOB)	0.08	g COD (g COD)$^{-1}$	Jubany et al., 2008
f_{SI}	Production of S_I in hydrolysis	0	g COD (g COD)$^{-1}$	Henze et al., 2000
f_{XI}	Fraction of X_I generated in biomass lysis	0.1	g COD (g COD)$^{-1}$	Henze et al., 2000
n_G	Anoxic growth factor	1	dimensionless	Hiatt and Grady, 2008

iv. Kinetic Parameters (wherever temperature-dependent the value was taken for 20 ºC)

Part A: Hydrolysis Processes				
Symbol	**Denotation**	**Value**	**Units**	**Reference**
K_H	Hydrolysis rate constant	3	d^{-1}	Henze et al., 2000
K_{O2_H}	Saturation/inhibition coefficient for O_2	0.2	g O_2 m^{-3}	Henze et al., 2000
K_{x_H}	Saturation coefficient for particulate COD	0.1	g X_S (g X_H) $^{-1}$	Henze et al., 2000
n_{NO3_H}	Anoxic hydrolysis reduction factor	0.6	Dimensionless	Henze et al., 2000
n_{NO2_H}	Anoxic hydrolysis reduction factor	0.6	Dimensionless	Massara et al., 2018
K_{NO3_H}	Saturation/inhibition coefficient for NO_3^-	0.5	g N m^{-3}	Henze et al., 2000
K_{NO2_H}	Saturation/inhibition coefficient for NO_2^-	0.5	g N m^{-3}	Massara et al., 2018
n_{fe_H}	Anaerobic hydrolysis reduction factor	0.4	Dimensionless	Henze et al., 2000

Part B: Heterotrophic Biomass X_H				
Symbol	**Denotation**	**Value**	**Units**	**Reference**
μ_H	Maximum growth rate on substrate	6	g X_S (g X_H) $^{-1}d^{-1}$	Henze et al., 2000
KO_2	Saturation/inhibition coefficient for O_2	0.2	g O_2 m^{-3}	Henze et al., 2000
K_F	Saturation coefficient for growth on S_F	4	g COD m^{-3}	Henze et al., 2000
K_{NH4}	Saturation coefficient for NH_4^+ (nutrient)	0.05	g N m^{-3}	Henze et al., 2000
K_P	Saturation coefficient for PO_4^{3-} (nutrient)	0.01	g P m^{-3}	Henze et al., 2000
K_{ALK}	Saturation coefficient for alkalinity (HCO_3^-)	0.1	mole HCO_3^- m^{-3}	Henze et al., 2000
K_{NO3}	Saturation/inhibition coefficient for NO_3^-	0.5	g N m^{-3}	Henze et al., 2000
n_{NO3_D}	Reduction factor for denitrification	0.8	Dimensionless	Henze et al., 2000
b_H	Rate constant for lysis and decay	0.4	d^{-1}	Henze et al., 2000
n_{G3}	Anoxic growth factor ($NO_2^- \rightarrow NO$)	0.16	Dimensionless	Hiatt and Grady, 2008
n_{G4}	Anoxic growth factor ($NO \rightarrow N_2O$)	0.35	Dimensionless	Hiatt and Grady, 2008
n_{G5}	Anoxic growth factor ($N_2O \rightarrow N_2$)	0.35	Dimensionless	Hiatt and Grady, 2008
K_{S3}	Half-saturation coefficient for substrate	20	mg COD L^{-1}	Hiatt and Grady, 2008
K_{S4}	Half-saturation coefficient for substrate	20	mg COD L^{-1}	Hiatt and Grady, 2008
K_{S5}	Half-saturation coefficient for substrate	40	mg COD L^{-1}	Hiatt and Grady, 2008
K_{NO2_Den}	Half-saturation coefficient for NO_2-N	0.2	mg N L^{-1}	Hiatt and Grady, 2008
K_{OH4}	Half-saturation coefficient for O_2	0.1	mg O_2 L^{-1}	Hiatt and Grady, 2008
K_{N2O_Den}	Half-saturation coefficient for N_2O-N	0.05	mg N L^{-1}	Hiatt and Grady, 2008
K_{OH3}	Half-saturation coefficient for O_2	0.1	mg O_2 L^{-1}	Hiatt and Grady, 2008
K_{NO_Den}	Half-saturation coefficient for NO-N	0.05	mg N L^{-1}	Hiatt and Grady, 2008
K_{OH5}	Half-saturation coefficient for O_2	0.1	mg O_2 L^{-1}	Hiatt and Grady, 2008
K_{I4NO}	NO inhibition coefficient ($NO \rightarrow N_2O$)	0.3	mg N L^{-1}	Hiatt and Grady, 2008

Part C: Nitrifying Organisms				
Symbol	**Denotation**	**Value**	**Units**	**Reference**
μ_{AOB_HAO}	Maximum AOB growth rate	0.78	d^{-1}	Hiatt and Grady, 2008
q_{AOB_AMO}	Maximum rate for the AMO reaction	5.2008	mg N $(mgCOD)^{-1}$ d^{-1}	Pocquet et al., 2016
K_{O2_AOB1}	AOB affinity constant for O_2 (AMO reaction)	1	mg O_2 L^{-1}	Pocquet et al., 2016
K_{NH4_AOB}	AOB affinity constant for NH_4^+	0.2	mg N L^{-1}	Pocquet et al., 2016
K_{O2_AOB2}	AOB affinity constant for O_2 (HAO reaction)	0.6	mg O_2 L^{-1}	Pocquet et al., 2016
K_{NH2OH_AOB}	AOB affinity constant for NH_2OH	0.9	mg N L^{-1}	Pocquet et al., 2016
q_{AOB_HAO}	Maximum rate for HAO reaction	5.2008	mg N $(mgCOD)^{-1}$ d^{-1}	Pocquet et al., 2016
$K_{NO\_AOB\_HAO}$	AOB affinity constant for NO (from HAO)	0.0003	mg N L^{-1}	Pocquet et al., 2016
$q_{AOB\_N2O\_NN}$	Maximum N_2O production rate by NH_2OH oxidation pathway	0.0078	mg N $(mgCOD)^{-1}$ d^{-1}	Pocquet et al., 2016
$K_{NO\_AOB\_NN}$	AOB affinity constant for NO (from NirK)	0.008	mg N L^{-1}	Pocquet et al., 2016
$K_{O2\_AOB\_ND}$	AOB constant for O_2 effect on the nitrifier denitrification pathway	0.5	mg O_2 L^{-1}	Pocquet et al., 2016
$K_{I\_O2\_AOB}$	N_2O constant for production inhibition by O_2	0.8	mg O_2 L^{-1}	Pocquet et al., 2016
K_{HNO2_AOB}	AOB affinity constant for HNO_2	0.004	mg N L^{-1}	Pocquet et al., 2016
$q_{AOB\_N2O\_ND}$	Maximum N_2O production rate by the nitrifier denitrification pathway	1.3008	mg N $(mgCOD)^{-1}$ d^{-1}	Pocquet et al., 2016
K_{ALK_AOB}	Saturation coefficient for alkalinity (HCO_3^-)	0.1	mole HCO_3^- m^{-3}	Massara et al., 2018
K_{P_AOB}	Saturation coefficient for PO_4^{3-} (nutrient)	0.01	g P m^{-3}	Massara et al., 2018
μ_{NOB}	Maximum NOB growth rate	0.78	d^{-1}	Hiatt and Grady, 2008
K_{O2_NOB}	Half-saturation coefficient for O_2	1.2	mg O_2 L^{-1}	Hiatt and Grady, 2008
K_{ALK_NOB}	Saturation coefficient for alkalinity (HCO_3^-)	0.1	mole HCO_3^- m^{-3}	Massara et al., 2018
K_{NO2_NOB}	Saturation coefficient for NO_2^-	0.5	mg N L^{-1}	Massara et al., 2018
K_{P_NOB}	Saturation coefficient for PO_4^{3-} (nutrient)	0.01	g P m^{-3}	Massara et al., 2018
b_{AOB}	Decay rate of AOB	0.096	d^{-1}	Hiatt and Grady, 2008
b_{NOB}	Decay rate of NOB	0.096	d^{-1}	Hiatt and Grady, 2008
Part D: Abiotic N_2O production				
Symbol	**Denotation**	**Value**	**Units**	**Reference**
kabiotic_1	Rate constant for NH_2OH decomposition to N_2O	0.168	L mg N^{-1} d^{-1}	Current study

kabiotic_2	Rate constant for N-nitrosation of NH_2OH with HNO_2 as nitrosating agent	0.024	L mg N^{-1} d^{-1}	Harper et al., 2015

v. Conversion Factors Matrix (ici)

Component	COD	N	P	Charge	TSS
S_{O2}	-1				
S_S	1	i_{NSF}	i_{PSF}		
S_{NH4}		1		1/14	
S_{NH2OH}	-8/7	1			
S_{N2O}	-16/7	1			
S_{NO}	-20/7	1			
S_{NO2}	-24/7	1		-1/14	
S_{NO3}	-32/7	1		-1/14	
S_{PO4}			1	-1.5/31	
S_I	1	i_{NSI}	i_{PSI}		
S_{ALK}				-1	
S_{N2}	-24/14	1			
X_I	1	i_{NXI}	i_{PXI}		i_{TSSXI}
X_S	1	i_{NXS}	i_{PXS}		i_{TSSXS}
X_H	1	i_{NBM}	i_{PBM}		i_{TSSBM}
X_{AOB}	1	i_{NBM}	i_{PBM}		i_{TSSBM}
X_{NOB}	1	i_{NBM}	i_{PBM}		i_{TSSBM}
X_{TSS}					-1

vi. Stoichiometric Matrix

Part A: Hydrolysis Processes				
Process	**1**	**2**	**3**	**4**
Component	**Aerobic Hydrolysis**	**Anoxic Hydrolysis (1st step: $NO_3^- \rightarrow NO_2^-$)**	**Anoxic Hydrolysis (2nd step: $NO_2^- \rightarrow N_2$)**	**Anaerobic Hydrolysis**
S_{O2}				
S_S	$1-f_{SI}$	$1-f_{SI}$	$1-f_{SI}$	$1-f_{SI}$
S_{NH4}	$i_{NXS}-(1-f_{SI}) \cdot i_{NSF}$	$i_{NXS}-(1-f_{SI}) \cdot i_{NSF}$	$i_{NXS}-(1-f_{SI}) \cdot i_{NSF}$	$i_{NXS}-(1-f_{SI}) \cdot i_{NSF}$
S_{NH2OH}				
S_{N2O}				
S_{NO}				
S_{NO2}				
S_{NO3}				
S_{PO4}	$i_{PXS}-(1-f_{SI}) \cdot i_{PSF}$	$i_{PXS}-(1-f_{SI}) \cdot i_{PSF}$	$i_{PXS}-(1-f_{SI}) \cdot i_{PSF}$	$i_{PXS}-(1-f_{SI}) \cdot i_{PSF}$
S_I	f_{SI}	f_{SI}	f_{SI}	f_{SI}
S_{ALK}[1]				
S_{N2}				
X_I				
X_S	-1	-1	-1	-1
X_H				
X_{AOB}				
X_{NOB}				
X_{TSS}[2]				

[1] The alkalinity stoichiometric coefficient for each one of the processes was calculated by multiplying its column of process coefficients by the 4th column of the Conversion Factors Matrix.

[2] The TSS stoichiometric coefficient for each one of the processes was calculated by multiplying its column of process coefficients by the 5th column of the Conversion Factors Matrix.

Part B: Heterotrophic Biomass X_H						
Process	**5**	**6**	**7**	**8**	**9**	**10**
Component	**Aerobic growth on S_S**	**S_S: Anoxic growth of X_H**				**Lysis**
		1st step: $NO_3^- \rightarrow NO_2^-$	**2nd step: $NO_2^- \rightarrow NO$**	**3rd step: $NO \rightarrow N_2O$**	**4th step: $N_2O \rightarrow N_2$**	
S_{O2}	$1-(1/Y_H)$					
S_S	$-1/Y_H$	$-1/Y_H$	$-1/(Y_H \cdot n_G)$	$-1/(Y_H \cdot n_G)$	$-1/(Y_H \cdot n_G)$	
S_{NH4}	$-i_{NBM}$	$-i_{NBM}$	$-i_{NBM}$	$-i_{NBM}$	$-i_{NBM}$	$i_{NBM}-i_{NXI} \cdot f_{XI}$
S_{NH2OH}						
S_{N2O}				$(1-Y_H \cdot n_G)/((4/7) \cdot Y_H \cdot n_G)$	$-(1-Y_H \cdot n_G)/((4/7) \cdot Y_H \cdot n_G)$	
S_{NO}			$(1-Y_H \cdot n_G)/((4/7) \cdot Y_H \cdot n_G)$	$-(1-Y_H \cdot n_G)/((4/7) \cdot Y_H \cdot n_G)$		
S_{NO2}		$(1-Y_H \cdot n_G)/((8/7) \cdot Y_H \cdot n_G)$	$-(1-Y_H \cdot n_G)/((4/7) \cdot Y_H \cdot n_G)$			
S_{NO3}		$-(1-Y_H \cdot n_G)/((8/7) \cdot Y_H \cdot n_G)$				
S_{PO4}	$-i_{PBM}$	$-i_{PBM}$	$-i_{PBM}$	$-i_{PBM}$	$-i_{PBM}$	$i_{PBM}-i_{PXI} \cdot f_{XI}$
S_I						
S_{ALK}[1]						
S_{N2}					$(1-Y_H \cdot n_G)/((4/7) \cdot Y_H \cdot n_G)$	
X_I						f_{XI}
X_S						$1-f_{XI}$
X_H	1	1	1	1	1	-1
X_{AOB}						
X_{NOB}						
X_{TSS}[2]						

Part C: Nitrifying Organisms								
Process	**11**	**12**	**13**	**14**	**15**	**16**	**17**	**18**
Component	**NH_3 oxidation to NH_2OH coupled with O_2 consumption**	**NH_2OH oxidation to NO coupled with O_2 reduction (*AOB growth here)**	**NO oxidation to NO_2^- coupled with O_2 reduction**	**NO reduction to N_2O coupled with the NH_2OH oxidation to NO_2^- (N_2O from the NH_2OH oxidation pathway)**	**HNO_2 reduction to N_2O coupled with NH_2OH oxidation to NO_2^- (N_2O from the nitrifier denitrification pathway)**	**Aerobic growth of NOB**	**Lysis of AOB**	**Lysis of NOB**
S_{O2}	-8/7	$-(12/7-Y_{AOB})/Y_{AOB}$	-4/7			$-((8/7)-Y_{NOB})/Y_{NOB}$		
S_S								
S_{NH4}	-1	$-i_{NBM}$				$-i_{NBM}$	$i_{NBM}-i_{NXI}\cdot f_{XI}$	$i_{NBM}-i_{NXI}\cdot f_{XI}$
S_{NH2OH}	1	$-1/Y_{AOB}$		-1	-1			
S_{N2O}				4	2			
S_{NO}		$1/Y_{AOB}$	-1	-4				
S_{NO2}			1	1	-1	$-1/Y_{NOB}$		
S_{NO3}						$1/Y_{NOB}$		
S_{PO4}		$-i_{PBM}$				$-i_{PBM}$	$i_{PBM}-i_{PXI}\cdot f_{XI}$	$i_{PBM}-i_{PXI}\cdot f_{XI}$
S_I								
S_{ALK}[1]								
S_{N2}								
X_I							f_{XI}	f_{XI}
X_S							$1-f_{XI}$	$1-f_{XI}$
X_H								
X_{AOB}		1					-1	
X_{NOB}						1		-1
X_{TSS}[2]								

Part D: Abiotic N_2O production		
Process	**19**	**20**
Component	**NH_2OH decomposition to N_2O**	**N-nitrosation of NH_2OH with HNO_2 as nitrosating agent**
S_{O2}		
S_S		
S_{NH4}	1/2	
S_{NH2OH}	-1	-1
S_{N2O}	1/2	2
S_{NO}		
S_{NO2}		-1
S_{NO3}		
S_{PO4}		
S_I		
S_{ALK}[1]		
S_{N2}		
X_I		
X_S		
X_H		
X_{AOB}		
X_{NOB}		
X_{TSS}[2]		

vii. Process Rates

Part A: Hydrolysis Processes		
Process	**Description**	**Process rate**
1	Aerobic hydrolysis	$K_H \cdot [S_{O2}/(K_{O2\_H}+S_{O2})] \cdot [(X_S/X_H)/(K_{x\_H}+(X_S/X_H))] \cdot X_H$
2	Anoxic hydrolysis (NO_3^-)	$K_H \cdot n_{NO3\_H} \cdot [K_{O2\_H}/(K_{O2\_H}+S_{O2})] \cdot [S_{NO3}/(K_{NO3\_H}+S_{NO3})] \cdot [(X_S/X_H)/(K_{x\_H}+(X_S/X_H))] \cdot X_H$
3	Anoxic hydrolysis (NO_2^-)	$K_H \cdot n_{NO2\_H} \cdot [K_{O2\_H}/(K_{O2\_H}+S_{O2})] \cdot [S_{NO2}/(K_{NO2\_H}+S_{NO2})] \cdot [(X_S/X_H)/(K_{x\_H}+(X_S/X_H))] \cdot X_H$
4	Anaerobic hydrolysis	$K_H \cdot n_{fe\_H} \cdot [K_{O2\_H}/(K_{O2\_H}+S_{O2})] \cdot [(K_{NO2\_H}/(K_{NO2\_H}+(S_{NO3}+S_{NO2}))] \cdot [(X_S/X_H)/(K_{x\_H}+(X_S/X_H))] \cdot X_H$
Part B: Heterotrophic Biomass X_H		
Process	**Description**	**Process rate**
5	Aerobic growth on S_S	$\mu_H \cdot [S_S/(K_F+S_S)] \cdot [S_{O2}/(K_{O2}+S_{O2})] \cdot [S_{NH4}/(K_{NH4}+S_{NH4})] \cdot [S_{PO4}/(K_P+S_{PO4})] \cdot [S_{ALK}/(K_{ALK}+S_{ALK})] \cdot X_H$
6	S_S: Anoxic growth of heterotrophs ($NO_3^- \rightarrow NO_2^-$)	$\mu_H \cdot n_{NO3\_D} \cdot [S_s/(K_F+S_s)] \cdot [K_{O2}/(K_{O2}+S_{O2})] \cdot [S_{NO3}/(K_{NO3}+S_{NO3})] \cdot [S_{NH4}/(K_{NH4}+S_{NH4})] \cdot [S_{PO4}/(K_P+S_{PO4})] \cdot [S_{ALK}/(K_{ALK}+S_{ALK})] \cdot X_H$
7	S_S: Anoxic growth of heterotrophs ($NO_2^- \rightarrow NO$)	$\mu_H \cdot n_{G3} \cdot [S_S/(K_{S3}+ S_S)] \cdot [S_{NO2}/(K_{NO2\_Den}+S_{NO2})] \cdot [K_{OH3}/(K_{OH3}+S_{O2})] \cdot [S_{NH4}/(K_{NH4}+S_{NH4})] \cdot [S_{PO4}/(K_P+S_{PO4})] \cdot [S_{ALK}/(K_{ALK}+S_{ALK})] \cdot X_H$
8	S_S: Anoxic growth of heterotrophs ($NO \rightarrow N_2O$)	$\mu_H \cdot n_{G4} \cdot [S_S/(K_{S4}+S_S)] \cdot [S_{NO}/(K_{NO\_Den} + S_{NO} + S_{NO}^2/K_{I4NO})] \cdot [K_{OH4}/(K_{OH4}+S_{O2})] \cdot [S_{NH4}/(K_{NH4}+S_{NH4})] \cdot [S_{PO4}/(K_P+S_{PO4})] \cdot [S_{ALK}/(K_{ALK}+S_{ALK})] \cdot X_H$
9	S_S: Anoxic growth of heterotrophs ($N_2O \rightarrow N_2$)	$\mu_H \cdot n_{G5} \cdot [S_S /(K_{S5}+S_S)] \cdot [S_{N2O}/(K_{N2O\_Den}+S_{N2O})] \cdot [K_{OH5}/(K_{OH5}+S_{O2})] \cdot [S_{NH4}/(K_{NH4}+S_{NH4})] \cdot [S_{PO4}/(K_P+S_{PO4})] \cdot [S_{ALK}/(K_{ALK}+S_{ALK})] \cdot X_H$
10	Lysis	$b_H \cdot X_H$
Part C: Nitrifying Organisms		
Process	**Description**	**Process rate**
11	NH_3 oxidation to NH_2OH with oxygen consumption	$q_{AOB\_AMO} \cdot [S_{O2}/(K_{O2\_AOB1}+S_{O2})] \cdot [S_{NH4}/(K_{NH4\_AOB}+S_{NH4})] \cdot X_{AOB}$
12	NH_2OH oxidation to NO with oxygen reduction (X_{AOB} growth)	$\mu_{AOB\_HAO} \cdot [S_{O2}/(K_{O2\_AOB2}+S_{O2})] \cdot [S_{NH2OH}/(K_{NH2OH\_AOB}+S_{NH2OH})] \cdot [S_{NH4}/(S_{NH4}+10^{-12})] \cdot [S_{PO4}/(K_{P\_AOB}+S_{PO4})] \cdot [S_{ALK}/(K_{ALK\_AOB}+S_{ALK})] \cdot X_{AOB}$
13	NO oxidation to NO_2^- with oxygen reduction	$q_{AOB\_HAO} \cdot [S_{O2}/(K_{O2\_AOB2}+S_{O2})] \cdot [S_{NO}/(K_{NO\_AOB\_HAO}+S_{NO})] \cdot X_{AOB}$
14	NO reduction to N_2O with the NH_2OH oxidation to NO_2^- (N_2O	$q_{AOB\_N2O\_NN} \cdot [S_{NH2OH}/(K_{NH2OH\_AOB}+S_{NH2OH})] \cdot [S_{NO}/(K_{NO\_AOB\_NN}+S_{NO})] \cdot X_{AOB}$

	from NH_2OH oxidation)	
15	HNO_2 reduction to N_2O with NH_2OH oxidation to NO_2^- (N_2O from nitrifier denitrification)	$q_{AOB\_N2O\_ND} \cdot [S_{NH2OH}/(K_{NH2OH\_AOB}+S_{NH2OH})] \cdot [S_{HNO2}/(K_{HNO2\_AOB}+S_{HNO2})] \cdot fS_{O2} \cdot X_{AOB}$ $fS_{O2} = S_{O2} / [(K_{O2\_AOB\_ND} + (1-2\cdot(K_{O2\_AOB\_ND}/K_{I\_O2\_AOB})^{1/2}) \cdot S_{O2} + ((S_{O2}^2)/K_{I\_O2\_AOB}))]$ • $S_{HNO2} = S_{NO2} / [(Ka\cdot 10^{pH} + 1) \cdot (47/14)]$ (Jubany, 2007) • $Ka = \exp(-2300/(273+T))$ (Jubany, 2007) • T = 20 ºC & pH = 7 (Massara et al., 2018)
16	Aerobic growth of X_{NOB}	$\mu_{NOB} \cdot [S_{O2}/(K_{O2\_NOB}+S_{O2})] \cdot [S_{NO2}/(K_{NO2\_NOB}+S_{NO2})] \cdot [S_{PO4}/(K_{P\_NOB}+S_{PO4})] \cdot [S_{ALK}/(K_{ALK\_NOB}+S_{ALK})] \cdot X_{NOB}$
17	Lysis of AOB	$b_{AOB} \cdot X_{AOB}$
18	Lysis of NOB	$b_{NOB} \cdot X_{NOB}$
Part D: Abiotic N_2O production		
Process	**Description**	**Process rate**
19	NH_2OH decomposition to N_2O	$k_{abiotic\_1} \cdot S_{NH2OH}$
20	N-nitrosation of NH_2OH with HNO_2 as nitrosating agent	$k_{abiotic\_2} \cdot S_{NH2OH} * S_{NO2}$

References (Accompanying Material of Chapter III)

Harper, W.F., Takeuchi, Y., Riya, S., Hosomi, M., Terada, A., 2015. Novel abiotic reactions increase nitrous oxide production during partial nitrification: Modelling and experiments. Chem. Eng. J. 281: 1017-1023.

Henze, M., Gujer, W., Mino, T., van Loosdrecht, M., 2000. Activated Sludge Models ASM1, ASM2, ASM2d and ASM3. IWA Publishing, London, United Kingdom.

Hiatt, W.C., Grady, C.P.L., 2008. An updated process model for carbon oxidation, nitrification, and denitrification. Water Environ. Res. 80: 2145-2156.

Jubany, I., 2007. Operation, modeling and automatic control of complete and partial nitrification of highly concentrated ammonium wastewater. PhD thesis in Chemical Engineering, Universitat Autònoma de Barcelona, Spain. http://tdx.cat/handle/10803/5310; accessed 15.03.2016.

Jubany, I., Carrera, J., Lafuente, J., Baeza, J.A., 2008. Start-up of a nitrification system with automatic control to treat highly concentrated ammonium wastewater: Experimental results and modelling. Chem. Eng. J. 144: 407-419.

Massara, T.M., Solís, B., Guisasola, A., Katsou, E., Baeza, J.A., 2018. Development of an ASM2d-N_2O model to describe nitrous oxide emissions in municipal WWTPs under dynamic conditions. Chem. Eng. J. 335: 185-196.

Pocquet, M., Wu, Z., Queinnec, I., Sperandio, M., 2016. A two-pathway model for N_2O emissions by ammonium oxidizing bacteria supported by the NO/N_2O variation. Water Res. 88: 948-959.

Accompanying Material of Chapter IV

i. Model Components

Variable	Definition	Unit
S_{O2}	Dissolved oxygen	mmol O_2 L^{-1}
S_{NH3}	Ammonia (NH_3)	mmol N-NH_3 L^{-1}
S_{NO3}	Nitrate (NO_3^-)	mmol N-NO_3^- L^{-1}
S_{NO2}	Nitrite (NO_2^-)	mmol N-NO_2^- L^{-1}
S_{NO}	Nitric oxide (NO)	mmol N-NO L^{-1}
S_{N2O}	Nitrous oxide (N_2O)	mmol N-N_2O L^{-1}
S_{NH2OH}	Hydroxylamine (NH_2OH)	mmol N-NH_2OH L^{-1}
S_{Mred_AOB}	Reduced form of electron carrier (AOB)	mmol as Mred L^{-1}
S_{Mox_AOB}	Oxidized form of electron carrier (AOB)	mmol as Mox L^{-1}
S_{Mred_HB}	Reduced form of electron carrier (HB)	mmol as Mred L^{-1}
S_{Mox_HB}	Oxidized form of electron carrier (HB)	mmol as Mox L^{-1}
X_{AOB}	Ammonia Oxidizing Bacteria (AOB)	g VSS L^{-1}
S_S	Readily biodegradable COD	mmol COD L^{-1}
X_S	Slowly biodegradable COD	mmol COD L^{-1}
X_H	Heterotrophic Biomass (HB)	g VSS L^{-1}
X_{NOB}	Nitrite Oxidizing Bacteria (NOB)	g VSS L^{-1}

ii. Kinetic rate expressions for the integrated N_2O production model

Process	Kinetic rate expression
Ammonium Oxidizing Bacteria (AOB)	
R1: NH_3 oxidation to NH_2OH	$r_{NH3\_Ox} \left(\frac{S_{O2}}{K_{O2\_NH3}+S_{O2}}\right) \left(\frac{S_{NH3}}{K_{NH3}+S_{NH3}}\right) \left(\frac{S_{Mred\_AOB}}{K_{Mred1\_AOB}+S_{Mred\_AOB}}\right) X_{AOB}$
R2: NH_2OH oxidation to NO	$r_{NH2OH\_Ox} \left(\frac{S_{NH2OH}}{K_{NH2OH}+S_{NH2OH}}\right) \left(\frac{S_{Mox\_AOB}}{K_{Mox\_AOB}+S_{Mox\_AOB}}\right) X_{AOB}$
R3: NO oxidation to NO_2^-	$r_{NO\_Ox} \left(\frac{S_{NO}}{K_{NO\_Ox}+S_{NO}}\right) \left(\frac{S_{Mox\_AOB}}{K_{Mox\_AOB}+S_{Mox\_AOB}}\right) X_{AOB}$
R4: NO reduction to N_2O	$r_{NO\_red} \left(\frac{S_{NO}}{K_{NO\_red}+S_{NO}}\right) \left(\frac{S_{Mred\_AOB}}{K_{Mred2\_AOB}+S_{Mred\_AOB}}\right) X_{AOB}$
R5: O_2 reduction to H_2O	$r_{O2\_red} \left(\frac{S_{O2}}{K_{O2\_red}+S_{O2}}\right) \left(\frac{S_{Mred\_AOB}}{K_{Mred3\_AOB}+S_{Mred\_AOB}}\right) X_{AOB}$
R6: NO_2^- reduction to N_2O	$r_{NO2\_red} \left(\frac{S_{NO2}}{K_{NO2\_AOB}+S_{NO2}}\right) \left(\frac{S_{Mred\_AOB}}{K_{Mred4\_AOB}+S_{Mred\_AOB}}\right) X_{AOB}$
R7: Decay of AOB	$b_{AOB} * X_{AOB}$
E1: Electron carriers equation for AOB	$SM_{red\_AOB} + SM_{ox\_AOB} = C_{tot\_AOB}$
Heterotrophic Bacteria (HB)	
R8: Xs hydrolysis	$k_H \left(\frac{X_S/X_H}{K_H+X_S/X_H}\right) X_H$
R9: Aerobic COD oxidation	$r_{COD\_max} \left(\frac{S_S}{K_S+S_S}\right) \left(\frac{S_{Mox\_HB}}{K_{Mox\_HB}+S_{Mox\_HB}}\right) \left(\frac{S_{O2}}{K_{O2\_HB}+S_{O2}}\right) X_H$
R10: Anoxic COD oxidation	$\eta\ r_{COD\_max} \left(\frac{S_S}{K_S+S_S}\right) \left(\frac{S_{Mox\_HB}}{K_{Mox\_HB}+S_{Mox\_HB}}\right) \left(\frac{K_{O2\_HB}}{K_{O2\_HB}+S_{O2}}\right) X_H$
R11: NO_3^- reduction to NO_2^-	$r_{NO3\_max} \left(\frac{S_{NO3}}{K_{NO3\_HB}+S_{NO3}}\right) \left(\frac{S_{Mred\_HB}}{K_{Mred1\_HB}+S_{Mred\_HB}}\right) \left(\frac{K_{O2\_HB}}{K_{O2\_HB}+S_{O2}}\right) X_H$
R12: NO_2^- reduction to NO	$r_{NO2\_max} \left(\frac{S_{NO2}}{K_{NO2\_HB}+S_{NO2}}\right) \left(\frac{S_{Mred\_HB}}{K_{Mred2\_HB}+S_{Mred\_HB}}\right) \left(\frac{K_{O2\_HB}}{K_{O2\_HB}+S_{O2}}\right) X_H$
R13: NO reduction to N_2O	$r_{NO\_max} \left(\frac{S_{NO}}{K_{NO\_HB}+S_{NO}}\right) \left(\frac{S_{Mred\_HB}}{K_{Mred3\_HB}+S_{Mred\_HB}}\right) \left(\frac{K_{O2\_HB}}{K_{O2\_HB}+S_{O2}}\right) X_H$
R14: N_2O reduction to N_2	$r_{N2O\_max} \left(\frac{S_{N2O}}{K_{N2O\_HB}+S_{N2O}}\right) \left(\frac{S_{Mred\_HB}}{K_{Mred4\_HB}+S_{Mred\_HB}}\right) \left(\frac{K_{O2\_HB}}{K_{O2\_HB}+S_{O2}}\right) X_H$
R15: Decay of HB	$b_H * X_H$
E2: Electron carriers equation for HB	$SM_{red\_HB} + SM_{ox\_HB} = C_{tot\_HB}$
Nitrite Oxidizing Bacteria (NOB)	
R16: NOB growth	$r_{NO2\_NOB} \left(\frac{S_{NO2}}{K_{NO2\_NOB}+S_{NO2}}\right) \left(\frac{S_{O2}}{K_{O2\_NOB}+S_{O2}}\right) X_{NOB}$
R17: Decay of NOB	$b_{NOB} * X_{NOB}$

iii. Stoichiometric matrix for the integrated N_2O production model

Process	S_{O2}	S_{NH3}	S_{NH2OH}	S_{NO3}	S_{NO2}	S_{NO}	S_{N2O}	S_S	S_{Mox_AOB}	S_{Mred_AOB}	S_{Mox_HB}	S_{Mred_HB}	X_S	X_{AOB}	X_{NOB}	X_H
Ammonium Oxidizing Bacteria (AOB)																
R1	-1	-1	1						1	-1				Y_{AOB}		
R2			-1			1			-3/2	3/2						
R3					1	-1			-1/2	1/2						
R4						-1	1/2		1/2	-1/2						
R5	-1/2								1	-1						
R6					-1		1/2		1	-1						
R7													35.5	-1		
Heterotrophic Bacteria (HB)																
R8								1					-1			
R9								-1			$-(1-Y_H)$	$(1-Y_H)$				Y_H
R10								-1			$-(1-Y_H)$	$(1-Y_H)$				Y_H
R11				-1	1						1	-1				
R12					-1	1					1/2	-1/2				
R13						-1	1/2				1/2	-1/2				
R14							-1				1	-1				
R15													35.5			-1
Nitrite Oxidizing Bacteria (NOB)																
R16	-1/2			1	-1										Y_{NOB}	
R17													35.5		-1	

iv. Kinetic and stoichiometric parameters of the integrated N_2O model

Parameter	Definition	Value	Unit	Source
r_{NH3_Ox}	Maximum NH_3 oxidation rate	16±1	mmol N-NH_3 (g VSS)$^{-1}$ h^{-1}	Calibrated
r_{NH2OH_Ox}	Maximum NH_2OH oxidation rate	22.86	mmol N-NH_2OH (g VSS)$^{-1}$ h^{-1}	Ni et al., 2014
r_{NO_Ox}	Maximum NO oxidation rate	22.86	mmol N-NO (g VSS)$^{-1}$ h^{-1}	Ni et al., 2014
r_{O2_red}	Maximum O_2 reduction rate	58.13±16	mmol as O_2 (g VSS)$^{-1}$ h^{-1}	Calibrated
r_{NO2_red}	Maximum NO_2^- reduction rate	3.2±0.6	mmol N-NO_2 (g VSS)$^{-1}$ h^{-1}	Calibrated
r_{NO_red}	Maximum NO reduction rate	0.022±0.002	mmol N-NO (g VSS)$^{-1}$ h^{-1}	Calibrated
K_{O2_NH3}	O_2 affinity constant for NH_3 oxidation	0.017±0.0009	mmol as O_2 L^{-1}	Calibrated
K_{NH3}	NH_3 affinity constant for NH_3 oxidation	0.17	mmol N-NH_3 L^{-1}	Ni et al., 2014
K_{NH2OH}	NH_2OH affinity constant for NH_2OH oxidation	0.05	mmol N-NH_2OH L^{-1}	Ni et al., 2014
K_{NO_Ox}	NO affinity constant for NO oxidation	0.0006	mmol N-NO L^{-1}	Ni et al., 2014
K_{O2_red}	O_2 affinity constant for O_2 reduction	0.0019	mmol as O_2 L^{-1}	Ni et al., 2014
K_{NO2_AOB}	NO_2^- affinity constant for NO_2^- reduction by AOB	0.01	mmol N-NO_2^- L^{-1}	Ni et al., 2014
K_{NO_red}	NO affinity constant for NO reduction (by AOB)	0.0006	mmol N-NO L^{-1}	Ni et al., 2014
K_{Mox_AOB}	Affinity constant for SMox (R3)	0.0001	mmol as Mox (g VSS)$^{-1}$	Ni et al., 2014
K_{Mred1_AOB}	Affinity constant for SMred (R1)	0.00001	mmol as Mred (g VSS)$^{-1}$	Ni et al., 2014
K_{Mred2_AOB}	Affinity constant for SMred (R4)	0.00001	mmol as Mred (g VSS)$^{-1}$	Ni et al., 2014
K_{Mred3_AOB}	Affinity constant for SMred (R5)	0.037	mmol as Mred (g VSS)$^{-1}$	Ni et al., 2014
K_{Mred4_AOB}	Affinity constant for SMred (R6)	0.15	mmol as Mred (g VSS)$^{-1}$	Ni et al., 2014
b_{AOB}	Decay rate of AOB	0.00625	h^{-1}	Henze et al., 2000
Y_{AOB}	AOB yield	0.00149	g VSS (mmol N)$^{-1}$	Mampaey et al., 2013
C_{tot_AOB}	Total electron carrier concentration for AOB	0.01	mmol as Ctot (g VSS)$^{-1}$	Ni et al., 2014
k_H	Hydrolysis rate constant	3.9	mmol COD (g VSS)$^{-1}$ h^{-1}	Henze et al., 2000
K_X	Hydrolysis saturation constant	3.125	mmol COD (g VSS)$^{-1}$	Henze et al., 2000
r_{COD_max}	Maximum COD oxidation rate	8.46	mmol COD (g VSS)$^{-1}$ h^{-1}	Pan et al., 2013
K_S	Affinity constant for S_S	0.1	mmol COD L^{-1}	Pan et al., 2013
K_{Mox_HB}	Affinity constant for S_{Mox} (R9)	0.0001	mmol COD L^{-1}	Pan et al., 2013

K_{O2_HB}	Half-saturation coefficient for O_2	0.003125	mmol as O_2 L^{-1}	Hiatt and Grady, 2008
Y_H	Yield coefficient for heterotrophic biomass	0.007143	g VSS (mmol COD)$^{-1}$	Henze et al., 2000
η	Denitrification reduction factor	0.8	-	Henze et al., 2000
r_{NO3_max}	Maximum NO_3^- reduction rate	3.99	mmol N-NO_3 (g VSS)$^{-1}$ h^{-1}	Pan et al., 2013
K_{NO3_HB}	Affinity constant for NO_3^-	0.0018	mmol N-NO_3^- L^{-1}	Pan et al., 2013
K_{Mred1_HB}	Affinity constant for SMred (R11)	0.00458	mmol as Mred (g VSS)$^{-1}$	Pan et al., 2013
r_{NO2_max}	Maximum NO_2^- reduction rate	5.27	mmol N-NO_2^- (g VSS)$^{-1}$ h^{-1}	Pan et al., 2013
K_{NO2_HB}	Affinity constant for NO_2^-	0.00413	mmol N-NO_2^- L^{-1}	Pan et al., 2013
K_{Mred2_HB}	Affinity constant for SMred (R12)	0.000393	mmol as Mred (g VSS)$^{-1}$	Pan et al., 2013
r_{NO_max}	Maximum NO reduction rate	50	mmol N-NO (g VSS)$^{-1}$ h^{-1}	Pan et al., 2013
K_{NO_HB}	Affinity constant for NO	0.0000107	mmol N-NO L^{-1}	Pan et al., 2013
K_{Mred3_HB}	Affinity constant for SMred (R13)	0.00001	mmol as Mred (g VSS)$^{-1}$	Pan et al., 2013
r_{N2O_max}	Maximum N_2O reduction rate	20	mmol N-N_2O (g VSS)$^{-1}$ h^{-1}	Pan et al., 2013
K_{N2O_HB}	Affinity constant for N_2O	0.025	mmol N-N_2O L^{-1}	Pan et al., 2013
K_{Mred4_HB}	Affinity constant for SMred (R14)	0.00323	mmol as Mred (g VSS)$^{-1}$	Pan et al., 2013
b_H	Decay rate of heterotrophic biomass	0.00833	h^{-1}	Henze et al., 2000
C_{tot_HB}	Total electron carrier concentration for HB	0.01	mmol as Ctot (g VSS)$^{-1}$	Ni et al., 2014
r_{NO2_NOB}	Maximum NO_2^- oxidation rate (NOB)	148.75	mmol N-NO_2^- (g VSS)$^{-1}$ h^{-1}	Wiesmann, 1994
K_{NO2_NOB}	Affinity constant for NO_2^- (NOB)	0.39	mmol N-NO_2^- L^{-1}	Wiesmann, 1994
K_{O2_NOB}	Half-saturation coefficient for O_2 (NOB)	0.069	mmol O_2 L^{-1}	Wiesmann, 1994
Y_{NOB}	Yield coefficient for NOB	0.0004114	g VSS (mmol N)$^{-1}$	Wiesmann, 1994
b_{NOB}	Decay rate of NOB	0.0025	h^{-1}	Wiesmann, 1994

References (Accompanying Material of Chapter IV)

Henze, M., Gujer, W., Mino, T., van Loosdrecht, M.C.M., 2000. Activated Sludge Models ASM1, ASM2, ASM2d, and ASM3, IWA Scientific and Technical Report n.9. IWA Publishing, London, UK.

Hiatt, W.C., Grady, C.P.L., 2008. An updated process model for carbon oxidation, nitrification, and denitrification. Water Environ. Res. 80: 2145-2156.

Mampaey, K.E., Beuckels, B., Kampschreur, M.J., Kleerebezem, R., van Loosdrecht, M.C.M., Volcke, E.I.P., 2013. Modelling nitrous and nitric oxide emissions by autotrophic ammonia-oxidizing bacteria. Environ. Technol. 34: 1555-1566.

Ni, B.J., Peng, L., Law, Y., Guo, J., Yuan, Z., 2014. Modeling of Nitrous Oxide Production by Autotrophic Ammonia-Oxidizing Bacteria with Multiple Production Pathways. Environ. Sci. Technol. 48: 3916-3924.

Pan, Y., Ni, B.J., Yuan, Z., 2013. Modeling electron competition among nitrogen oxides reduction and N_2O accumulation in denitrification. Environ. Sci. Technol. 47: 11083-11091.

Wiesmann, U., 1994. Biological nitrogen removal from wastewater. In: Biotechnics/Wastewater, pp. 113-154, Springer Berlin Heidelberg, Germany.

Supporting Information

List of Publications related to this Thesis

	JOURNAL ARTICLES
November 2017	**Massara, T.M.,** Solís, B., Guisasola, A., Katsou, E., Baeza, J.A., 2018. **Development of an ASM2d-N_2O model to describe nitrous oxide emissions in municipal WWTPs under dynamic conditions.** Chem. Eng. J. 335: 185-196. doi:10.1016/j.cej.2017.10.119
April 2017	**Massara, T.M.,** Malamis, S., Guisasola, A., Baeza, J.A., Noutsopoulos, C., Katsou, E., 2017. **A review on nitrous oxide (N_2O) emissions during biological nutrient removal from municipal wastewater and sludge reject water.** Sci. Total Environ. 596-597: 106-123. doi:10.1016/j.scitotenv.2017.03.191
	BOOK CHAPTERS
May 2017	**Massara, T.M.,** Katsou, E., Guisasola, A., Rodriguez-Caballero, A., Pijuan, M., Baeza, J.A., 2017. **Modelling of N_2O emissions in a full-scale activated sludge sequencing batch reactor.** In: Mannina, G. Ed. *Frontiers in Wastewater Treatment and Modelling.* Palermo, Italy: Springer, pp. 98-104. https://link.springer.com/chapter/10.1007/978-3-319-58421-8_15